Alma Mater Studiorum - Università di Bologna

DOTTORATO DI RICERCA IN

CHIMICA

Ciclo 35

Settore Concorsuale: 03/B1 - FONDAMENTI DELLE SCIENZE CHIMICHE E SISTEMI INORGANICI

Settore Scientifico Disciplinare: CHIM/03 - CHIMICA GENERALE E INORGANICA

CRYSTAL ENGINEERING STRATEGIES AGAINST ANTIMICROBIAL
RESISTANCE: A SOLID CONTRIBUTION TO A CONTEMPORARY PROBLEM.

Presentata da: Cecilia Fiore

Coordinatore Dottorato   **Supervisore**

Luca Prodi   Dario Braga

                                              Co-supervisore

                                              Lucia Maini

Esame finale anno 2023

ABSTRACT

This PhD thesis sets its goal in the application of crystal engineering strategies to the design, formulation, synthesis, and characterization of innovative materials obtained by combining well established biologically active molecules and/or GRAS (*generally recognized as safe*)[1,2] compounds with co-formers able to modulate specific properties of the molecule of interest. The solid-state association, via non-covalent interactions, of an active ingredient with another molecular component, a metal salt or a complex, may alter in a useful way the physicochemical properties of the active ingredient and/or may allow to explore new ways to enhance, in a synergistic way, the overall biological performance.[3,4]

More specifically this thesis will address the threat posed by the increasing antimicrobial resistance (AMR) developed by microorganisms, which call for novel therapeutic strategies.[5,6] Crystal engineering provides new tools to approach this crisis in a greener and cost-effective way.[3,7,8]

This PhD work has been developed along two main research lines aiming to contribute to the search for innovative solutions to the AMR problem.

Design, preparation and characterization of novel metal-based antimicrobials, whereby organic molecules with known antimicrobial properties are combined with metal atoms also known to exert antimicrobial action.

Design, preparation and characterization of co-crystals obtained by combining antibacterial APIs (*active pharmaceutical ingredients*) with natural antimicrobials.

References

(1)   *Generally Recognized as Safe (GRAS) | FDA*. https://www.fda.gov/food/food-ingredients-packaging/generally-recognized-safe-gras (accessed 2023-01-09).

(2)   Burdock, G. A.; Carabin, I. G. Generally Recognized as Safe (GRAS): History and Description. *Toxicol. Lett.* **2004**, *150* (1), 3–18. https://doi.org/10.1016/J.TOXLET.2003.07.004.

(3)   Almarsson, Ö.; Zaworotko, M. J. Crystal Engineering of the Composition of Pharmaceutical Phases. Do Pharmaceutical Co-Crystals Represent a New Path to Improved Medicines? *Chem. Commun.* **2004**, No. 17, 1889–1896. https://doi.org/10.1039/B402150A.

(4)   Desiraju, G. R. R. Crystal Engineering : The Design of Organic Solids. *Elsevier Sci.* **1989**.

(5)   *Antimicrobial resistance*. https://www.who.int/news-room/fact-sheets/detail/antimicrobial-resistance (accessed 2023-01-09).

(6)   *Antimicrobial resistance | European Medicines Agency*. https://www.ema.europa.eu/en/human-regulatory/overview/public-health-threats/antimicrobial-resistance (accessed 2023-01-09).

(4)   Burdock, G. A.; Carabin, I. G. Generally Recognized as Safe (GRAS): History and Description. *Toxicol. Lett.* **2004**, *150* (1), 3–18. https://doi.org/10.1016/J.TOXLET.2003.07.004.

(7)   Shemchuk, O.; Braga, D.; Grepioni, F.; Turner, R. J. Co-Crystallization of Antibacterials with Inorganic Salts: Paving the Way to Activity Enhancement. *RSC Adv.* **2020**, *10* (4), 2146–2149. https://doi.org/10.1039/C9RA10353H.

(8)   Fiore, C.; Shemchuk, O.; Grepioni, F.; Turner, R. J.; Braga, D. Proflavine and Zinc Chloride "Team Chemistry": Combining Antibacterial Agents via Solid-State Interaction. *CrystEngComm* **2021**, *23* (25), 4494–4499. https://doi.org/10.1039/D1CE00612F.

INDEX

Chapter 1 – Introduction

1.1 Overview

The overuse of antimicrobials during the last half-century is the primary cause of the development of antimicrobial resistance (AMR) in pathogenic and opportunistic microorganisms.[1,2] AMR has become one of the most important challenges in pharmacology and modern medicine. In the era of antimicrobial resistance, with an increasing need to find novel therapeutic strategies, the crystal engineering approach provides some different tools to approach this crisis in a greener and cost-effective way. This PhD thesis sets its goal in the application of crystal engineering strategies in the design, formulation and production of innovative materials combining well established biologically active molecules and/or compounds of the GRAS (*generally recognized as safe*)[3,4] type with co-formers able to modulate some specific property of the molecule of interest.

Paying great attention to the production process, following the principles of green chemistry, during this PhD work two main research lines were developed, aiming to progress in the search of innovative solutions to fight the AMR issue.

Line 1 – Design, preparation and characterization of novel metal-based antimicrobials, whereby organic molecules with known antimicrobial properties are combined with metal atoms also known to exert antimicrobial activity.

The results of the work discussed herein lend further support to the idea that co-crystallization of antibacterial compounds or GRAS molecules with metal salts is a viable, eco-friendly, and inexpensive way to obtain new materials with enhanced antibacterial properties.[5,6] Beyond organic antimicrobial molecules, metal-based antimicrobials are

of great interest as new means of dealing with the AMR threat.[7] Silver, zinc, copper, and other metals have been used for millennia as antimicrobial agents.[8,9] In this thesis I have applied a crystal engineering approach to the preparation, characterization and antimicrobial activity evaluation of novel compounds obtained from the assembling of antibacterial agents or GRAS molecules with salts of these metals.

Line 2 – **Design, preparation and characterization of co-crystals** obtained by combining antibacterial APIs (*active pharmaceutical ingredients*) with natural antimicrobials.

The basic idea is that the solid-state association, via non-covalent interactions, of an active ingredient with a molecular component, may alter in a useful way physicochemical properties such as solubility, dissolution rate, thermal stability, photoreactivity [10] *etc.* of the active ingredient and/or may allow to explore new ways to enhance, in a synergistic way, the overall antimicrobial performance. Co-crystals have become especially attractive in the pharmaceutical field, since they can lead to new pharmaceutical formulations compared, for example, to conventional salts.[10] This goal is usually pursued by co-crystallizing the API with a non-active (GRAS accepted) molecule. In more advanced applications, however, the API may also be co-crystallized with another active ingredient, yielding a so-called co-drug, whereby not only the solid-state physicochemical properties of the API are altered with respect to those of the pure crystal, but also the pharmaceutical and biological activity may result significantly different.[11–13] In this thesis, co-crystallization strategies are applied to alter/enhance the antibacterial properties of well-known classes of antibiotics, namely cephalosporines and ciprofloxacin.

In the following, the operative principles of crystal engineering utilized to carry out the work along the two lines outlined above, will be briefly described. This thesis will then

touch upon the general approach of the mechanochemical, and solution preparations of the compounds obtained by co-crystallization and then describe briefly how the antimicrobial performance of the products has been evaluated. For this latter aspect, however, a *caveat* is in order: the assessment of the antimicrobial activity has been possible thanks to the collaborations with research groups at the University of Calgary, Alberta – Canada and at the University of Bologna – Italy, who also share the authorship of the papers and works generated by this thesis and presented in the following chapters.

1.2   Crystal engineering: meaning and purpose

Crystal engineering, the design of functional molecular solids and coordination polymers, has emerged as one of the most appealing areas of chemical research in recent years.[14] The subject attracts attention for both fundamental and applied reasons. The goal of this field of research is that of assembling functionalized molecular and ionic components into a target network of supramolecular interactions.[15,16] Making crystals by design is the paradigm of crystal engineering.[19] The concept of crystal engineering was introduced by Pepinsky in 1955[19] and further implemented and elaborated by Schmidt in[20] the context of organic solid-state photochemical reactions. Desiraju subsequently defined crystal engineering as "*the understanding of intermolecular interactions in the context of crystal packing and in the utilization of such understanding in the design of new solids with desired physical and chemical properties*".[11]

Crystal engineering has matured into methods for the supramolecular synthesis of new compounds. The understanding of intermolecular interactions in chemical and energy terms represents the first step in the design of a crystal engineering experiment.

Substantially, crystal engineering is a powerful tool to gain control on the arrangement of the molecules/ions in the solid state via non-covalent intermolecular interactions such as hydrogen and halogen bonding, van der Waals and π-interactions as well as coordination bonds.[21,22] The solid-state packing arrangement of the building blocks (molecular and/or ionic) can dramatically affect the materials properties.[23,24]

1.2.1 Intermolecular interactions

It is from the perspective of understanding molecular properties in an environment, in terms of interactions between molecules, that the intermolecular interactions will be considered in what follows. [22,24,25] In Table 1 are summarized the main intermolecular interactions with their corresponding range of energies involved.[26,27]

Table 1. Summary of main intermolecular interactions and their energy ranges

Interaction	Energy (kJ/mol)
Hydrogen bonding	
Strong	>85
Moderate	15-85
Weak	5-15
Halogen bonding	5-45
Ionic and dipolar interactions	
ion - ion	200-300
Ion - dipole	50-200
dipole - dipole	5-50
π-interactions	2-50

1.2.2 Hydrogen bonding

Hydrogen bonding is surely the most frequently encountered and most important interaction in molecular crystals.[28] The frequency with which typical hydrogen bond acceptor/donor elements such as nitrogen and oxygen occur in organic compounds, coupled with the strength and directionally of the hydrogen-bond as compared to other intermolecular forces accounts for its significance. The hydrogen bonding can be considered as the strongest tool for molecular recognition. [29]

The hydrogen bond can be generally defined as "*an attractive interaction between a hydrogen atom from a molecule or a molecular fragment X-H in which X is more electronegative than H, and an atom or a group of atoms in the same or a different molecule (Y), in which there is evidence of bond formation* ".[30] The energy of a hydrogen bond depends on several parameters such as the nature of the donor and acceptor atoms which constitute the bond, *e.g.* the electronegativity of the atoms *X* and *Y*, their geometry, and environment.[31] As a result, one can commonly divide hydrogen bonds into three categories, *i.e.* strong, moderate and weak. The importance of weak and moderate hydrogen bonds should not be underestimated since they can play a significant role in the landscape of the non-covalent interactions in the lack of strong hydrogen bonds. To the most typically observed weak hydrogen bonds belong such interactions as C-H···N, C-H···O, C-H···X (X= Cl, F), and N-H···π.[32,33] In Figure 1 are depicted some strong and moderate hydrogen bond motifs.
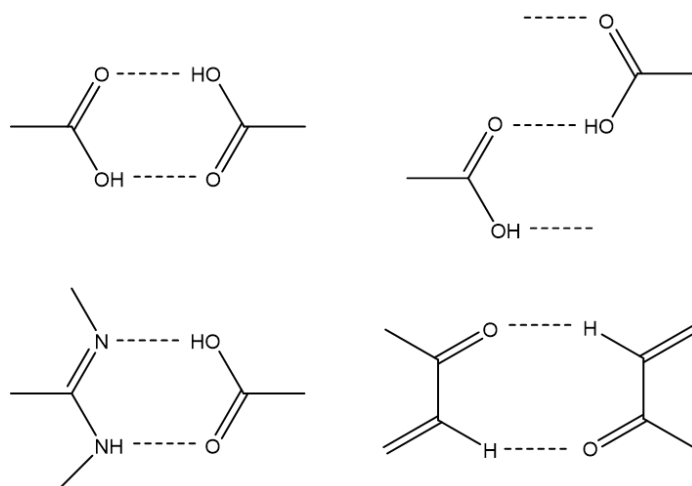
Figure 1. Schematic representation of some strong and moderate hydrogen bond motifs.

One more important aspect that influences the strength of a hydrogen bond is the *pKa* value of both hydrogen bond donor and acceptor. If an ionic charge is present on the donor and/or the acceptor of a hydrogen bond, the electrostatic dipole-dipole component of hydrogen bonding is enhanced. The hydrogen bonds of this type are called "*charge assisted hydrogen bonds*". They are usually obtained via proton transfer in acid-base reactions. [27]

1.2.3 Halogen bonding

Halogen atoms can work as acceptor sites resulting into the interaction called halogen bond. *The halogen bond occurs when there is evidence of a net attractive interaction between an electrophilic region associated with a halogen atom in a molecular entity and a nucleophilic region in another, or the same, molecular entity.*[34] The interaction energy follows the trend I>Br>Cl>F, with I-atoms involved in the strongest bonds. Thus, halogen bonding is a particular non-covalent interaction in which a halogen atom acts as an electrophilic species with electron donors.[34,35] Like hydrogen bonds, halogen bonds can be also used to control recognition, self-assembly, and aggregation processes in the solid. [36] The notable energies of certain halogen bonds allow these interactions to

prevail over other non-covalent interactions such as dipole–dipole interactions, π–π stacking, etc.[40] Some of the most common halogen bond kind of interactions are given in Figure 2.
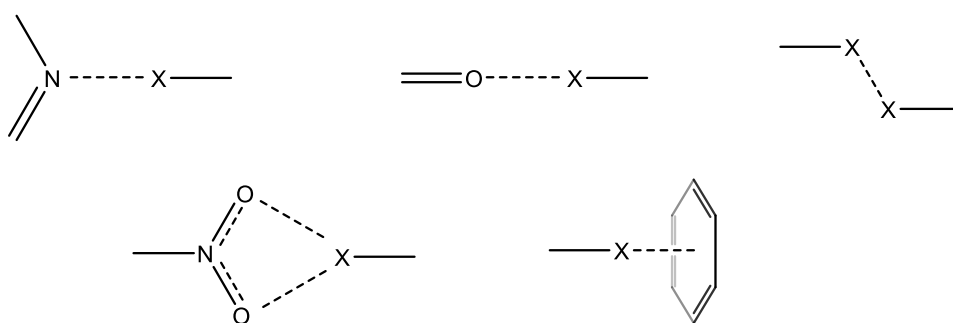

Figure 2. Common examples of halogen bond motifs.

1.2.4 Ionic and dipolar interactions

Ionic and dipolar interactions - ion-ion, ion-dipole, and dipole-dipole interactions - arise from the electrostatic interactions between charges.[39,40] The ion-ion interactions - the strongest ones - rely on high charge densities, therefore they generally act on long range distances and do not display a directional arrangement. For the ion-dipole interactions, it is possible to drive the spatial arrangement especially regarding the metal-ligand coordination, since the number of links expected as well as the geometry of the binding center are (at least in the case of d-block metals) predictable. Finally, the dipole-dipole interaction can arrange itself in a parallel or orthogonal way - thus displaying a sort of directional preference - because of the balance between repulsive and attractive forces and of the shape of the components involved.[27,41] All these features make these interactions extensively exploited in the crystal engineering field for the design of new materials.[15,18]

1.2.5 Van der Waals and π-interactions

Van der Waals and π-interactions are resulting from the direct overlap of regions of strong electronic accumulation (lone pairs, π-orbitals) in atoms or molecules. These bonds are usually indicated as A · · · B (or π · · · π, Ar · · · Ar), where A and B are the atoms (or group of atoms) with strong electronic localization.[27,42,43] π-interactions are typical of highly aromatic regions and can be essentially of two types, depending on how the aromatic rings are oriented towards each other: the aryl edge-face (EF) mode and the aryl offset face-face (OFF) mode (Figure 3). In the first case, the C-H···π interaction is formed due to the herringbone arrangement of the molecules, while the OFF mode is based on π···π interactions between molecules on top of each other (π stacking). Generally, small molecules base their arrangement on the EF mode, large molecules on the OFF mode while intermediate size molecules can form both the interactions giving rise to a sandwich herringbone crystal. [44,45]
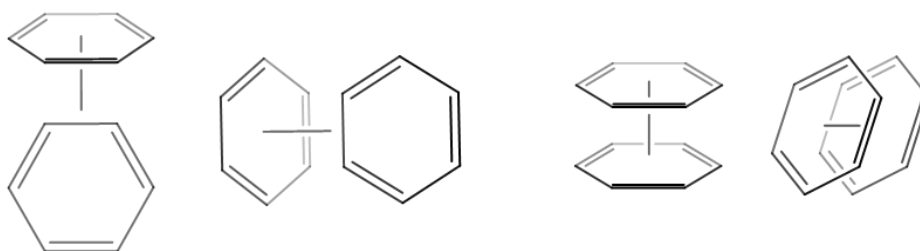
Figure 3. The aryl edge-face (EF) mode and the aryl offset face-face (OFF) mode.

1.2.6 Supramolecular synthons

In the crystal making process, the choice of "*supramolecular synthons*" is typically involved. Desiraju defined supramolecular synthons as "*an identifiable pattern of interacting molecular groups that is likely to be repeated in other crystal structures that contain the same molecular functional groups. These linkers largely control how the individual molecules will assemble as crystals for both organic and inorganic substances*".[16] The main goal of crystal engineering is to recognize and to use wisely supramolecular synthons and intermolecular interactions, in the design of materials.[46,47]

In Figure 4 some examples of supramolecular synthons formed via hydrogen bonding are represented.[48–51] Synthons **1-3** are homosynthons exhibited by carboxylic acid (**1** and **2**) and amide dimers (**3**). Synthon **4-6** are examples of heterosynthons. Synthon **1-6** have strong C=O···H–O; N–H···O; and O–H···N interactions. Synthons **7** and **8** are less favoured with either one weak C–H···O=C and one strong O–H···N (**7**) or both weak C–H···O=C hydrogen bonds (**8**).
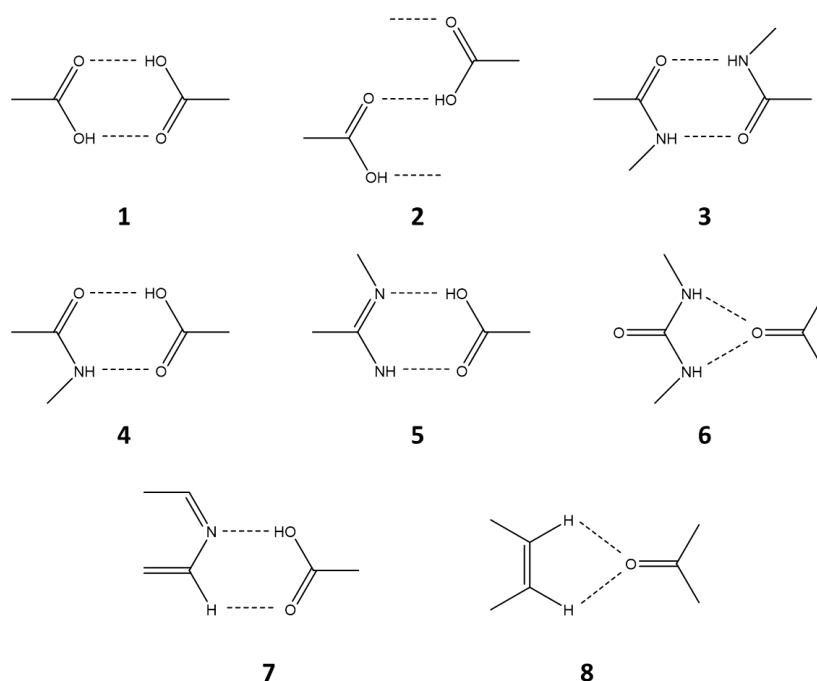
Figure 4. Arrangements of supramolecular synthons formed via hydrogen bonds.

1.2.7 Coordination networks

The properties of a solid can be engineered by arranging or assembling organic and inorganic species able to establish intermolecular interactions of the types described above and/or to coordinate and linking metal centres in a required fashion. [55]

Crystal engineering with coordination bonds is an attractive area or research owing to the inherent stability of coordination bonds and the versatility of coordination modes of transition metal atoms.[54] Coordination molecular architectures can be assembled with metal ions in different geometries and various multifunctional ligands, into complex frameworks. The coordination behaviour of the ligands and of the metal ions play a fundamental role in controlling the framework structures, which can exhibit a wide range of coordination architectures from zero-dimensional (0-D) complexes, to 1-D coordination polymers, 2-D coordination networks and to 3-D metal organic frameworks.[55]

Besides the above-mentioned supramolecular interactions, other weak intermolecular interactions, such as metallophilic interactions between d^{10} metal ions (e.g copper(I), silver(I), gold(I)), can also significantly influence the assembly of a polymeric/ supramolecular structure. [56–58]

1.3 Possible outcomes of a crystallization process

The understanding of all the possible intra- and intermolecular interactions does not guarantee the predictability of the outcome of a crystallization process. Especially, the prediction becomes more difficult if more than one molecular and/or ionic building block is involved in the crystallization process.[59] Depending on the design strategy and on the experimental conditions there is a great diversity of crystal forms that can be obtained starting from a building block of choice, which may well be an active

pharmaceutical ingredient or a biologically active molecule (vide infra). The crystallization process of a given molecule or complex of interest, may result in a variety of solid forms, from amorphous materials,[60] to single molecule crystals, to polymorphs,[61–64] solvates,[62,65] hydrates,[66] salts,[67] molecular[68–70] or ionic [71–73] co-crystals, and solid solutions[73,74] depending on the crystallization conditions and/or on the presence of other crystallization components. The possible outcomes are represented in Scheme 1.
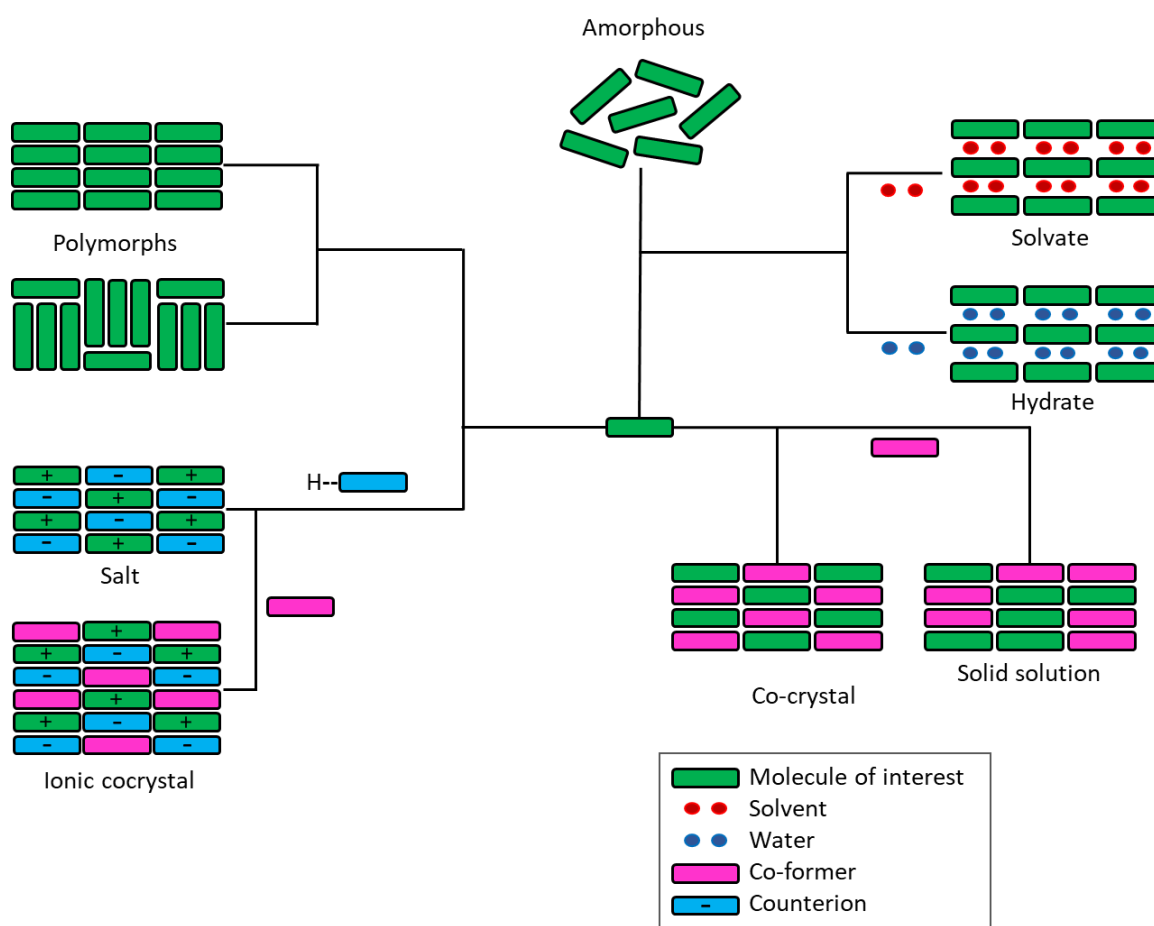
Scheme 1. Outline representation of the structural relationship between polymorphs, hydrates, solvates, co-crystals, salts, solid solutions, and amorphous materials obtained from a molecule of interest crystallized in different experimental conditions.

1.3.1 Molecular and ionic co-crystals

Multicomponent crystalline assemblies are relevant targets in the quest for novel solid forms exhibiting enhancement of physicochemical properties such as solubility, intrinsic dissolution rate, morphology, thermal and hydration stability compared to those of the separate components. Due to their potential utilization to tune these crucial properties, multicomponent crystalline solids are of interest in a variety of applications (pharmaceuticals, pigments, high energetic materials, nutraceuticals, agrochemicals, cosmetics etc.).[75–80] Several strategies can be employed to modify the chemical and physical solid-state properties of the material of interest (see scheme 1): the formation of polymorphs, salts, hydrates, solvates, molecular and ionic co-crystals, and solid solutions. The most well-established approach in the formulation of a new multicomponent crystalline solid with enhanced physicochemical properties is the formation of a salt.[85,86] The main limitation of salts is that the compound of interest must contain ionizable (basic or acidic) moieties.[87] A different pathway can be the formation of a molecular or ionic co-crystal.[85]

The definition of co-crystal has been extensively debated in the academic literature over the last years.[69,70,86] Starting from the generic assumption that a co-crystal is a multi-component molecular crystal, more specific definitions have been proposed, with the aim of ruling out other types of crystalline materials such as solvates, hydrates, clathrates, salts, and non-stoichiometric compounds. Zaworotko and co-workers have stated that a molecular co-crystal is a multiple component crystal where neutral molecular components are present in a definite stoichiometric ratio and all the components, when pure, are solid under ambient conditions.[86] Similarly, Aakeröy and Salmon have proposed the following criteria to define a molecular co-crystal, i.e. (1) only

compounds constructed from discrete neutral molecular species are considered (this statement excludes all solids containing ions, namely salts and complexes of transition-metal ions), (2) the components should be solid at ambient conditions (this assertion allows to distinguish co-crystals from solvates and hydrates as well as from clathrates or inclusion compounds with a solvent/gas molecule as a guest component) and (3) the crystal must be a structurally homogeneous crystalline material containing two or more neutral building blocks in well-defined stoichiometric amounts (this statement allows to draw a borderline between co-crystals and solid solutions).[68]

Depending on the nature of a co-former, co-crystals can be divided into "molecular" or "ionic" co-crystals.[75] A "molecular" co-crystal is composed of at least two neutral co-formers in a stoichiometric ratio, the components typically held together by hydrogen and/or halogen bonds, π-π stacking or other weak intermolecular interactions. The term "ionic co-crystal" (ICC) was introduced by our research group.[87] Initially this term was used to define co-crystals formed by a neutral organic molecule and an inorganic salt of a non-transition metal. The main interactions in such organic–inorganic systems are those established by metal cations with the organic moieties (typically, oxygen or nitrogen atoms donate electrons towards the metal cation).[87] To date, the use of the term has been extended to define the co-crystals of neutral molecules with organic or organic-inorganic salts.[88] Strictly speaking, ICCs do not meet one of the requirements – necessary to define a co-crystal – mentioned above, since one of the co-formers is not neutral. However, they are not proper salts either since no proton transfer took place between the molecule of interest and the co-former. Consequently, one can say that ICCs lie on the borderline between salts and co-crystals.

1.4 Mechanochemistry: a tool for a *sustainable* crystal engineering

Paul Anastas and John C. Warner co-authored the cornerstone book, *Green Chemistry: Theory and Practice* in 1998, and they defined Green Chemistry as the *"design of chemical products and processes to reduce or eliminate the use and generation of hazardous substances"*.[89] From a first ideal concept, the Green Chemistry manifesto was then structured, with the Twelve Principles as a guide for the design of new chemical products and processes.[90] Sustainable and green chemistry in very simple terms is just a different way of thinking about how chemistry and chemical engineering can be done.[91] Mechanochemistry, nowadays, is considered one of the most relevant techniques used in the field of green chemistry.[92] It is an ancient tool, recently rediscovered to meet the demand for clean processes and environmentally friendly solvent-free reaction.[93,94]

The term "mechanochemistry" was coined by Ostwald in 1893 and it consists in the application of mechanical forces to promote phenomena and chemical reactions. [95,96]

A mechanochemical reaction is defined as "a chemical reaction that is induced by the direct absorption of mechanical energy",[93,95] in fact, the energy that is released by the movement and collision of grinding bodies does not only lead to a reduction in particle size but can also be enough to allow the activation of chemicals in reaction environments.[97,101,102]

Recent works in mechano-synthesis of small organic molecules and metal–organic materials suggest that mechanochemical methods can bring about approximately 10000-fold improvements in the solvent- and energy-usage.[98,100,101] From a green chemistry perspective, mechanochemical activation conducted by milling or ultrasonic irradiation allows for the possibility to drastically reduce the amount of solvent needed

during chemical reactions, even to the point of achieving chemical reactivity under solvent-free conditions.[98,102,105]

Regarding the crystal engineering field, this method presents a whole range of benefits such as the control on stoichiometric composition and the ability to generate crystalline materials regardless of the relative solubilities of the starting components. [103–105] Typically, molecular and ionic co-crystals are prepared by slow solvent evaporation, the limitation being the solubility of the components in a given solvent or solvent mixture, but also the solubility of the co-crystal with respect to that of the single components.[106]

The mechanical grinding of molecular materials, with or without the addition of a small quantity of solvent (liquid assisted grinding- *LAG*), has revealed itself a greener and cost-effective way to prepare molecular and ionic co-crystals. [103,106]

The mortar and its pestle is the simplest mechanochemical reactor and with this practical and ancient "instrument", chemical reactions were already carried out in the Middle Ages, such as the conversion of cinnabar (HgS) into liquid mercury. [107–109]

Mechanochemical reactions, nowadays, are mostly performed with a ball milling instrument, planetary or vibrating.[110,111] The ball mills are instruments designed for the reduction and homogenization of the particle size of powder mixtures. Thanks to the continuous frictions that occur between the particles and the milling bodies of the mills, in fact, the dimensions of the introduced powders are reduced and a more even distribution of the particle dimensions is obtained. The mills, partially filled with spheres acting as grinding media, allow in a single instrument to have a homogeneous mixing of the introduced reagents, the increase of the surface area of the powders with the grinding action and a high energy supply, thanks to the friction forces taking place.[110,112,113] These forces can promote the activation of many phenomena inside the

milling jars, such as organic reactions,[97,100] breaking and rearranging bonds, [101,112] solid

state transitions and transformations,[103,104,106] particle size reduction, crashing, alloying,

etc. [95,110,114]

The grinding media and the material of the milling vessel can variate from ceramics to

plastic and stainless steel. The planetary mill rotates on a horizontal axis, describing a

planetary movement around the rotation center. The vibrating mill oscillates with a

frequency that can reach 60 Hz, commonly with a horizontal movement. In Figure 5 are

illustrated possible milling movements and grinding directions.
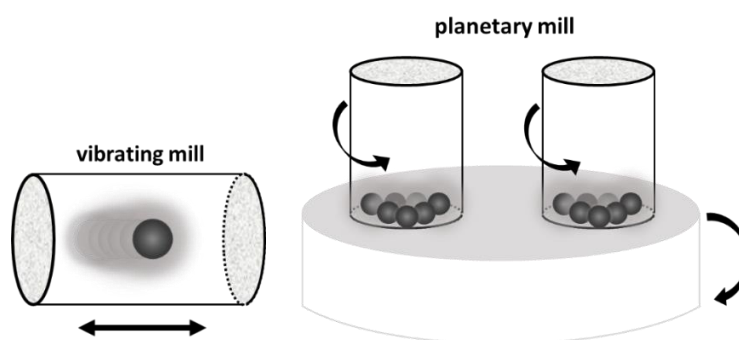
Figure 5. Description of milling movements and grinding directions.

The course of a reaction can be modulated by changing the milling conditions, such as

the amount of solvent, the milling time, the material of the jar and the grinding media.

[115–117]

From all these considerations, it follows that mechanochemistry is the preferred

synthetic technique applied in this research work to obtain bulk materials, performed

along with the solution-based synthesis, to obtain single crystals suitable for single

crystal X-ray diffraction.

1.5 Methods and techniques used for the preparation and characterization of solid products.

A brief overview of crystal growth techniques, bulk material preparation, sample analysis and characterization methods used in this thesis is presented in the following section.

As mentioned in the previous paragraph, the mechanochemical synthetic strategy was the preferred technique applied for the preparation of bulk materials, along with the synthesis from slurry. To obtain highly crystalline samples, in most of the cases, was performed a slow evaporation of solvent from solution, in various conditions and reaction parameters. Crystallization from melt was also applied in some peculiar case, for example when a reagent was almost completely insoluble in each accessible solvent. The resulting solid samples were then analysed with the following techniques:

- **Single Crystal X-ray Diffraction (SCXRD)** is the main technique used for structure determination from suitable single crystal samples.
- **X-ray Powder Diffraction (XRPD)** allowed to characterize the bulk material. In co-crystallization experiments it was mainly used to determine if a change of the phase was taking place, whether there were any new peaks different from those of the starting materials and, if so, whether some traces of the starting materials were still present in the bulk. When it was not possible to grow the single crystal of suitable quality to solve the structure using SCXRD, XRPD was applied for this purpose.
- **Variable Temperature X-ray Powder Diffraction (VTXRPD)** was used to follow the possible changes in the crystalline structure of the investigated solids upon change of the temperature.
- **Differential Scanning Calorimetry (DSC)** is a thermo-analytical technique used to detect and measure the enthalpy change associated with phase changes (dehydration/desolvation, polymorphic transition, melting).
- **Thermogravimetric Analysis (TGA)** was performed to quantify the mass loss of the sample upon heating.

- **Hot-Stage Microscopy (HSM)** was used for preparation of the crystals from melt and for visual estimation of the effect of temperature on the investigated solids.
- **Solubility tests** were performed to determine the maximum quantity of a compound capable of dissolving in a defined amount and type of solvent.
- **Solid-state NMR** – performed by collaborators of the group of Professor Roberto Gobetto at the University of Torino, Italy – used to characterize solid-state products when a better understanding of the structural features was needed.

1.6 Evaluation of the antimicrobial and bactericidal activity

The evaluation of the antimicrobial performance of the products obtained by applying the methods outlined above was possible thanks to a number of experts and synergistic collaborations with research groups at the University wasof Calgary (Canada), prof. Raymond Turner, and at the University of Bologna (Italy), groups of prof. Vittorio Sambri and of prof. Vincenzo Scarlato. Without entering in the details of the work carried out by these groups, with the objective of assisting the reader of this thesis to appreciate the results described in the published papers and in this thesis, the main parameters that have been evaluated are described hereafter.

Minimum inhibitory concentration (MIC) is defined as the lowest concentration of an antimicrobial that will inhibit the visible growth of a microorganism after overnight incubation. MICs are used by diagnostic laboratories mainly to confirm resistance, but most often as a research tool to determine the *in vitro* activity of new antimicrobials.[118,119]

Minimum bactericidal concentration (MBC) is the lowest concentration of antimicrobial that will prevent the growth of an organism after subculturing on to antibiotic-free media. The MBC is identified by determining the lowest concentration of antibacterial

agent that reduces the viability of the initial bacterial inoculum by ≥99.9%. The MBC is complementary to the MIC; whereas the MIC test demonstrates the lowest level of antimicrobial agent that inhibits growth, the MBC demonstrates the lowest level of antimicrobial agent that results in microbial death.[120]

References

(1)   *Antimicrobial resistance*. https://www.who.int/news-room/fact-sheets/detail/antimicrobial-resistance (accessed 2023-01-09).

(2)   *Antimicrobial resistance | European Medicines Agency*. https://www.ema.europa.eu/en/human-regulatory/overview/public-health-threats/antimicrobial-resistance (accessed 2023-01-09).

(3)   *Generally Recognized as Safe (GRAS) | FDA*. https://www.fda.gov/food/food-ingredients-packaging/generally-recognized-safe-gras (accessed 2023-01-09).

(4)   Burdock, G. A.; Carabin, I. G. Generally Recognized as Safe (GRAS): History and Description. *Toxicol. Lett.* **2004**, *150* (1), 3–18. https://doi.org/10.1016/J.TOXLET.2003.07.004.

(5)   Shemchuk, O.; Braga, D.; Grepioni, F.; Turner, R. J. Co-Crystallization of Antibacterials with Inorganic Salts: Paving the Way to Activity Enhancement. *RSC Adv.* **2020**, *10* (4), 2146–2149. https://doi.org/10.1039/C9RA10353H.

(6)   Fiore, C.; Shemchuk, O.; Grepioni, F.; Turner, R. J.; Braga, D. Proflavine and Zinc Chloride "Team Chemistry": Combining Antibacterial Agents via Solid-State Interaction. *CrystEngComm* **2021**, *23* (25), 4494–4499. https://doi.org/10.1039/D1CE00612F.

(7)   Lekhan, A.; Fiore, C.; Shemchuk, O.; Grepioni, F.; Braga, D.; Turner, R. J. Comparison of Antimicrobial and Antibiofilm Activity of Proflavine Co-Crystallized with Silver, Copper, Zinc, and Gallium Salts. *ACS Appl. Bio Mater.* **2022**. https://doi.org/10.1021/ACSABM.2C00404.

(8)   Turner, R. J. Metal-Based Antimicrobial Strategies. *Microb. Biotechnol.* **2017**, *10* (5), 1062–1065. https://doi.org/10.1111/1751-7915.12785.

(9)   Alexander, J. W. History of the Medical Use of Silver. *https://home.liebertpub.com/sur* **2009**, *10* (3), 289–292. https://doi.org/10.1089/SUR.2008.9941.

(10)   Almarsson, Ö.; Zaworotko, M. J. Crystal Engineering of the Composition of Pharmaceutical Phases. Do Pharmaceutical Co-Crystals Represent a New Path to Improved Medicines? *Chem. Commun.* **2004**, No. 17, 1889–1896. https://doi.org/10.1039/B402150A.

(11)   Bordignon, S.; Cerreia Vioglio, P.; Priola, E.; Voinovich, D.; Gobetto, R.; Nishiyama, Y.; Chierotti, M. R. Engineering Codrug Solid Forms: Mechanochemical Synthesis of an Indomethacin-Caffeine System. *Cryst. Growth Des.* **2017**, *17* (11), 5744–5752. https://doi.org/10.1021/ACS.CGD.7B00748.

(12)   Sekhon, B. S. Drug-Drug Co-Crystals. *DARU, J. Pharm. Sci.* **2012**, *20* (1), 1–2. https://doi.org/10.1186/2008-2231-20-45.

(13)   Qiao, N.; Li, M.; Schlindwein, W.; Malek, N.; Davies, A.; Trappitt, G. Pharmaceutical Co-Crystals: An Overview. *Int J Pharm* **2011**, *419* (1–2), 1–11. https://doi.org/10.1016/j.ijpharm.2011.07.037.

(14)   Tiekink, E. R. T.; Vittal, J. J. Frontiers in Crystal Engineering. *Front. Cryst. Eng.* **2006**, 1–332. https://doi.org/10.1002/0470022612.

(15)   Braga, D.; Grepioni, F. Intermolecular Interactions in Nonorganic Crystal Engineering. *Acc. Chem. Res.* **2000**, *33* (9), 601–608. https://doi.org/10.1021/AR990143U.

(16) Desiraju, G. R. Supramolecular Synthons in Crystal Engineering—A New Organic Synthesis. *Angew. Chemie Int. Ed. English* **1995**, *34* (21), 2311–2327. https://doi.org/10.1002/ANIE.199523111.

(17) Desiraju, G. R. R. Crystal Engineering : The Design of Organic Solids. *Elsevier Sci.* **1989**, 312.

(18) Braga, D.; Grepioni, F.; Desiraju, G. R. Crystal Engineering and Organometallic Architecture. *Chem. Rev.* **1998**, *98* (4), 1375–1405. https://doi.org/10.1021/CR960091B.

(19) Pepinsky, R. Crystal Engineering: A New Concept in Crystallography. *Phys. Rev.* **1955**, *100*, 971.

(20) Schmidt, G. M. J. Photodimerization in the Solid State. *Pure Appl. Chem.* **1971**, *27* (4), 647–678. https://doi.org/10.1351/PAC197127040647.

(21) Braga, D.; Grepioni, F. Making Crystals by Design: Methods, Techniques and Applications. *Mak. Cryst. by Des. Methods, Tech. Appl.* **2007**, 1–346. https://doi.org/10.1002/9783527610112.

(22) Novoa, J. J.; D'Oria, E.; Carvajal, M. A. Understanding the Nature of the Intermolecular Interactions in Molecular Crystals. A Theoretical Perspective. *Mak. Cryst. by Des. Methods, Tech. Appl.* **2007**, 25–57. https://doi.org/10.1002/9783527610112.CH2.

(23) Corpinot, M. K.; Bučar, D. K. A Practical Guide to the Design of Molecular Crystals. *Cryst. Growth Des.* **2019**, *19* (2), 1426–1453. https://doi.org/10.1021/ACS.CGD.8B00972.

(24) Vologzhanina, A. V. Intermolecular Interactions in Functional Crystalline Materials: From Data to Knowledge. *Cryst.* **2019**, *9* (9), 478. https://doi.org/10.3390/CRYST9090478.

(25) Kaplan, I. G. Intermolecular Interactions: Physical Picture, Computational Methods and Model Potentials. *Intermol. Interact. Phys. Pict. Comput. Methods Model Potentials* **2006**, 1–367. https://doi.org/10.1002/047086334X.

(26) Kaplan, I. G. Types of Intermolecular Interactions: Qualitative Picture. *Intermol. Interact.* **2006**, 25–79. https://doi.org/10.1002/047086334X.CH2.

(27) Sommerer, S. O. Intermolecular Interactions. *Intermol. Interact.* **1998**, 1–2. https://doi.org/10.1007/978-1-4615-4829-4_1.

(28) Aakeröy, C. B.; Seddon, K. R. The Hydrogen Bond and Crystal Engineering. *Chem. Soc. Rev.* **1993**, *22* (6), 397–407. https://doi.org/10.1039/CS9932200397.

(29) van der Lubbe, S. C. C.; Fonseca Guerra, C. The Nature of Hydrogen Bonds: A Delineation of the Role of Different Energy Components on Hydrogen Bond Strengths and Lengths. *Chem. - An Asian J.* **2019**, *14* (16), 2760–2769. https://doi.org/10.1002/ASIA.201900717.

(30) Arunan, E.; Desiraju, G. R.; Klein, R. A.; Sadlej, J.; Scheiner, S.; Alkorta, I.; Clary, D. C.; Crabtree, R. H.; Dannenber, J. J.; Hobza, P.; Kjaergaard, H. G.; Legon, A. C.; Mennucci, B.; Nesbitt, D. J. Definition of the Hydrogen Bond (IUPAC Recommendations 2011). *Pure Appl. Chem.* **2011**, *83* (8), 1637–1641. https://doi.org/10.1351/PAC-REC-10-01-02.

(31) Steiner, T. The Hydrogen Bond in the Solid State. *Angew. Chemie Int. Ed.* **2002**, *41*, 49--76.

(32) Jeffrey, G. A. *An Introduction to Hydrogen Bonding*; Oxford University Press, **1997.**

(33) Umeyama, H.; Morokuma, K. The Origin of Hydrogen Bonding. An Energy Decomposition Study. *J. Am. Chem. Soc.* **1977**, *99* (5), 1316–1332. https://doi.org/10.1021/JA00447A007.

(34) Metrangolo, P.; Meyer, F.; Pilati, T.; Resnati, G.; Terraneo, G. Halogen Bonding in Supramolecular Chemistry. *Angew. Chemie Int. Ed.* **2008**, *47* (33), 6114–6127. https://doi.org/10.1002/ANIE.200800128.

(35) Saccone, M.; Cavallo, G.; Metrangolo, P.; Pace, A.; Pibiri, I.; Pilati, T.; Resnati, G.; Terraneo, G. Halogen Bond Directionality Translates Tecton Geometry into Self-Assembled Architecture Geometry. *CrystEngComm* **2013**, *15* (16), 3102–3105. https://doi.org/10.1039/C3CE40268A.

(36) Metrangolo, P.; Neukirch, H.; Pilati, T.; Resnati, G. Halogen Bonding Based Recognition Processes: A World Parallel to Hydrogen Bonding. *ChemInform* **2005**, *36* (29). https://doi.org/10.1002/CHIN.200529294.

(37) Aakeröy, C. B.; Baldrighi, M.; Desper, J.; Metrangolo, P.; Resnati, G. Supramolecular Hierarchy among Halogen-Bond Donors. *Chem. - A Eur. J.* **2013**, *19* (48), 16240–16247. https://doi.org/10.1002/CHEM.201302162.

(39) Fuoss S, R. M. Ionic Interactions. *Nat.* **1971**, *233*, 572–573. https://doi.org/10.1038/233572b0.

(40) Petrucci, S. Ionic Interactions : From Dilute Solutions to Fused Salts. Elsevier, **2012**.

(41) Zeegers-Huyskens, T.; Huyskens, P. Intermolecular Forces. *Intermol. Forces* **1991**, 1–30. https://doi.org/10.1007/978-3-642-76260-4_1.

(42) Speight, J. G. Aromatic Hydrocarbons. *Rules Thumb Pet. Eng.* **2017**, 59–60. https://doi.org/10.1002/9781119403647.CH27.

(43) Fagnani, D. E.; Sotuyo, A.; Castellano, R. K. π–π Interactions. *Compr. Supramol. Chem. II* **2017**, 121–148. https://doi.org/10.1016/B978-0-12-409547-2.12485-0.

(44) Chen, T.; Li, M.; Liu, J. π-π Stacking Interaction: A Nondestructive and Facile Means in Material Engineering for Bioapplications. *Cryst. Growth Des.* **2018**, *18* (5), 2765–2783. https://doi.org/10.1021/ACS.CGD.7B01503.

(45) Desiraju, G. R.; Gavezzotti, A. Crystal Structures of Polynuclear Aromatic Hydrocarbons. Classification, Rationalization and Prediction from Molecular Structure. *Acta Crystallogr. Sect. B* **1989**, *45* (5), 473–482. https://doi.org/10.1107/S0108768189003794.

(46) Desiraju, G. R.; Sharma, C. V. K. Crystal Engineering and Molecular Recognition-Twin Facets of Supramolecular Chemistry. *Cryst. as a Supramol. Entity* **2007**, *2*, 31–61. https://doi.org/10.1002/9780470511459.CH2.

(47) Desiraju, G. R. The Crystal as a Supramolecular Entity. *Cryst. as a Supramol. Entity* **2007**, *2*, 1–314. https://doi.org/10.1002/9780470511459.

(48) Moulton, B.; Zaworotko, M. J. From Molecules to Crystal Engineering: Supramolecular Isomerism and Polymorphism in Network Solids. *Chem. Rev.* **2001**, *101* (6), 1629–1658. https://doi.org/10.1021/CR9900432.

(49) Philp, D.; Fraser Stoddart, J. Self-Assembly in Natural and Unnatural Systems. *Angew. Chemie (International Ed. English)* **1996**, *35* (11), 1154–1196. https://doi.org/10.1002/ANIE.199611541.

(50) Sauvage, J. P.; Gaspard, P. From Non-Covalent Assemblies to Molecular Machines. *From Non-Covalent Assem. to Mol. Mach.* **2011**. https://doi.org/10.1002/9783527632817.

(51) Fujita, M.; Murase, T. Noncovalent Assemblies: Design and Synthesis: Report. *From Non-Covalent Assem. to Mol. Mach.* **2011**, 7–30.

https://doi.org/10.1002/9783527632817.CH2.

(52)   Desiraju, G. R. Supramolecular Synthons in Crystal Engineering—A New Organic Synthesis. *Angew. Chemie Int. Ed. English* **1995**, *34* (21), 2311–2327. https://doi.org/10.1002/ANIE.199523111.

(53)   Desiraju, G. R. (Gautam R. . *Crystal Design : Structure and Function*; Gautam R. Desiraju, Ed.; Wiley, **2003**.

(54)   Robson, R. A Net-Based Approach to Coordination Polymers. *J. Chem. Soc. Dalt. Trans.* **2000**, No. 21, 3735–3744. https://doi.org/10.1039/B003591M.

(55)   Steed, J. W.; Atwood, J. L. Supramolecular Chemistry: Second Edition. *Supramol. Chem. Second Ed.* **2009**, 1–970. https://doi.org/10.1002/9780470740880.

(56)   Hayashi, A.; Olmstead, M. M.; Attar, S.; Balch, A. L. Crystal Chemistry of the Gold (I) Trimer, Au3(NC5H4)3: Formation of Hourglass Figures and Self-Association through Aurophilic Attraction. *J. Am. Chem. Soc.* **2002**, *124* (20), 5791–5795. https://doi.org/10.1021/JA012416Y.

(57)   Zheng, J.; Lu, Z.; Wu, K.; Ning, G. H.; Li, D. Coinage-Metal-Based Cyclic Trinuclear Complexes with Metal-Metal Interactions: Theories to Experiments and Structures to Functions. *Chem. Rev.* **2020**, *120* (17), 9675–9742. https://doi.org/10.1021/ACS.CHEMREV.0C00011.

(58)   Schmidbaur, H.; Graf, W.; Müller, G. Weak Intramolecular Bonding Relationships: The Conformation-Determining Attractive Interaction between Gold(I) Centers. *Angew. Chemie* **1988**, *27* (3), 417–419. https://doi.org/10.1002/ANIE.198804171.

(59)   Vippagunta, S. R.; Brittain, H. G.; Grant, D. J. W. Crystalline Solids. *Adv. Drug Deliv. Rev.* **2001**, *48* (1), 3–26. https://doi.org/10.1016/S0169-409X(01)00097-7.

(60)   Malek, J. Kinetic Analysis of Crystallization Processes in Amorphous Materials. *Thermochim. Acta* **2000**, *355* (1–2), 239–253. https://doi.org/10.1016/S0040-6031(00)00449-4.

(61)   Y. Matsuda et all. Kinetic Study of the Polymorphic Transformations of Phenylbutazone. *J. Pharm. Sci.* **1984**, *73*, 1453–1460.

(62)   G. A. Stephenson et all. Solid-State Analysis of Polymorphic, Isomorphic, and Solvated Forms of Dirithromycin. *J. Am. Chem. Soc.* **1994**, *116*, 5766–5773.

(63)   W. I. Higuchi et all. Polymorphism and Drug Availability. *J. Pharm. Sci.* **1963**, *52*, 150–153.

(64)   Byrn, S.; Pfeiffer, R.; Ganey, M.; Hoiberg, C.; Poochikian, G. Pharmaceutical Solids: A Strategic Approach to Regulatory Considerations. *Pharm. Res. An Off. J. Am. Assoc. Pharm. Sci.* **1995**, *12* (7), 945–954. https://doi.org/10.1023/A:1016241927429.

(65)   Giron, D. Thermal Analysis and Calorimetric Methods in the Characterisation of Polymorphs and Solvates. *Thermochim. Acta* **1995**, *248* (C), 1–59. https://doi.org/10.1016/0040-6031(94)01953-E.

(66)   Khankari, R. K.; Grant, D. J. W. Pharmaceutical Hydrates. *Thermochim. Acta* **1995**, *248* (C), 61–79. https://doi.org/10.1016/0040-6031(94)01952-D.

(67)   Adams, C. J.; Haddow, M. F.; Lusi, M.; Orpen, A. G. Crystal Engineering of Lattice Metrics of Perhalometallate Salts and MOFs. *Proc. Natl. Acad. Sci. U. S. A.* **2010**, *107* (37), 16033–16038. https://doi.org/10.1073/PNAS.0910146107.

(68)   Aakeröy, C. B.; Salmon, D. J. Building Co-Crystals with Molecular Sense and

Supramolecular Sensibility. *CrystEngComm* **2005**, *7* (72), 439–448. https://doi.org/10.1039/B505883J.

(69) Desiraju, G. R. Crystal and Co-Crystal. *CrystEngComm* **2003**, *5* (82), 466–467. https://doi.org/10.1039/B313552G.

(70) Dunitz, J. D. Crystal and Co-Crystal: A Second Opinion. *CrystEngComm* **2003**, *5* (91), 506–506. https://doi.org/10.1039/B315687G.

(71) Braga, D.; Grepioni, F.; Shemchuk, O. Organic–Inorganic Ionic Co-Crystals: A New Class of Multipurpose Compounds. *CrystEngComm* **2018**, *20* (16), 2212–2220. https://doi.org/10.1039/C8CE00304A.

(72) Braga, D.; Grepioni, F.; Lampronti, G. I.; Maini, L.; Turrina, A. Ionic Co-Crystals of Organic Molecules with Metal Halides: A New Prospect in the Solid Formulation of Active Pharmaceutical Ingredients. *Cryst. Growth Des.* **2011**, *11* (12), 5621–5627. https://doi.org/10.1021/CG201177P.

(73) Ocak, S.; Birolo, R.; Carì, G.; Bordignon, S.; Chierotti, M. R.; Braga, D.; Gobetto, R.; Salzillo, T.; Venuti, E.; Yaffe, O.; d'Agostino, S. Engineering Plastic Phase Transitions via Solid Solutions: The Case of "Reordering Frustration" in Ionic Plastic Crystals of Hydroxyquinuclidinium Salts. *Mol. Syst. Des. Eng.* **2022**, *7* (8), 950–962. https://doi.org/10.1039/D2ME00040G.

(74) Lusi, M. Engineering Crystal Properties through Solid Solutions. *Cryst. Growth Des.* **2018**, *18* (6), 3704–3712. https://doi.org/10.1021/ACS.CGD.7B01643.

(75) Duggirala, N. K.; Perry, M. L.; Almarsson, Ö.; Zaworotko, M. J. Pharmaceutical Cocrystals: Along the Path to Improved Medicines. *Chem. Commun.* **2015**, *52* (4), 640–655. https://doi.org/10.1039/C5CC08216A.

(76) Golob, S.; Perry, M.; Lusi, M.; Chierotti, M. R.; Grabnar, I.; Lassiani, L.; Voinovich, D.; Zaworotko, M. J. Improving Biopharmaceutical Properties of Vinpocetine Through Cocrystallization. *J. Pharm. Sci.* **2016**, *105* (12), 3626–3633. https://doi.org/10.1016/J.XPHS.2016.09.017.

(77) Meng, S. S.; Yu, Y. M.; Bu, F. Z.; Yan, C. W.; Wu, Z. Y.; Li, Y. T. Directional Self-Assembly of Ofloxacin and Syringic Acid: The First Salt Cocrystal of Ofloxacin with Phenolic Acid Displays Superior in Vitro/Vivo Biopharmaceutical Property and Enhanced Antibacterial Activity. *Cryst. Growth Des.* **2022**, *22* (11), 6735–6750. https://doi.org/10.1021/ACS.CGD.2C00896.

(78) Bučar, D. K.; Filip, S.; Arhangelskis, M.; Lloyd, G. O.; Jones, W. Advantages of Mechanochemical Cocrystallisation in the Solid-State Chemistry of Pigments: Colour-Tuned Fluorescein Cocrystals. *CrystEngComm* **2013**, *15* (32), 6289–6291. https://doi.org/10.1039/C3CE41013G.

(79) Schultheiss, N.; Newman, A. Pharmaceutical Cocrystals and Their Physicochemical Properties. *Cryst. Growth Des.* **2009**, *9* (6), 2950–2967. https://doi.org/10.1021/CG900129F.

(80) Aakeröy, C. B.; Forbes, S.; Desper, J. Using Cocrystals to Systematically Modulate Aqueous Solubility and Melting Behavior of an Anticancer Drug. *J. Am. Chem. Soc.* **2009**, *131* (47), 17048–17049. https://doi.org/10.1021/JA907674C.

(81) Aitipamula, S.; Banerjee, R.; Bansal, A. K.; Biradha, K.; Cheney, M. L.; Choudhury, A. R.; Desiraju, G. R.; Dikundwar, A. G.; Dubey, R.; Duggirala, N.; Ghogale, P. P.; Ghosh, S.; Goswami, P. K.; Goud, N. R.; Jetti, R. R. K. R.; Karpinski, P.; Kaushik, P.; Kumar, D.; Kumar,

V.; Moulton, B.; Mukherjee, A.; Mukherjee, G.; Myerson, A. S.; Puri, V.; Ramanan, A.; Rajamannar, T.; Reddy, C. M.; Rodriguez-Hornedo, N.; Rogers, R. D.; Row, T. N. G.; Sanphui, P.; Shan, N.; Shete, G.; Singh, A.; Sun, C. C.; Swift, J. A.; Thaimattam, R.; Thakur, T. S.; Kumar Thaper, R.; Thomas, S. P.; Tothadi, S.; Vangala, V. R.; Variankaval, N.; Vishweshwar, P.; Weyna, D. R.; Zaworotko, M. J. Polymorphs, Salts, and Cocrystals: What's in a Name? *Cryst. Growth Des.* **2012**, *12* (5), 2147–2152. https://doi.org/10.1021/CG3002948.

(82)   Berge, S. M.; Bighley, L. D.; Monkhouse, D. C. Pharmaceutical Salts. *J. Pharm. Sci.* **1977**, *66* (1), 1–19. https://doi.org/10.1002/JPS.2600660104.

(83)   Stahl, P. H.; Wermuth, C. G.; International Union of Pure and Applied Chemistry. Handbook of Pharmaceutical Salts : Properties, Selection, and Use. **2008**, 374.

(84)   Childs, S. L.; Stahly, G. P.; Park, A. The Salt-Cocrystal Continuum: The Influence of Crystal Structure on Ionization State. *Mol. Pharm.* **2007**, *4* (3), 323–338. https://doi.org/10.1021/MP0601345

(85)   Aakeröy, C. B.; Fasulo, M. E.; Desper, J. Cocrystal or Salt: Does It Really Matter? *Mol. Pharm.* **2007**, *4* (3), 317–322. https://doi.org/10.1021/MP060126O.

(86)   Shan, N.; Zaworotko, M. J. The Role of Cocrystals in Pharmaceutical Science. *Drug Discov. Today* **2008**, *13* (9–10), 440–446. https://doi.org/10.1016/J.DRUDIS.2008.03.004.

(87)   Braga, D.; Grepioni, F.; Maini, L.; Prosperi, S.; Gobetto, R.; Chierotti, M. R. From Unexpected Reactions to a New Family of Ionic Co-Crystals: The Case of Barbituric Acid with Alkali Bromides and Caesium Iodide. *Chem. Commun.* **2010**, *46* (41), 7715–7717. https://doi.org/10.1039/C0CC02701D.

(88)   Shemchuk, O.; Braga, D.; Grepioni, F.; Turner, R. J. Co-Crystallization of Antibacterials with Inorganic Salts: Paving the Way to Activity Enhancement. *RSC Adv.* **2020**, *10* (4), 2146–2149. https://doi.org/10.1039/C9RA10353H.

(89)   Anastas, P. T.; Warner, J. C. Green Chemistry: Theory and Practice - Oxford University Press. **1998**, 148.

(90)   *12 Principles of Green Chemistry - American Chemical Society.* https://www.acs.org/greenchemistry/principles/12-principles-of-green-chemistry.html (accessed 2023-01-03).

(91)   Anastas, P.; Eghbali, N. Green Chemistry: Principles and Practice. *Chem. Soc. Rev.* **2009**, *39* (1), 301–312. https://doi.org/10.1039/B918763B.

(92)   Friščić, T.; Mottillo, C.; Titi, H. M. Mechanochemistry for Synthesis. *Angew. Chemie - Int. Ed.* **2020**, *59* (3), 1018–1029. https://doi.org/10.1002/ANIE.201906755.

(93)   Liu, X.; Li, Y.; Zeng, L.; Li, X.; Chen, N.; Bai, S.; He, H.; Wang, Q.; Zhang, C. A Review on Mechanochemistry: Approaching Advanced Energy Materials with Greener Force. *Adv. Mater.* **2022**, *34* (46), 2108327. https://doi.org/10.1002/ADMA.202108327.

(94)   Cuccu, F.; De Luca, L.; Delogu, F.; Colacino, E.; Solin, N.; Mocci, R.; Porcheddu, A. Mechanochemistry: New Tools to Navigate the Uncharted Territory of "Impossible" Reactions. *ChemSusChem* **2022**, *15* (17). https://doi.org/10.1002/CSSC.202200362.

(95)   Do, J. L.; Friščić, T. Mechanochemistry: A Force of Synthesis. *ACS Cent. Sci.* **2017**, *3* (1), 13–19. https://doi.org/10.1021/ACSCENTSCI.6B00277.

(96)   Takacs, L. The Historical Development of Mechanochemistry. *Chem. Soc. Rev.* **2013**, *42* (18), 7649–7659. https://doi.org/10.1039/C2CS35442J.

(97) Margetic, D.; Štrukil, V. *Mechanochemical Organic Synthesis*, 1st ed., Elsevier, **2016.**

(98) James, S. L.; Adams, C. J.; Bolm, C.; Braga, D.; Collier, P.; Friščic, T.; Grepioni, F.; Harris, K. D. M.; Hyett, G.; Jones, W.; Krebs, A.; Mack, J.; Maini, L.; Orpen, A. G.; Parkin, I. P.; Shearouse, W. C.; Steed, J. W.; Waddell, D. C. Mechanochemistry: Opportunities for New and Cleaner Synthesis. *Chem. Soc. Rev.* **2011**, *41* (1), 413–447. https://doi.org/10.1039/C1CS15171A.

(99) Friščić, T. New Opportunities for Materials Synthesis Using Mechanochemistry. *J. Mater. Chem.* **2010**, *20* (36), 7599–7605. https://doi.org/10.1039/C0JM00872A.

(100) Wang, G. W. Mechanochemical Organic Synthesis. *Chem. Soc. Rev.* **2013**, *42* (18), 7668–7700. https://doi.org/10.1039/C3CS35526H.

(101) Szuppa, T.; Stolle, A.; Ondruschka, B.; Hopfe, W. Solvent-Free Dehydrogenation of γ-Terpinene in a Ball Mill: Investigation of Reaction Parameters. *Green Chem.* **2010**, *12* (7), 1288–1294. https://doi.org/10.1039/C002819C.

(102) Anastas, N. D.; Warner, J. D. The Incorporation of Hazard Reduction as a Chemical Design Criterion in Green Chemistry. *Chem. Heal. Saf.* **2005**, *12* (2), 9–13. https://doi.org/10.1016/J.CHS.2004.10.001.

(103) Jones, W. Mechanochemistry and Its Role in Novel Crystal Form Discovery. *NATO Sci. Peace Secur. Ser. A Chem. Biol.* **2017**, *PartF1*, 341–351. https://doi.org/10.1007/978-94-024-1117-1_21.

(104) Boldyrev, V. V. Mechanochemistry and Mechanical Activation of Solids. *Russ. Chem. Rev.* **2006**, *75* (3), 177–189. https://doi.org/10.1070/RC2006V075N03ABEH001205.

(105) Boldyreva, E. Mechanochemistry of Inorganic and Organic Systems: What Is Similar, What Is Different? *Chem. Soc. Rev.* **2013**, *42* (18), 7719–7738. https://doi.org/10.1039/c3cs60052a.

(106) Braga, D.; Maini, L.; Grepioni, F. Mechanochemical Preparation of Co-Crystals. *Chem. Soc. Rev.* **2013**, *42* (18), 7638–7648. https://doi.org/10.1039/C3CS60014A.

(107) Takacs, L. Quicksilver from Cinnabar the First Documented Mechanochemical Reaction? *JOM* **2000**, *52* (1), 12–13. https://doi.org/10.1007/S11837-000-0106-0.

(108) Marchini, M.; Gandolfi, M.; Maini, L.; Raggetti, L.; Martelli, M. Exploring the Ancient Chemistry of Mercury. *Proc. Natl. Acad. Sci. U. S. A.* **2022**, *119* (24), e2123171119. https://doi.org/10.1073/PNAS.2123171119.

(109) Tanaka, K.; Toda, F. Solvent-Free Organic Synthesis. *Chem. Rev.* **2000**, *100* (3), 1025–1074. https://doi.org/10.1021/CR940089P.

(110) Matthey, J.; Rivas, M. E. "Ball Milling Towards Green Synthesis: Applications, Projects, Challenges." *Technol. Rev* **2016**, No. 2, 148–150. https://doi.org/10.1595/205651316X691375.

(111) Sahoo, B. M.; Banik, B. K. Solvent-Less Reactions: Green and Sustainable Approaches in Medicinal Chemistry. *Green Approaches Med. Chem. Sustain. Drug Des.* **2020**, 523–548. https://doi.org/10.1016/B978-0-12-817592-7.00014-9.

(112) Ohara, S.; Tan, Z. Q.; Yamamoto, K.; Qiu, N.; Hashishin, T. Collision-Friction Synthesis of Carbon Nanomaterials by a High-Speed Ball-Milling Process. *Proc. 1st Int. Jt. Symp. Join. Weld.* **2013**, 509–510. https://doi.org/10.1533/978-1-78242-164-1.509.

(113) El-Eskandarany, M. S. Mechanically Induced Gas-Solid Reactiоn. *Mech. Alloy.* **2001**, 94–

117. https://doi.org/10.1016/B978-081551462-6.50008-1.

(114)	Kaupp, G. Mechanochemistry: The Varied Applications of Mechanical Bond-Breaking. *CrystEngComm* **2009**, *11* (3), 388–403. https://doi.org/10.1039/b810822f.

(115)	Tavares, L. M. A Review of Advanced Ball Mill Modelling. *KONA Powder Part. J.* **2017**, *2017* (34), 106–124. https://doi.org/10.14356/KONA.2017015.

(116)	Okamoto, Y.; Harada, Y.; Ohta, N.; -, al; Ju Lee, J.; Young Oh, M.; Suk Nahm -, K.; Tayyebi, A.; Ogino, N.; Hayashi, T.; Shinde, S.; Momin, T.; Karkaria, V.; Karandikar, P. Investigation of Substitute Jar Materials for Laboratory Grade Ball Milling Machine to Process Electrode Materials for Energy Storage Devices. *IOP Conf. Ser. Mater. Sci. Eng.* **2021**, *1206* (1), 012018. https://doi.org/10.1088/1757-899X/1206/1/012018.

(117)	Piras, C. C.; Fernández-Prieto, S.; De Borggraeve, W. M. Ball Milling: A Green Technology for the Preparation and Functionalisation of Nanocellulose Derivatives. *Nanoscale Adv.* **2019**, *1* (3), 937–947. https://doi.org/10.1039/C8NA00238J.

(118)	Andrews, J. M. Determination of Minimum Inhibitory Concentrations. *J. Antimicrob. Chemother.* **2001**, *48* (suppl_1), 5–16. https://doi.org/10.1093/JAC/48.SUPPL_1.5.

(119)	Amyes, S. G. B. Antimicrobial Chemotherapy : Pocketbook. CRC Press, **1996**.

(120)	Craig, W. A.; Nadler, H.; Ph, D. Methods for Determining Bactericidal Activity of Antimicrobial Agents; FDA Approved Guideline. **1999**.

Chapter 2 – Design of novel metal-based antimicrobials

Metal compounds have been used as antimicrobial agents for thousands of years, only to be mostly replaced by organic antibiotics in the 20th century.[1]

Traditional antibiotics tend to follow the *bullet-target* concept, acting on specific biochemical processes: replication, transcription, translation, and metabolic enzymes, which provide ease of progressive resistance. Alternatively, metals appear to target multiple cellular processes.[1,2]

The extended overuse of antimicrobials during the last half-century is the primary cause of the development of antimicrobial resistance in pathogenic and opportunistic microorganisms,[3] which has become one of the most important challenges in pharmacology and modern medicine.[4,5] It follows that a synergistic multi-target strategy, based on metal-organic combinations could open a new window of opportunity.

Since metal-based antimicrobials have the potential for designing novel sustainable solutions for health,[1,6] progress has been made in the area of molecular inorganic-organic hybrid compounds.[7,8] These materials are engineered to combine a bactericidal metal center with bioactive ligands or with ancillary ligands selected from the GRAS (*generally recognized as safe*) list.[9] Indeed, the coordination of organic ligands with metals, showing antibacterial activities, has proved to be a valid route to tackle antimicrobial resistance (AMR).[10] In this part of my research work the attention has been focused on the design of new bioactive salts, complexes and coordination polymers (CPs). In the following sections are reported the results obtained concerning the matter described in this brief introduction.

References

(1)   Turner, R. J. Metal-Based Antimicrobial Strategies. *Microb. Biotechnol.* **2017**, *10* (5), 1062–1065. https://doi.org/10.1111/1751-7915.12785.

(2)   Aminov, R. I. A Brief History of the Antibiotic Era: Lessons Learned and Challenges for the Future. *Front. Microbiol.* **2010**, *1* (DEC), 134. https://doi.org/10.3389/FMICB.2010.00134.

(3)   Lewis, K. Persister Cells: Molecular Mechanisms Related to Antibiotic Tolerance. *Handb. Exp. Pharmacol.* **2012**, *211*, 121–133. https://doi.org/10.1007/978-3-642-28951-4_8.

(4)   *Antimicrobial resistance*. https://www.who.int/news-room/fact-sheets/detail/antimicrobial-resistance (accessed 2023-01-09).

(5)   *Antimicrobial resistance | European Medicines Agency*. https://www.ema.europa.eu/en/human-regulatory/overview/public-health-threats/antimicrobial-resistance (accessed 2023-01-09).

(6)   Wright, J. B.; Lam, K.; Burrell, R. E. Wound Management in an Era of Increasing Bacterial Antibiotic Resistance: A Role for Topical Silver Treatment. *Am. J. Infect. Control* **1998**, *26* (6), 572–577. https://doi.org/10.1053/ic.1998.v26.a93527.

(7)   Haas, K. L.; Franz, K. J. Application of Metal Coordination Chemistry to Explore and Manipulate Cell Biology. *Chem. Rev.* **2009**, *109* (10), 4921–4960. https://doi.org/10.1021/CR900134A.

(8)   Lemire, J. A.; Kalan, L.; Gugala, N.; Bradu, A.; Turner, R. J. Silver Oxynitrate – an Efficacious Compound for the Prevention and Eradication of Dual-Species Biofilms. *http://dx.doi.org/10.1080/08927014.2017.1322586* **2017**, *33* (6), 460–469. https://doi.org/10.1080/08927014.2017.1322586.

(9)   *Generally Recognized as Safe (GRAS) | FDA*. https://www.fda.gov/food/food-ingredients-packaging/generally-recognized-safe-gras (accessed 2023-01-09).

(10)   Levy, S. B.; Bonnie, M. Antibacterial Resistance Worldwide: Causes, Challenges and Responses. *Nat. Med. 2004 1012* **2004**, *10* (12), S122–S129. https://doi.org/10.1038/nm1145.

2.1 Proflavine and zinc chloride "team chemistry": combining antibacterial agents via solid-state interaction

Abstract

Co-crystallization of the antibacterial agent proflavine (PF) with the inorganic salt $ZnCl_2$ by mechanochemical and solution methods results in the formation of novel compounds $ZnCl_3(HPF)$ (1) and $[HPF]_2[ZnCl_4] \cdot H_2O$ (2), both containing the proflavinium cation $(HPF)+$. Both compounds show a 50–125% enhanced antimicrobial activity with respect to a reference standard of $AgNO_3$, and a 25–50% enhancement to the behaviour of the separate components against pathogen indicator strains of Pseudomonas aeruginosa, Staphylococcus aureus, and Escherichia coli. In terms of crystal structure, both compounds $ZnCl_3(HPF)$ and $[HPF]_2[ZnCl_4] \cdot H_2O$ are characterized by extensive π-stacking interactions between the proflavine moieties. The same interaction is predominant in the previously unknown crystal structures of neutral proflavine (PF), as well as in that of its dihydrated monochloride salt, $[HPF]Cl \cdot 2H_2O$, which are also described in this paper.

CrystEngComm

ROYAL SOCIETY
OF CHEMISTRY

PAPER

Check for updates

Proflavine and zinc chloride "team chemistry": combining antibacterial agents via solid-state interaction†

Cecilia Fiore, [ID] [a] Oleksii Shemchuk, [ID] [a] Fabrizia Grepioni, [ID] [a] Raymond J. Turner [ID] *[b] and Dario Braga [ID] *[a]

Co-crystallization of the antibacterial agent proflavine (PF) with the inorganic salt $ZnCl_2$ by mechanochemical and solution methods results in the formation of novel compounds $ZnCl_3(HPF)$ (**1**) and $[HPF]_2[ZnCl_4]\cdot H_2O$ (**2**), both containing the proflavinium cation $(HPF)^+$. Both compounds show a 50–125% enhanced antimicrobial activity with respect to a reference standard of $AgNO_3$, and a 25–50% enhancement to the behaviour of the separate components against pathogen indicator strains of *Pseudomonas aeruginosa*, *Staphylococcus aureus*, and *Escherichia coli*. In terms of crystal structure, both compounds $ZnCl_3(HPF)$ and $[HPF]_2[ZnCl_4]\cdot H_2O$ are characterized by extensive π-stacking interactions between the proflavine moieties. The same interaction is predominant in the previously unknown crystal structures of neutral proflavine (PF), as well as in that of its dihydrated monochloride salt, $[HPF]Cl\cdot 2H_2O$, which are also described in this paper.

Introduction

Antimicrobial resistance (AMR)[1] is rapidly developing as the major health problems of our time, mainly caused by the abuse of antibiotics to control infections in humans and animals.[2] Most of the common pathogenic strains already have antibiotic-resistant genes and, presumably, more antibiotic-resistant pathogens will emerge in the future.[3] The quest for new antimicrobial agents can nowadays rely on the important conceptual tools provided by crystal engineering,[4] namely the possibility of associating within the same crystalline material two or more components[5] via co-crystallization. As a matter of fact, co-crystallization is being actively explored in the pharmaceutical field,[6] since the association of an active ingredient and a coformer, which, in turn, can also be an active molecule, can generate new pharmaceuticals or alter significantly the physico-chemical and pharmacokinetic properties of known ones.[7] In the quest for a crystal engineering-based answer to the AMR problem, we have recently shown that co-crystallization of the

antibacterial compounds proflavine[8] and methyl viologen,[9] with metal salts, such as CuCl, CuCl₂ and AgNO₃, is a viable, eco-friendly, and inexpensive way to obtain new materials with enhanced antibacterial properties.[10] An analogous co-crystallization approach has been used to prepare new associations of known antibiotics, such as ciprofloxacin, with natural antimicrobials, such as thymol and carvacrol.[11] Based on the same approach, a multicomponent solid consisting of an antibacterial (norfloxacin) and an antimicrobial (sulfathiazole) has been recently reported by Desiraju et al.[12] showing enhanced in vitro biological properties and improved physicochemical behaviour. Besides organic antimicrobial molecules, metal-based antimicrobials are of great interest as new means of dealing with the AMR threat.[13,14] Silver, zinc, copper and others have been used for millennia as antimicrobial agents.[15] Moreover, the combination of metals with organic antimicrobials as metal-coordinated ligands and/or co-crystals may represent an alternative resource in the quest for new and diverse solutions.[16] In this work, we apply a crystal engineering approach to the preparation,

[a] Dipartimento di Chimica "Giacomo Ciamician", Università di Bologna, Via Selmi, 2, 40126 Bologna, Italy. E-mail: dario.braga@unibo.it
[b] Department of Biological Sciences, University of Calgary, 2500 University Drive NW, Calgary, Alberta T2N 4, Canada
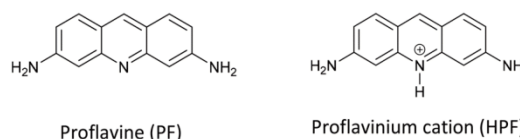
Scheme 1 Neutral PF and monoprotonated proflavine HPF used in this work.

characterization and antimicrobial activity evaluation of two novel compounds obtained from the known antibacterial agent proflavine (see Scheme 1 for neutral proflavine, PF) which is reacted as its hydrochloride proflavinium cation (HPF)$^+$ with zinc chloride. Depending on the stoichiometric ratio between (HPF)$^+$ and zinc chloride and on the preparation conditions, new compounds $ZnCl_3(HPF)$ (**1**) and $[HPF]_2[ZnCl_4]\cdot H_2O$ (**2**) have been obtained by both solution and mechanochemical methods and characterized by X-ray diffraction, DSC and TGA.

The structure of **1** has been determined from powder diffraction data, as it proved impossible to grow single crystals, while that of **2** has been determined from single-crystal X-ray data. Correspondence between the bulk mechanochemical products and the structures of **1** and **2** has been verified by comparing the observed and calculated X-ray powder diffraction patterns. The monohydrate nature of **2** has been ascertained by TGA. The antimicrobial activity of **1** and **2** has been tested against the pathogen indicator strains *Pseudomonas aeruginosa* ATCC27853, *Staphylococcus aureus* ATCC25923, and *Escherichia coli* ATCC 25922. To evaluate the efficacy of the antimicrobials, we have used the established method of measuring a zone of growth inhibition and contact killing using a compound impregnated antimicrobial susceptibility filter disk.

In this paper, we also report the structural characterization of two novel forms of proflavine, namely the anhydrous proflavine (PF), obtained by dehydration of proflavine monohydrate PF·H_2O (CSD refcode PROFLV[17]), and that of its hydrochloride salt, $[HPF]Cl\cdot 2H_2O$, the monoprotonated form of the known dichloride salt $[H_2PF]Cl_2\cdot 2H_2O$ (CSD refcode PROFLC[18]). Despite the different nature of the four compounds, the neutral organic molecule (PF), a hydrated salt $[HPF]Cl\cdot 2H_2O$ and coordination compounds between PF and zinc chloride (**1**) and a salt (**2**), all these crystals share the common feature of extensive π-stacking and of herringbone interactions between the proflavine/proflavinium moieties.

Experimental

Materials and methods

All reagents and solvents used in this work were purchased from Sigma-Aldrich and used without further purification.

Preparation of PF·H_2O. Commercial $[HPF]_2[SO_4]\cdot xH_2O$ (1 g) was dissolved in 25 mL of water and 3.10 g (0.077 mol) of NaOH was added to the solution, yielding PF·H_2O as a crystalline powder, which was filtered and washed several times with water. The experimental X-ray powder pattern of the product matched the one calculated on the basis of single crystal data for PROFLV (Fig. S1†). A sample of the polycrystalline PF·H_2O was analyzed *via* hot stage microscopy (HSM), using a Linkam TMS94 device connected to a Linkam LTS350 platinum plate and an Olympus optical microscope; a heating rate of 10 °C min^{-1} was applied. Crystal growth of the anhydrous proflavine was observed on the original

powder at *ca.* 100 °C, concomitantly with the dehydration process of PF·H_2O. The sample was cooled down to room temperature and the yellow single crystals were structurally characterized and analyzed *via* X-ray diffraction.

Synthesis of the anhydrous PF. The anhydrous phase of PF was obtained by thermal treatment in an oven for 20 min at 85 °C. The product was characterized by X-ray powder diffraction and the pattern was compared with the one calculated from the single crystals of anhydrous PF. The single crystals of anhydrous proflavine were obtained directly upon dehydration of PF·H_2O under the microscope during hot-stage heating to 100 °C.

Solution synthesis of $ZnCl_3(HPF)$ (1) (PF·H_2O : $ZnCl_2$ = 1 : 1). A solution of PF·H_2O (113.62 mg, 0.5 mmol) in HCl 0.1 M (2.5 mL, 0.25 mmol) was added to a solution of $ZnCl_2$ (68.14 mg, 0.5 mmol) in water (1 mL). A crystalline powder was recovered after slow evaporation of the solvent and used for structural characterization.

Solution synthesis of $[HPF]_2[ZnCl_4]\cdot H_2O$ (2) (PF·H_2O : $ZnCl_2$ = 2 : 1). A solution of PF·H_2O (113.62 mg, 0.5 mmol) in HCl 0.1 M (5 mL, 0.5 mmol) was added to a solution of $ZnCl_2$ (34.07 mg, 0.25 mmol) in water (0.5 mL). A crystalline powder was recovered after slow evaporation of the solvent. Single crystals of **2** were recovered and used for the diffraction experiments (see below). Serendipitously, single crystals of $[HPF]Cl\cdot 2H_2O$ were also recovered from one of the crystallization batches and subjected to X-ray diffraction.

Solid-state synthesis of $ZnCl_3(HPF)$ (1). Crystalline **1** was also obtained by kneading a 1 : 1 stoichiometric amount of $[HPF]Cl$ (obtained by reacting the free base of proflavine with HCl 0.1 M and drying in a rotavapor – the purity of the product was checked by solution NMR) and $ZnCl_2$, in the presence of 2–3 drops of acetone, for 1 hour in a Retsch MM200 Mixer Mill, operated at a frequency of 15 Hz, with 5 mL agate jars and 2 balls of 5 mm diameter. The same reaction in a 2 : 1 stoichiometric ratio still yielded compound **1**.

Powder X-ray diffraction. For phase identification purposes, room temperature X-ray powder diffraction (XRPD) patterns were collected on a PANalytical X'Pert PRO automated diffractometer equipped with an X'celerator detector in the 2θ range of 3–40° (step size: 0.011, time/step: 50 s, *V* × *A*: 40 × 40).

For the structural characterization of $ZnCl_3(HPF)$ (**1**) from the powder diffraction data, a room temperature X-ray diffraction pattern was collected in transmission geometry on a PANalytical X'Pert PRO automated diffractometer, equipped with a focusing mirror and pixel detector, in the 2θ range of 3–60° (step size: 0.0130°, time/step: 118.32 s, *V* × *A*: 40 kV × 40 mA). To improve the quality of the obtained XRPD patterns, 3 repetitions were performed and the scans were merged. The compound was indexed in the triclinic $P\bar{1}$ space group with the auto-indexing module of N-TREOR[19] as implemented in the program EXPO2014.[20] A simulated annealing method was performed with EXPO2014, using one zinc, three chloride ions and one proflavine cation per

Paper

asymmetric unit. Ten runs for the simulated annealing trial were set, and a cooling rate (defined as the ratio T_n/T_{n-1}) of 0.95 was used. A Rietveld refinement (Fig. S6†) was subsequently performed with TOPAS 5.0,[21] treating the proflavine molecule as a rigid body. Structural details are listed in Table S1.†

Single crystal X-ray diffraction. Single crystal data for **2** as well as for PF and for [HPF]Cl·2H$_2$O were collected at room temperature with an Oxford Diffraction X'Calibur diffractometer equipped with a graphite monochromator and a CCD detector. Mo-Kα radiation (λ = 0.71073 Å) was used. The unit cell parameters for both complexes discussed herein are reported in Table S1.† The structure was solved by the intrinsic phasing methods and refined by least squares methods against F^2 using SHELXT-2016 (ref. 22) and SHELXL-2018 (ref. 23) with the Olex2 interface.[24] Non-hydrogen atoms were refined anisotropically. H$_{CH}$ atoms were added in calculated positions; H$_{OH}$ and H$_{NH}$ atoms were either located from a Fourier map or added in calculated positions and refined riding on their respective carbon, nitrogen or oxygen atoms. The software Mercury 4.3 (ref. 25) was used for graphical representations and for powder pattern simulations on the basis of single crystal data.

Differential scanning calorimetry (DSC). DSC measurements were performed for PF·H$_2$O, ZnCl$_3$(HPF) (**1**) and [HPF]$_2$[ZnCl$_4$]·H$_2$O (**2**) with a Perkin-Elmer Diamond. The samples (3–5 mg) were placed in sealed aluminium pans, and heating was carried out at 5 °C min^{-1}.

Thermogravimetric analysis (TGA). TGA measurements for PF·H$_2$O, ZnCl$_3$(HPF) (**1**) and [HPF]$_2$[ZnCl$_4$]·H$_2$O (**2**) were performed using a Perkin-Elmer TGA7 in the temperature range of 25–450 °C under a N$_2$ gas flow, at a heating rate of 5 °C min^{-1}.

Antimicrobial activity. Antimicrobial efficacy was assessed similarly to previous work.[10] Inocula from frozen stocks of each of the three bacterium species strains were cultured in test tubes, prepared with 2 mL of Luria-Bertani (LB) and incubated at 37 °C for 16 h. These cultures were then used to inoculate spread plates (for the zone of inhibition and contact killing). LB agar plates were spread inoculated with 100 μL of overnight culture and were then allowed to dry while disks were prepared. Antimicrobial filter disks (Oxoid Basingstoke Hants, UK Lot# 1872714) were inserted into metal salt or crystal solutions/slurries of 25 mg mL^{-1} using sterile tweezers to soak and adsorb materials. The disks were exposed for 1 hour with inversions every 15 min. The disks were then placed on the spread plates and all the plates received a disk of AgNO$_3$ (also prepared from 25 mg mL^{-1}) as the internal control. The plates were incubated overnight at 37 °C prior to photography and measurement of the zone of inhibition by average diameter (mm). The zones of inhibition were ratioed to the zone of the AgNO$_3$ control on each plate to remove plate to plate variances. For contact killing efficacy, a pre-grown spread plate received disks on the surface of the bacteria growth lawn and left for 24 h and then removed to observe clearing of the bacterial growth due to cell lysis (as
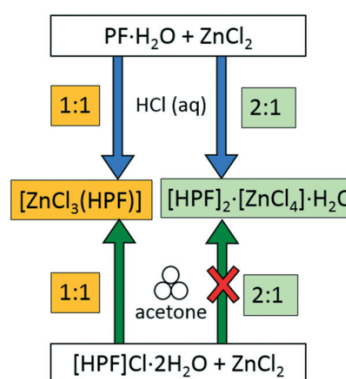

Scheme 2 Different reaction pathways for the synthesis of ZnCl$_3$(HPF) (**1**) and [HPF]$_2$[ZnCl$_4$]·H$_2$O (**2**).

well as swabbing underneath the disk to see if any exposed bacteria could be recovered).

Results and discussion

Proflavine (PF), obtained as a free base from the commercial sulphate salt (see Experimental), was co-crystallized with ZnCl$_2$ both *via* mechanochemistry (in the form of its chloride salt) and from solution in 1:1 and 2:1 stoichiometric ratios (see Scheme 2), yielding the neutral, anhydrous complex ZnCl$_3$(HPF) (**1**) and the hydrated salt [HPF]$_2$[ZnCl$_4$]·H$_2$O (**2**), both containing the proflavinium cation (HPF)$^+$, *i.e.* proflavine in its monoprotonated form (see Scheme 1). Crystallization from solution yielded higher purity target products, which were subsequently utilized for the investigation of the antimicrobial activity. It should be stressed here that the term co-crystallization, in this paper as in other related studies,[10] is used to emphasize that the products are obtained *via* direct mixing of solid compounds that form stable crystalline phases under ambient conditions and that the target of the investigation is the behaviour of the crystalline products in comparison with the crystalline phases of the separate components (*vide infra*).

Single crystals of anhydrous proflavine PF were grown directly from polycrystalline PF·H$_2$O upon dehydration at *ca.* 100 °C. Fig. 1 shows a photograph of the yellow crystals of PF growing from the powder of PF·H$_2$O while undergoing dehydration under the microscope.
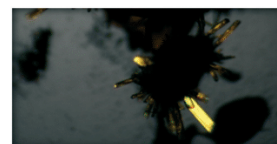
Fig. 1 Yellow crystals of the anhydrous proflavine, obtained directly upon dehydration of PF·H$_2$O under the microscope during hot-stage heating to 100 °C.
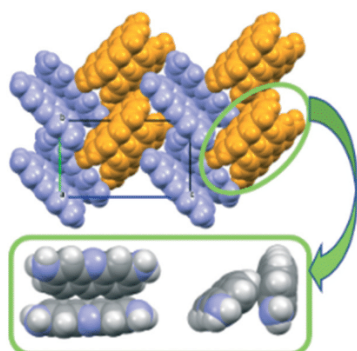
33

Fig. 2 (Top) "double" herringbone pattern in anhydrous PF, and (bottom) front/side views evidencing the C–H···π interactions within a pair of facing molecules.

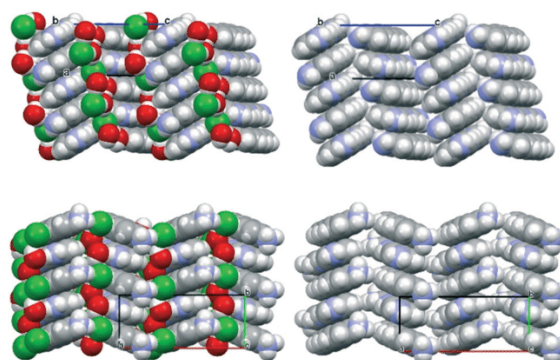**Fig. 4** Comparison of the π-stacking arrangements of aromatic mono- and di-cations in the monochloride [HPF]Cl·2H₂O (top) and dichloride [H₂PF]Cl₂·2H₂O (PROFLC) (bottom) proflavine salts. For the sake of clarity, the cation layers are shown on the right-hand side.

Its structure was determined from the single crystal X-ray diffraction data (see the ESI†) and is characterized by a double herringbone motif shown in Fig. 2, where pairs of PF molecules are stacked along the *b*-axis direction.

This arrangement is reminiscent of the one observed in the crystalline PF·H₂O (PROFLV), but in this last crystal, a simple herringbone pattern is present. In both crystals (see the insets in Fig. 2 and 3), the PF molecules within a pair are facing each other so as to maximize the number of C–H···π interactions.

Single crystals of [HPF]Cl·2H₂O were also recovered from one of the crystallization batches of [HPF]₂[ZnCl₄]·H₂O (**2**) and were subjected to a data collection revealing the unexpected formation of a novel hydrochloride form of PF. It is interesting to note that in this solid, analogously to what is observed for the known dichloride salt [H₂PF]Cl₂·2H₂O (PROFLC), the protonation of the acridine nitrogen and the concomitant presence of good hydrogen bond acceptors – the chloride ion and the water molecule – favor the formation of π–π stacking arrangements of the aromatic units within the crystal, as shown in Fig. 4.

The reaction of proflavine with $ZnCl_2$ in a 1:1 stoichiometric ratio (see Experimental) yields the complex $ZnCl_3(HPF)$ (**1**), which contains the ligand $(HPF)^+$, *i.e.* monoprotonated proflavine. Fig. 5 shows how the $ZnCl_3(HPF)$ molecules are piled along the crystallographic *c*-axis, with short interplanar distances of 3.30(1) and 3.37(1) Å.

Reaction of proflavine with $ZnCl_2$ in a 2:1 stoichiometric ratio (see Experimental) yields the hydrated molecular salt $[HPF]_2ZnCl_4·H_2O$ (**2**), which contains monoprotonated proflavine as a counterion, instead of the coordinated ligand as in compound **1**. Fig. 6 shows how the pairs of proflavinium cations are π-stacked in the crystal, with pairs arranged in a herringbone fashion; interplanar distances are 3.34(1) and 3.41(1) Å (see Fig. 6).

A standard antimicrobial disk-diffusion approach[26] was used to evaluate the relative antimicrobial activity. Both proflavine and zinc are antimicrobial and the question here is if they would retain their antimicrobial activity in a co-crystal. Rather than reporting the absolute zone of inhibition of growth, the amount of inhibition was ratioed in comparison to $AgNO_3$ (Fig. 7). Silver is the most established metal-based antimicrobial[27] and thus is an excellent comparator to evaluate new formulations. Under the medium conditions used here, $AgNO_3$ gives a minimal inhibitory concentration value of 0.125 mM towards all three bacterial
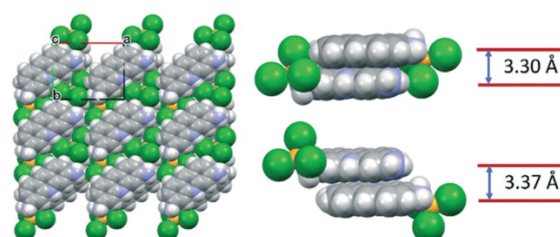

Fig. 3 (Top) herringbone pattern of the proflavine molecules in the monohydrated free base PF·H₂O (PROFLV) (water molecules are not shown for clarity), and (bottom) front/side views evidencing the C–H···π interactions, analogously to what is observed in the crystalline PF.

3.30 Å

3.37 Å

Fig. 5 (Left) projection in the *ab*-plane of the crystalline ZnCl₃(HPF) (**1**). The molecules are arranged in piles along the *c*-axis direction, with short interplanar distances between the aromatic moieties (right).
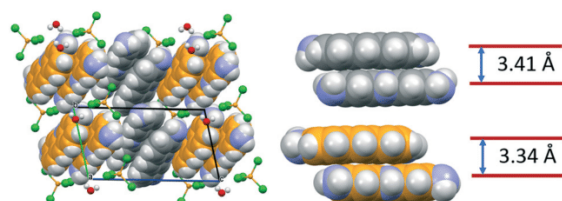
34

Fig. 6 Projection down the crystallographic b-axis of the crystalline $[HPF]_2[ZnCl_4]\cdot H_2O$ (**2**), showing the herringbone pattern of the HPF$^+$ cationic pairs (left) and the π-stacking arrangement of the cations within each pair (right; compared with crystalline **1** in Fig. 5) (grey and orange spheres represent the carbon atoms belonging to the two independent molecules).

strains used here.[28] We see that $ZnCl_2$ has a similar efficacy to AgNO$_3$ towards *P. aeruginosa*, but slightly better efficacy towards *E. coli* and best for *S. aureus*. Proflavine is a planar molecule that effectively intercalates into DNA as its mode of toxicity, making it an effective antimicrobial antiseptic and potential anticancer agent.[29] Proflavine shows a higher antimicrobial activity than silver in our assays. Combining the two compounds shows a 50 to 125% better efficacy than AgNO$_3$ towards all three of the pathogen indicator strains we tested. Additionally, all compounds had contact killing capability against all three strains. This was evaluated by placing the compound impregnated disks onto a lawn of live bacteria and assessing the ability to kill the bacteria in contact. These data demonstrate that the mixture as a crystal did not decrease the biocidal activity of the compounds and potentially enhances them, which was unexpected and somewhat remarkable. Given that the crystal mixtures by weight would actually have less proflavine by moles, the data imply that the presence of Zn enhances the antimicrobial efficacy of proflavine more than what one interprets from Fig. 7.
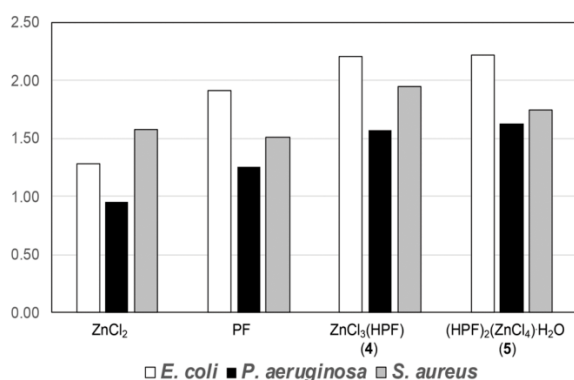

Fig. 7 Fold antimicrobial activity in comparison to AgNO$_3$ (the value of 1.00 is equal to the efficacy of silver nitrate). Data from the 3 independent biological trials (2 technical trials each) are given; variance between the trials was removed through ratioing to a control on each plate (silver nitrate) which leads to negligible differences in fold activity.

Conclusions

The increasing concern in the development of antimicrobial resistance is motivating the quest for new materials to be used in the battle against pathogens. A promising approach using co-crystallization has been used to synthesise new materials and/or to enhance the properties of active molecules. With this idea in mind, we have prepared by both solution and solid-state methods and structurally characterized two novel compounds of the antibacterial proflavine with $ZnCl_2$, namely $ZnCl_3(HPF)$ (**1**) and $[HPF]_2[ZnCl_4]\cdot H_2O$ (**2**). Interestingly, **1** can be obtained mechanochemically as the unique product starting from $[HPF]Cl\cdot 2H_2O$ while reaction in solution of $PF\cdot H_2O$ and $ZnCl_2$ yields **1** or **2** depending on whether a 1:1 or 2:1 stoichiometric ratio of the reactants is used. The fact that mechanochemical and solution synthesis may yield different products is not surprising[30] and has been observed in several cases. In terms of antimicrobial activity, the two compounds appear to be 1.5 to 2 times more efficient towards the pathogen indicator strains with respect to the reagents and towards AgNO$_3$ used as a standard of metal antimicrobial activity. We envisage the use of our compounds as coating materials in the prevention of infectious disease transfer or microbial fouling. The challenges that exist are producing a crystal that releases the active ingredients at a level that sustains antimicrobial properties and that is stable to the physical manipulation and use of the material that has been coated. This opens avenues for the development of unique metal chelates and organo-metal compounds for AMB applications.

Conflicts of interest

There are no conflicts to declare.

Acknowledgements

Notes and references

1 S. B. Levy and M. Bonnie, *Nat. Med.*, 2004, **10**, S122–S129.

2 E. D. Brown and G. D. Wright, *Nature*, 2016, **529**, 336–343.

3 L. M. Streicher, *J. Glob. Antimicrob. Resist.*, 2021, **24**, 285–295.

4 G. R. Desiraju, *Angew. Chem., Int. Ed.*, 2007, **46**, 8342–8356.

5 Ö. Almarsson and M. J. Zaworotko, *Chem. Commun.*, 2004, 1889–1896.

6 J. Wouters and L. Quéré, *Pharmaceutical salts and co-crystals*, Royal Society of Chemistry, 2011.

7 N. Schultheiss and A. Newman, *Cryst. Growth Des.*, 2009, **9**, 2950–2967.

35

CrystEngComm   **Paper**

8 M. Wainwright, *J. Antimicrob. Chemother.*, 2001, **47**, 1–13.

9 M. C. Sulavik, C. Houseweart, C. Cramer, N. Jiwani, N. Murgolo, J. Greene, B. Didomenico, K. J. Shaw, G. H. Miller, R. Hare and G. Shimer, *Antimicrob. Agents Chemother.*, 2001, **45**, 1126–1136.

10 O. Shemchuk, D. Braga, F. Grepioni and R. J. Turner, *RSC Adv.*, 2020, **10**, 2146–2149.

11 O. Shemchuk, S. D'Agostino, C. Fiore, V. Sambri, S. Zannoli, F. Grepioni and D. Braga, *Cryst. Growth Des.*, 2020, **20**, 6796–6803.

12 S. P. Gopi, S. Ganguly and G. R. Desiraju, *Mol. Pharmaceutics*, 2016, **13**, 3590–3594.

13 R. J. Turner, *Microb. Biotechnol.*, 2017, **10**, 1062–1065.

14 J. A. Lemire, J. J. Harrison and R. J. Turner, *Nat. Rev. Microbiol.*, 2013, **11**, 371–384.

15 J. W. Alexander, History of the medical use of silver, *Surg. Infect.*, 2009, **10**, 289–292.

16 A. S. Abd-El-Aziz, C. Agatemor and N. Etkin, *Biomaterials*, 2017, **118**, 27–50.

17 A. Achari and S. Neidle, *Acta Crystallogr., Sect. B: Struct. Crystallogr. Cryst. Chem.*, 1976, **32**, 2537–2539.

18 S. K. Obendorf, H. L. Carrell and J. P. Glusker, *Acta Crystallogr., Sect. B: Struct. Crystallogr. Cryst. Chem.*, 1974, **30**, 1408–1411.

19 A. Altomare, C. Giacovazzo, A. Guagliardi, A. G. G. Moliterni, R. Rizzi and P. E. Werner, *J. Appl. Crystallogr.*, 2000, **33**, 1180–1186.

20 A. Altomare, C. Cuocci, C. Giacovazzo, A. Moliterni, R. Rizzi, N. Corriero and A. Falcicchio, *J. Appl. Crystallogr.*, 2013, **46**, 1231–1235.

21 A. A. Coelho, *J. Appl. Crystallogr.*, 2018, **51**, 210–218.

22 G. M. Sheldrick, *Acta Crystallogr., Sect. A: Found. Adv.*, 2015, **71**, 3–8.

23 G. M. Sheldrick, *Acta Crystallogr., Sect. C: Struct. Chem.*, 2015, **71**, 3–8.

24 O. V. Dolomanov, L. J. Bourhis, R. J. Gildea, J. A. K. Howard and H. Puschmann, *J. Appl. Crystallogr.*, 2009, **42**, 339–341.

25 C. F. MacRae, I. Sovago, S. J. Cottrell, P. T. A. Galek, P. McCabe, E. Pidcock, M. Platings, G. P. Shields, J. S. Stevens, M. Towler and P. A. Wood, *J. Appl. Crystallogr.*, 2020, **53**, 226–235.

26 M. Balouiri, M. Sadiki and S. K. Ibnsouda, *J. Pharm. Anal.*, 2016, **6**, 71–79.

27 J. S. Möhler, W. Sim, M. A. T. Blaskovich, M. A. Cooper and Z. M. Ziora, *Biotechnol. Adv.*, 2018, **36**, 1391–1411.

28 A. Pormohammad and R. J. Turner, *Antibiotics*, 2020, **9**, 853.

29 V. M. Hridya, J. T. Hynes and A. Mukherjee, *J. Phys. Chem. B*, 2019, **123**, 10904–10914.

30 S. L. James, C. J. Adams, C. Bolm, D. Braga, P. Collier, T. Friščić, F. Grepioni, K. D. M. Harris, G. Hyett, W. Jones, A. Krebs, J. Mack, L. Maini, A. G. Orpen, I. P. Parkin, W. C. Shearouse, J. W. Steed and D. C. Waddell, *Chem. Soc. Rev.*, 2012, **41**, 413–447.

36

2.1.1 Supporting information

Proflavine and zinc chloride "team chemistry": Combining antibacterial agents via solid-state interaction
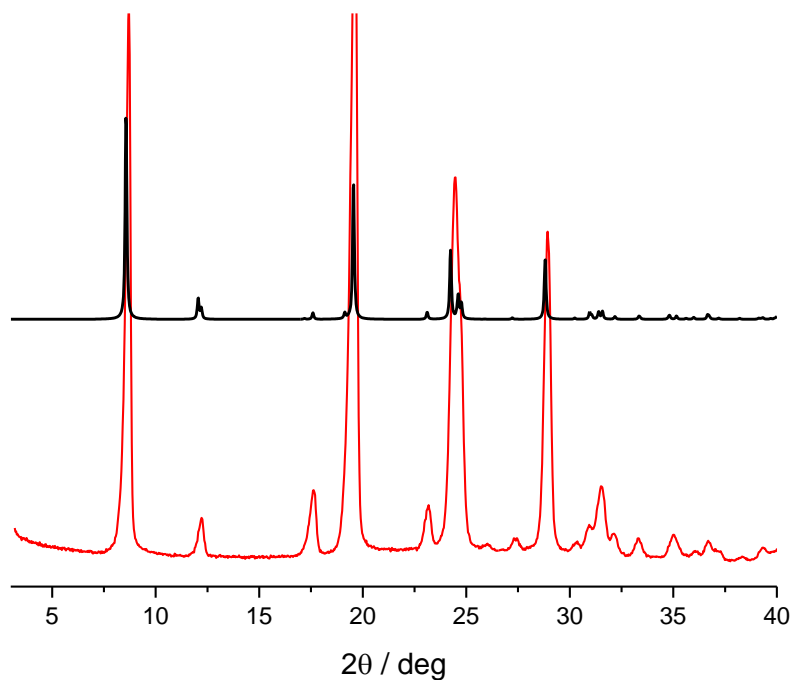
Cecilia Fiore, [a] Oleksii Shemchuk,[a] Dario Braga*,[a] Fabrizia Grepioni,[a] and Raymond J. Turner*[b]

[a] Dipartimento di Chimica "Giacomo Ciamician", Università di Bologna, Via Selmi, 2 – 40126 Bologna – Italy.

[b] Department of Biological Sciences, University of Calgary, 2500 University Drive NW, Calgary, Alberta T2N 1N4, Canada.

X-RAY POWDER DIFFRACTION PATTERNS

Figure SI-1. Comparison between the experimental XRPD pattern for PF·H$_2$O (red line) and the pattern calculated on the basis of single crystal data from the CSD (PROFLV) (black line).
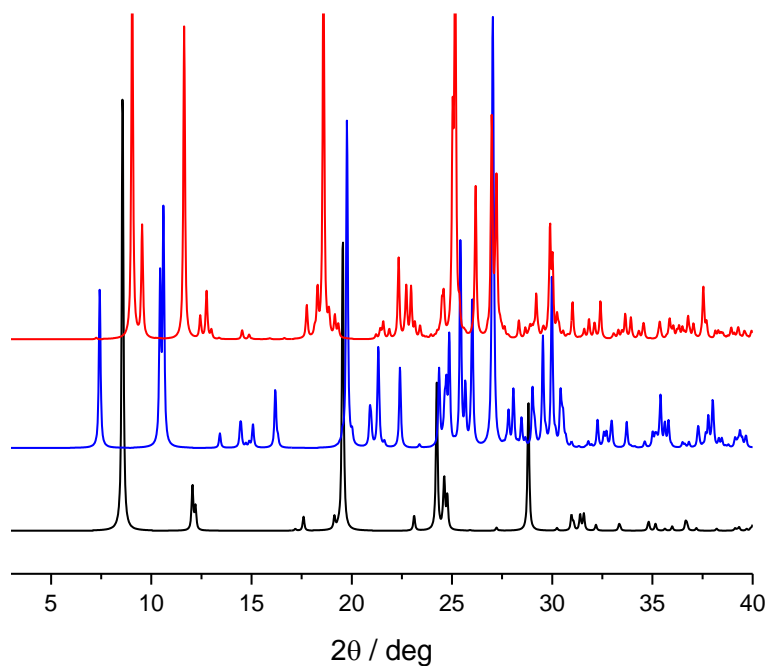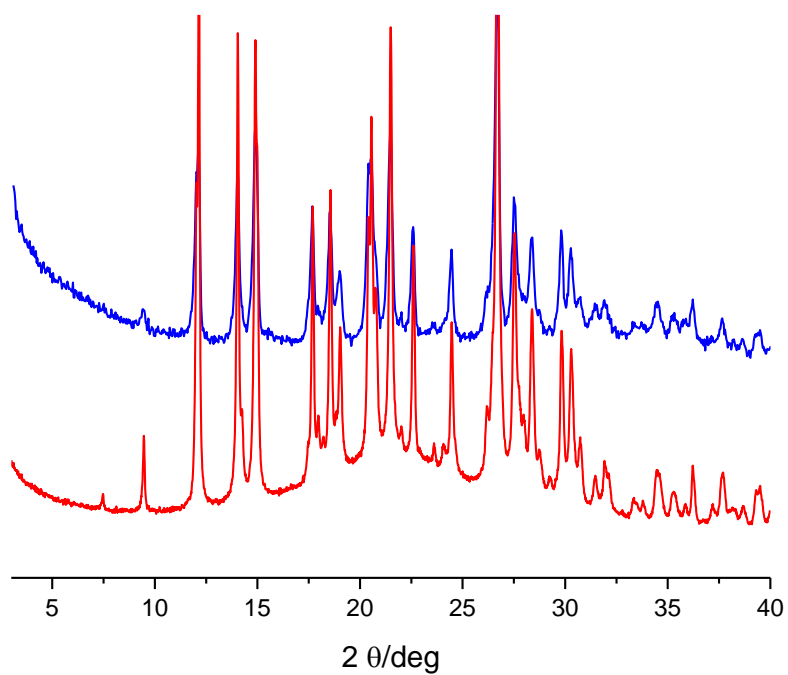

Figure SI-2. Comparison between the experimental pattern for [HPF]Cl·2H$_2$O (red line) and the patterns calculated on the basis of single crystal data for [H$_2$PF]Cl$_2$·2H$_2$O (PROFLC) (blue line) and PF·H$_2$O (PROFLV) (black line) as a reference.
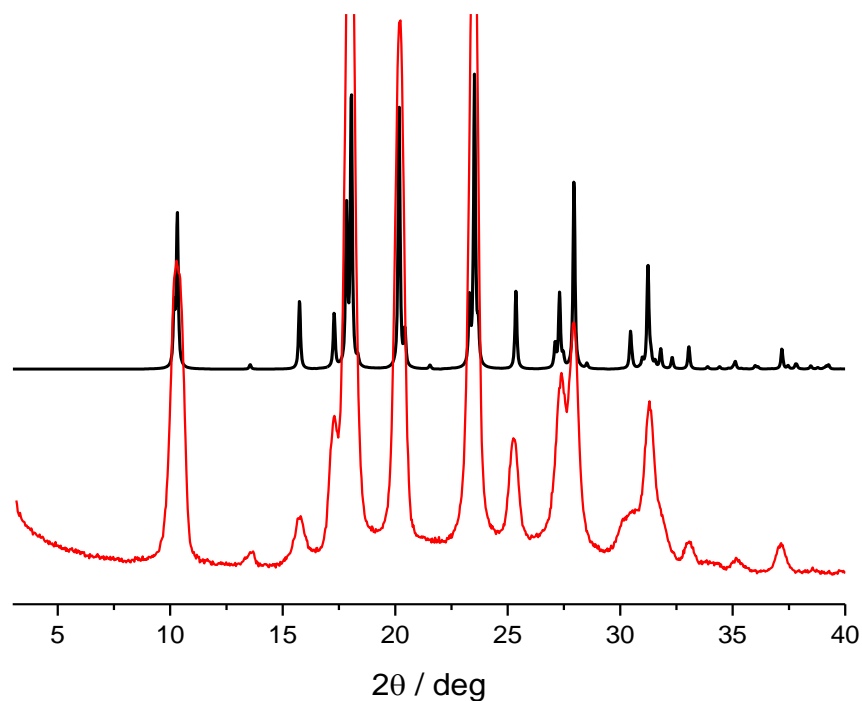
Figure SI-3. Comparison between calculated (black line) and experimental (red line) patterns for anhydrous PF.
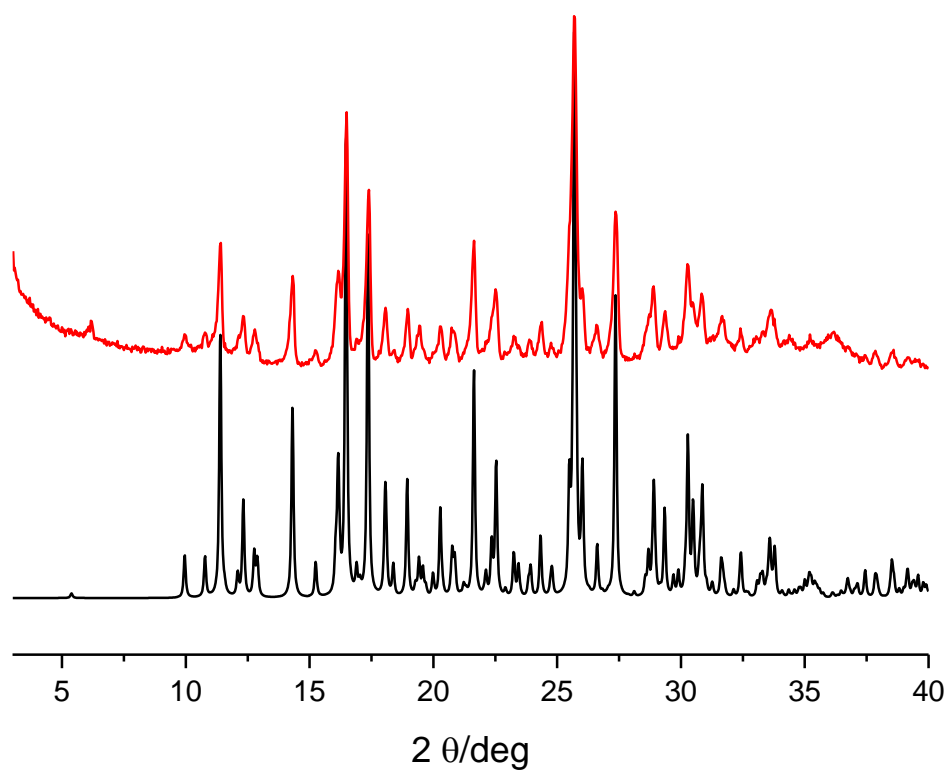
Figure SI-4. Comparison between the calculated pattern for $[HPF]_2[ZnCl_4]\cdot H_2O$ **(2)** (black line) and the experimental XRPD pattern of $[HPF]_2[ZnCl_4]\cdot H_2O$ as obtained from solution (red line).

Figure SI-5. Comparison between the experimental XRPD pattern of ZnCl$_3$(HPF) **(1)** obtained from solution (red line) and the XRPD pattern of ZnCl$_3$(HPF) obtained from ball milling (blue line).
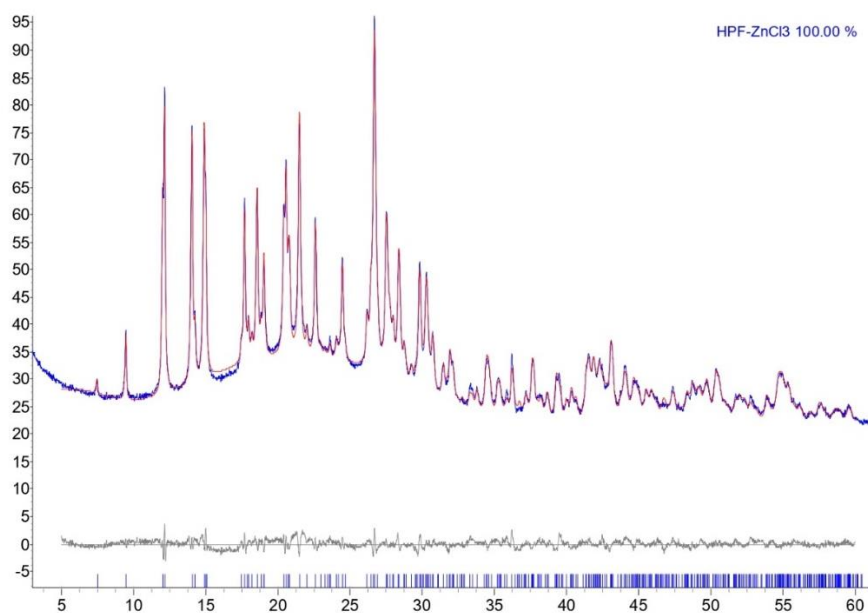
Figure SI-6. Rietveld analysis plot of ZnCl$_3$(HPF) **(1)**: In red the calculated pattern, in blue the experimental one, and in grey the difference plot.

CRYSTALLOGRAPHIC DATA

Table ESI-1. Crystal data and details of measurements (T = 298 K) for PF anhydrous, [HPF]Cl·2H₂O, ZnCl₃(HPF) (**1**) and [HPF]₂·[ZnCl₄]·H₂O (**2**).

	PF anhydrous	[HPF]Cl·2H₂O	ZnCl₃(HPF) (1)[a]	[HPF]₂·[ZnCl₄]·H₂O (2)
Chemical formula	$C_{13}H_{11}N_3$	$(C_{13}H_{12}N_3^+)$, Cl^-, $2H_2O$	$ZnCl_3(C_{13}H_{12}N_3^+)$	$2(C_{13}H_{12}N_3^+)$, $(ZnCl_4^{2-})$, H_2O
M_r /g mol⁻¹	209.25	281.74	382.00	603.71
Crystal system	Orthorhombic	Triclinic	Triclinic	Triclinic
Space group	$P2_12_12_1$	P-1	P-1	P-1
a / Å	5.9524 (6)	7.5170 (5)	12.1724 (1)	8.7727 (4)
b / Å	10.0773 (9)	12.5737 (10)	9.6326 (3)	10.1439 (5)
c / Å	17.1337 (14)	15.5867 (10)	6.7045 (1)	16.8688 (9)
α / °	90	89.941 (6)	104.8578 (3)	100.796 (4)
β / °	90	77.478 (5)	104.4355 (1)	93.143 (4)
γ / °	90	75.976 (6)	85.7581 (1)	112.422 (4)
V / Å³	1027.75 (16)	1393.23 (18)	735.81 (3)	1349.85 (12)
Z, Z'	4, 1	4, 2	2, 1	2, 1
d / mg cm⁻³	1.352	1.343	-	1.589
μ / mm⁻¹	0.08	0.28	-	1.34
Measd reflns	3178	9921	-	9389
Indep reflns	2005	4882	-	4754
Reflns with $I > 2\sigma(I)$	893	2209	-	3296
R_{int}	0.046	0.046	-	0.037
$R1$ [$F^2 > 2\sigma(F^2)$]	0.071	0.062	-	0.064
$wR(F^2)$	0.223	0.128	-	0.103
R_wp	-	-	0.0389	-
R_p	-	-	0.0308	-
R_exp	-	-	0.0302	-
χ^2	-	-	1.2921	-

Crystal data can be obtained free of charge from the Cambridge Crystallographic Data Centre via https://www.ccdc.cam.ac.uk and have been allocated the accession numbers CCDC 2081498-2081501.
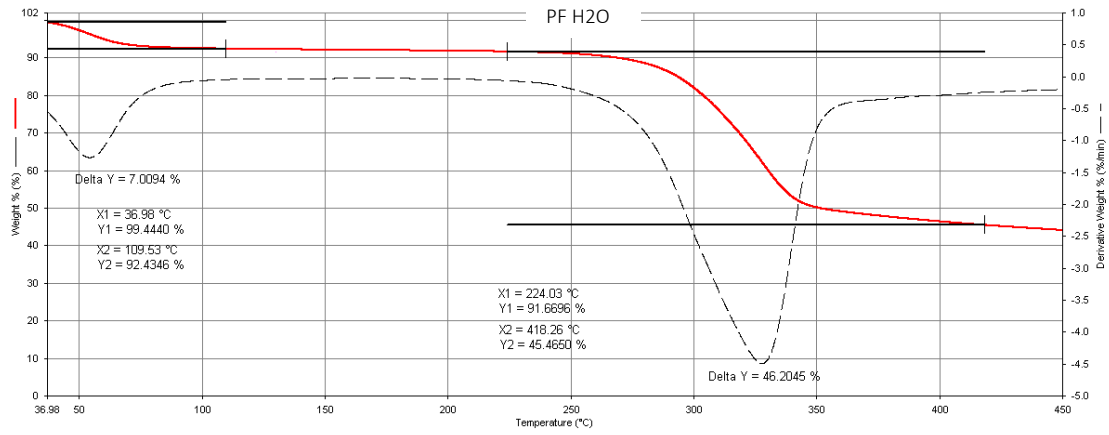
TGA AND DSC DATA

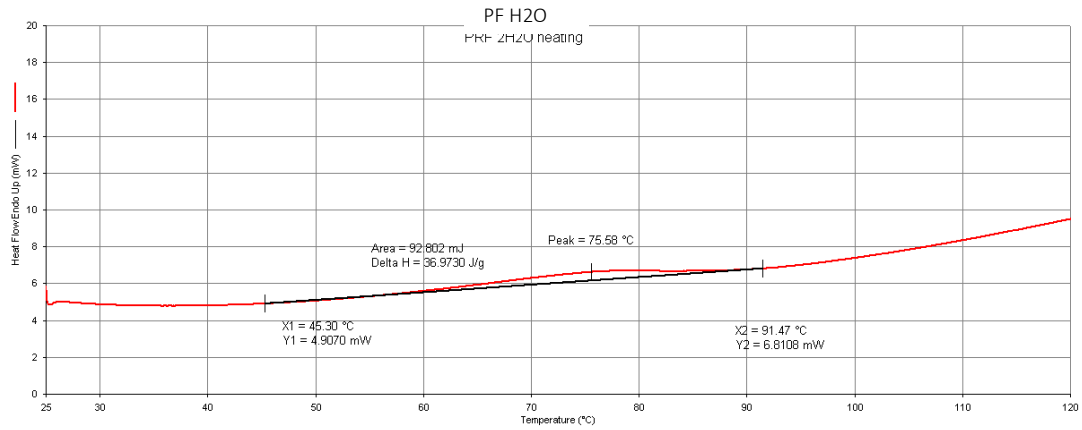**Figure SI-7.** TGA trace for PF·H$_2$O.

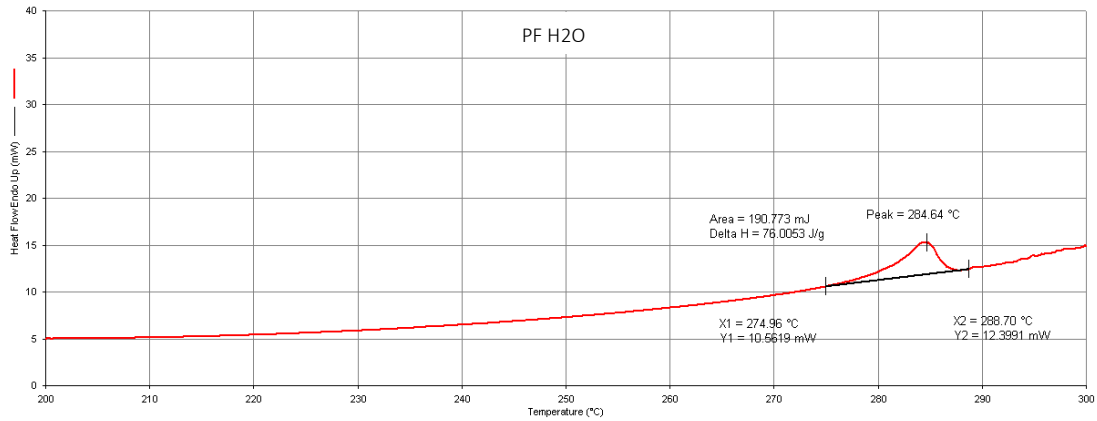**Figure SI-8.** DSC trace for PF·H$_2$O from 25°C to 120°C.

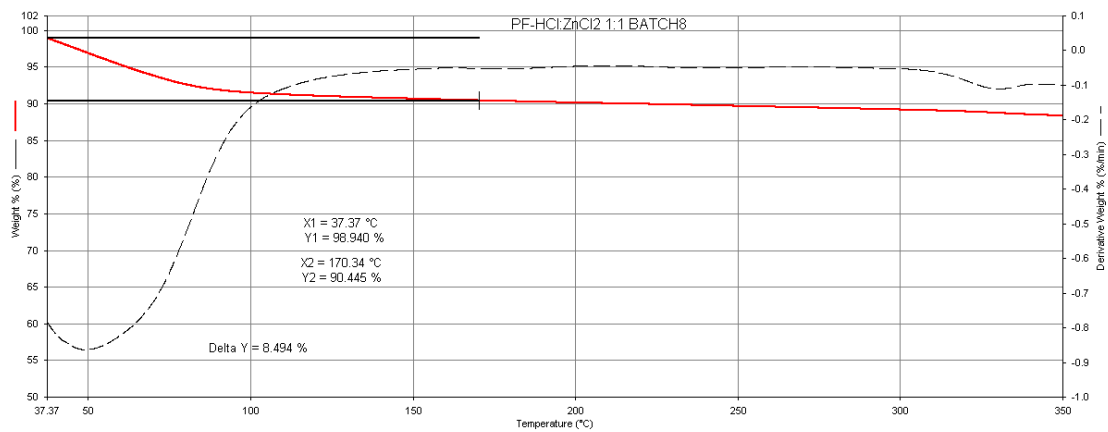**Figure SI-9.** DSC trace for PF·H$_2$O from 200°C to 300°C.

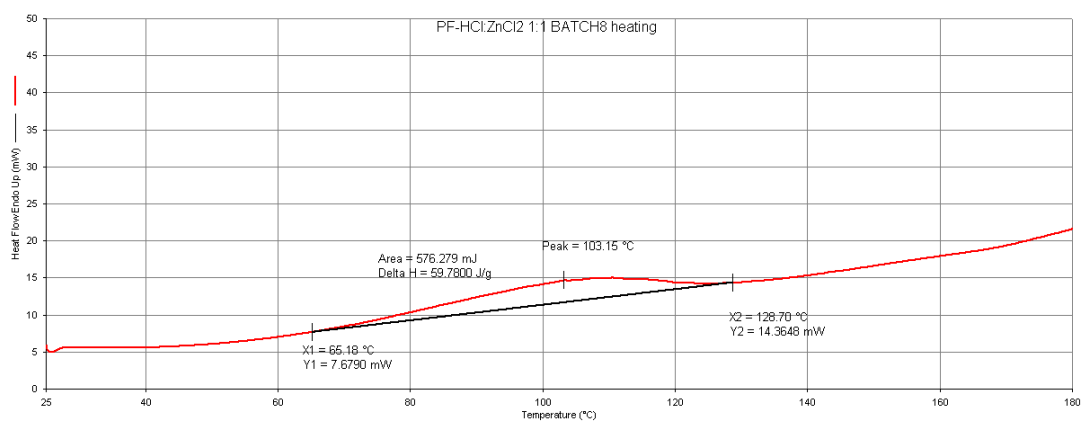**Figure SI-10.** TGA trace for $ZnCl_3(HPF)$ (**1**).
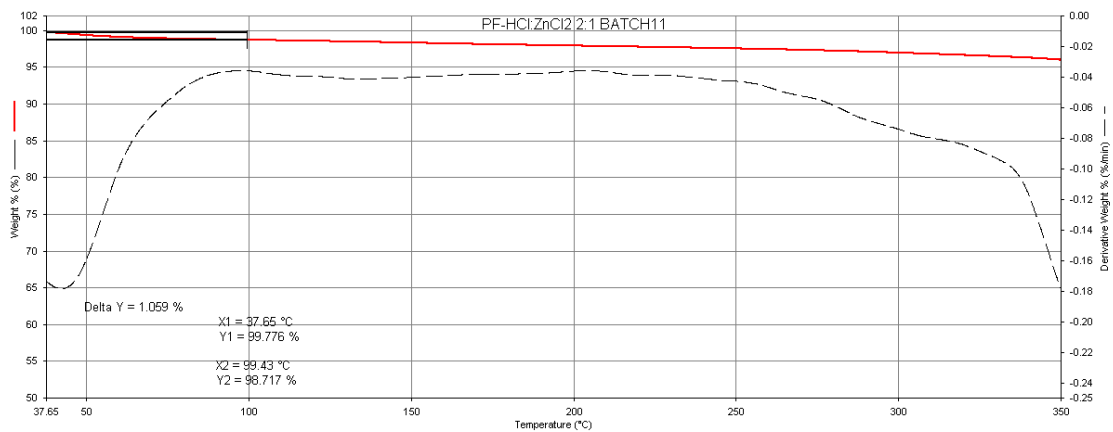

Figure SI-11. DSC trace for $ZnCl_3(HPF)$ (**1**).

Figure SI-12. TGA trace for $[HPF]_2[ZnCl_4] \cdot H_2O$ (**2**).
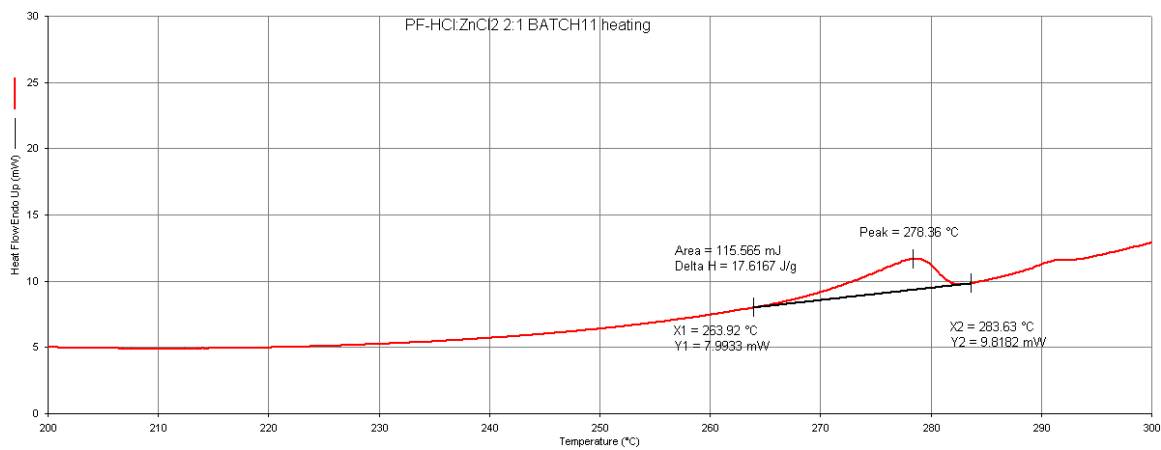
Figure SI-13. DSC trace for [HPF]$_2$[ZnCl$_4$]·H$_2$O (**2**).

2.2 Comparison of Antimicrobial and Antibiofilm Activity of Proflavine Co-crystallized with Silver, Copper, Zinc, and Gallium Salts

Abstract

Here, we exploit our mechanochemical synthesis for co-crystallization of an organic antiseptic, proflavine, with metal-based antimicrobials (silver, copper, zinc, and gallium). Our previous studies have looked for general antimicrobial activity for the co-crystals: proflavine·AgNO$_3$, proflavine·CuCl, ZnCl$_3$[Proflavinium], [Proflavinium]$_2$[ZnCl$_4$]·H$_2$O, and [Proflavinium]$_3$[Ga(oxalate)$_3$]·4H$_2$O. Here, we explore and compare more precisely the bacteriostatic (minimal inhibitory concentrations) and antibiofilm (prevention of cell attachment and propagation) activities of the co-crystals. For this, we choose three prominent "ESKAPE" bacterial pathogens of Pseudomonas aeruginosa, Escherichia coli, and Staphylococcus aureus. The antimicrobial behavior of the co-crystals was compared to that of the separate components of the polycrystalline samples to ascertain whether the proflavine–metal complex association in the solid state provided effective antimicrobial performance. We were particularly interested to see if the co-crystals were effective in preventing bacteria from initiating and propagating the biofilm mode of growth, as this growth form provides high antimicrobial resistance properties. We found that for the planktonic lifestyle of growth of the three bacterial strains, different co-crystal formulations gave selectivity for best performance. For the biofilm state of growth, we see that the silver proflavine co-crystal has the best overall antibiofilm activity against all three organisms. However, other proflavine–metal co-crystals also show practical antimicrobial efficacy against E. coli and S. aureus. While not all proflavine–metal co-crystals demonstrated enhanced antimicrobial efficacy over their constituents alone, all possessed acceptable antimicrobial properties while trapped in

the co-crystal form. We also demonstrate that the metal−proflavine crystals retain

antimicrobial activity in storage. This work defines that co-crystallization of metal

compounds and organic antimicrobials has a potential role in the quest for

antimicrobials/antiseptics in the defence against bacteria in our antimicrobial resistance

era.

Comparison of Antimicrobial and Antibiofilm Activity of Proflavine Co-crystallized with Silver, Copper, Zinc, and Gallium Salts

Andrii Lekhan, Cecilia Fiore, Oleksii Shemchuk, Fabrizia Grepioni, Dario Braga,* and Raymond J. Turner*

Read Online

ACCESS | Metrics & More | Article Recommendations | Supporting Information

ABSTRACT: Here, we exploit our mechanochemical synthesis for co-crystallization of an organic antiseptic, proflavine, with metal-based antimicrobials (silver, copper, zinc, and gallium). Our previous studies have looked for general antimicrobial activity for the co-crystals: proflavine·AgNO$_3$, proflavine·CuCl, ZnCl$_3$[Proflavinium], [Proflavinium]$_2$[ZnCl$_4$]·H$_2$O, and [Proflavinium]$_3$[Ga(oxalate)$_3$]·4H$_2$O. Here, we explore and compare more precisely the bacteriostatic (minimal inhibitory concentrations) and antibiofilm (prevention of cell attachment and propagation) activities of the co-crystals. For this, we choose three prominent "ESKAPE" bacterial pathogens of *Pseudomonas aeruginosa*, *Escherichia coli*, and *Staphylococcus aureus*. The antimicrobial behavior of the co-crystals was compared to that of the separate components of the polycrystalline samples to ascertain whether the proflavine−metal complex association in the solid state provided effective antimicrobial performance. We were particularly interested to see if the co-crystals were effective in preventing bacteria from initiating and propagating the biofilm mode of growth, as this growth form provides high antimicrobial resistance properties. We found that for the planktonic lifestyle of growth of the three bacterial strains, different co-crystal formulations gave selectivity for best performance. For the biofilm state of growth, we see that the silver proflavine co-crystal has the best overall antibiofilm activity against all three organisms. However, other proflavine−metal co-crystals also show practical antimicrobial efficacy against *E. coli* and *S. aureus*. While not all proflavine−metal co-crystals demonstrated enhanced antimicrobial efficacy over their constituents alone, all possessed acceptable antimicrobial properties while trapped in the co-crystal form. We also demonstrate that the metal−proflavine crystals retain antimicrobial activity in storage. This work defines that co-crystallization of metal compounds and organic antimicrobials has a potential role in the quest for antimicrobials/antiseptics in the defense against bacteria in our antimicrobial resistance era.

KEYWORDS: antimicrobials, quaternary-ammonium compound, silver, copper, gallium, zinc, co-crystallization

■ INTRODUCTION

The current state of the antibiotic resistance crisis puts pressure for more research toward the development of new and novel antimicrobial agents, as we find ourselves in the antimicrobial resistance (AMR) era.[1] The rates at which clinically and agriculturally relevant pathogens are gaining resistance toward treatment with available antimicrobials are outpacing the rates at which new antimicrobials arrive at the market.[1] WHO now considers AMR the hidden pandemic, claiming that we will see 10 million human deaths per year by 2050, which will be greater than those due to cancer. The issues of the emerging crisis of antibiotic resistance and inadequate focus in bacterial susceptibility assessment call for re-evaluation of conventional approaches in antimicrobial development. We also have the issue of the paradigm of antibiotic research and development almost exclusively focusing on the planktonic (free-swimming) form of microbial growth. However, it is now well appreciated that in nature, bacteria predominantly appear in the form of aggregations or surface-attached communities—biofilms.[2] Biofilms are far less susceptible to antibiotics, due to their extracellular matrix of exopolysaccharides, proteins, nucleic acids, and other bio-molecules such as metabolites, which are thought to generate a barrier of penetration from the external environment.[2] Additionally, there are remarkable changes in cellular biochemistry and physiology, compared to the planktonic
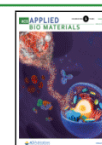
form.[2] Thus, biofilms provide a unique challenge in antimicrobial formulation development.

Among the promising directions to address AMR are metal- and metalloid-based antimicrobials (MBAs).[3] Unlike conventional antibiotics, which tend to demonstrate target-specific biochemical activities, metal ions and their related chemical species are believed to have multiple biochemical targets within the bacterial cell, providing multifactorial modes of action. As recently reviewed in detail,[4] MBAs may cause protein damage by direct redox chemistry of biomolecules and substitution of the essential metals both in active and structural sites of proteins. Some MBAs interfere with nutrient intake, damage the cell membrane, and may lead to electron transport chain (ETC) decoupling. MBAs may bind to nucleic acids leading to differential regulation and/or mutations. Another MBA toxicity factor is the generation of various reactive oxygen species (ROS) that may be catalyzed directly by the metal or indirectly (via ETC decoupling or [Fe−S] disruption), leading to further cellular damage.

Although many metals have antimicrobial activities, those that have shown strong potential and are in use include Ag(I),[5] Cu(II),[6] Zn(II),[7] and Ga(III).[8] Ag(I) and Cu(II) are examples of "soft" acids according to hard−soft acids and bases theory[9] and a major part of their antibacterial activity depends on interactions with "soft" bases (thiols) within the bacterial cell. Cu(II) and Cu(I) ions were shown to interact with thiol groups, such as cysteine side chains and glutathione, interfering with natural thiol biochemistry and depleting their ability to act as antioxidants.[10] Ag(I) and Cu(II) bind and/or oxidize "soft" sulfur atoms and thus cause functional changes in proteins, frequently inactivating them. [Fe−S] clusters are yet another target,[11,12] and destruction of [Fe−S] clusters by replacing the Fe with the antimicrobial metal leads, first, to the respective protein malfunction and, second, to the release of highly Fenton-active Fe(II) ions leading to oxidative damage by means of ROS production. As such, exposure to excessive amounts of Ag(I) and Cu(II) leads directly to the impairment of [Fe−S] reactions in the ETC and indirectly to ROS generation due to increased Fe activity. Zn(II) has been shown to interfere with essential metal uptake, specifically Mn.[13] Ag(I) is known to disrupt bacterial cell wall continuity in as yet undefined mechanism.[14] Cu(II) can also interfere with bacterial cell wall biosynthesis by inhibiting LD-transpeptidase.[15] Ag(I) has also been shown to inhibit urease through restricting key conformational changes.[16] Antimicrobial activity of the Ga(III) ion is based on its chemical similarity to Fe(III). Ga(III) competes for Fe(III) transport systems, thus depleting the bacterial Fe(III) supply. Ga(III) may also be incorporated in metalloproteins instead of Fe(III); however, unlike Fe(III), Ga(III) is not redox-active under physiological conditions.[17]

Using a combination of antimicrobials that affect a cell very differently is an approach to combat AMR, as it reduces the rate of resistance. The probability that mutations will occur in a single cell within two different genes at the same time to provide resistance to both antimicrobials is astronomically low. An additional advantage of the combinatorial approach of any two different antimicrobials is that one may obtain a greater efficacy than would be expected from summing their effects up and demonstrate synergistic outcomes. Previous work has shown MBAs to have synergistic effects with some quaternary cation compounds (QCCs) used as antiseptics.[18] QCCs are a class of molecules that possess a positively charged quaternary atom, typically nitrogen, and less frequently arsenic or

phosphorus. Amphiphilic members of the group demonstrate antimicrobial activity due to their ability to be incorporated into lipid bilayers and thus impair bacterial membrane functions.[19] Planar QCC molecules can also be intercalated between the nucleic acid bases and thus are genotoxic.

We have begun to use co-crystallization in our exploration to mix metal-based antimicrobials with QCCs. We have chosen proflavine (acridine-3,6-diamine), a notable example of planar QCCs,[20] which has been used as a disinfectant since early in the 20th century and has continued to find use as a topical antimicrobial in 21st century. Its antimicrobial properties are based on three principles: (i) photosensitizing the intercalated region of DNA and causing frameshift mutations, (ii) inhibition of DNA and RNA polymerases, thus interfering with DNA replication and transcription, and (iii) affecting cell membrane fluidity. The molecular diagrams of proflavine (PF) and of its monoprotonated proflavinium cation (HPF$^+$) are shown in Scheme 1. The character of this QCC provided a foundational compound for co-crystallization with metals for proof of principle work.

Scheme 1. Neutral PF and Its Monoprotonated Proflavinium Cation (HPF$^+$)

Proflavine (PF)   Proflavinium cation (HPF$^+$)
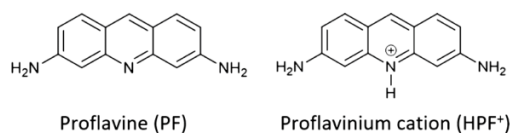
There are several strategies that aim to mix organics with metals to provide novel superior antimicrobial, anti-cancer, and anti-fungal drugs and those for other purposes. Crystal engineering, that is, the design, preparation, and characterization of multi-component systems based on supramolecular interactions,[21] is now being actively exploited also to tackle the problem of AMR. Crystal engineering approaches utilizing metal−organic complexes and coordination networks can enhance the delivery and pharmaceutical properties of both the counterparts.

Examples of metals containing multi-component materials are metal organic frameworks, metal−organic gels, incorporation of antimicrobial metals into nanopolymers, or metal-based coordination polymers. An alternative to these approaches is that of antimicrobial co-crystals, that is, multicomponent solid materials whereby the antimicrobial activity of metal ions could be used together with that of an active organic molecule to enhance the physicochemical and microbiological properties of the constituent compounds. The focus of this approach is not on the properties of the individual components, but rather on collective properties of the extended supramolecular aggregates formed in the solid state via non-covalent interactions such as hydrogen bonds and coordination interactions.[22] There is increasing literature on applications of co-crystallization in the quest for new drugs or as a means to rejuvenate old drugs.[23,24] However, in most cases, the focus of studies is on the changes in the physical properties of the crystalline phase of the active ingredient (solubility, dissolution rate, thermal stability, etc.) imparted by the association with an ancillary component and not on the mechanism of action. We and others have concentrated our efforts on exploring if the roles of the organic/inorganic constituents may be enabling, enhancing, or inhibiting the

respective antimicrobial activities. This is the case of metal salts of Lauric acid[25] or a metabolite such as urea,[26] or that of enhancing the activity of an organic antiseptic.[27−29]

In this study, we aim to quantify and compare the antimicrobial properties of earlier reported co-crystals and supramolecular complex/salts of PF and MBAs: PF·AgNO$_3$,[27] PF·CuCl,[27] ZnCl$_3$(HPF),[28] [HPF]$_2$[ZnCl$_4$]·H$_2$O,[28] and [HPF]$_3$[Ga(ox)$_3$]·4H$_2$O.[29] Characteristic antimicrobial concentrations of these crystals and their constituents were established for inhibition of planktonic growth (minimum inhibitory concentration, MIC) and biofilm growth (minimum biofilm inhibitory concentration, MBIC) for three WHO priority list pathogens.[30] The Gram-negative bacteria *Pseudomonas aeruginosa* and *Escherichia coli* are listed as critical priority pathogens and the Gram-positive *Staphylococcus aureus* as high priority; all three are part of the concerning ESKAPE list of pathogens.

■ METHODS

Crystal Preparation. The compounds investigated in this study, namely, PF·AgNO$_3$,[27] PF·CuCl,[27] ZnCl$_3$(HPF),[28] [HPF]$_2$[ZnCl$_4$]· H$_2$O,[28] and [HPF]$_3$[Ga(ox)$_3$]·4H$_2$O,[29] have all been prepared and fully characterized by solid state methods, as summarized in Table 1.

Table 1. Crystalline Materials Investigated in This Work

crystalline material	synthetic method
PF·CuCl	slurry/grinding[27]
PF·AgNO$_3$	slurry/grinding[27]
ZnCl$_3$(HPF)	slurry/grinding[28]
[HPF]$_2$[ZnCl$_4$]·H$_2$O	slurry/grinding/solution[28]
[HPF]$_3$[Ga(ox)$_3$]·4H$_2$O	slurry/grinding/solution[29]

PF has been used in the co-crystallization processes either as neutral PF·H$_2$O or as its hydrochloride salt [HPF]Cl$_2$·H$_2$O. All compounds discussed herein were prepared by mechanochemical (grinding) or slurry methods, that is, by direct mixing of solid PF·H$_2$O or [HPF]Cl$_2$·H$_2$O with the inorganic salts, CuCl$_2$, AgNO$_3$, ZnCl$_2$, as well as with K$_3$[Ga(ox)$_3$]. This approach yielded, in most cases, higher purity target products with respect to conventional crystallization from solution. Structural characterization for all materials was conducted via single crystal and/or powder X-ray diffraction.

When single crystal structure information was obtained, correspondence between the structure of the single crystal and that of the bulk polycrystalline material was verified by comparing observed powder patterns to those calculated based on single crystal data. The preparation methods are briefly described below; however, the interested reader is addressed to the original crystal engineering papers (and their supplementary structural material) for more specific details.

Figure 1 shows the structure of the PF copper(I) chloride co-crystal, PF·CuCl. The crystal is formed by a 1-D polymer of CuCl monomers and by the neutral PF molecules arranged in a herring-bone fashion.
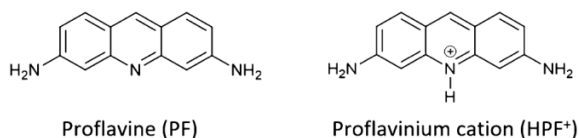

Figure 1. Relevant packing features in crystalline PF·CuCl, showing the herring-bone arrangement of the PF molecules (a) and the 1D (CuCl···CuCl···)$_n$ chains (b); H atoms omitted for clarity.

The reaction of PF and AgNO$_3$, both by slurry and grinding, yielded the anhydrous solid PF·AgNO$_3$.[27] The reaction with ZnCl$_2$ yielded two different products, depending on the preparation method (grinding or slurry) and based on the Zn-PF stoichiometric ratio and on the experimental conditions. The two materials contain the (HPF$^+$) cation and were characterized as the complex ZnCl$_3$(HPF) and the monohydrate supramolecular salt [HPF]$_2$[ZnCl$_4$]·H$_2$O.[28] The structures of the two compounds are compared in Figures 2 and
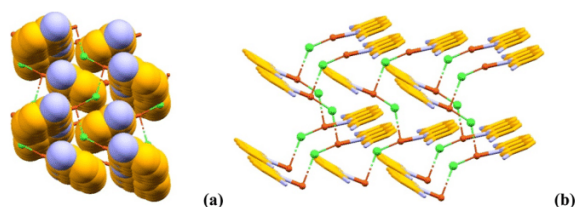

Figure 2. (a) Projection along the *a*-axis of crystalline ZnCl$_3$(HPF), showing the stackings of proflavinium ligands along the *c*-axis direction. (b) Space-filling representation. H atoms omitted for clarity.
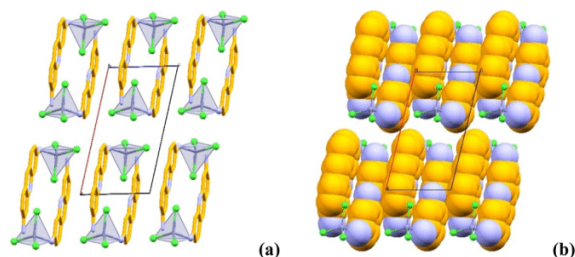
Figure 3. (a) Projection down the crystallographic *b*-axis of crystalline [HPF]$_2$[ZnCl$_4$]·H$_2$O, showing the herring-bone pattern of HPF$^+$ cationic pairs. (b) Space-filling representation. Water oxygens in blue; H atoms omitted for clarity.

3. In both materials, stacking of the proflavinium cations is observed. The same interaction is present in the crystal structures of neutral PF and of the hydrochloride salt [HPF]Cl$_2$·H$_2$O.

Here, our study also comprises the co-crystals obtained by using as a preformed building unit a gallium oxalate complex [Ga(ox)$_3$]$^{3−}$ in order to prepare the tetrahydrate [HPF]$_3$[Ga(ox)$_3$]·4H$_2$O.[29] The structure of [HPF]$_3$[Ga(ox)$_3$]·4H$_2$O is shown in Figure 4. The proflavinium cations envelop the [Ga(ox)$_3$]$^{3−}$ anions forming stackings of PF cations analogous to those observed in the neutral co-crystals discussed above.
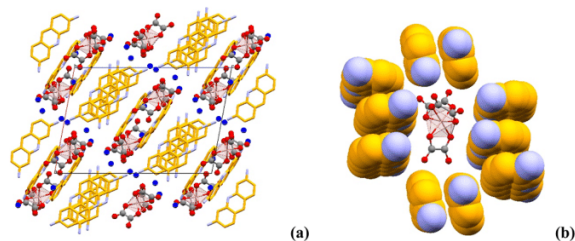
Figure 4. Packing in crystalline [HPF]$_3$[Ga(ox)$_3$]·4H$_2$O viewed along the crystallographic *b*-axis (a). Proflavinium cations envelop around the [Ga(ox)$_3$]$^{3−}$ anion (b). O$_W$ in blue; H atoms omitted for clarity.

49

Antimicrobial Testing; Strains and Growth Medium. *P. aeruginosa* ATCC27853, *S. aureus* ATCC25923, and *E. coli* ATCC25922 pathogen indicator strains were used in this study. Lysogeny broth (LB) was prepared in distilled water with 10 g/L NaCl (VWR International Co., Mississauga, Canada), 5 g/L yeast extract (EMD Chemicals Inc., Darmstadt, Germany), and 10 g/L tryptone (VWR Chemicals LLC, Solon, USA). The pH of the media was not altered by the addition of any of the compounds used in the antimicrobial testing.

Working Stocks. 24 mg/mL stock solutions of metal salts or suspensions/slurries of target co-crystals was prepared. Stocks were prepared freshly and used within 24 h. No experiments were performed to determine the speciation of released metals nor the decomposition of the crystals in the complex microbial media during the time course of the experiment. Crystal violet (CV) (VWR Chemicals LLC, Solon, USA) was prepared with distilled water to 0.1% (w/v) stock for biofilm biomass assessment.

Inoculum. Frozen cultures were revived on LB agar plates overnight at 37 °C, subsequently passaged on fresh LB agar, and incubated overnight again. From the second passage of overnight cultures, several colonies were picked using sterile cotton swab and transferred to saline until the suspension reached McFarland 1.0 turbidity that approximately corresponds to the concentration of colony forming units in the suspension of 3×10^8 CFU/mL. Bacterial suspension then was diluted 30-fold in LB and used as inoculum for minimum effective concentration assays.

Antimicrobial Assays. For all assays, the original metal salt and the PF were assayed as comparator controls. The original studies[27−29] evaluated if the compounds worked additively or not, and as such, experiments of adding the individual components of each co-crystal into solution were not performed here, allowing us to focus on comparing the co-crystals to each other. These earlier studies provided the list of compounds for this study (Table 2). All

Table 2. Antimicrobials under Evaluation

compound	number
AgNO$_3$	**1**
CuCl$_2$	**2**
ZnCl$_2$	**3**
Ga(NO$_3$)$_3$	**4**
K$_3$[Ga(ox)$_3$]·3H$_2$O	**5**
K$_2$[Ga$_2$(ox)$_2$(OH)$_2$]·2H$_2$O	**6**
PF	**7**
PF·AgNO$_3$	**CC-1**
PF·AgNO$_3$ (aged)	**CC-2**
PF·CuCl	**CC-3**
PF·CuCl (aged)	**CC-4**
ZnCl$_3$(HPF)	**CC-5**
[HPF]$_2$[ZnCl$_4$]·H$_2$O	**CC-6**
[HPF]$_3$[Ga(ox)$_3$]·4H$_2$O	**CC-7**

antimicrobial assays were repeated with two to four biological replicates from a fresh bacterial culture inoculated from the ATCC stock. Each biological replicate also had three technical replicates within a given experiment. Variation between trials is observed in standard deviations. If no deviations are indicated, there was no variation between experiments or replicates. AMR data are presented (Figures 5 and 6) as log-2 scale as per the dilution series.

Note that in Table 2, compounds **CC-1** and **CC-2** are the same co-crystal formulation, as well as **CC-3** and **CC-4**. Samples **CC-2** and **CC-3** were synthesized 3 years earlier (March 2019) and used for the preliminary antimicrobial testing by disk diffusion.[27] The samples were stored in the lab at room temperature in the dark in a stoppered vial.

Minimum Inhibitory Concentration. Classical broth dilution assay[31] was used to quantitate the antimicrobial activity serial two-fold dilutions of compounds were prepared in LB broth in a standard

microtiter plate, which thus had 8 sterility control wells (150 μL of medium), 8 growth control wells (135 μL of medium), and 2 replicates of dilution series for different compound (total of 80 wells, 135 μL of medium/compound mixture). Growth and test wells were inoculated with 15 μL of inoculum and incubated for 24 h (*E. coli* and *P. aeruginosa*) or 48 h (*S. aureus*) under 37 °C and 150 rpm shaking. Cultured plates were analyzed visually and by optical density at 600$_{nm}$, and MICs were identified as the concentration of the compound in the first well that has no turbidity increase and/or coloration change, adjacent to the well with such changes present.

Minimal Biocidal Concentration. Ten microliters from each well from the MIC determination plate was either spot-plated to solid media or used to inoculate 150 μL of fresh media and incubated for 36 h at 37 °C. The lack of colony growth on solid media and/or no growth as determined by an OD$_{600}$ measurement was defined as the end point defining the MBC values, that is, MBC gives an impression of bactericidal activity compared to MIC's suggestion of bacteriostatic activity.

Minimum Biofilm Inhibition Concentration. Total biofilm biomaterial was evaluated using the popular method of biomass staining with CV detected with spectrophotometric analysis.[32] The remaining liquid from the initial MIC plates was removed by inverting the plate upside-down and shaking three times. Plates were then rinsed twice by submerging into the distilled water. 170 μL of 0.1% (w/v) CV solution was added into each well and left at room temperature for 10 min. Then the CV solution was removed by inverting the plate with subsequent double rinsing in distilled water by submerging. After rinsing, plates were inverted and tapped on paper towel five times to remove the remaining free dye solution. Plates were then left at room temperature for 2 h for drying. The dye in each well, which would be bound to microbial biofilm biomass, was solubilized by adding 200 μL of acetic acid and mixed pipetting up and down for 5 times. 150 μL of solubilized dye from each well was then transferred to a new microtiter plate, and absorbance was evaluated by a microtiter plate reader. MBICs were identified as the concentration of the compound in the respective well of the initial MIC plate that has no observable coloration increase in the MBIC plate compared to sterility control, adjacent to a well in the MBIC plate that has the same coloration or higher than that of a growth control well. Although the rinsing step removed the co-crystal slurry, a control experiment performed showed no spectroscopic modification of the CV by trace co-crystals.

■ RESULTS

The antimicrobial activity of all compounds is shown for *P. aeruginosa*, *E. coli*, and *S. aureus* together in Figures 5 and 6. The raw data numbers are available in Tables S1 (MIC), S2 (MBC), and S3 (MBIC). Evaluation of the antimicrobial activity saw good reproducibility as seen by the absence of standard deviation error bars for most of the compounds for both MIC and MBIC endpoints of the biological replicants. Note that to read these figures, the smaller bar height reflects superior antimicrobial activity. This is highlighted by compound **1** (AgNO$_3$), which is known for its superior antimicrobial activity and thus also a good comparator to evaluate novel metal-based antimicrobials.

A cursory comparison of the antimicrobial data for the three test bacteria highlights the remarkable difference in efficacy of the same metal ions against these strains. Even the two Gram-negative strains (*P. aeruginosa* and *E. coli*) show striking differences in their susceptibility profiles.

Antimicrobial Efficacy. The MIC is an effective measure of how bacteriostatic an antimicrobial agent is against microbial growth in the free-swimming planktonic state. The MIC data are seen in Figure 5. For these planktonic MIC data, we see some compounds showing poor efficacy (**4**, **5**, **6**), yet have improved efficacy in their co-crystal forms. For a

50
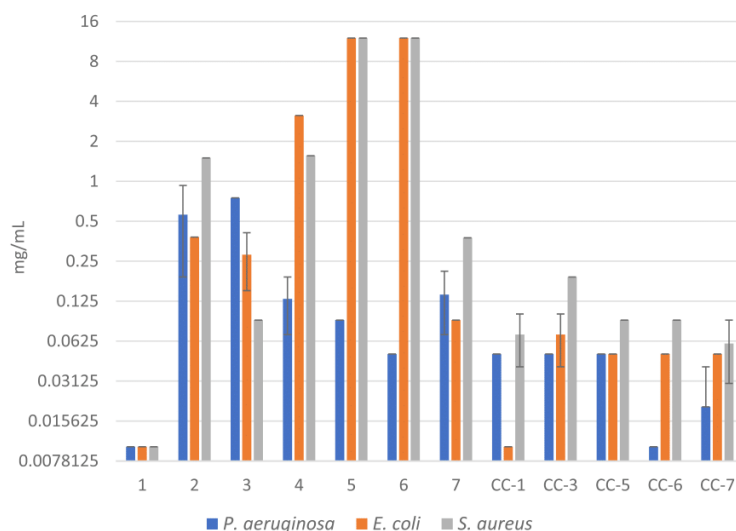
Figure 5. Bacteriostatic MIC efficacy of the metal salt and PF starter compounds and their co-crystallization products. Bars with no visible errors indicate that there was no variation in the values obtained between trials. Note *y*-axis scale is log-2.
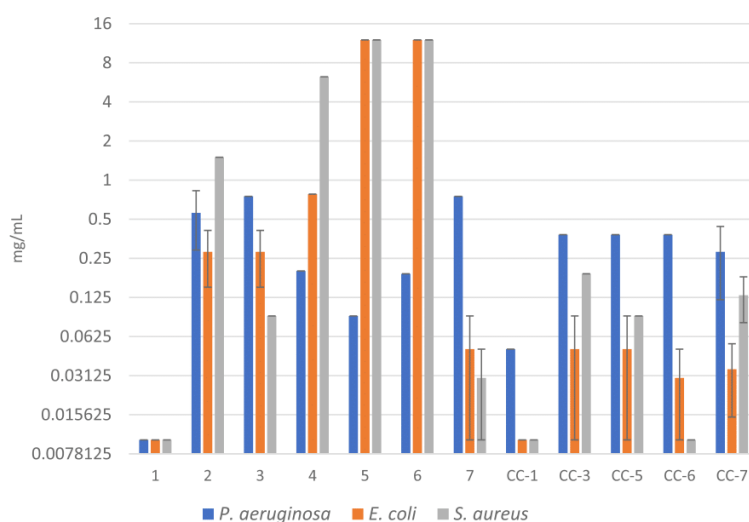
Figure 6. MBIC efficacy of the metal salt and PF starter compounds and their co-crystallization products. These values represent the ability of the compounds to inhibit cell attachment and proliferation of biofilm biomass. Bars with no visible error bars indicate that there was no variation in the values obtained between trials. Note the y-axis scale is log-2.

compound to be considered to have good antimicrobial activity, one generally looks for MIC concentrations below 0.125 mg/mL. Overall, we see that the co-crystals gave MIC values against all three organisms at or below this value, and in many cases, there is greater bactericidal activity than the PF alone (compound **7**). Looking at the data of *P. aeruginosa*, we see the potential of the gallium compounds (**5**, **6**) acting specifically to this strain and for our co-crystallization products **CC-6** and **CC-7** also showing superior performance. $ZnCl_3(HPF)$ (**CC-5**) MIC was at least 2-fold lower than that of PF (**7**) and more than 10-fold lower than that of Zn^{2+} alone (**3**). $[HPF]_2[ZnCl_4]\cdot H_2O$ (**CC-6**) had stronger anti-planktonic properties against this strain—at least 4-fold, compared to PF, and more than 60-fold, compared to Zn^{2+}. The PF·CuCl (**CC-3**) co-crystal had 2-fold and 10-fold

decreased MIC, compared to PF and Cu^{2+} alone, respectively. $[HPF]_3[Ga(ox)_3]\cdot 4H_2O$ (**CC-7**), although presenting a range of MIC values (large error bar), was at least 2 times more effective than $K_3[Ga(ox)_3]\cdot 3H_2O$ (**6**) or PF (**7**) alone.

For *E. coli* and *S. aureus*, we see that all the co-crystallization products provided good bacteriostatic activities being below the 0.125 mg/mL cut off except for **CC-3** against *S. aureus*. Certainly *E. coli* appeared the most susceptible in the planktonic state to the silver co-crystals, with **CC-1** showing the lowest MIC values, and as such, the highest efficacy. Although not as impressive, both **CC-1** and **CC-7** would be quite effective to control growth of *S. aureus*.

Bactericidal activity as the minimal biocidal concentration (MBC) at 100% kill was determined (Table S2). Biocidal assay reflects the lack of ability of a microbe to recover and grow
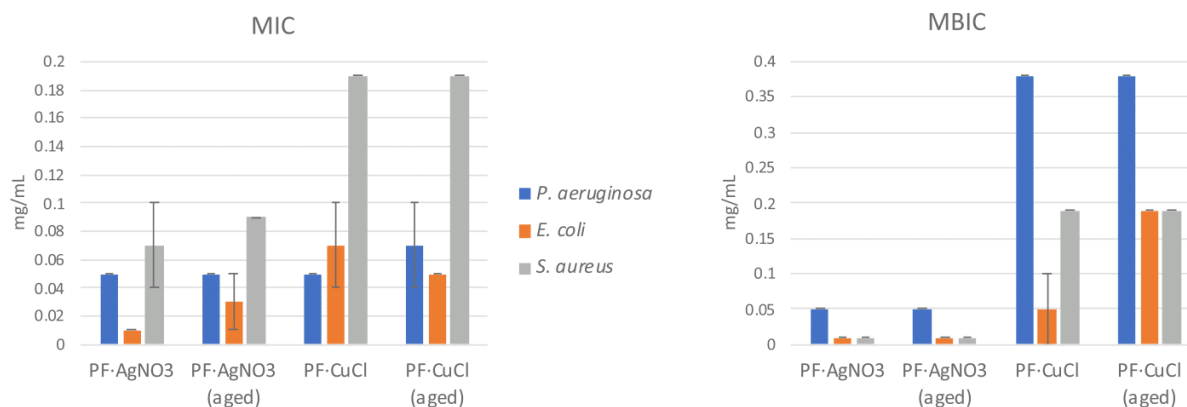
Figure 7. Comparison of efficacy from storage of co-crystals **CC-1**, **CC-2**, **CC-3**, and **CC-4**.

after the antimicrobial has been removed. All the co-crystal compounds demonstrated biocidal properties. The MBC values generally followed the same trend as the MIC values for the various antimicrobials tested but at higher concentrations than those of MIC, which is typical, and were more variable, particularly for the *S. aureus* strain.

Prevention of Biofilm. Here, we assayed the antimicrobial plate for the ability of cells to attach to the surface to initiate and proliferate a biofilm. Often the MBIC is expected to be equal to the MIC values as seen with most antibiotics. However, we have observed often for projects within the Calgary Biofilm Research group that for many non-"antibiotic" antimicrobials, antiseptics, and biocides, particularly those that are bacterial static versus bactericidal, the MBIC can be quite different from the MIC. Many bacteriostatic compounds still allow slow growth, and bacteria can adsorb to a surface still viable. This changes their physiology to biofilm state, and thus they begin a biofilm growth cycle. Thus, in our case, we expect and see MBIC > MIC or MBC.

The CV dye assay measures surface-adhered biomass (both live and dead cells as well as the variety of biomolecules of the biofilm matrix). Our comparator control of silver nitrate (**1**) showed strong biofilm inhibition as expected (Figure 6) and reflects why this simple metal salt is so popular as an antimicrobial.[5] The other metals on their own did not have very good antibiofilm activity, but for each strain, we see interesting second choices (based on a 0.25 mg/mL target) such as ZnCl₂ (**3**) for *S. aureus* and *E. coli* and CuCl₂ (**2**) for *E. coli*. The gallium oxalate chelates $K_3[Ga(ox)_3] \cdot 3H_2O$ (**5**) and $K_2[Ga_2(ox)_2(OH)_2] \cdot 2H_2O$ (**6**) only showed antimicrobial activity against *P. aeruginosa,* supporting our previous observations.[29]

P. aeruginosa is a robust biofilm-forming bacterial species, and thus there is a need for novel antibiofilm compounds. Of our tested antimicrobials, the PF-silver co-crystals (**CC-1**) showed strong antibiofilm activity at useful concentrations and this compound showed remarkable antibiofilm activity toward *S. aureus* and *E. coli*. For *E. coli*, all the co-crystals were able to prevent this organism from forming and proliferating a biofilm below 0.065 mg/mL. *S. aureus* biofilm production was effectively inhibited with the Zn co-crystal, **CC-6**. Although the other PF-metal compounds showed efficacy within very effective MBIC values below the 0.25 mg/mL cut off for both *S. aureus* and *E. coli*.

Effect on Extended Storage Time. Due to COVID-19 isolation restrictions, we paused working and stored co-crystal samples of PF with silver (**CC-2**) and copper (**CC-4**), which were used in our original pilot study published in 2020.[27] The compounds were at room temperature and ~35% relative humidity (on average) in a covered container away from direct light exposure. This fortuitous event allowed us to revisit these older samples in our present study and evaluate them besides freshly prepared co-crystals of the same compounds (**CC-1** and **CC-3**) Figure 7. The only observable difference was that the aged compounds had an overall larger grain size by 2−4 times, which may have originated by using a different grinding apparatus in the earlier preparations. We observed only minor changes in antimicrobial efficacy between the fresh and aged co-crystals, suggesting that they are very stable to room temperature storage conditions.

■ DISCUSSION

This study explores novel antimicrobial formulation efficacies against these pathogens by means of co-crystallization of potential metal atom-based antimicrobials (MBAs) with PF. Co-crystallization of pharmaceuticals is a growing research field that harvests the change of physicochemical properties of the co-crystal, compared to properties of single compound crystals as reviewed in detail elsewhere.[33] Briefly, co-crystallization has been shown to increase solubility, photo and mechanical stability, as well as bioavailability.[33] As a part of the whole combinatorial approach in dealing with antibiotic resistance development, which was proposed more than 30 years ago, co-crystallization of antimicrobials is viewed by us as a viable way of combining antimicrobials which have different modes of action into a single drug complex. Such a combination would deliver both antimicrobials with the possibility for increased antimicrobial efficacy, compared to the single antimicrobials used to produce it.

MBAs were used to treat microbial infections and preserve food well before discovery of conventional antibiotics.[34] MBAs, including metals, metal salts, and metal complexes, are viewed as a viable alternative to antibiotics.[3] QCCs are well known antimicrobial agents and are currently used as antiseptics, biocides, and preservatives.[35] PF and proflavinium cation, as an example of a ridged planar QCC, is of our interest due to its previous use. We see co-crystallization of MBAs with QCCs as a unique area of combinatorial antimicrobials, and it provides

52

an excellent test case for further antimicrobial co-crystallization development.

In our previous works,[27−29] we described the co-crystalline materials of PF with the MBAs of Ag, Cu, Zn, and Ga, exploring their antimicrobial properties by means of disk diffusion assays. The disk diffusion assay, however, does not provide quantitative data regarding antimicrobial properties of the compound, which is required for adequate assessment and further development of any antimicrobial agent. Thus, in the present study, we provide quantification of anti-planktonic and anti-biofilm efficacy of those compounds in a direct comparison to each other. We evaluated the standard approach of determining the MIC required for inhibition of planktonic growth of bacteria (bacteriostatic effect). Growing awareness of the dramatic difference in physiology and biochemistry between planktonic and biofilm mode of bacterial growth and a realization of the prevalence of biofilm in biofouling, infection spread, and chronic infections[36] led us to also evaluate the anti-biofilm activity (MIBC) of all crystalline materials. Both the spread of infection and infection itself are tightly associated with biofilms, as bacteria tend to form biofilms on inanimate surfaces that serve as hotspots of institutional and nosocomial infection transfer.[37] Thus, our study here is a crucial initial step that compares the potential of co-crystals of antimicrobial efficacy of metal ions with a QCC antiseptic. Below, we briefly overview strategies against the three bacterial species studied here providing literature examples of other organo-metal complexes as comparators to the co-crystal results we present here.

Co-crystallization Products' Antimicrobial Activity against *P. aeruginosa*. Studies have been performed using silver against either planktonic and biofilm growth of *P. aeruginosa*, demonstrating good antimicrobial and antifouling properties.[38] However, besides economic burden caused by high price of silver, there are other factors that limit its practical use in free ionic form, such as low photostability and possible precipitation in the form of AgCl or Ag-thiol group aggregates under physiological conditions.[39] To address the issue of silver's bioavailability and stability, multiple approaches have been proposed, such as stabilized speciation and/or complexation of silver with organic ligands. Copper, similar to silver, is a coinage metal and was used since ancient times to preserve water and treat infectious diseases.[40] Zinc ions were shown to interfere with *P. aeruginosa* biofilm formation and inhibit planktonic growth of the bacterium.[41] Gallium is attracting attention as an antimicrobial agent,[42] with forms of gallium-containing drugs currently being discussed with regard to *P. aeruginosa* treatment, such as gallium complexes with organic molecules, such as acetate[43] or desferrioxamin.[44]

Co-crystallization of silver with PF in our work reflected MIC values between those of PF and AgNO₃ individually. Biofilm prevention properties of these two co-crystals (**CC-1** and **CC-2**) were at the level of AgNO₃ (**1**). It is worth noting that the molar presence of silver in co-crystal is half that for the dosage provided by **1**. This suggests that the physicochemical properties of the Ag-PF co-crystal enhance the Ag efficacy and thus provide an advantage in the use of the silver-PF co-crystals over AgNO₃ alone. Our studies demonstrated decrease in MIC with PF-CuCl co-crystals (**CC-3**) compared to PF (**7**) or CuCl₂ (**2**) alone. Antibiofilm properties of (**CC-3**) were on the same order as that of (**7**) or (**2**), suggesting no advantage of the crystal form. However, **CC-4** did not lose any efficacy with storage over 3 years, whereas PF was unstable when stored in a

similar fashion. This suggests that the co-crystal of PF-CuCl could be useful for applications against *P. aeruginosa* requiring longevity or shelf-life stability.

Our approach also demonstrated impressive results where the Zn-PF co-crystals had lower MICs of PF or ZnCl₂ alone for *P. aeruginosa*. Promising data were also obtained regarding ZnCl₃(HPF) anti-biofilm properties—2-fold decrease in MBIC, compared to PF alone. Gallium, as an effective bacteriostatic agent, is also recently receiving attention in various organometallic complexes. Here, we see that the Ga-oxalate ligand complexes **5** and **6** showed selective antimicrobial activity toward *P. aeruginosa* compared to the other two strains. The co-crystal **CC-7** retained antibiofilm properties to the level of Ga(NO₃)₃ (**4**).

Co-crystallization Products' Antimicrobial Activity against *E. coli*. Like *P. aeruginosa*, silver is the most studied and widely applied antimicrobial metal against *E. coli*. Dozens of patents were assigned over 21st century,[5] yet silver resistance is now widespread including resistance to the nanoparticle form.[45] Following the combinatorial narrative, silver−sulfodiazine combination is used in clinic settings for various microbes including *E. coli*.[46] Copper has also been shown to increase efficacy of several organic compounds against *E. coli*, including lactic acid[47] and chloro-catechols.[48] Although on its own Zn is less antimicrobial to *E. coli* compared to silver or copper, Zn²⁺ is being explored in combinations with other therapeutics, in part due to its immunostimulant properties and its ability to reverse *E. coli* resistance to amikacin,[49] for example.

PF-silver co-crystals (**CC-1/2**) demonstrated good bacteriostatic results against planktonic growth of *E. coli*, where they remained as effective as AgNO₃ (**1**) or averaged between MICs of **1** and **7**. Antibiofilm properties of **CC1/2** provided equal or better efficacy level of the constituents. Here, we also see the same trend for the copper-PF co-crystals (**CC3/4**) in both bacteriostatic and antibiofilm properties toward *E. coli*. This trend continues with the two different zinc−PF complexes (**CC-5** and **CC-6**) and the gallium co-crystal (**CC-7**), where higher bacteriostatic activity was observed over the metal salts (**3** and **4**) or Ga- oxalate chelates (**5** and **6**) alone. The Cu, Zn, and Ga PF co-crystals showed anti-biofilm properties with efficacy comparable to or better than PF (**7**) alone for *E. coli*. It is worth reiterating that the molar presence of metal and/or PF in the co-crystal is considerably smaller than that of these compounds on their own, which implies that the same or better antimicrobial activity is seen when using less of each antimicrobial. At this stage, we cannot define this observation to be synergistic or additive.

Co-crystallization Products' Antimicrobial Activity against *S. aureus*. Generally, silver has been shown to demonstrate only moderate activity against *S. aureus*, although the silver−sulfodiazine combination is reasonably active against *S. aureus* biofilms.[50] Multiple attempts have been made to increase its antimicrobial properties against Gram-positive bacteria, including complexation with carbene compounds[51] or coordination with camphorimines.[52] Considerable attention has also been dedicated to anti-*Staphylococcal* research of copper compounds. High-throughput screening of copper complexation with organic molecules yielded several active bis(thiosemicarbazone)−Cu complexes, including specific copper-dependent as glyoxal-bis(N4-methylthiosemicarbazone) (GTSM)-Cu as an anti-MRSA complex.[53] Cu-Schiff base complexes were also studied for interactions with oxacillin

and vancomycin and were shown to be additive/synergistic. $[Cu(bitpy)_2](ClO_4)_2$ was demonstrated to possess *S. aureus* anti-biofilm properties.[54] Zn is the MBA that is receiving the most attention regarding *S. aureus* treatment. Multiple complexes of Zn(II) with heterocyclic ligands were reported to have antimicrobial activity.[55] Phthalocyanine[56] and menthol–phthalocyanine[57] complexes with Zn(II) are viewed as a viable photo-assisted solution to *S. aureus* infection. Like copper, zinc Schiff-bases complexes such as (*N*-allylsalicylide-neiminato)-zinc are reported to be twice as effective as zinc acetate alone.[58] The Ga(III) complex with maltolate[59] was reported to show anti-planktonic properties against *S. aureus*, while recent success of galbofloxacin, a ciprofloxacin-containing gallium compound, demonstrates success of a combinational approach to gallium-bearing drugs development against *S. aureus*.[60]

In our studies, bacteriostatic properties against *S. aureus* were observed from all co-crystallization products. Beyond the silver co-crystals (**CC-1/2**) having good antibiofilm properties, the zinc co-crystal (**CC-6**) has excellent antibiofilm activity, even though its bacteriostatic activity is less effective. This gives another example of the co-crystalline structure showing selective antimicrobial efficacy, but in this case in antibiofilm properties.

Overall, at this time, it is not clear if the co-crystal activity mechanism is simply a delivery platform for the two different antimicrobials or it is that features of their structures mediate bacterial cell structure and physiology damage as well. Our previous work[26−28] suggested that the co-crystals are more than simply the additive efficacy of the components and as a co-crystal are enhancing the interaction with the bacteria or perhaps and facilitating a localized "burst" of combined antimicrobials. It is well known that the toxicity of a metal is in its speciation. Given the chemical complexity of the microbial growth media and the bacterium's biochemistry, one can imagine an overwhelming diversity and complexity of different metal species and chelates in the biological soup. With this in mind, we can postulate further that our crystalline materials are able to deliver, at least initially, a unique and/or uniform metal species to the bacterium cell.

CONCLUSIONS

It is well appreciated in toxicology that a metal's chemical speciation influences its bioavailability, and as such, the metal organic co-crystal provides a unique speciation that warranted the antimicrobial investigation here. We find that all metal-PF co-crystals explored here have merit as antimicrobials. Although the best broad-spectrum antibiofilm compound is the silver-based **CC-1**, we identified other effective co-crystals for each species and growth state that could also move forward for specific bacterial problem situations. We find that select co-crystals are required for best results against each bacterium and growth state. We observe that no single metal-PF co-crystal works equally well against all three bacterial species. This is not too much of a surprise, given the dramatic difference in physiology between the strains and growth states. While not all metal-PF co-crystals demonstrated enhanced antimicrobial efficacy over one or both of their constituents, their compounds did not lose their antimicrobial properties while trapped in the crystal form. This is an excellent observation, and it clearly shows that co-crystallization of MBAs with an antiseptic QCC (PF) does not affect the activity of individual antimicrobials and potentially protects them within the co-

crystal. How the antimicrobial activity might be related to changes in thermodynamic solubility or kinetic dissolution rate, at least for some of the best performing co-crystals, will require further studies, and how co-crystallization may be further used to fine-tune physicochemical properties of metal–organic antimicrobial combinations must be explored. This work gives a solid proof of principle to apply these co-crystals to specific applications such as in cosmetics, biofouling, agriculture, general antiseptic, disinfectant, coatings, and so forth.

ASSOCIATED CONTENT

Supporting Information

The Supporting Information is available free of charge at https://pubs.acs.org/doi/10.1021/acsabm.2c00404.

AMR values (PDF)

AUTHOR INFORMATION

Corresponding Authors

Dario Braga − *Dipartimento di Chimica "Giacomo Ciamician", Università di Bologna, 40126 Bologna, Italy;* orcid.org/0000-0003-4162-4779; Email: dario.braga@unibo.it

Raymond J. Turner − *Department of Biological Sciences, University of Calgary, Calgary, Alberta T2N 1N4, Canada;* orcid.org/0000-0002-9263-0776; Email: turnerr@ucalgary.ca

Authors

Andrii Lekhan − *Department of Biological Sciences, University of Calgary, Calgary, Alberta T2N 1N4, Canada*

Cecilia Fiore − *Dipartimento di Chimica "Giacomo Ciamician", Università di Bologna, 40126 Bologna, Italy;* orcid.org/0000-0002-2483-1867

Oleksii Shemchuk − *Institute of Condensed Matter and Nanosciences, Université Catholique de Louvain, 1348 Louvain-la-Neuve, Belgium;* orcid.org/0000-0003-3003-3922

Fabrizia Grepioni − *Dipartimento di Chimica "Giacomo Ciamician", Università di Bologna, 40126 Bologna, Italy;* orcid.org/0000-0003-3895-0979

Complete contact information is available at:
https://pubs.acs.org/10.1021/acsabm.2c00404

Notes

The authors declare no competing financial interest.

REFERENCES

(1) Ventola, C. The antibiotic resistance crisis: part 1: causes and threats. *Pharm. Ther.* **2015**, *40*, 277−283.

(2) Harrison, J.; Turner, R.; Marques, L.; Ceri, H. Biofilms. *Am. Sci.* **2005**, *93*, 508.

(3) Turner, R. J. Metal-Based Antimicrobial Strategies. *Microbiol. Biotechnol.* **2017**, *10*, 1062−1065.

(4) Lemire, J. A.; Harrison, J. J.; Turner, R. J. Antimicrobial Activity of Metals: Mechanisms, Molecular Targets and Applications. *Nat. Rev. Microbiol.* **2013**, *11*, 371−384.

(5) Sim, W.; Barnard, R. T.; Blaskovich, M. A. T.; Ziora, Z. M. Antimicrobial Silver in Medicinal and Consumer Applications: A Patent Review of the Past Decade (2007−2017). *Antibiotics* **2018**, *7*, 93.

(6) Arendsen, L. P.; Thakar, R.; Sultan, A. H. The Use of Copper as an Antimicrobial Agent in Health Care, Including Obstetrics and Gynecology. *Clin. Microbiol. Rev.* **2019**, *32*, SEP19.

(7) David, R. Why Zinc Is Bad for Bacteria. *Nat. Rev. Microbiol.* **2011**, *10*, 4.

(8) Hijazi, S.; Visaggio, D.; Pirolo, M.; Frangipani, E.; Bernstein, L.; Visca, P. Antimicrobial Activity of Gallium Compounds on ESKAPE Pathogens. *Front. Cell. Infect. Microbiol.* **2018**, *8*, 316.

(9) Pearson, R. G. Hard and Soft Acids and Bases. *J. Am. Chem. Soc.* **2002**, *85*, 3533−3539.

(10) Rigo, A.; Corazza, A.; Luisa di Paolo, M.; Rossetto, M.; Ugolini, R.; Scarpa, M. Interaction of Copper with Cysteine: Stability of Cuprous Complexes and Catalytic Role of Cupric Ions in Anaerobic Thiol Oxidation. *J. Inorg. Biochem.* **2004**, *98*, 1495−1501.

(11) Macomber, L.; Imlay, J. A. The Iron-Sulfur Clusters of Dehydratases Are Primary Intracellular Targets of Copper Toxicity. *Proc. Natl. Acad. Sci. U.S.A.* **2009**, *106*, 8344−8349.

(12) Xu, F. F.; Imlay, J. A. Silver(I), Mercury(II), Cadmium(II), and Zinc(II) Target Exposed Enzymic Iron-Sulfur Clusters When They Toxify Escherichia Coli. *Appl. Environ. Microbiol.* **2012**, *78*, 3614−3621.

(13) Eijkelkamp, B. A.; Morey, J. R.; Ween, M. P.; Ong, C. L. Y.; McEwan, A. G.; Paton, J. C.; McDevitt, C. Extracellular Zinc Competitively Inhibits Manganese Uptake and Compromises Oxidative Stress Management in Streptococcus Pneumoniae. *PLoS One* **2014**, *9*, No. e89427.

(14) Feng, Q. L.; Wu, J.; Chen, G. Q.; Cui, F. Z.; Kim, T. N.; Kim, J. O. A Mechanistic Study of the Antibacterial Effect of Silver Ions on Escherichia Coli and Staphylococcus Aureus. *J. Biomed. Mater. Res.* **2000**, *52*, 662−668.

(15) Peters, K.; Pazos, M.; Edoo, Z.; Hugonnet, J. E.; Martorana, A. M.; Polissi, A.; VanNieuwenhze, M. S.; Arthur, M.; Vollmer, W. Copper Inhibits Peptidoglycan LD-Transpeptidases Suppressing β-Lactam Resistance Due to Bypass of Penicillin-Binding Proteins. *Proc. Natl. Acad. Sci. U.S.A.* **2018**, *115*, 10786−10791.

(16) Mazzei, L.; Cianci, M.; Gonzalez Vara, A.; Ciurli, S. The Structure of Urease Inactivated by Ag(I): A New Paradigm for Enzyme Inhibition by Heavy Metals. *Dalton Trans.* **2018**, *47*, 8240−8247.

(17) Bernstein, L. R. Mechanisms of Therapeutic Activity for Gallium. *Pharmacol. Rev.* **1998**, *50*, 665−682.

(18) Harrison, J. J.; Turner, R. J.; Joo, D. A.; Stan, M. A.; Chan, C. S.; Allan, N. D.; Vrionis, H. A.; Olson, M. E.; Ceri, H. Copper and Quaternary Ammonium Cations Exert Synergistic Bactericidal and Antibiofilm Activity against Pseudomonas Aeruginosa. *Antimicrob. Agents Chemother.* **2008**, *52*, 2870−2881.

(19) Zhang, C.; Cui, F.; Zeng, G. M.; Jiang, M.; Yang, Z.; Yu, Z. G.; Zhu, M. Y.; Shen, L. Q. Quaternary Ammonium Compounds (QACs): A Review on Occurrence, Fate and Toxicity in the Environment. *Sci. Total Environ.* **2015**, *518−519*, 352−362.

(20) Wainwright, M. Acridine–a neglected antibacterial chromophore. *J. Antimicrob. Chemother.* **2001**, *47*, 1−13.

(21) Desiraju, G. R. Crystal Engineering: A Holistic View. *Angew. Chem., Int. Ed.* **2007**, *46*, 8342−8356.

(22) Grepioni, F.; Casali, L.; Fiore, C.; Mazzei, L.; Sun, R.; Shemchuk, O.; Braga, D. Steps towards nature inspired inorganic crystal engineering. *Dalton Trans.* **2022**, *51*, 7390−7400.

(23) Pharmaceutical Salts and Co-Crystals; Wouters, J., Quéré, L., Eds.; *Drug Discovery*; Royal Society of Chemistry: Cambridge, 2011.

(24) Steed, J. W. The Role of Co-Crystals in Pharmaceutical Design. *Trends Pharmacol. Sci.* **2013**, *34*, 185−193.

(25) Yamamoto, Y.; Morikawa, T.; Kawai, T.; Nonomura, Y. Selective Bactericidal Activity of Divalent Metal Salts of Lauric Acid. *ACS Omega* **2017**, *2*, 113−121.

(26) Casali, L.; Mazzei, L.; Shemchuk, O.; Honer, K.; Grepioni, F.; Ciurli, S.; Braga, D.; Baltrusaitis, J. Smart Urea Ionic Co-Crystals with Enhanced Urease Inhibition Activity for Improved Nitrogen Cycle Management. *Chem. Commun.* **2018**, *54*, 7637−7640.

(27) Shemchuk, O.; Braga, D.; Grepioni, F.; Turner, R. J. Co-Crystallization of Antibacterials with Inorganic Salts: Paving the Way to Activity Enhancement. *RSC Adv.* **2020**, *10*, 2146−2149.

(28) Fiore, C.; Shemchuk, O.; Grepioni, F.; Turner, R. J.; Braga, D. Proflavine and Zinc Chloride "Team Chemistry": Combining Antibacterial Agents via Solid-State Interaction. *CrystEngComm* **2021**, *23*, 4494−4499.

(29) Guerrini, M.; d'Agostino, S.; Grepioni, F.; Braga, D.; Lekhan, A.; Turner, R. J. Antimicrobial Activity of Supramolecular Salts of Gallium(III) and Proflavine and the Intriguing Case of Trioxalate Complex. *Sci. Rep.* **2022**, *12*, 3673.

(30) World Health Organization. "Global Priority List of Antibiotic-Resistant Bacteria To Guide Research, Discovery, And Development Of New Antibiotics" [Online]. Available: https://www.who.int/medicines/publications/WHO-PPL-Short_Summary_25Feb-ET_NM_WHO.pdf (accessed April 5, 2022).

(31) Balouiri, M.; Sadiki, M.; Ibnsouda, S. K. Methods for in vitro evaluating antimicrobial activity: A review. *J. Pharm. Anal.* **2016**, *6*, 71−79.

(32) Allkja, J.; Bjarnsholt, T.; Coenye, T.; Cos, P.; Fallarero, A.; Harrison, J. J.; Lopes, S. P.; Oliver, A.; Pereira, M. O.; Ramage, G.; Shirtliff, M. E.; Stoodley, P.; Webb, J. S.; Zaat, S. A. J.; Goeres, D. M.; Azevedo, N. F. Minimum information guideline for spectrophotometric and fluorometric methods to assess biofilm formation in microplates. *Biofilm* **2020**, *2*, 100010.

(33) Karimi-Jafari, M.; Padrela, L.; Walker, G. M.; Croker, D. M. Creating Cocrystals: A Review of Pharmaceutical Cocrystal Preparation Routes and Applications. *Cryst. Growth Des.* **2018**, *18*, 6370−6387.

(34) Landecker, H. Antimicrobials before Antibiotics: War, Peace, and Disinfectants. *Palgrave Commun.* **2019**, *5*, 45.

(35) Gerba, C. P. Quaternary Ammonium Biocides: Efficacy in Application. *Appl. Environ. Microbiol.* **2015**, *81*, 464−469.

(36) Bjarnsholt, T. The Role of Bacterial Biofilms in Chronic Infections. *APMIS* **2013**, *121*, 1−58.

(37) Kramer, A.; Schwebke, I.; Kampf, G. How Long Do Nosocomial Pathogens Persist on Inanimate Surfaces? A Systematic Review. *BMC Infect. Dis.* **2006**, *6*, 130.

(38) Bjarnsholt, T.; Kirketerp-møller, K.; Kristiansen, S.; Phipps, R.; Nielsen, A. K.; Jensen, P. Ø.; Høiby, N.; Givskov, M. Silver against Pseudomonas Aeruginosa Biofilms. *APMIS* **2007**, *115*, 921−928.

(39) Betts, H. D.; Neville, S. L.; McDevitt, C. A.; Sumby, C. J.; Harris, H. H. The Biochemical Fate of Ag+ Ions in Staphylococcus Aureus, Escherichia Coli, and Biological Media. *J. Inorg. Biochem.* **2021**, *225*, 111598.

(40) Dollwet, H. H. A.; Sorenson, J. R. J. Historic Uses of Copper Compounds in Medicine. In *Trace Elements in Medicine*; The Humana Press Inc.: Arkansas, 2001; pp 80−87.

(41) Wu, C.; Labrie, J.; Tremblay, Y. D. N.; Haine, D.; Mourez, M.; Jacques, M. Zinc as an Agent for the Prevention of Biofilm Formation by Pathogenic Bacteria. *J. Appl. Microbiol.* **2013**, *115*, 30−40.

(42) Kaneko, Y.; Thoendel, M.; Olakanmi, O.; Britigan, B. E.; Singh, P. K. The Transition Metal Gallium Disrupts Pseudomonas Aeruginosa Iron Metabolism and Has Antimicrobial and Antibiofilm Activity. *J. Clin. Invest.* **2007**, *117*, 877−888.

(43) Wang, Y.; Han, B.; Xie, Y.; Wang, H.; Wang, R.; Xia, W.; Li, H.; Sun, H. Combination of Gallium(III) with Acetate for Combating Antibiotic Resistant Pseudomonas Aeruginosa. *Chem. Sci.* **2019**, *10*, 6099−6106.

(44) Banin, E.; Lozinski, A.; Brady, K. M.; Berenshtein, E.; Butterfield, P. W.; Moshe, M.; Chevion, M.; Greenberg, E. P.; Banin, E. The Potential of Desferrioxamine-Gallium as an Anti-

Pseudomonas Therapeutic Agent. *Proc. Natl. Acad. Sci. U.S.A.* **2008**, *105*, 16761−16766.

(45) Graves, J. L.; Tajkarimi, M.; Cunningham, Q.; Campbell, A.; Nonga, H.; Harrison, S. H.; Barrick, J. E. Rapid Evolution of Silver Nanoparticle Resistance in Escherichia Coli. *Front. Genet.* **2015**, *6*, 42.

(46) White, R.; Cooper, R. *Silver Sulfadiazine: A Review of the Evidence*; Wounds UK, 2005; Vol. *1*.

(47) Gyawali, R.; Ibrahim, S. A.; Abu Hasfa, S. H.; Smqadri, S. Q.; Haik, Y. Antimicrobial Activity of Copper Alone and in Combination with Lactic Acid against Escherichia Coli O157:H7 in Laboratory Medium and on the Surface of Lettuce and Tomatoes. *J. Pathog.* **2011**, *2011*, 650968.

(48) Schweigert, N.; Hunziker, R. W.; Escher, B. I.; Eggen, R. I. L. Acute Toxicity of (Chloro-)Catechols and (Chloro-)Catechol-Copper Combinations in Escherichia Coli Corresponds to Their Membrane Toxicity in Vitro. *Environ. Toxicol. Chem.* **2001**, *20*, 239−247.

(49) Lin, D. L.; Tran, T.; Alam, J. Y.; Herron, S. R.; Ramirez, M. S.; Tolmasky, M. E. Inhibition of Aminoglycoside 6′-N-Acetyltransferase Type Ib by Zinc: Reversal of Amikacin Resistance in Acinetobacter Baumannii and Escherichia Coli by a Zinc Ionophore. *Antimicrob. Agents Chemother.* **2014**, *58*, 4238−4241.

(50) Ueda, Y.; Miyazaki, M.; Mashima, K.; Takagi, S.; Hara, S.; Kamimura, H.; Jimi, S. The Effects of Silver Sulfadiazine on Methicillin-Resistant Staphylococcus Aureus Biofilms. *Microorg* **2020**, *8*, 1551.

(51) Esarte Palomero, O.; Cunningham, A. L.; Davies, B. W.; Jones, R. A. Antibacterial Thiamine Inspired Silver (I) and Gold (I) N-Heterocyclic Carbene Compounds. *Inorg. Chim. Acta* **2021**, *517*, 120152.

(52) Cardoso, J. M. S.; Galvão, A. M.; Guerreiro, S. I.; Leitão, J. H.; Suarez, A. C.; Carvalho, M. F. N. N. Antibacterial Activity of Silver Camphorimine Coordination Polymers. *Dalton Trans.* **2016**, *45*, 7114−7123.

(53) Haeili, M.; Moore, C.; Davis, C. J. C.; Cochran, J. B.; Shah, S.; Shrestha, T. B.; Zhang, Y.; Bossmann, S. H.; Benjamin, W. H.; Kutsch, O.; Wolschendorf, F. Copper Complexation Screen Reveals Compounds with Potent Antibiotic Properties against Methicillin-Resistant Staphylococcus Aureus. *Antimicrob. Agents Chemother.* **2014**, *58*, 3727−3736.

(54) Rajalakshmi, S.; Fathima, A.; Rao, J. R.; Nair, B. U. Antibacterial Activity of Copper(II) Complexes against Staphylococcus Aureus. *RSC Adv.* **2014**, *4*, 32004−32012.

(55) Yamgar, R. S.; Nivid, Y.; Nalawade, S.; Mandewale, M.; Atram, R. G.; Sawant, S. S. Novel Zinc(II) Complexes of Heterocyclic Ligands as Antimicrobial Agents: Synthesis, Characterisation, and Antimicrobial Studies. *Bioinorg. Chem. Appl.* **2014**, *2014*, 276598.

(56) Tunçel, A.; Öztürk, I.; Ince, M.; Ocakoglu, K.; Hoşgör-Limoncu, M.; Yurt, F. Antimicrobial Photodynamic Therapy against Staphylococcus Aureus Using Zinc Phthalocyanine and Zinc Phthalocyanine-Integrated TiO2 Nanoparticles. *J. Porphyrins Phthalocyanines* **2019**, *23*, 206−212.

(57) Szymczak, J.; Sobotta, L.; Dlugaszewska, J.; Kryjewski, M.; Mielcarek, J. Menthol Modified Zinc(II) Phthalocyanine Regioisomers and Their Photoinduced Antimicrobial Activity against Staphylococcus Aureus. *Dyes Pigm.* **2021**, *193*, 109410.

(58) Poulter, N.; Donaldson, M.; Mulley, G.; Duque, L.; Waterfield, N.; Shard, A. G.; Spencer, S.; Jenkins, A. T. A.; Johnson, A. L. Plasma Deposited Metal Schiff-Base Compounds as Antimicrobials. *New J. Chem.* **2011**, *35*, 1477−1484.

(59) Arnold, C. E.; Bordin, A.; Lawhon, S. D.; Libal, M. C.; Bernstein, L. R.; Cohen, N. D. Antimicrobial Activity of Gallium Maltolate against Staphylococcus Aureus and Methicillin-Resistant S. Aureus and Staphylococcus Pseudintermedius: An in Vitro Study. *Vet. Microbiol.* **2012**, *155*, 389−394.

(60) Pandey, A.; Śmiłowicz, D.; Boros, E. Galbofloxacin: A Xenometal-Antibiotic with Potent in Vitro and in Vivo Efficacy against S. Aureus. *Chem. Sci.* **2021**, *12*, 14546−14556.

2.2.1 Supporting information

Comparison of antimicrobial and antibiofilm activity of Proflavine co-crystallized with Silver, Copper, Zinc, and Gallium salts.

Andrii Lekhan,[a] Cecilia Fiore,[b] Oleksii Shemchuk,[c] Fabrizia Grepioni,[b] Dario Braga,[b*] Raymond J. Turner[a*]

[a] Department of Biological Sciences, University of Calgary, Calgary, Alberta, Canada, T2N1N4.

[b] Dipartimento di Chimica "Giacomo Ciamician", Università di Bologna, Via Selmi 2, 40126 Bologna, Italy.

[c] Institute of Condensed Matter and Nanosciences, Université Catholique de Louvain, Place Louis Pasteur 1, 1348 Louvain-la-Neuve, Belgium.

Table S1: Minimal Inhibitory Concentrations (mg/mL)

Antimicrobial agent	Compound code	P. aeruginosa	E. coli	S. aureus
$AgNO_3$	1	0.01	0.01	0.01
$CuCl_2$	2	0.56 ± 0.27	0.38	1.5
$ZnCl_2$	3	0.75	0.28 ± 0.13	0.09
$Ga(NO_3)_3$	4	0.13 ± 0.06	3.13	1.56
$K_3[Ga(ox)_3] \cdot 3H_2O$	5	0.09	12	12
$K_2[Ga_2(ox)_2(OH)_2] \cdot 2H_2O$	6	0.05	12	12
PF	7	0.14 ± 0.07	0.09	0.375
$PF \cdot AgNO_3$	CC-1	0.05	0.01	0.07 ± 0.03
$PF \cdot CuCl$	CC-3	0.05	0.07 ± 0.03	0.19
$ZnCl_3[HPF]$	CC-5	0.05	0.05	0.09
$[HPF]_2[ZnCl_4] \cdot H_2O$	CC-6	0.01	0.05	0.09
$[HPF]_3[Ga(ox)_3] \cdot 4H_2O$	CC-7	0.02 ± 0.02	0.05	0.06 ± 0.03

Table S2. Minimal biocidal concentrations (mg/mL)

Antimicrobial agent	Compound code	*P. aeruginosa*	*E. coli*	*S. aureus*
AgNO$_3$	1	0.05	0.01	0.05 ± 0.02
CuCl$_2$	2	0.75	0.03 ± 0.02	6.25 ± 1.5
ZnCl$_2$	3	1.5	1.25 ± 0.75	0.56 ± 0.27
Ga(NO$_3$)$_3$	4	1.5	6.25	6.25 ± 1.5
K$_3$[Ga(ox)$_3$]·3H$_2$O	5	1.5 ± 0.25	12	12
K$_2$[Ga$_2$(ox)$_2$(OH)$_2$]·2H$_2$O	6	N/D	N/D	N/D
PF	7	0.75	0.56 ± 0.27	1.25 ± 0.75
PF·AgNO$_3$	CC-1	0.05	0.01	0.56 ± 0.27
PF·CuCl	CC-3	0.56 ± 0.27	0.13 ± 0.05	1.25 ± 0.75
ZnCl$_3$[HPF]	CC-5	1.5	0.56 ± 0.27	0.56 ± 0.27
[HPF]$_2$[ZnCl$_4$]·H$_2$O	CC-6	1.25 ± 0.75	0.56 ± 0.27	0.56 ± 0.27
[HPF]$_3$[Ga(ox)$_3$]·4H$_2$O	CC-7	0.75	0.28 ± 0.13	0.56 ± 0.27

N/D. not determined.

Table S3: Minimal Biofilm Inhibition Concentrations (mg/mL).

Antimicrobial agent	Compound code	*P. aeruginosa*	*E. coli*	*S. aureus*
AgNO$_3$	1	0.01	0.01	0.01
CuCl$_2$	2	0.56 ± 0.27	0.28 ± 0.13	1.5
ZnCl$_2$	3	0.75	0.28 ± 0.13	0.09
Ga(NO$_3$)$_3$	4	0.2	0.78	6.25
K$_3$[Ga(ox)$_3$]·3H$_2$O	5	0.09	12	12
K$_2$[Ga$_2$(ox)$_2$(OH)$_2$]·2H$_2$O	6	0.19	12	12
PF	7	0.75	0.05 ± 0.04	0.03 ± 0.02
PF·AgNO$_3$	CC-1	0.05	0.01	0.01
PF·CuCl	CC-3	0.38	0.05 ± 0.04	0.19
ZnCl$_3$[HPF]	CC-5	0.38	0.05 ± 0.04	0.09
[HPF]$_2$[ZnCl$_4$]·H$_2$O	CC-6	0.38	0.03 ± 0.02	0.01
[HPF]$_3$[Ga(ox)$_3$]·4H$_2$O	CC-7	0.28 ± 0.16	0.035 ± 0.02	0.13 ± 0.05

2.3 Mechanochemical preparation, solid-state characterization, and antimicrobial performance of copper and silver nitrate coordination polymers with L-and DL-arginine and histidine.

Abstract

The antimicrobial activity of the novel coordination polymers obtained by co-crystallizing the amino acids arginine or histidine, as both enantiopure L and racemic DL forms, with the salts $Cu(NO_3)_2$ and $AgNO_3$ has been investigated to explore the effect of chirality in the cases of enantiopure and racemic forms. The compounds were prepared by mechanochemical, slurry and solution methods and characterized by X-ray single-crystal, powder diffraction and, in the cases of the silver compounds, by solid-state NMR* spectroscopy. The activity against bacterial pathogens *Pseudomonas aeruginosa, Escherichia coli*, and *Staphylococcus aureus* was assessed by carrying out disk diffusion assays on lysogeny agar media.

*The solid-state NMR experiments were carried out at the University of Torino in collaboration with the group of Prof. Roberto Gobetto (see authors list).

Article

Mechanochemical Preparation, Solid-State Characterization, and Antimicrobial Performance of Copper and Silver Nitrate Coordination Polymers with L- and DL-Arginine and Histidine

Cecilia Fiore [1] , Andrii Lekhan [2], Simone Bordignon [3], Michele R. Chierotti [3] , Roberto Gobetto [3] , Fabrizia Grepioni [1], Raymond J. Turner [2,*] and Dario Braga [1,*]

[1]   Dipartimento di Chimica "Giacomo Ciamician", University of Bologna, Via Selmi, 2, 40126 Bologna, Italy
[2]   Department of Biological Sciences, University of Calgary, 2500 University Drive NW,
       Calgary, AB T2N 1N4, Canada
[3]   Dipartimento di Chimica and NIS Centre, University of Torino, Via P. Giuria, 7, 10125 Torino, Italy
*   Correspondence: turnerr@ucalgary.ca (R.J.T.); dario.braga@unibo.it (D.B.)

Abstract: The antimicrobial activity of the novel coordination polymers obtained by co-crystallizing the amino acids arginine or histidine, as both enantiopure L and racemic DL forms, with the salts $Cu(NO_3)_2$ and $AgNO_3$ has been investigated to explore the effect of chirality in the cases of enantiopure and racemic forms. The compounds $[Cu \cdot AA \cdot (NO_3)_2]_{CPs}$ and $[Ag \cdot AA \cdot NO_3]_{CPs}$ (AA = L-Arg, DL-Arg, L-His, DL-His) were prepared by mechanochemical, slurry, and solution methods and characterized by X-ray single-crystal and powder diffraction in the cases of the copper coordination polymers, and by powder diffraction and by solid-state NMR spectroscopy in the cases of the silver compounds. The two pairs of coordination polymers, $[Cu \cdot L\text{-}Arg \cdot (NO_3)_2 \cdot H_2O]_{CP}$ and $[Cu \cdot DL\text{-}Arg \cdot (NO_3)_2 \cdot H_2O]_{CP}$, and $[Cu \cdot L\text{-}Hys \cdot (NO_3)_2 \cdot H_2O]_{CP}$ and $[Cu \cdot DL\text{-}His \cdot (NO_3)_2 \cdot H_2O]_{CP}$, have been shown to be isostructural in spite of the different chirality of the amino acid ligands. A similar structural analogy could be established for the silver complexes on the basis of SSNMR. The activity against the bacterial pathogens *Pseudomonas aeruginosa*, *Escherichia coli*, and *Staphylococcus aureus* was assessed by carrying out disk diffusion assays on lysogeny agar media showing that, while there is no significant effect arising from the use of enantiopure or chiral amino acids, the coordination polymers exert an appreciable antimicrobial activity comparable, when not superior, to that of the metal salts alone.

Keywords: antimicrobials; coordination polymers; crystal engineering; co-crystallization; silver; copper; amino acids; mechanochemistry

1. Introduction

The overuse of antimicrobials during the last half-century is the primary cause of the development of antimicrobial resistance in pathogenic and opportunistic microorganisms, which has become one of the most important challenges in pharmacology and modern medicine [1,2]. Since metal-based antimicrobials have the potential for new sustainable solutions for health [3,4], progress has been made in the area of molecular inorganic–organic hybrid compounds [5,6]. Indeed, the coordination of organic ligands with metals, showing antibacterial activities, has proved to be a valid route to tackle antimicrobial resistance (AMR) [7–9]. Attention has been focused on the design of new bioactive metal–organic frameworks (bioMOFs) [10,11], coordination polymers [12,13], salts [14–16], and complexes [17,18]. These materials are engineered in order to combine a bactericidal metal center with bioactive ligands or with ancillary ligands selected from the GRAS (*generally recognized as safe*) list [19].

In this work, we extend the quest for novel antimicrobials to the investigation of a series of novel coordination polymers of copper nitrate and silver nitrate with the amino

acids arginine and histidine, reacted as both enantiopure L and racemic DL forms. Hereafter, we elaborate on the reasons for choosing these metals and the amino acids as ligands.

The coinage metals copper and silver have a history of medicinal use through antiquity. It is worth recalling that silver is presently widely used in wound dressings and medical devices because it exerts broad-spectrum antimicrobial activity against Gram-positive and -negative bacteria, viruses, fungi, and protozoa [20,21], while copper is an esteemed antimicrobial agent and has long been used for its medical properties [22,23]. Nowadays, copper is widely studied in different forms and formulations for the antimicrobial treatment of surfaces [24,25] and on medical devices and implants [26,27]. We can find various examples of copper used in its metallic state [28–30], in a nanoparticle form [31], and as a coordination compound or ionic co-crystal [32–34]. The mechanism of action of silver and copper, although not fully established, consists of the disruption of cell membranes, enzymes, and nucleic acids, and interfering with cell division, inducing an oxidative stress response involving endogenous ROS (reactive oxygen species), thus leading to cell death [35–41].

Even though one does not regularly associate amino acids with antimicrobial properties, many antimicrobials are built upon amino acid scaffolds or incorporate amino acids into their structures [42]. Additionally, some studies have shown antimicrobial activity in particular forms [43]. Arginine is also a key building block of antimicrobial peptide structures and performs best in a polymeric configuration [44]. Histidine also acts as an antimicrobial in peptides, but requires a lower pH in order to be sure that the imidazole side chain holds a positive charge [45]. A report of efficacy against *Helicobacter pylori* suggests that its major mechanism of antimicrobial activity is the inhibition of cell wall synthesis [46].

Many examples of complexes and coordination compounds with silver and other metals (zinc, copper) [32,33,47,48] showing antimicrobial activity are available in the literature that have *basic* amino acids (arginine, histidine) as ligands [49–51] or compounds with N-protonated functionalities (imidazole, guanidine) [52–54]. In 2015, the structure of a coordination polymer with silver nitrate and the amino acid L-arginine (IWOFUX [Ag·L-Arg·NO$_3$·0.5H$_2$O]$_{CP}$ [55]) was reported, showing a remarkable activity against two Gram-negative bacteria (*E. coli*, *P. aeruginosa*). Moderate activity was observed against molds (*A. niger*, *P. citrinum*) and some activity was observed for the yeasts *C. albicans*, *S. cerevisiae*, although it was not significant [51]. The structure of a silver nitrate complex with L-histidine in its zwitterionic form was also described in 2012 (TIGHEY [Ag·*bis*(L-His)·NO$_3$·0.5H$_2$O]$_{CP}$ [56]) while discussing a pH-dependent and selective behavior of amino acids coordinating silver ions.

Here, we extend on our theme of combining antimicrobial metals with organic molecules in coordination polymers. In this case, we also took the opportunity to use both enantiopure and racemic forms of the amino acids with the aim of ascertaining whether the bacteriostatic activity could show differences attributable to chirality. All coordination polymers as bulk materials were investigated in terms of antimicrobial activity by the standard Kirby–Bauer disk diffusion zone of inhibition assay [57] against *Pseudomonas aeruginosa*, *Escherichia coli*, and *Staphylococcus aureus*. It can be anticipated, but *vide infra*, that, while no significant difference could be detected in terms of antimicrobial behavior between enantiopure and racemic products, all compounds are active against these bacterial strains. Moreover, this study has enabled us to find a remarkable structural analogy between enantiopure and racemic coordination polymers, which will be discussed hereafter.

2. Results and Discussion

Mechanochemical and solution methods (see below) were applied to prepare a family of compounds, which, as will be explained below, are all characterized by the assembly of the metals and of the amino acid ligands in coordination polymers. The chemical formulae and the corresponding abbreviated names are listed in Table 1.

Table 1. List of the coordination polymers prepared and discussed in this work, with the respective adopted abbreviations.

[Cu·AA·(NO$_3$)$_2$]$_{CPs}$	Abbreviation	[Ag·AA·NO$_3$]$_{CPs}$	Abbreviation
[Cu·L-Arg·(NO$_3$)$_2$·H$_2$O]$_{CP}$	L-Arg·Cu	[Ag·L-Arg·NO$_3$·0.5H$_2$O]$_{CP}$ [55]	L-Arg·Ag
[Cu·DL-Arg·(NO$_3$)$_2$·H$_2$O]$_{CP}$	DL-Arg·Cu	[Ag·DL-Arg·NO$_3$·0.5H$_2$O]$_{CP}$	DL-Arg·Ag
[Cu·L-His·(NO$_3$)$_2$·H$_2$O]$_{CP}$ form I	L-His·Cu form I	[Ag·L-His·NO$_3$]$_{CP}$	L-His·Ag
[Cu·L-His·(NO$_3$)$_2$·H$_2$O]$_{CP}$ form II	L-His·Cu form II	/	/
[Cu·DL-His·(NO$_3$)$_2$·H$_2$O]$_{CP}$	DL-His·Cu	[Ag·DL-His·NO$_3$]$_{CP}$	DL-His·Ag
/	/	[Ag·*bis*(L-His)·NO$_3$·0.5H$_2$O]$_{CP}$ [56]	L-His$_2$·Ag
/	/	[Ag·*bis*(DL-His)·NO$_3$·0.5H$_2$O]$_{CP}$	DL-His$_2$·Ag

The copper coordination polymers were all characterized by single-crystal X-ray diffraction, whereas, in the silver cases, due to the difficulty in growing suitable single crystals, the structural characterization was based on a combination of X-ray powder diffraction (XRPD) and solid-state NMR (SSNMR) spectroscopy experiments. SSNMR is known to be highly complementary to diffraction methods, providing insight into the structural and dynamic features of solid materials. Its multinuclear approach, i.e., the possibility of probing the local environment of several NMR-active nuclei, is one of the main strengths of the technique. For instance, ^{13}C CPMAS spectra can give information about the purity and the degree of crystallinity of a sample, as well as the number of independent molecules in the unit cell. Moreover, the chemical shift of carboxylic moieties is quite sensitive to the protonation state of the acid group, or to the involvement of the carboxyl in the formation of hydrogen bonds, allowing for the distinction between salts and co-crystals [58]. Multinuclear SSNMR measurements have been carried out on the silver compounds listed above, as well as on the previously reported silver coordination polymers IWOFUX ([Ag·L-Arg·NO$_3$·0.5H$_2$O]$_{CP}$) [55] and TIGHEY ([Ag·*bis*(L-His)·NO$_3$·0.5H$_2$O]$_{CP}$) [56].

2.1. Structures of Enantiopure and Racemic [Cu·AA·(NO$_3$)$_2$]$_{CPs}$

As pointed out in the introduction and discussed later in this manuscript, one of the purposes of this work was to establish whether the enantiopure and racemic derivatives would show a different or similar antimicrobial activity when tested against the same bacteria strains (vide infra). However, hereafter, we focus on the remarkable structural analogies between the two pairs of compounds. All of the compounds are coordination polymers in which the amino acid molecules act as bridging ligands between the metal atoms. Because of the structural similarity between the arginine and histidine compounds, it is convenient to begin with a discussion of the structures of the two pairs of copper coordination polymers, namely, the arginine compounds L-Arg·Cu and DL-Arg·Cu and the histidine compounds L-His·Cu and DL-His·Cu. These compounds were obtained by reacting copper nitrate with the L-enantiomer and the DL racemic mixture of arginine and histidine, respectively. The coordination polymers consist of amino acid moieties (in zwitterionic form) bridging consecutive copper atoms. Both histidine and arginine link metals by a bidentate-chelating Cu—N(-CHRC)O—Cu unit on one side, and by a coordination O—Cu bond on the other side. In such a way, each copper atom formally receives three electron pairs from each amino acid molecule, fulfilling a distorted octahedral coordination via two interactions with nitrate ions and with one water molecule. The close resemblance between the resulting enantiopure and racemic chains in both the arginine and histidine compounds is remarkable, even more so because the same feature is shared by both the histidine and the arginine compounds. However, in the enantiopure polymers, the bridging ligands obviously have the same chirality, while in the racemic polymers, L and D enantiomers neatly alternate in the structure, but in such a way that the polymers always show an "enantiopure side". In other words, in the DL polymers, L and D enantiomers occupy opposite sites along the chains.

The polymeric chains in L-Arg·Cu and DL-Arg·Cu are compared in Figure 1, while those of the histidine compounds L-His·Cu and DL-His·Cu are compared in Figure 2.
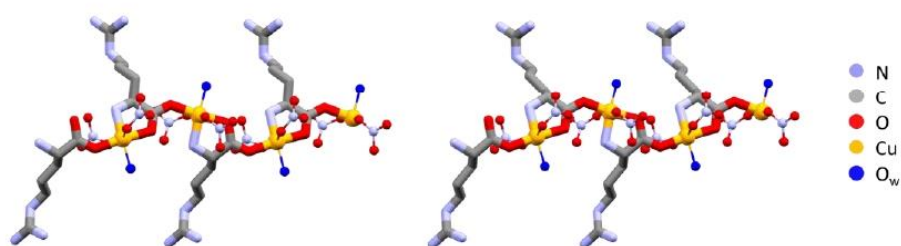
Figure 1. Polymeric chains in L-Arg·Cu (**left**) and DL-Arg·Cu (**right**). Note the remarkable structural similarity, with all arginine ligands having the same chirality on the left and alternate chirality on the right. Hydrogens omitted for clarity.
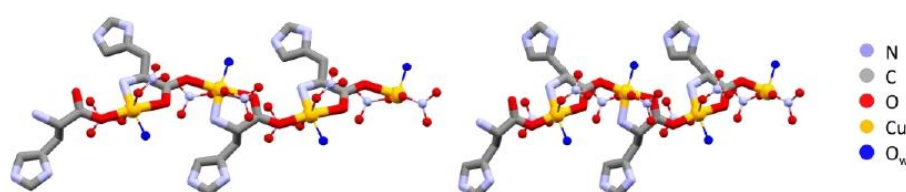
Figure 2. Polymeric chains in L-His·Cu form II (**left**) and DL-His·Cu (**right**). As in the case of arginine (Figure 1), the coordination polymers are structurally very similar despite the different chirality. Hydrogens omitted for clarity.

In the L-arginine case, the compound obtained from ball milling and from slurry show different diffraction patterns, i.e., different compounds were obtained, which calls for an explanation. While ball milling generates the 1:1 L-arginine–copper compound for which single crystals were also obtained, the slurry procedure yielded a compound with a powder pattern corresponding to the structure of the 2:1 derivative LAHNOX [59] for which a calculated pattern could be obtained from the data available in the Cambridge Structural Database (CSD). The four patterns are compared in Figure 3a. No such difference was otherwise observed when reacting DL-arginine. Figure 3b compares the powder diffraction calculated based on the single-crystal structure of DL-Arg·Cu with those measured on the sample obtained from slurry and from ball milling.
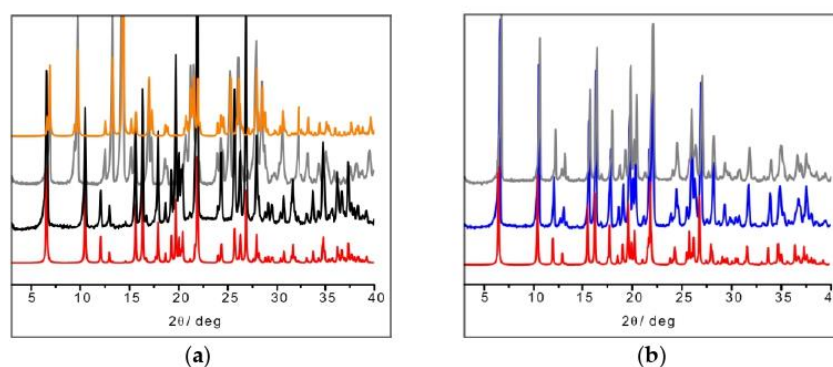
Figure 3. (**a**) From bottom to top: calculated pattern from single-crystal data of L-Arg·Cu (in red); powder pattern from ball milling experiment (in black); powder pattern from slurry experiment resulting in the more stable 2:1 product LAHNOX (in gray) and calculated pattern of LAHNOX [59] from database (in orange).; (**b**) From bottom to top: calculated pattern from single-crystal data of DL-Arg·Cu (in red); powder pattern from ball milling experiment (in blue) and from slurry (in gray).

The result in the case of L-His·Cu also deserves a closer look, since the crystallization product corresponding to the structure depicted in Figure 2 appears to be unstable with respect to a polymorphic transition upon manual grinding. After grinding, the powder pattern of the L-His·Cu compound closely resembles that calculated for the DL-His·Cu compound (Figure 4). It seems reasonable to conclude that the two polymorphs (I and II) of L-His·Cu are structurally very similar, with form I being the more stable phase.
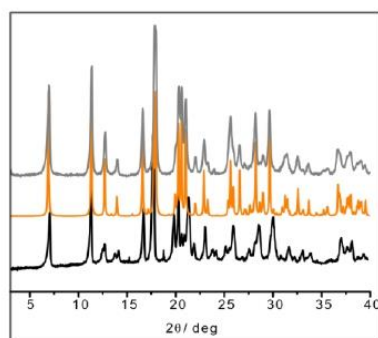
Figure 4. XRPD of ball-milling product of L-His·Cu (in black); calculated pattern from SCXRD of DL-His·Cu (in orange); XRPD of ball-milling product of DL-His·Cu synthesis (in gray).

2.2. Structures of Enantiopure and Racemic [Ag·AA·NO$_3$]$_{CPs}$

As pointed out in the Introduction, because of the paucity of structural information obtained from diffraction, we recurred to SSNMR spectroscopy to characterize the silver compounds. ^{13}C, ^{15}N, and ^{1}H are usually the nuclei of choice to detect the presence of hydrogen bonds and evaluate their strengths, as well as to ascertain whether a protonic transfer has occurred, i.e., whether a salt has formed [60]. Specifically, in the case of ^{15}N SSNMR spectra, the resonance frequency of nitrogen nuclei is significantly influenced by their partaking in protonic transfer or in the formation of hydrogen bonds. For example, the chemical shift of aliphatic nitrogen atoms increases by up to 20 ppm in the case of protonation; for an aromatic nitrogen, the change in chemical shift upon salification is much more pronounced, with a decrease of up to 120 ppm. In general, the entity of the change in the chemical shift of the signal of interest is related to the position of the proton along the hydrogen bond axis (i.e., it is less pronounced if the protonic transfer was not complete and a simple hydrogen bond was formed) [60]. Even in the case of metal coordination by a nitrogen-based moiety, the ^{15}N SSNMR chemical shift proves highly informative: both aliphatic and aromatic nitrogen atoms are shielded upon donation of their lone pairs, yielding lower chemical shifts for their signals in the complex [61,62].

^{13}C and ^{15}N CPMAS analyses were performed in the cases of L-His·Ag, DL-His·Ag, L-His$_2$·Ag [56], and DL-His$_2$·Ag. The full ^{13}C and ^{15}N CPMAS SSNMR spectra of the coordination polymers and the pure amino acids are reported in Figure S3A–D in the Supplementary Materials; isotropic ^{13}C and ^{15}N SSNMR chemical shift values and J$_{AgN}$ coupling constants for the pure amino acids and the obtained coordination polymers are reported in Table S3a,b, respectively, in the Supplementary Materials.
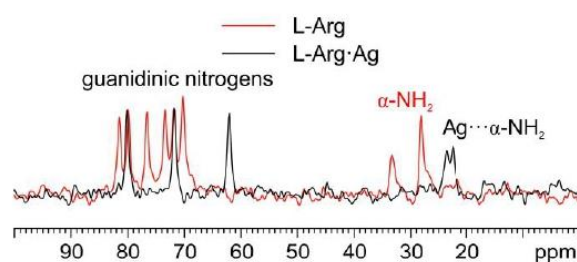
2.2.1. L-Arg·Ag and DL-Arg·Ag

Starting with the ^{13}C CPMAS spectra (Figure 5), the first observation is that while the spectrum of pure L-arginine (L-Arg) corresponds to that expected for the presence of two molecules in its asymmetric unit, the presence of a single set of resonances in the spectrum of L-Arg·Ag indicates that the coordination polymer only contains one amino acid molecule in the asymmetric unit. The spectrum also indicates that the crystalline powder of the obtained product corresponds to a pure compound of good crystallinity (average full width at half maximum, FWHM = 93 Hz).
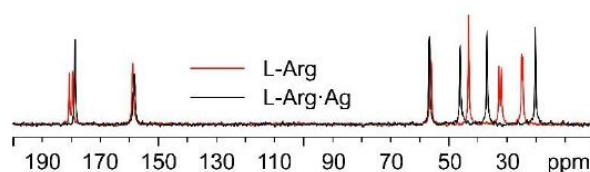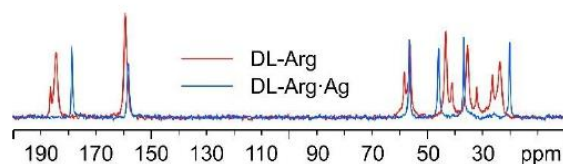
Figure 5. Overlay of the ^{13}C CPMAS spectra of L-Arg·Ag (in black) and pure L-Arg (in red).

As for the ^{15}N analyses (Figure 6), the observation of the shift towards lower frequencies of the α nitrogen signal (from 32.7 and 27.5 ppm in pure L-Arg to an average value of 23.0 ppm in L-Arg·Ag) and its splitting makes it possible to ascertain that the α-NH$_2$ group of L-Arg is the one coordinating Ag.


Figure 6. Overlay of a detail of the ^{15}N CPMAS spectra of L-Arg·Ag (in black) and pure L-Arg (in red).

In Figure 7, the ^{13}C CPMAS spectra of DL-Arg·Ag and pure DL-arginine (DL-Arg) are displayed. The overlay demonstrates that DL-Arg·Ag is a new pure and moderately crystalline (average FWHM = 95 Hz) phase, different from the pure AA.

**Figure 7.** Overlay of the ^{13}C CPMAS spectra of DL-Arg·Ag (in blue) and pure DL-Arg (in red).

Interestingly, as can be observed from Figure 8, the ^{13}C spectral features of DL-Arg·Ag coincide with those of L-Arg·Ag; this suggests that the two CPs are isomorphous, which may well be indicative of the formation of a conglomerate of crystals of L-Arg·Ag and of D-Arg·Ag. Indeed, this agrees with a possible spontaneous resolution of the DL-Arg·Ag racemic compound into crystals of L-Arg·Ag and of D-Arg·Ag, giving the same spectral features as those of enantiopure L-Arg·Ag. This likeness would also apply to the X-ray powder diffraction patterns.
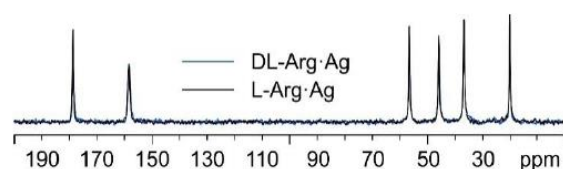
Figure 8. Overlay of the ^{13}C CPMAS spectra of L-Arg·Ag (in black) and DL-Arg·Ag (in blue).

The comparison of the powder diffraction patterns measured on DL-Arg·Ag and on L-Arg·Ag supports this hypothesis. As can be seen in Figure 9, the patterns coincide and

correspond to the pattern calculated on the basis of the single-crystal structure of L-Arg·Ag, for which data are available in the CSD.
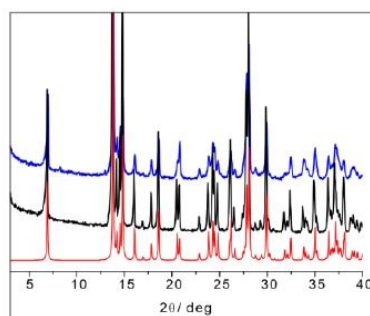
Figure 9. From bottom to top: calculated pattern from single-crystal data of IWOFUX (L-Arg·Ag) in red), experimental powder pattern of L-Arg·Ag (in black), and experimental powder pattern.

2.2.2. L-Arg·Ag and DL-Arg·Ag

As mentioned above, in the case of the L-histidine complexes for the sake of the identification of the reaction products, it is necessary to consider the formation of both the 1:1 and 1:2 compounds, namely, L-His·Ag and L-His$_2$·Ag. Figure 10 shows the comparison between the ^{13}C CPMAS spectra of L-His$_2$·Ag and pure L-histidine (L-His). A pure crystalline (average FWHM = 72 Hz) phase, different from the pure amino acid, was obtained, characterized by the presence of two independent molecules of L-His in the unit cell.
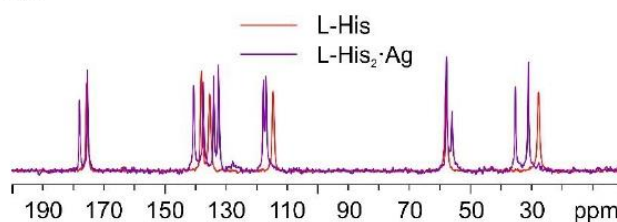
Figure 10. Overlay of the ^{13}C CPMAS spectra of L-His$_2$·Ag (in purple) and pure L-His (in red).

Figure 11 displays an overlay of the ^{15}N CPMAS spectrum of L-His$_2$·Ag with that of pure L-His. From the comparison, it is easy to notice how the α-NH$_3^+$ group of the pure amino acid stays charged in the coordination polymer, with the aromatic δ nitrogen being the one that binds the silver nucleus. This is proved by the shift of its ^{15}N signal from 245.7 ppm in pure L-His to 211.6 and 208.5 ppm (isotropic values) in the coordination polymer, for which the signals of both molecules of L-His are split by the $^{107/109}$Ag-^{15}N J-coupling [61].
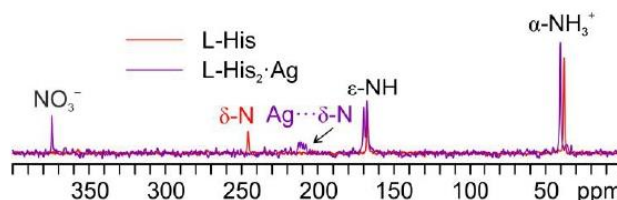

Figure 11. Overlay of a detail of the ^{15}N CPMAS spectra of L-His$_2$·Ag (in purple) and pure L-His (in red).

Regarding L-His·Ag, Figure 12 shows a comparison of its ^{13}C spectrum and that of pure L-His, as for the case of L-His$_2$·Ag above. As can be easily observed, the sharp signals

in the spectrum of L-His·Ag fall at different chemical shifts than those of the pure amino acid. Nonetheless, very broad shoulders at the base of said peaks clearly indicate the presence of consistent amounts of amorphous material. Moreover, the weak resonances at about 20, 60, and 80 ppm can be ascribed to impurities, possibly coming from the solvents used for the synthesis. All of this confirms the sample to be quite unstable, which made the acquisition of the ^{15}N CPMAS spectrum of L-His·Ag unfeasible.
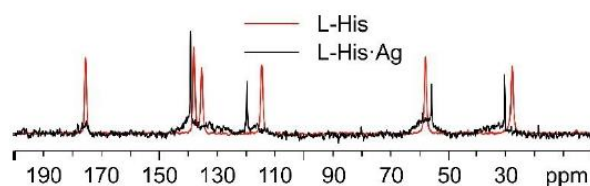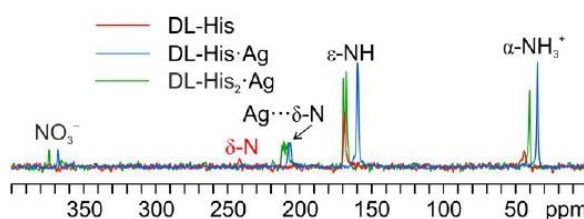

Figure 12. Overlay of the ^{13}C CPMAS spectra of L-His·Ag (in black) and pure L-His (in red).

As for DL-histidine (DL-His), two pure different crystalline phases were obtained, namely, DL-His·Ag and DL-His$_2$·Ag. This can be visually assessed from Figure 13, which displays their ^{13}C CPMAS spectra, together with that of pure DL-His.
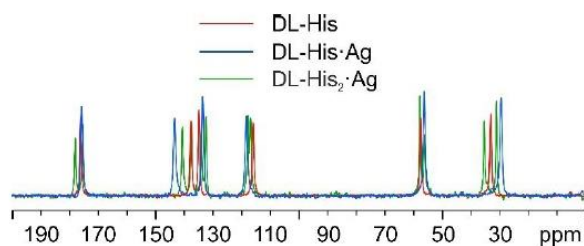
Figure 13. Overlay of the ^{13}C CPMAS spectra of DL-His$_2$·Ag (in green), DL-His·Ag (in blue), and pure DL-His (in red).

As in the other cases, the main piece of information about the identity of the coordinating N atom comes from a comparison of their ^{15}N CPMAS spectra (Figure 14).


Figure 14. Overlay of a detail of the ^{15}N CPMAS spectra of DL-His$_2$·Ag (in green), DL-His·Ag (in blue), and pure DL-His (in red).

Indeed, in both coordination polymers, the δ nitrogen is the one that binds Ag, as witnessed by the chemical shifts of the corresponding signals, i.e., 207.3 ppm in DL-His·Ag and 211.6/208.5 ppm in DL-His$_2$·Ag, with respect to that of the same nitrogen in pure DL-His (241.8 ppm). Moreover, in both spectra, the usual splitting of the resonances due to the coordinating N site can be observed.

Once again, by comparing the ^{13}C CPMAS spectra of L-His$_2$·Ag and DL-His$_2$·Ag (Figure 15), it is easy to notice that the two phases are isomorphous, as in the case of the L/DL-Arg systems.
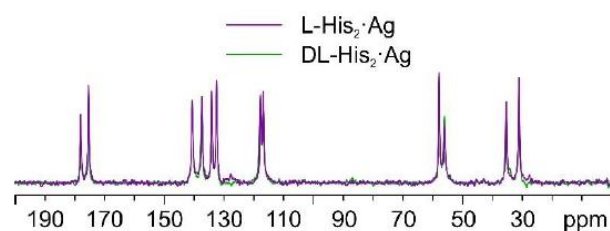
Figure 15. Overlay of the ^{13}C CPMAS spectra of L-His$_2$·Ag (in purple) and DL-His$_2$·Ag (in green).

The SSNMR information can thus be used to analyze the X-ray powder diffraction patterns in comparison with the available data from single-crystal structure determination retrieved from the CSD database. Figure 16a shows the calculated powder pattern on L-His$_2$·Ag (TIGHEY) [56] in comparison with the experimental XRPD pattern measure on the product from the slurry synthetic procedure of L-His$_2$·Ag (in black) and DL-His$_2$·Ag (in blue). The experimental XRPD patterns of the 1:1 compounds L-His·Ag and DL-His·Ag are also compared (Figure 16b).
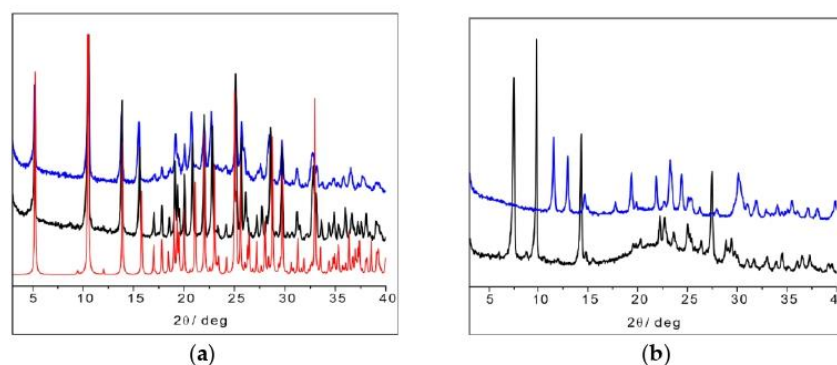

Figure 16. (**a**) L-His$_2$·Ag (TIGHEY) [56] calculated pattern from database (in red), experimental XRPD pattern from slurry synthetic procedure of L-His$_2$·Ag (in black), and DL-His$_2$·Ag (in blue); (**b**) experimental XRPD pattern from slurry of L-His·Ag (in black) and DL-His·Ag (in blue).

2.3. Antimicrobial Activity

The antimicrobial activity was evaluated using the established Kirby–Bauer disk diffusion assay [57]. As expected, silver nitrate gave robust antimicrobial activity with 10–15 mm zones of growth inhibition on lysogeny agar media plates. Copper nitrate provided slightly larger zones under these experimental conditions for *E. coli* and *S. aureus*. Smaller zones of inhibition were observed for each of the tested amino acids, except for L-Arg, where no inhibition was observed for the Gram-positive strain *S. aureus.* These data are shown in Figure S4A in the Supplementary Materials as zones of inhibition normalized to that of silver nitrate. Silver nitrate is a well-known antimicrobial agent and thus provides a good comparator for this study as well as an internal control to deal with plate-to-plate variation.

Figure 17A shows the normalized antimicrobial efficacy of silver nitrate and copper nitrate in combination with arginine or histidine as their coordination polymers. As a comparison, we performed direct mixing of the amino acid and the metal salt at a 1:1 ratio in order to determine whether the coordination polymer changed the antimicrobial properties (Figure 17B). Generally, there is not a large difference between the amino acids with metals presented as a combination versus a coordination polymer. Regardless, several combinations are shown to have antimicrobial activity superior to silver nitrate, particularly against *P. aeruginosa*. The variation between trials for all conditions was quite small at

+/− 0.05. Thus, for these figures, one is looking for the normalized value to be >1.05 for superior antimicrobial activity and <0.95 for decreased activity, compared to silver nitrate.
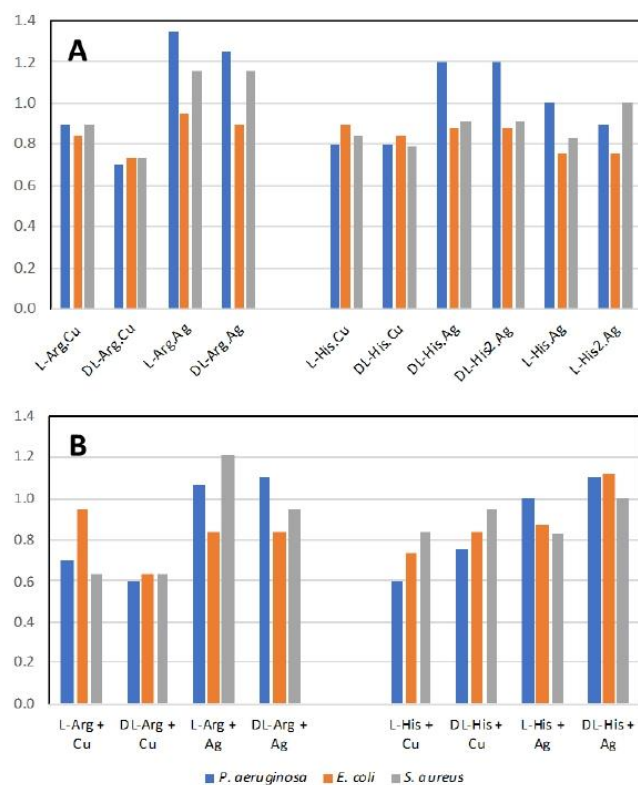
Figure 17. Antimicrobial activity. (**A**) Normalized antimicrobial activity from disk diffusion assay on lysogeny agar media for the coordination polymers of the metal salts with the amino acids; (**B**) mixture of the amino acid with the metal salt at 1:1 ratio. Values normalized to silver nitrate value of 1.0. Values above 1.05 are more antimicrobial than silver nitrate alone.

In our past studies, mechanochemistry was employed to co-crystallize antimicrobial metal salts with quaternary cation compound (QCC) antiseptics, such as proflavine [15,16]. In the present study, we replaced the QCC antiseptic with the biological cation compounds of the amino acids arginine and histidine and investigated their crystal structures and properties, as well as their antimicrobial activities to three different pathogen indicator strains. The amino acids on their own have low-level antimicrobial activity compared to silver (Figure S4A). However, from the literature, we may assume that a formulation containing amino acids with side chains in their cationic state, and acting in a "polymeric" structure type, can potentially exhibit antimicrobial activity similar to cationic antimicrobial peptides (CAPs). Since our compounds have a polymeric structure, they could be considered molecular mimes of CAPs. However, overall, we observed similar activities for when the metals and amino acids were simply mixed (Figure 17B). Although we do notice a substantial enhancement of the activity for the arginine–metal coordination polymer, we should consider that a similar structure of the coordination polymer may be produced in solution, as the amino acids can generate a pseudo-molecular organic framework or metallophore complex(es).

The effect of the difference of the amino acid enantiomer is that of repressing the antimicrobial activity of the copper coordination polymer with arginine when in racemic form. The same applies to Arg·Ag, but only for *P. aeruginosa*. A minor effect on the

antimicrobial activity was observed on comparing the racemic and enantiopure amino acid in the specific case of histidine coordination polymers with silver, particularly against *P. aeruginosa*. Combining the highly antimicrobial metal salt of copper nitrate with these amino acids reduces the antimicrobial activity. The simplest explanation for this is that the amino acid ligands form stable interactions both in solution and in the coordination polymer aggregate, thus diminishing the release of the metal ion and its bioavailability to attack the microbial cell biochemistry. On the other hand, mixing silver nitrate with the two amino acids led to superior antimicrobial activity against *P. aeruginosa* and *S. aureus*, suggesting that the amino acid ligands aid in silver ion delivery to the bacteria cells or enhance the amino acid cationic polymer character.

Further studies will tell whether the physicochemical nature of the co-crystal leads to superior 'drug-delivery' features over the combination of the components. There is a considerable need for biocompatible, eco-friendly, cost-effective antimicrobials with long term stability/activity in food packaging, cosmetic preservatives, and corrosion/biofouling control. It is in these areas that we envision possible applications of these and similar co-crystal compounds.

3. Materials and Methods

All reagents and solvents used in this work were purchased from Merck (Sigma-Aldrich) (Darmstadt, Germany) TCI Europe (Zwijndrecht, Belgium), or Fluorochem (Hadfield, UK) and then used without further purification.

3.1. Synthetic Procedures

All of the products were obtained using a 1:1 or 2:1 stoichiometry between the AA and the metal salts $AgNO_3$ or $Cu(NO_3)_2 \cdot 3H_2O$. All of the AAs were in their anhydrous form.

3.1.1. Synthesis from Slurry

$[Cu \cdot AA \cdot (NO_3)_2]_{CPs}$ and $[Ag \cdot AA \cdot NO_3]_{CPs}$ were synthesized from slurry in ethanol (0.5 mL) and water (0.5 mL) in a 1:1 stoichiometric ratio of the reactants. For each reactant, 1 mmol was used (mass quantities reported in Table 2) and the reaction was left to stir at room temperature for 3 days in a 10 mL glass vial closed with a *PE pressure plug*. The same procedure was applied for the synthesis of the 2:1 silver-coordination compounds, in which 0.5 mmol of silver nitrate was used instead. The solid products were recovered and analyzed after filtration and drying.

Table 2. Mass quantities of the materials used in the solid-state synthesis (expressed in mg).

	L-Arginine	DL-Arginine	L-Histidine	DL-Histidine	$AgNO_3$	$Cu(NO_3)_2 \cdot 3H_2O$
mg	174.20	174.20	155.16 (1:1)	155.16 (1:1)	169.87 (1:1)	241.55
mg	data	data	155.16 (2:1)	155.16 (2:1)	84.94 (2:1)	

3.1.2. Synthesis from Ball Milling

All of the $[Cu \cdot AA \cdot (NO_3)_2]_{CPs}$ were synthesized mechanochemically using a Retsch MM200 Mixer Mill (Verder Group, Haan, Germany), operated at a frequency of 25 Hz for 1 h, with 5 mL agate jars and 2 agate balls of 5 mm diameter, using a 1:1 mixture of ethanol and water (100 μL). The same methodology was also applied for the $[Ag \cdot AA \cdot NO_3]_{CPs}$, successfully obtaining L-Arg·Ag [55] and DL-Arg·Ag. For the $[Ag \cdot His \cdot NO_3]_{CPs}$ (L and DL), the synthesis gave slightly crystalline powders with quasi-amorphous patterns (synthesis scale 1 mmol, mass quantities as reported in Table 2). The products were left to dry out at room temperature, collected from the jar, and analyzed with XRPD.

3.1.3. Synthesis from Solution

$[Cu \cdot AA \cdot (NO_3)_2]_{CPs}$ were synthesized from a 1:1 solution of ethanol and water (1 mL) and 0.25 mmol of reactants; the mass quantities are reported in Table 3. Crystals suitable

for single-crystal X-ray analysis were collected 2 weeks after the slow evaporation of the solvent mixture. All of the attempts to crystallize the [Ag·AA·NO$_3$]$_{CPs}$ series led to the reduction of silver nitrate or to the obtainment of small sized crystals that were difficult to collect and analyze.

Table 3. Mass quantities of the materials used in the solution-based synthesis (expressed in mg).

	L-Arginine	DL-Arginine	L-Histidine	DL-Histidine	AgNO$_3$	Cu(NO$_3$)$_2$·3H$_2$O
mg	174.20	174.20	155.16 (1:1)	155.16 (1:1)	169.87 (1:1)	241.55
mg	data	data	155.16 (2:1)	155.16 (2:1)	84.94 (2:1)	

3.2. Solid-State Characterization

3.2.1. Single-Crystal X-ray Diffraction (SCXRD)

Structural data for [Cu·AA·(NO$_3$)$_2$]$_{CPs}$ were collected at room temperature with an Oxford Diffraction X'Calibur diffractometer (Rigaku, Tokyo, Japan) equipped with a graphite monochromator and a CCD detector. The unit cell parameters for all compounds discussed herein are reported in Table S1 in the Supplementary Materials. The structures were solved by the Intrinsic Phasing methods and refined by least squares methods against F^2 using SHELXT-2016 and SHELXL-2018 [63,64] with the Olex2 [65] interface. Non-hydrogen atoms were refined anisotropically. Hydrogen atoms were added in calculated positions. The software Mercury 2020.2.0 [66] was used to analyze and represent the crystal packing. Crystal data can be obtained free of charge via www.ccdc.cam.ac.uk/conts/retrieving.html (or from the Cambridge Crystallographic Data Centre, 12 Union Road, Cambridge CB21EZ, UK; fax: (+44)1223-336-033; or e-mail: deposit@ccdc.cam.ac.uk). CCDC 2238350-2238353.

3.2.2. Powder X-ray Diffraction (XRPD)

Room-temperature powder X-ray diffraction patterns were collected on a PANalytical X'Pert Pro automated diffractometer (was PHILIPS, now Malvern PANalytical-Spectris, London, UK) equipped with an X'Celerator detector in Bragg–Brentano geometry, using Cu Kα radiation (λ = 1.5418 Å) without monochromator in the 3–40° 2θ range (step size: 0.033°; time/step: 20 s; Soller slit: 0.04 rad; anti-scatter slit: ½; divergence slit: ¼; 40 mA*40 kV).

3.2.3. Variable-Temperature X-ray Powder Diffraction (VT-XRPD)

X-ray powder diffractograms in the 3–40° 2θ range were collected for L-His·Ag on a PANalytical X'Pert Pro automated diffractometer (was PHILIPS, now Malvern PANalytical-Spectris, London, UK) equipped with an X'Celerator detector and an Anton Paar TTK 450 system (Graz, Austria) for measurements at controlled temperature. Data were collected in open air in Bragg–Brentano geometry using Cu Kα radiation without a monochromator.

3.2.4. Differential Scanning Calorimetry (DSC)

DSC measurements were performed for all CPs with a Perkin–Elmer Diamond instrument (Waltham, MA, USA). The samples (3–5 mg) were placed in sealed aluminum pans, and heating was carried out at 5 °C min^{-1}.

3.2.5. Thermogravimetric Analysis (TGA)

TGA measurements for all CPs were performed using a Perkin-Elmer TGA7 instrument (Waltham, MA, USA) in the temperature range 35–350/400 °C under an N$_2$ gas flow, at a heating rate of 5 °C min^{-1}. Data for DSC and TGA results are reported in the Supplementary Materials, Table S2.

3.2.6. Solid-State NMR (SSNMR)

The solid-state ^{13}C and ^{15}N CPMAS spectra were acquired with a Jeol (Tokyo, Japan) ECZR 600 instrument, operating at 600.17, 150.91, and 60.81 MHz, respectively, for ^{1}H,

^{13}C, and ^{15}N nuclei. The powder samples were packed into a cylindrical zirconia rotor with a 3.2 mm o.d. and a 60 µL volume. A certain amount of sample was collected from each batch and used without further preparations to fill the rotor. The ^{13}C CPMAS spectra were acquired at room temperature, at a spinning speed of 20 kHz, using a ramp cross-polarization pulse sequence with a 90° ^{1}H pulse of 2.0 µs and a contact time of 3.5 ms. An optimized recycle delay ranging from 1.1 to 29.7 s was used for a number of scans in the 20–22,000 range, depending on the sample. The ^{15}N CPMAS spectra were acquired at room temperature, at a spinning speed of 12 kHz, using a ramp cross-polarization pulse sequence with a 90° ^{1}H pulse of 2.0 µs and a contact time of 0.5, 1 or 4 ms, depending on the sample. An optimized recycle delay ranging from 1.1 to 29.7 s was used for a number of scans in the 2000–80,000 range, depending on the sample. For every spectrum, a two-pulse phase modulation (TPPM) decoupling scheme was used, with a radiofrequency field of 108.5 kHz. The ^{13}C chemical shift scale was calibrated through the carboxylic signal of external standard glycine (at 176.5 ppm); the ^{15}N chemical shift scale was calibrated through the signal of external standard glycine (at 33.4 ppm with reference to NH$_3$).

3.3. Antimicrobial Activity

3.3.1. Strains and Growth Medium

Pseudomonas aeruginosa ATCC27853, *Escherichia coli* ATCC25922, and *Staphylococcus aureus* indicator strains were used in this study. Lysogeny broth (LB) was prepared in distilled water with 10 g/L NaCl (VWR International Co., Mississauga, ON, Canada), 5 g/L yeast extract (EMD Chemicals Inc., Darmstadt, Germany), and 10 g/L tryptone (VWR Chemicals LLC, Solon, OH, USA). The agar medium for the disk diffusion assays was obtained by adding 15 g/L bacteriological agar (VWR International LLC, Solon, OH, USA) to the above-mentioned LB. Frozen cultures were revived on LB agar plates overnight at 37 °C. Colonies were transferred to liquid LB using a sterile cotton swab and incubated for 16 h at 37 °C and 150 rpm shaking, and this saturated culture was then used for the inoculant for the disk diffusion assay.

3.3.2. Disk Diffusion Assay

In an aseptic environment, 150 µL of overnight culture was spread on LB agar plates per each organism and left to dry at room temperature for 1 h. Then, 25 mg/mL stock solutions or suspensions of CPs and initial compounds were prepared from powder. Controls of initial compounds were prepared as mixtures by 1:1 mixing of the 25 mg/mL stocks (i.e., 12.5 mg/mL final concentration of each compound). Kirby–Bauer blank disks were placed into a vial with 300 µL of a solution or suspension of the compound(s) of interest and left to soak for 30 min with mixing every 10 min by the inversion of the vial. The disks were then transferred to the agar culture plates (total of two replicates per compound per organism) and the plates were left in the incubator at 37 °C for 24 h, where the zone of growth inhibition was measured. Three of these biological trials were performed. To address plate-to-plate and trial variance, the average zone of inhibition measurement in mm was normalized where the zone for disk containing silver nitrate (placed on every plate) was defined as a zone of 1.0 in each biological replicate. Overall, the variance in this approach is 0.05 normalized units. This then gives an effective break point for any value >1.05 to have greater antimicrobial activity than the comparator of silver nitrate.

4. Conclusions

Solid formulations of metal complexes of active ingredients are being investigated for antimicrobial applications, particularly in response to the increasing threat of antimicrobial resistance. The co-crystallization of organic active molecules, such as active pharmaceutical ingredients (APIs) or naturally occurring antimicrobials or inorganic metals and complexes, has proved a fruitful way to access a great variety of new compounds, which may integrate or replace existing antimicrobials experiencing resistance. As a part of our ongoing studies, we have shown, for example, that proflavine co-crystals of metal complexes with silver,

copper, zinc, and gallium can be used selectively for the best results against different bacteria strains and growth states [67].

In this paper, we investigated a family of complexes obtained by the mechanochemical and solution co-crystallization of copper and silver salts with the amino acids arginine and histidine in both enantiopure and racemic forms. The goal of this work was manifold. First, we aimed to explore the outcome of the co-crystallization of the metal salts silver nitrate and copper nitrate with arginine and histidine, which resulted in the formation of novel coordination polymers that required a combination of single-crystal and powder diffraction as well as of solid-state NMR experiments for their characterization.

In terms of structures, the two pairs of copper coordination polymers, namely, the arginine compounds L-Arg·Cu and DL-Arg·Cu and the histidine compounds L-His·Cu and DL-His·Cu, have been found to show remarkable similarities. Not only do they form isostructural coordination polymers, with the amino acid ligands bridging consecutive copper atoms, but also show that, in the DL cases, amino acids of the same chirality occupy the same side along the chains. As a consequence, the enantiopure and racemic coordination polymers are basically isostructural. Multinuclear ^{15}N and ^{13}C CPMAS solid-state NMR spectroscopy also revealed the same structural relationship between the L- and DL-pairs of the L/DL-Arg as well as of the L-His$_2$·Ag and DL-His$_2$·Ag systems.

We also evaluated the potential antibacterial activity of the resulting coordination polymers against common bacterial strains. The consequence of using both the enantiopure and the racemic amino acids in the formation of the coordination polymers was also investigated, as it was the possible presence of any "chiral preference" in the interaction of the enantiopure or racemic products with the bacteria. Even though chirality seems to add nuances to the antibacterial capacity of the compounds, our primary observation is that the amino acids arginine and histidine form coordination polymers with silver and copper, which had a level of antimicrobial activity with primary differences depending on the nature of the metal atom. Overall, this study lends further support to the idea that co-crystallization, especially in solvent-free conditions, is a cheap and effective way to explore the possibility of enhancing the properties of crystal formers, whether as a combination of active organic molecules with other organic ones or with inorganic partners. The mechanism of interactions of the coordination polymers with the bacteria membranes remains to be fully understood and will be the subject of future work.

References

1. Antimicrobial Resistance. Available online: https://www.who.int/news-room/fact-sheets/detail/antimicrobial-resistance (accessed on 23 January 2023).
2. Antimicrobial Resistance | European Medicines Agency. Available online: https://www.ema.europa.eu/en/human-regulatory/overview/public-health-threats/antimicrobial-resistance (accessed on 23 January 2023).
3. Turner, R.J. Metal-Based Antimicrobial Strategies. *Microb. Biotechnol.* **2017**, *10*, 1062–1065. [CrossRef] [PubMed]

4. Wright, J.B.; Lam, K.; Burrell, R.E. Wound Management in an Era of Increasing Bacterial Antibiotic Resistance: A Role for Topical Silver Treatment. *Am. J. Infect. Control* **1998**, *26*, 572–577. [CrossRef] [PubMed]

5. Haas, K.L.; Franz, K.J. Application of Metal Coordination Chemistry to Explore and Manipulate Cell Biology. *Chem. Rev.* **2009**, *109*, 4921–4960. [CrossRef]

6. Lemire, J.A.; Kalan, L.; Gugala, N.; Bradu, A.; Turner, R.J. Silver Oxynitrate–an Efficacious Compound for the Prevention and Eradication of Dual-Species Biofilms. *Biofouling* **2017**, *33*, 460–469. [CrossRef] [PubMed]

7. Levy, S.B.; Bonnie, M. Antibacterial Resistance Worldwide: Causes, Challenges and Responses. *Nat. Med.* **2004**, *10*, S122–S129. [CrossRef]

8. Lewis, K. Persister Cells: Molecular Mechanisms Related to Antibiotic Tolerance. Antibiotic Resistance. *Handb. Exp. Pharmacol.* **2011**, *211*, 121–133. [CrossRef]

9. Frei, A.; Verderosa, A.D.; Elliott, A.G.; Zuegg, J.; Blaskovich, M.A. Metals to combat antimicrobial resistance. *Nat. Rev. Chem.* **2023**. [CrossRef]

10. Pettinari, C.; Pettinari, R.; Di Nicola, C.; Tombesi, A.; Scuri, S.; Marchetti, F. Antimicrobial MOFs. *Coord. Chem. Rev.* **2021**, *446*, 214121. [CrossRef]

11. Jaros, S.W.; Król, J.; Bazanów, B.; Poradowski, D.; Chrószcz, A.; Nesterov, D.S.; Kirillov, A.M.; Smoleński, P. Antiviral, Antibacterial, Antifungal, and Cytotoxic Silver(I) BioMOF Assembled from 1,3,5-Triaza-7-Phoshaadamantane and Pyromellitic Acid. *Molecules* **2020**, *25*, 2119. [CrossRef]

12. Jaros, S.W.; Guedes Da Silva, M.F.C.; Florek, M.; Smoleński, P.; Pombeiro, A.J.L.; Kirillov, A.M. Silver(I) 1,3,5-Triaza-7-Phosphaadamantane Coordination Polymers Driven by Substituted Glutarate and Malonate Building Blocks: Self-Assembly Synthesis, Structural Features, and Antimicrobial Properties. *Inorg. Chem.* **2016**, *55*, 5886–5894. [CrossRef]

13. Wu, F.; He, D.; Chen, L.; Liu, F.; Huang, H.; Dai, J.; Zhang, S.; You, J. Antibacterial Coordination Polymer Hydrogels Composed of Silver(I)-PEGylated Bisimidazolylbenzyl Alcohol. *RSC Adv.* **2018**, *8*, 20829–20835. [CrossRef] [PubMed]

14. Yamamoto, Y.; Morikawa, T.; Kawai, T.; Nonomura, Y. Selective Bactericidal Activity of Divalent Metal Salts of Lauric Acid. *ACS Omega* **2017**, *2*, 113–121. [CrossRef] [PubMed]

15. Shemchuk, O.; Braga, D.; Grepioni, F.; Turner, R.J. Co-Crystallization of Antibacterials with Inorganic Salts: Paving the Way to Activity Enhancement. *RSC Adv.* **2020**, *10*, 2146–2149. [CrossRef] [PubMed]

16. Fiore, C.; Shemchuk, O.; Grepioni, F.; Turner, R.J.; Braga, D. Proflavine and Zinc Chloride "Team Chemistry": Combining Antibacterial Agents via Solid-State Interaction. *CrystEngComm* **2021**, *23*, 4494–4499. [CrossRef]

17. Fiori, A.T.M.; Nakahata, D.H.; Cuin, A.; Lustri, W.R.; Corbi, P.P. Synthesis, Crystallographic Studies, High Resolution Mass Spectrometric Analyses and Antibacterial Assays of Silver(I) Complexes with Sulfisoxazole and Sulfadimethoxine. *Polyhedron* **2017**, *121*, 172–179. [CrossRef]

18. Matiadis, D.; Karagiaouri, M.; Mavroidi, B.; Nowak, K.E.; Katsipis, G.; Pelecanou, M.; Pantazaki, A.; Sagnou, M. Synthesis and Antimicrobial Evaluation of a Pyrazoline-Pyridine Silver(I) Complex: DNA-Interaction and Anti-Biofilm Activity. *BioMetals* **2021**, *34*, 67–85. [CrossRef]

19. Generally Recognized as Safe (GRAS) | FDA. Available online: https://www.fda.gov/food/food-ingredients-packaging/generally-recognized-safe-gras (accessed on 23 January 2023).

20. Lansdown, A.B.G. Silver in Health Care: Antimicrobial Effects and Safety in Use. *Curr. Probl. Dermatol.* **2006**, *33*, 17–34. [CrossRef] [PubMed]

21. Mijnendonckx, K.; Leys, N.; Mahillon, J.; Silver, S.; Van Houdt, R. Antimicrobial Silver: Uses, Toxicity and Potential for Resistance. *BioMetals* **2013**, *26*, 609–621. [CrossRef] [PubMed]

22. Mitra, D.; Kang, E.T.; Neoh, K.G. Antimicrobial Copper-Based Materials and Coatings: Potential Multifaceted Biomedical Applications. *ACS Appl. Mater. Interfaces* **2020**, *12*, 21159–21182. [CrossRef]

23. Dollwet, H.; Sorenson, J. *Historic Uses of Copper Compounds in Medicine. Trace Elements in Medicine*, 2nd ed.; The Humana Press Inc.: Clifton, AR, USA, 2001.

24. Casey, A.L.; Adams, D.; Karpanen, T.J.; Lambert, P.A.; Cookson, B.D.; Nightingale, P.; Miruszenko, L.; Shillam, R.; Christian, P.; Elliott, T.S.J. Role of Copper in Reducing Hospital Environment Contamination. *J. Hosp. Infect.* **2010**, *74*, 72–77. [CrossRef]

25. Airey, P.; Verran, J. Potential Use of Copper as a Hygienic Surface; Problems Associated with Cumulative Soiling and Cleaning. *J. Hosp. Infect.* **2007**, *67*, 271–277. [CrossRef]

26. Wang, Y.; Zhang, W.; Yao, Q. Copper-Based Biomaterials for Bone and Cartilage Tissue Engineering. *J. Orthop. Transl.* **2021**, *29*, 60–71. [CrossRef]

27. Shen, Q.; Qi, Y.; Kong, Y.; Bao, H.; Wang, Y.; Dong, A.; Wu, H.; Xu, Y. Advances in Copper-Based Biomaterials With Antibacterial and Osteogenic Properties for Bone Tissue Engineering. *Front. Bioeng. Biotechnol.* **2022**, *9*, 1526. [CrossRef] [PubMed]

28. Quaranta, D.; Krans, T.; Santo, C.E.; Elowsky, C.G.; Domaille, D.W.; Chang, C.J.; Grass, G. Mechanisms of Contact-Mediated Killing of Yeast Cells on Dry Metallic Copper Surfaces. *Appl. Environ. Microbiol.* **2011**, *77*, 416–426. [CrossRef] [PubMed]

29. Santo, C.E.; Lam, E.W.; Elowsky, C.G.; Quaranta, D.; Domaille, D.W.; Chang, C.J.; Grass, G. Bacterial Killing by Dry Metallic Copper Surfaces. *Appl. Environ. Microbiol.* **2011**, *77*, 794–802. [CrossRef] [PubMed]

30. Grass, G.; Rensing, C.; Solioz, M. Metallic Copper as an Antimicrobial Surface. *Appl. Environ. Microbiol.* **2011**, *77*, 1541–1547. [CrossRef]

31. Sánchez-Sanhueza, G.; Fuentes-Rodríguez, D.; Bello-Toledo, H. Copper Nanoparticles as Potential Antimicrobial Agent in Disinfecting Root Canals: A Systematic Review. *Int. J. Odontostomatol.* **2016**, *10*, 547–554. [CrossRef]

32. Gungor, O.; Kocer, F.; Kose, M. Cu(II) Complexes of Biguanidine Ligands: Structural Characterisation, DNA Binding and Antimicrobial Properties. *J. Mol. Struct.* **2020**, *1204*, 127533. [CrossRef]

33. Zalevskaya, O.A.; Gur'eva, Y.A. Recent Studies on the Antimicrobial Activity of Copper Complexes. *Russ. J. Coord. Chem. Khimiya* **2021**, *47*, 861–880. [CrossRef]

34. Grepioni, F.; Casali, L.; Fiore, C.; Mazzei, L.; Sun, R.; Shemchuk, O.; Braga, D. Steps towards a nature inspired inorganic crystal engineering. *Dalton Trans.* **2022**, *51*, 7390–7400. [CrossRef]

35. Celik, S.; Yurdakul, S.; Erdem, B. New Silver(I) Complex as Antibiotic Candidate: Synthesis, Spectral Characterization, DFT, QTAIM and Antibacterial Investigations and Docking Properties. *J. Mol. Struct.* **2022**, *1261*, 132902. [CrossRef]

36. Lansdown, A.B. Silver I: Its Antibacterial Properties and Mechanism of Action. *J. Wound Care* **2013**, *11*, 125–130. [CrossRef] [PubMed]

37. Dakal, T.C.; Kumar, A.; Majumdar, R.S.; Yadav, V. Mechanistic Basis of Antimicrobial Actions of Silver Nanoparticles. *Front. Microbiol.* **2016**, *7*, 1831. [CrossRef]

38. Hong, R.; Kang, T.Y.; Michels, C.A.; Gadura, N. Membrane Lipid Peroxidation in Copper Alloy-Mediated Contact Killing of Escherichia Coli. *Appl. Environ. Microbiol.* **2012**, *78*, 1776–1784. [CrossRef]

39. Tian, W.X.; Yu, S.; Ibrahim, M.; Almonaofy, A.W.; He, L.; Hui, Q.; Bo, Z.; Li, B.; Xie, G. lin Copper as an Antimicrobial Agent against Opportunistic Pathogenic and Multidrug Resistant Enterobacter Bacteria. *J. Microbiol.* **2012**, *50*, 586–593. [CrossRef]

40. Mathews, S.; Hans, M.; Mücklich, F.; Solioz, M. Contact Killing of Bacteria on Copper Is Suppressed If Bacterial-Metal Contact Is Prevented and Is Induced on Iron by Copper Ions. *Appl. Environ. Microbiol.* **2013**, *79*, 2605–2611. [CrossRef]

41. Gutierrez, H.; Portman, T.; Pershin, V.; Ringuette, M. Evaluation of Biocidal Efficacy of Copper Alloy Coatings in Comparison with Solid Metal Surfaces: Generation of Organic Copper Phosphate Nanoflowers. *J. Appl. Microbiol.* **2013**, *114*, 680–687. [CrossRef] [PubMed]

42. Nowak, M.G.; Skwarecki, A.S.; Milewska, M.J. Amino Acid Based Antimicrobial Agents—Synthesis and Properties. *ChemMedChem* **2021**, *16*, 3513–3544. [CrossRef]

43. Cutrona, K.J.; Kaufman, B.A.; Figueroa, D.M.; Elmore, D.E. Role of Arginine and Lysine in the Antimicrobial Mechanism of Histone-Derived Antimicrobial Peptides. *FEBS Lett.* **2015**, *589*, 3915–3920. [CrossRef]

44. Sepahi, M.; Jalal, R.; Mashreghi, M. Antibacterial Activity of Poly-l-Arginine under Different Conditions. *Iran. J. Microbiol.* **2017**, *9*, 103–111.

45. Kacprzyk, L.; Rydengård, V.; Mörgelin, M.; Davoudi, M.; Pasupuleti, M.; Malmsten, M.; Schmidtchen, A. Antimicrobial Activity of Histidine-Rich Peptides Is Dependent on Acidic Conditions. *Biochim. Biophys. Acta—Biomembr.* **2007**, *1768*, 2667–2680. [CrossRef] [PubMed]

46. Minami, M.; Ando, T.; Hashikawa, S.N.; Torii, K.; Hasegawa, T.; Israel, D.A.; Ina, K.; Kusugami, K.; Goto, H.; Ohta, M. Effect of Glycine on Helicobacter Pylori in Vitro. *Antimicrob. Agents Chemother.* **2004**, *48*, 3782–3788. [CrossRef]

47. Kalarani, R.; Sankarganesh, M.; Kumar, G.G.V.; Kalanithi, M. Synthesis, Spectral, DFT Calculation, Sensor, Antimicrobial and DNA Binding Studies of Co(II), Cu(II) and Zn(II) Metal Complexes with 2-Amino Benzimidazole Schiff Base. *J. Mol. Struct.* **2020**, *1206*, 127725. [CrossRef]

48. Repon, R.; Islam, T.; Sadia, H.T.; Mikučionienė, D.; Hossain, S.; Kibria, G.; Kaseem, M. Development of Antimicrobial Cotton-Fabric-Impregnating AgNPs Utilizing Contemporary Practice. *Coatings* **2021**, *11*, 1413. [CrossRef]

49. Kasuga, N.C.; Takagi, Y.; Tsuruta, S.I.; Kuwana, W.; Yoshikawa, R.; Nomiya, K. Synthesis, Structure and Antimicrobial Activities of Meso Silver(I) Histidinate [Ag2(D-His)(L-His)]n (Hhis = Histidine) Showing Different Self-Assembly from Those of Chiral Silver(I) Histidinates. *Inorg. Chim. Acta* **2011**, *368*, 44–48. [CrossRef]

50. Nomiya, K.; Takahashi, S.; Noguchi, R.; Nemoto, S.; Takayama, T.; Oda, M. Synthesis and Characterization of Water-Soluble Silver(I) Complexes with L-Histidine (H2his) and (S)-(-)-2-Pyrrolidone-5-Carboxylic Acid (H2pyrrld) Showing a Wide Spectrum of Effective Antibacterial and Antifungal Activities. Crystal Structures of Chiral Helical Polymers [Ag(Hhis)](n) and {[Ag(Hpyrrld)]2}(n) in the Solid State. *Inorg. Chem.* **2000**, *39*, 3301–3311. [CrossRef]

51. Legler, A.V.; Kazachenko, A.S.; Kazbanov, V.I.; Per'yanova, O.V.; Veselova, O.F. Synthesis and Antimicrobial Activity of Silver Complexes with Arginine and Glutamic Acid. *Pharm. Chem. J.* **2001**, *35*, 501–503. [CrossRef]

52. Abuskhuna, S.; Briody, J.; McCann, M.; Devereux, M.; Kavanagh, K.; Fontecha, J.B.; McKee, V. Synthesis, Structure and Anti-Fungal Activity of Dimeric Ag(I) Complexes Containing Bis-Imidazole Ligands. *Polyhedron* **2004**, *23*, 1249–1255. [CrossRef]

53. Nomiya, K.; Tsuda, K.; Sudoh, T.; Oda, M. Ag(I)-N Bond-Containing Compound Showing Wide Spectra in Effective Antimicrobial Activities: Polymeric Silver(I) Imidazolate. *J. Inorg. Biochem.* **1997**, *68*, 39–44. [CrossRef]

54. Kasuga, N.C.; Yoshikawa, R.; Sakai, Y.; Nomiya, K. Syntheses, Structures, and Antimicrobial Activities of Remarkably Light-Stable and Water-Soluble Silver Complexes with Amino Acid Derivatives, Silver(I) N-Acetylmethioninates. *Inorg. Chem.* **2012**, *51*, 1640–1647. [CrossRef]

55. Ahmad, S.; Yousaf, A.; Tahir, M.N.; Isab, A.A.; Monim-Ul-Mehboob, M.; Linert, W.; Saleem, M. Structural Characterization and Antimicrobial Activity of a Silver(I) Complex of Arginine. *J. Struct. Chem.* **2016**, *56*, 1653–1657. [CrossRef]

56. Mirolo, L.; Schmidt, T.; Eckhardt, S.; Meuwly, M.; Fromm, K.M. PH-Dependent Coordination of AgI Ions by Histidine: Experiment, Theory, and a Model for SilE. *Chem. Eur. J.* **2013**, *19*, 1754–1761. [CrossRef]

57. Balouiri, M.; Sadiki, M.; Ibnsouda, S.K. Methods for in Vitro Evaluating Antimicrobial Activity: A Review. *J. Pharm. Anal.* **2016**, *6*, 71–79. [CrossRef]

58. Aramini, A.; Bianchini, G.; Lillini, S.; Bordignon, S.; Tomassetti, M.; Novelli, R.; Mattioli, S.; Lvova, L.; Paolesse, R.; Chierotti, M.R.; et al. Unexpected Salt/Cocrystal Polymorphism of the Ketoprofen–Lysine System: Discovery of a New Ketoprofen–l-Lysine Salt Polymorph with Different Physicochemical and Pharmacokinetic Properties. *Pharmaceuticals* **2021**, *14*, 555. [CrossRef] [PubMed]

59. Hu, R.; Yu, Q.; Liang, F.; Ma, L.; Chen, X.; Zhang, M.; Liang, H.; Yu, K. Syntheses and Crystal Structures of Cis—And Trans-Copper(II) Complexes of L-Arginine. *J. Coord. Chem.* **2008**, *61*, 1265–1271. [CrossRef]

60. Cerreia Vioglio, P.; Chierotti, M.R.; Gobetto, R. Pharmaceutical Aspects of Salt and Cocrystal Forms of APIs and Characterization Challenges. *Adv. Drug Deliv. Rev.* **2017**, *117*, 86–110. [CrossRef]

61. Daolio, A.; Pizzi, A.; Calabrese, M.; Terraneo, G.; Bordignon, S.; Frontera, A.; Resnati, G. Molecular Electrostatic Potential and Noncovalent Interactions in Derivatives of Group 8 Elements. *Angew. Chemie Int. Ed.* **2021**, *60*, 20723–20727. [CrossRef]

62. Pettinari, R.; Marchetti, F.; Pettinari, C.; Condello, F.; Skelton, B.W.; White, A.H.; Chierotti, M.R.; Gobetto, R. Self-Assembly of Arene Ruthenium Acylpyrazolone Fragments to Tetranuclear Metallacycles. Molecular Structures and Solid-State 15N CPMAS NMR Correlations. *Dalt. Trans.* **2016**, *45*, 3974–3982. [CrossRef]

63. Sheldrick, G. SHELXT: Integrating Space Group Determination and Structure Solution. *Acta Crystallogr. Sect. A Found. Adv.* **2014**, *70*, C1437. [CrossRef]

64. Sheldrick, G.M. SHELXT—Integrated Space-Group and Crystal-Structure Determination. *Acta Crystallogr. Sect. A Found. Crystallogr.* **2015**, *71*, 3–8. [CrossRef]

65. Dolomanov, O.V.; Bourhis, L.J.; Gildea, R.J.; Howard, J.A.K.; Puschmann, H. OLEX2: A Complete Structure Solution, Refinement and Analysis Program. *J. Appl. Crystallogr.* **2009**, *42*, 339–341. [CrossRef]

66. MacRae, C.F.; Sovago, I.; Cottrell, S.J.; Galek, P.T.A.; McCabe, P.; Pidcock, E.; Platings, M.; Shields, G.P.; Stevens, J.S.; Towler, M.; et al. Mercury 4.0: From Visualization to Analysis, Design and Prediction. *J. Appl. Crystallogr.* **2020**, *53*, 226–235. [CrossRef] [PubMed]

67. Lekhan, A.; Fiore, C.; Shemchuk, O.; Grepioni, F.; Braga, D.; Turner, R.J. Comparison of Antimicrobial and Antibiofilm Activity of Proflavine Co-crystallized with Silver, Copper, Zinc, and Gallium Salts. *ACS Appl. Biomat.* **2022**, *5*, 4203–4212. [CrossRef]

2.3.1 Supporting information

Mechanochemical preparation, solid-state characterization, and antimicrobial performance of copper and silver nitrate coordination polymers with L-and DL-arginine and histidine.

Cecilia Fiore[1], Andrii Lekhan[2], Simone Bordignon[3], Michele R. Chierotti[3], Roberto Gobetto[3*], Fabrizia Grepioni[1], Raymond J. Turner[2*] and Dario Braga[3*]

[1]Dipartimento di Chimica "Giacomo Ciamician", University of Bologna, Via Selmi, 2 – 40126 Bologna – Italy.
[2]Department of Biological Sciences, University of Calgary, 2500 University Drive NW, Calgary, Alberta T2N 1N4 – Canada.
[3]Department of Chemistry and NIS Centre, University of Turin, Via P. Giuria, 7 – 10125 Torino – Italy.
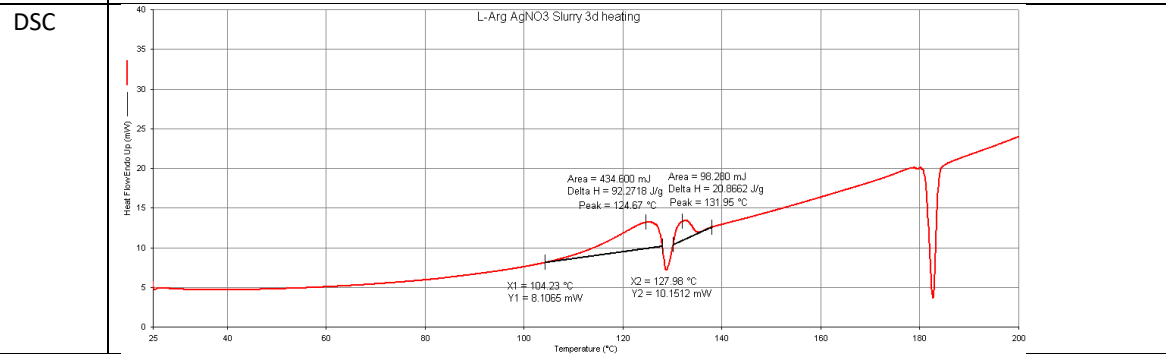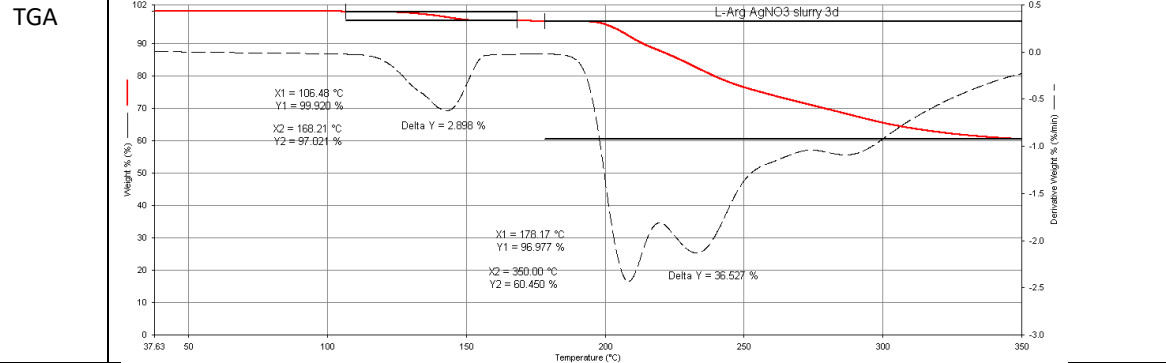
CRYSTALLOGRAPHIC DATA

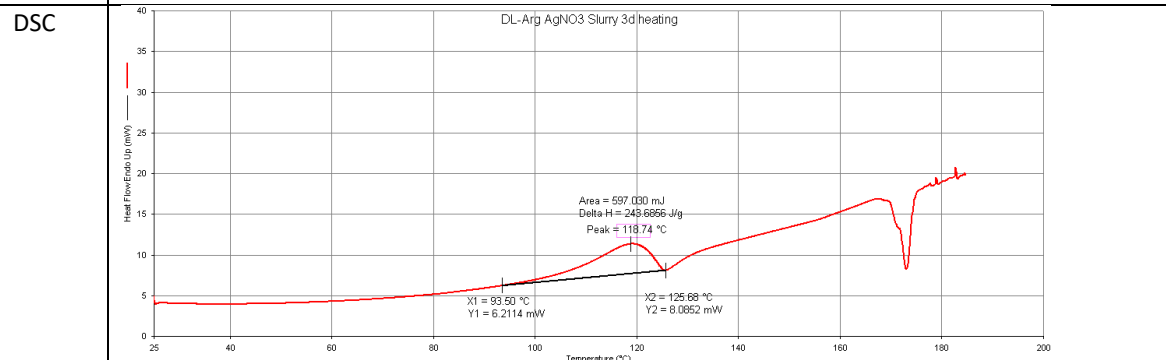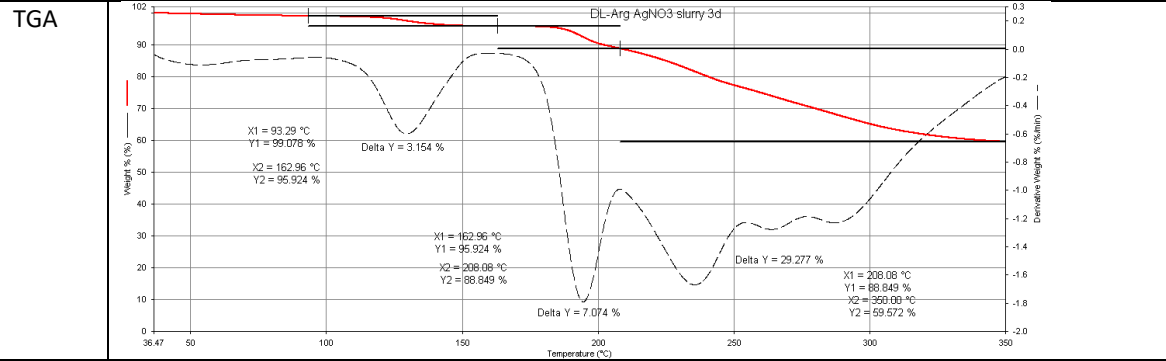| Table S1. Crystallographic table for data obtained from single-crystal XRD.				
	L-Arg·Cu	**DL-Arg·Cu**	**L-His·Cu**	**DL-His·Cu**
Chemical formula	$C_6H_{14}N_6O_8Cu\cdot H_2O$	$C_6H_{14}N_6O_8Cu\cdot H_2O$	$C_6H_9N_5O_8Cu\cdot H_2O$	$C_6H_9N_5O_8Cu\cdot H_2O$
M_r /g mol^{-1}	379.79	379.79	720.61	360.74
Crystal system	Monoclinic	Monoclinic	Monoclinic	Monoclinic
Space group	$P2_1$	$P2_1/c$	$P2_1$	$P2_1/c$
a / Å	10.0142 (2)	13.4092 (7)	9.9964 (4)	12.9972 (12)
b / Å	10.7768 (2)	10.7584 (4)	9.9530 (4)	9.8254 (5)
c / Å	13.4634 (3)	10.0233 (4)	12.2937 (5)	10.0294 (8)
α / °	90	90	90	90
β / °	100.950 (2)	100.181 (4)	97.009 (4)	104.187 (8)
γ / °	90	90	90	90
V / Å^3	1426.53 (5)	1423.21 (11)	1214.02 (8)	1241.72 (17)
Z, Z'	4, 2	4, 1	2, 1	4, 1
d / mg cm^{-3}	1.768	1.773	1.970	1.930
μ / mm^{-1}	1.59	1.59	1.86	1.82
Measd reflns	11944	6492	6121	9894
Indep reflns	6517	3294	4125	3018
Reflns with $I > 2\sigma(I)$	5706	2581	3613	2732
R_{int}	0.026	0.031	0.035	0.033
$R1\ [F^2 > 2\sigma(F^2)]$	0.042	0.050	0.062	0.100
$wR(F^2)$	0.075	0.121	0.163	0.240

TGA AND DSC DATA
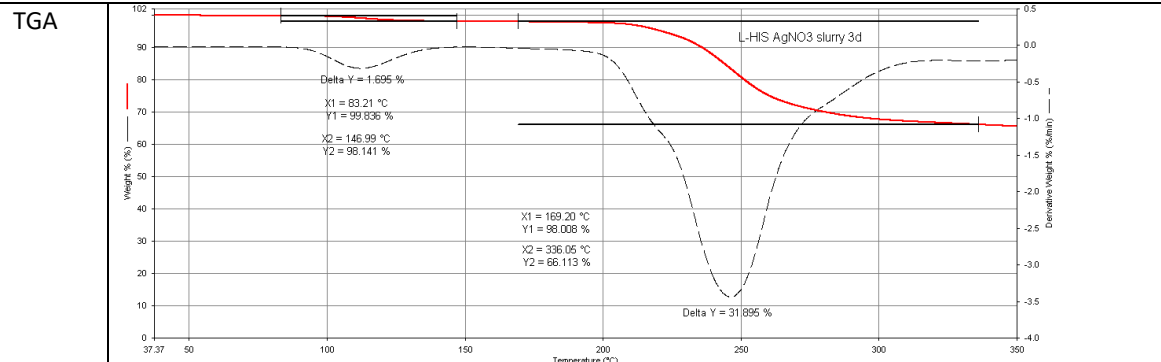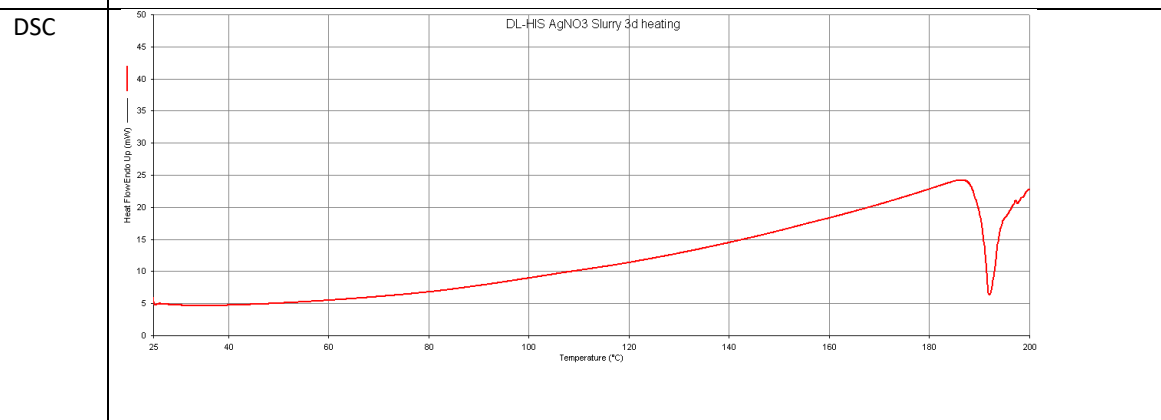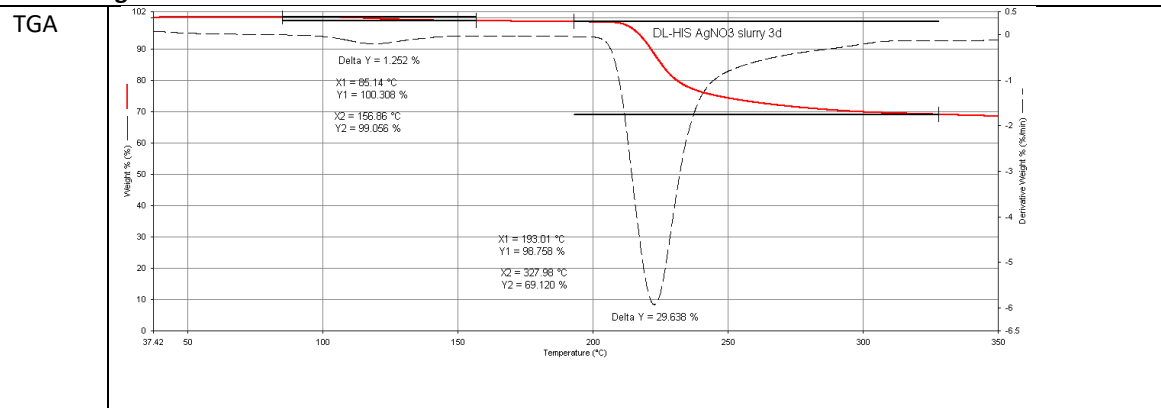
Table S2. TGA and DSC results.

L-Arg·Ag (IWOFUX)

TGA	

L-Arg AgNO3 slurry 3d

X1 = 106.48 °C
Y1 = 99.920 %

X2 = 168.21 °C
Y2 = 97.021 %

Delta Y = 2.898 %

X1 = 178.17 °C
Y1 = 96.977 %

X2 = 350.00 °C
Y2 = 60.450 %

Delta Y = 36.527 %

DSC	

L-Arg AgNO3 Slurry 3d heating

Area = 434.600 mJ
Delta H = 92.2718 J/g
Peak = 124.67 °C

Area = 98.280 mJ
Delta H = 20.8662 J/g
Peak = 131.95 °C

X1 = 104.23 °C
Y1 = 8.1065 mW

X2 = 127.98 °C
Y2 = 10.1512 mW

DL-Arg·Ag

TGA	

DL-Arg AgNO3 slurry 3d

X1 = 93.29 °C
Y1 = 99.078 %

X2 = 162.96 °C
Y2 = 95.924 %

Delta Y = 3.154 %

X1 = 162.96 °C
Y1 = 95.924 %

X2 = 208.08 °C
Y2 = 88.849 %

Delta Y = 7.074 %

Delta Y = 29.277 %

X1 = 208.08 °C
Y1 = 88.849 %
X2 = 350.00 °C
Y2 = 59.572 %

DSC	

DL-Arg AgNO3 Slurry 3d heating

Area = 597.030 mJ
Delta H = 243.6856 J/g
Peak = 118.74 °C

X1 = 93.50 °C
Y1 = 6.2114 mW

X2 = 125.68 °C
Y2 = 8.0852 mW

L-His₂·Ag (TIGHEY)

TGA

L-HIS AgNO3 slurry 3d

Delta Y = 1.695 %

X1 = 83.21 °C
Y1 = 99.836 %

X2 = 146.99 °C
Y2 = 98.141 %

X1 = 169.20 °C
Y1 = 98.008 %

X2 = 336.05 °C
Y2 = 66.113 %

Delta Y = 31.895 %

DSC

L-HIS AgNO3 Slurry 3d heating

DL-His₂·Ag

TGA

DL-HIS AgNO3 slurry 3d

Delta Y = 1.252 %

X1 = 85.14 °C
Y1 = 100.308 %

X2 = 156.86 °C
Y2 = 99.056 %

X1 = 193.01 °C
Y1 = 98.758 %

X2 = 327.98 °C
Y2 = 69.120 %

Delta Y = 29.638 %

DSC

DL-HIS AgNO3 Slurry 3d heating

82

L-His·Ag	
TGA	
DSC	

DL-His·Ag	
TGA	
DSC	

L-Arg·Cu	
TGA	

DSC	L-Arg Cu(NO3)2 BM 1:1 heating

DL-Arg·Cu

TGA	DL-Arg:Cu(NO3)2 1:1 BM Batch 2 recryst
DSC	DL-Arg:Cu(NO3)2 1:1 BM Batch 2 recryst heating

L-His·Cu

TGA	L-His Cu(NO3)2 1:1 BM
DSC	L-His Cu(NO3)2 BM 1:1

84

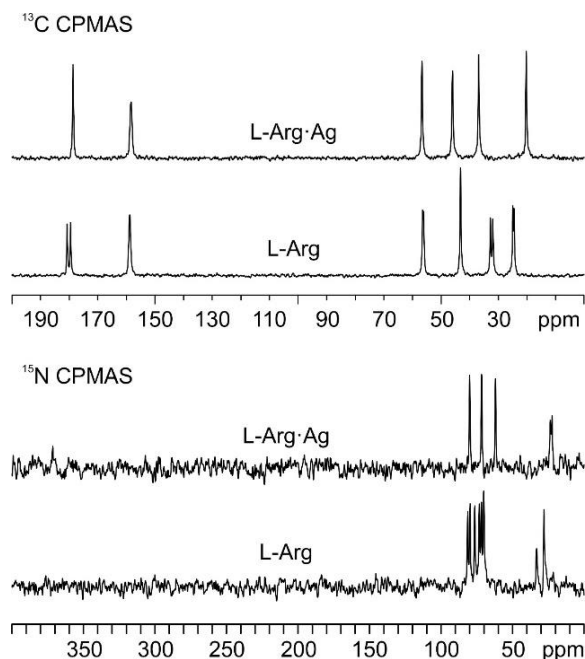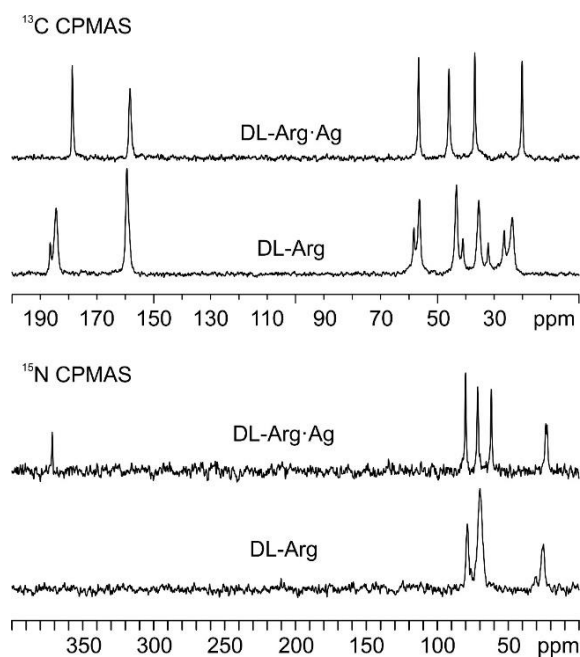| DL-His·Cu	
TGA	
DSC	

SOLID-STATE NMR

Figure S3A. Top: ^{13}C (150.9 MHz) CPMAS spectra of L-Arg·Ag and pure L-Arg, acquired at a spinning speed of 20 kHz at room temperature; bottom: ^{15}N (60.8 MHz) CPMAS spectra of L-Arg·Ag and pure L-Arg, acquired at a spinning speed of 12 kHz at room temperature.
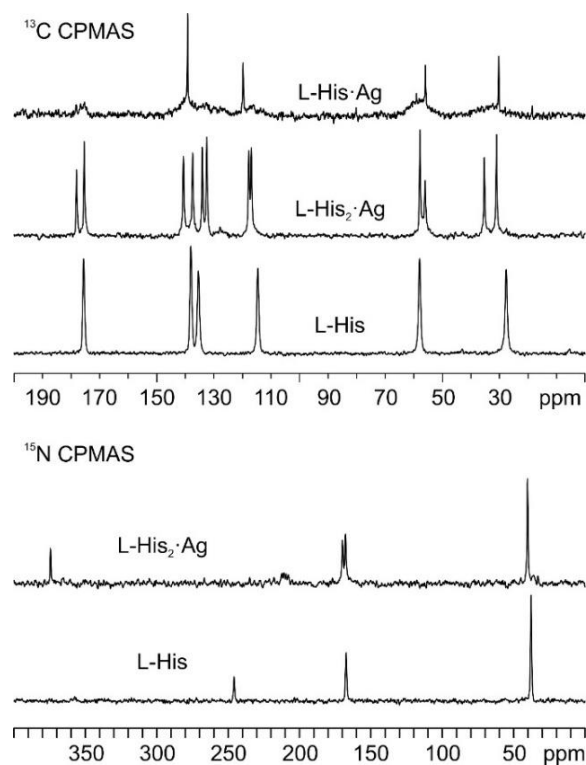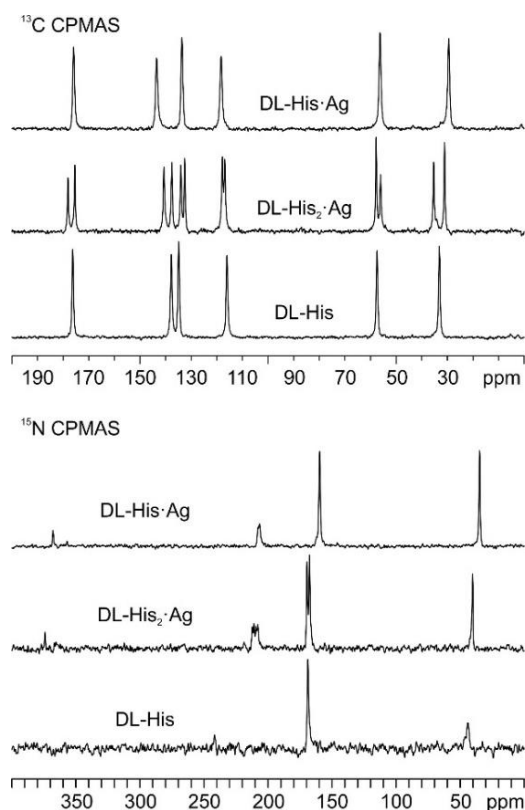
Figure S3B. Top: ^{13}C (150.9 MHz) CPMAS spectra of DL-Arg·Ag and pure DL-Arg, acquired at a spinning speed of 20 kHz at room temperature; bottom: ^{15}N (60.8 MHz) CPMAS spectra of DL-Arg·Ag and pure DL-Arg, acquired at a spinning speed of 12 kHz at room temperature.

Figure S3C. Top: ^{13}C (150.9 MHz) CPMAS spectra of L-His·Ag, L-His$_2$·Ag and pure L-His, acquired at a spinning speed of 20 kHz at room temperature; bottom: ^{15}N (60.8 MHz) CPMAS spectra of L-His$_2$·Ag and pure L-His, acquired at a spinning speed of 12 kHz at room temperature.

86

Figure S3D. Top: ^{13}C (150.9 MHz) CPMAS spectra of DL-His·Ag, DL-His$_2$·Ag and pure DL-His, acquired at a spinning speed of 20 kHz at room temperature; bottom: ^{15}N (60.8 MHz) CPMAS spectra of DL-His·Ag, DL-His$_2$·Ag and pure DL-His, acquired at a spinning speed of 12 kHz at room temperature.

Table S3a. ^{13}C and ^{15}N SSNMR isotropic chemical shift values (in ppm) of the peaks observed in the CPMAS spectra of the employed AAs.

L-Arg	DL-Arg	L-His	DL-His
^{13}C SSNMR chemical shift (ppm)			
179.9	186.5	175.6	176.2
178.7	184.3	138.1	137.7
158.1	159.5	135.4	134.9
55.6	58.3	114.6	116.0
55.3	56.3	58.0	57.5
42.3	43.3	27.7	33.1
31.9	41.0		
31.1	35.4		
24.0	32.1		
23.6	26.4		
	23.6		
^{15}N SSNMR chemical shift (ppm)			
80.6	78.9	245.7	241.8
79.0	70.1	167.3	168.9
75.8	25.2	37.8	43.8
72.6			
71.1			
69.5			
32.7			
27.5			

Table S3b. ^{13}C and ^{15}N SSNMR isotropic chemical shift values (in ppm) of the peaks observed in the CPMAS spectra of the achieved coordination polymers. When observed, J_{AgN} coupling constants (Hz) are reported in parentheses as averaged values between J_{109AgN} and J_{107AgN}.

L-Arg·Ag	DL-Arg·Ag	L-His·Ag	L-His₂·Ag	DL-His·Ag	DL-His₂·Ag
^{13}C SSNMR chemical shift (ppm)					
178.7	178.7	178.3	178.1	175.9	178.1
158.3	158.3	139.2	175.4	143.5	175.4
56.7	56.6	119.8	140.6	133.6	140.6
45.9	45.9	55.9	137.4	118.3	137.5
36.8	36.8	30.3	134.1	56.3	134.0
20.2	20.2		132.5	29.4	132.5
			117.8		117.8
			116.9		116.9
			57.8		57.8
			56.1		56.0
			35.3		35.3
			31.1		31.1
^{15}N SSNMR chemical shift (ppm)					
371.6	371.6	/	374.3	368.0	374.1
80.1	80.1	/	211.6 (91)	207.3 (73)	211.6 (83)
71.7	71.5	/	208.5 (96)	159.7	208.7 (83)
62.0	62.0	/	169.9	34.8	169.6
23.0 (70)	23.1 (59)		167.7		167.6
			40.2		40.2

ANTIMICROBIAL ACTIVITY TESTS
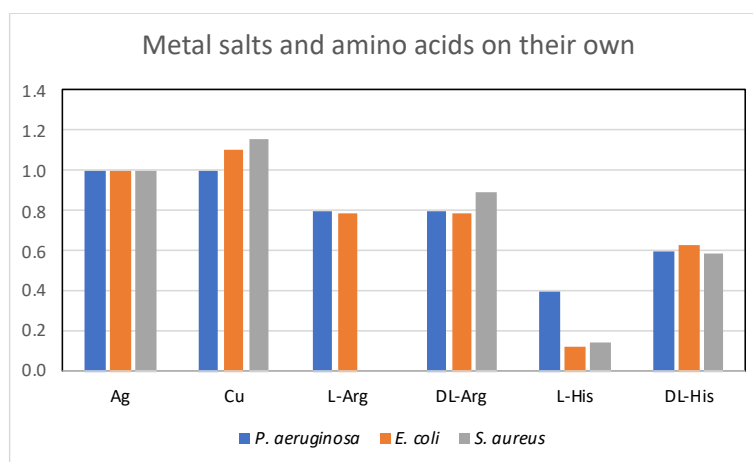
Figure S4A. Normalized antimicrobial activity of compounds used in this study on their own as obtained by disk diffusion experiments on lysogeny media agar media. Values normalized to silver nitrate value of 1.0. Values above 1.05 are more antimicrobial than silver. N = 3.

Chapter 3 – Co-crystallization of antibacterial APIs with natural antimicrobials

Co-crystals have become especially attractive in the pharmaceutical field, since they can lead to new pharmaceutical formulations compared, for example, to conventional salts.[1] Co-crystallization provides alternative routes to the synthesis of new materials and/or to the enhancement of the properties of active molecules, including solubility, dissolution rate, mechanical properties, hygroscopicity, physical stability and chemical stability. [2] Pharmaceutical co-crystals composed of an Active Pharmaceutical Ingredient (API) and a non-active ancillary co-former, selected from the *Generally Recognized as Safe* (GRAS) list of substances, are being actively investigated by crystal engineers. It is also possible to co-crystallize an API with another API or active molecule, thus forming a drug-drug (or co-drug) co-crystal.[3] The solid-state association of an antibacterial API with a molecular co-former may also allow to explore new ways to enhance, in a synergistic way, the antimicrobial performance.[4]

In the search of new sustainable and cost-effective response to the AMR issue, crystal engineering intervenes with different strategies, respect to the common procedures applied in the pharmaceutical industry. In this thesis chapter are reported the results obtained applying crystal engineering tools, especially co-crystallization, to modify and evaluate new antimicrobial properties to novel active antibacterial materials (co-crystals), composed by a synthetic antibiotic and a natural product with antimicrobial properties as co-former.

References

(1) Qiao, N.; Li, M.; Schlindwein, W.; Malek, N.; Davies, A.; Trappitt, G. Pharmaceutical Co-Crystals: An Overview. *Int J Pharm* **2011**, *419* (1–2), 1–11. https://doi.org/10.1016/j.ijpharm.2011.07.037.

(2) Almarsson, Ö.; Zaworotko, M. J. Crystal Engineering of the Composition of Pharmaceutical Phases. Do Pharmaceutical Co-Crystals Represent a New Path to Improved Medicines? *Chem. Commun.* **2004**, No. 17, 1889–1896. https://doi.org/10.1039/B402150A.

(3) Sekhon, B. S. Drug-Drug Co-Crystals. *DARU, J. Pharm. Sci.* **2012**, *20* (1), 1–2. https://doi.org/10.1186/2008-2231-20-45.

(4) *Antimicrobial resistance | European Medicines Agency*. https://www.ema.europa.eu/en/human-regulatory/overview/public-health-threats/antimicrobial-resistance (accessed 2023-01-09).

(5) *Antimicrobial resistance*. https://www.who.int/news-room/fact-sheets/detail/antimicrobial-resistance (accessed 2023-01-09).

3.1 Natural antimicrobials meet a synthetic antibiotic: carvacrol/thymol and ciprofloxacin co-crystals as a promising solid-state route to activity enhancement

Abstract

The antibiotic ciprofloxacin (CIP) zwitterion has been co-crystallized via slurry and/or ball-milling with carvacrol (CAR) and thymol (THY), also known to exert antimicrobial activity, with the aim of improving the antibacterial activity of ciprofloxacin. In the case of CAR, the 1:4 cocrystal $CIP \cdot CAR_4$ appears to be the most stable phase, where the intermediate phases $CIP \cdot CAR_3$ and $CIP \cdot CAR_2$ have been isolated by stepwise loss of CAR. In the case of THY, the 1:2 cocrystal $CIP \cdot THY_2$ is the most stable, while the 1:4 cocrystal $CIP \cdot THY_4$ easily loses THY to yield the bisadduct. All cocrystals were structurally characterized by single crystal or powder diffraction: in both cocrystals sheets of CIP molecules are intercalated with layers of CAR and THY, respectively, that can be released stepwise upon heating as followed by DSC, TGA and variable temperature XRPD. Preliminary antimicrobial experiments provide encouraging evidence of the enhanced activity of the cocrystals $CIP \cdot CAR_4$ and $CIP \cdot THY_2$ against Escherichia coli (ATCC 25922) with respect to pure ciprofloxacin as well as to physical mixtures of ciprofloxacin with carvacrol or thymol.

Article

Natural Antimicrobials Meet a Synthetic Antibiotic: Carvacrol/Thymol and Ciprofloxacin Cocrystals as a Promising Solid-State Route to Activity Enhancement

Oleksii Shemchuk, Simone d'Agostino, Cecilia Fiore, Vittorio Sambri, Silvia Zannoli, Fabrizia Grepioni, and Dario Braga*

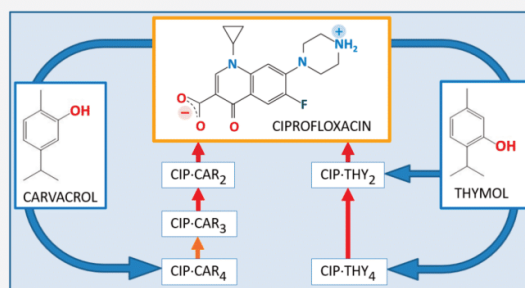Read Online

ACCESS | Metrics & More | Article Recommendations | Supporting Information

ABSTRACT: The antibiotic ciprofloxacin (CIP) zwitterion has been cocrystallized via slurry and/or ball-milling with carvacrol (CAR) and thymol (THY), also known to exert antimicrobial activity, with the aim of improving the antibacterial activity of ciprofloxacin. In the case of CAR, the 1:4 cocrystal $CIP\cdot CAR_4$ appears to be the most stable phase, where the intermediate phases $CIP\cdot CAR_3$ and $CIP\cdot CAR_2$ have been isolated by stepwise loss of CAR. In the case of THY, the 1:2 cocrystal $CIP\cdot THY_2$ is the most stable, while the 1:4 cocrystal $CIP\cdot THY_4$ easily loses THY to yield the bisadduct. All cocrystals were structurally characterized by single crystal or powder diffraction: in both cocrystals sheets of CIP molecules are intercalated with layers of CAR and THY, respectively, that can be released stepwise upon heating as followed by DSC, TGA and variable temperature XRPD. Preliminary antimicrobial experiments provide encouraging evidence of the enhanced activity of the cocrystals $CIP\cdot CAR_4$ and $CIP\cdot THY_2$ against *Escherichia coli* (ATCC 25922) with respect to pure ciprofloxacin as well as to physical mixtures of ciprofloxacin with carvacrol or thymol.

■ INTRODUCTION

Cocrystallization, an application of crystal engineering principles,[1−5] provides alternative routes to the synthesis of new materials and/or to the enhancement of the properties of active molecules.[6−11] As a matter of fact, cocrystals are finding applications in diverse areas: pharmaceuticals,[12−16] agrochemistry,[17−20] high-energy materials,[21−23] food,[24−26] etc. The basic idea is that the solid state association, via noncovalent interactions, of an active ingredient with a molecular component may alter in a useful way physicochemical properties such as solubility, dissolution rate, thermal stability, photoreactivity, etc. of the active ingredient. Cocrystals have become especially attractive in the pharmaceutical field, since they can lead to new pharmaceutical formulations compared, for example, to conventional salts.

This goal is usually pursued by cocrystallizing the API with a nonactive (GRAS accepted[27]) molecule, as in molecular cocrystals, or with a salt, as in ionic cocrystals.[28] The large choice of molecular and/or ionic building blocks makes the number of possible combinations between active pharmaceutical ingredients (APIs) and ancillary coformers virtually limitless.

In more advanced applications, however, the API may also be cocrystallized with another active ingredient, yielding a so-called codrug,[29−33] whereby not only are the solid state

physicochemical properties of the API altered with respect to those of the pure crystal but also the pharmaceutical and biological activity may give significantly different results.[34−36]

In this paper, we apply cocrystallization strategies to approach a problem of extraordinary contemporary importance, namely that of "antimicrobial resistance" (AMR). As a matter of fact, the AMR phenomenon is one of the major medical challenges in most healthcare systems, both in developed countries and in low financial income areas.[37] AMR has increased dramatically in the recent years and represents a global public health threat.[38] A number of diseases that were thought to be under control by the application of antibacterial remedies are getting back being resistant to these therapies. One of the main reasons for *drug*-resistance in microorganisms is the intensive overuse of treatments to control infections in humans and animals as well as in the agricultural sector.[39] Actually, the reason AMR is a significant

concern is the high mortality level attributed to infections caused by multi drug resistant germs.[40] A number of common pathogenic strains are already bearing antibiotic-resistant genes, and presumably, more antibiotic-resistant pathogens will emerge in the future, if no different and more cautious use of antimicrobials takes place.[41]

To cope with the problem of AMR, two possible strategies can be used: the first is the quest for novel active ingredients, but this is facing increasing bench-to-market costs and times;[42] the second is the exploration of ways to improve the activity of existing antibacterials, and it is more promising. In a recent paper, we showed that cocrystallization of the antibacterial agents proflavine and methyl viologen with the inorganic salts CuCl, CuCl$_2$, and AgNO$_3$ results in enhanced antimicrobial activity with respect to the separate components.[43]

In this paper we report our results in the cocrystallization of the known antibiotic ciprofloxacin (CIP hereafter) with the natural antimicrobials carvacrol (CAR) and thymol (THY) (see Scheme 1). At ambient conditions THY is a molecular

Scheme 1. Ciprofloxacin (CIP) Zwitterion and the Two Antimicrobial Molecules, Carvacrol (CAR) and Thymol (THY), Used as Coformers
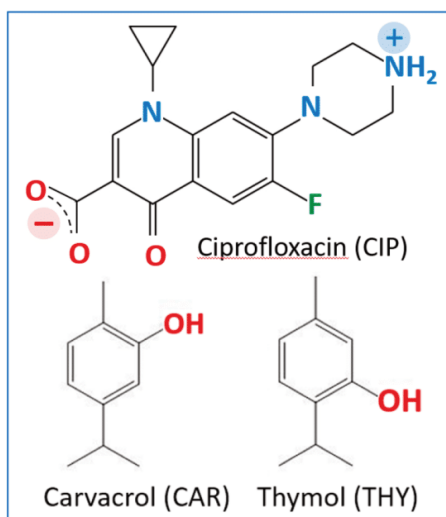
solid (mp 51.5 °C),[44] while carvacrol is a liquid (mp 3.5 °C);[44] therefore, crystalline solids containing ciprofloxacin and this latter coformer should be strictly regarded as "pharmaceutical solvates".[45−47] However, as it will be apparent in the following, the distinction between cocrystals and solvates is rather semantic in the contest of this study and does not reflect specific differences in physicochemical behaviors.

Ciprofloxacin (1-cyclopropyl-6-fluoro-1,4-dihydro-4-oxo-7-(1-piperazinyl)-3-quinoline carboxylic acid) is an antibiotic belonging to the class of fluoroquinolones, which are effective antibacterial agents against a broad spectrum of Gram-positive and Gram-negative bacteria. Thymol [5-methyl-2-(propan-2-yl)benzenol, also known as m-thymol] is a natural mono-terpenoid phenol derivative of p-cymene, and it is the most abundant component of the oil extracted from *Thymus vulgaris* (thyme). Carvacrol [2-methyl-5-(propan-2-yl)benzenol, also known as o-thymol], is present in the essential oils of *Origanum vulgare* (oregano), thyme, pepperwort, and wild bergamot. The

effective antibacterial properties of both essential oils have been investigated *in vitro* and *in vivo* against diverse Gram-negative and Gram-positive bacteria such as *Salmonella typhimurium*, *Escherichia coli*, and *Listeria monocytogenes*.[48−52] Both THY and CAR are generally used as natural preservatives in food treatment and packaging.[53−56] They are both components of "Thymi aetheroleum", a herbal medicinal product,[57] and have been assigned the GRAS (generally recognized as safe) status of flavor additives[58] by FEMA.[59] Recently cocrystals of thymol and carvacrol, among a number of essential oils components, have been investigated for agricultural applications.[60]

In the following, we describe preparation, solid state characterization and thermal behavior of the two families of ciprofloxacin cocrystals with carvacrol, CIP·CAR$_n$ (n = 2, 3, 4) and with thymol, CIP·THY$_n$ (n = 2, 4). The effect of cocrystals formation on the antibiotic activity of ciprofloxacin has also been evaluated by means of standard antimicrobial tests in the case of CIP·CAR$_4$ and CIP·THY$_2$ and compared with the results for the pure components and their physical mixtures. Preliminary results are encouraging, and they have prompted a thorough antimicrobial investigation, which will be the subject of a separate research project.

■ EXPERIMENTAL PART

Materials and Instrumentation. All reagents and solvents used in this work were purchased from Sigma-Aldrich and used without further purification.

Synthesis of Ciprofloxacin Cocrystals with Carvacrol. *CIP·CAR$_4$.* CIP·CAR$_4$ was obtained by three different methods: solution, mechanochemistry, and slurry. In the first one, ciprofloxacin (30 mg, 0.09 mmol) was dissolved in carvacrol (2 mL, 12.99 mmol), and upon solvent evaporation single crystals were obtained after 2 weeks. In the second one, 100 mg (0.30 mmol) of ciprofloxacin were manually ground with 4−5 drops of carvacrol, added in a stepwise manner: the powder was ground until dryness, and then an additional drop of CAR was added. In the third method, ciprofloxacin was slurried for 60 h in 3 mL of ethanol with a slight excess of carvacrol with respect to the CIP:CAR 1:4 stoichiometric ratio; after filtration, the solid material was left to dry out at room temperature.

CIP·CAR$_3$. CIP·CAR$_3$ was obtained in two steps starting from CIP·CAR$_4$: first CIP·CAR$_4$ was heated to 80 °C in an oven and kept at this temperature for 30 min; the sample was then cooled to 40 °C and kept at this temperature for 4 h.

CIP·CAR$_2$. CIP·CAR$_2$ was obtained in two steps starting from CIP·CAR$_4$: first CIP·CAR$_4$ was heated to 100 °C in an oven and kept at this temperature for 30 min; the sample was then cooled to 40 °C and kept at this temperature for 4 h.

All attempts to synthesize CIP·CAR$_2$ and CIP·CAR$_3$ by direct mixing of the reactants in the correct stoichiometric ratios were unsuccessful.

Synthesis of Ciprofloxacin Cocrystals with Thymol. *CIP·THY$_2$.* CIP·THY$_2$ was obtained mechanochemically by ball milling ciprofloxacin (100 mg, 0.30 mmol) and thymol (90.7 mg, 0.60 mmol) for 30 min in a Retsch MM200 ball miller, operated at a frequency of 20 Hz, in the presence of 2 drops (100 μL) of ethanol.

CIP·THY$_4$. A solid mixture of ciprofloxacin (30 mg, 0.09 mmol) and thymol (150 mg, 1.00 mmol) was gently ground and subsequently heated to 55 °C, to induce the melting of thymol (mp of 51.5 °C).[44] Upon slow cooling the growth of single crystals was observed. CIP·THY$_4$ was also obtained via slurry: ciprofloxacin (100 mg, 0.30 mmol) and excess thymol (272 mg, 1.80 mmol) were slurried in 2 mL of ethanol for 60 h in a closed vial; the vial was then opened, still under slurry conditions, to allow the complete evaporation of ethanol.

Thermogravimetric Analysis (TGA). TGA measurements (Figures SI-6 to SI-11) for all compounds were performed with a

PerkinElmer TGA7 in the temperature range 30−400 °C, under an N_2 gas flow, at the heating rate of 5 °C min^{-1}.

Differential Scanning Calorimetry (DSC). DSC measurements (Figures SI-12 to SI-16) for all compounds were performed with a Perkin−Elmer Diamond, at the heating rate of 5 °C min^{-1}. Samples (3−5 mg) were placed in hermetic aluminum pans.

X-ray Powder Diffraction Measurements. Room temperature X-ray powder diffraction (XRPD) patterns were collected on a PANalytical X'Pert Pro automated diffractometer equipped with an X'Celerator detector in Bragg−Brentano geometry, using Cu Kα radiation (λ = 1.5418 Å) without monochromator in the 3−40° 2θ range (step size, 0.033°; time/step, 20 s; Soller slit, 0.04 rad; antiscatter slit, 1/2; divergence slit, 1/4; 40 mA × 40 kV). For structure solution purposes, X-ray diffraction patterns were collected on a PANalytical X'Pert Pro automated diffractometer with transmission geometry equipped with a focusing mirror and Pixcel detector, using Cu Kα radiation (λ = 1.5418 Å) without monochromator in the 2θ range 3−70° (step size, 0.0130°; time/step, 170.595 s; Soller slit, 0.04 rad; antiscatter slit, 1/2; divergence slit, 1/2; 40 kV × 40 mA). To improve the quality of the obtained XRPD patterns, three repetitions were performed, and the scans were merged. Data analyses were carried out using the PANalytical X'Pert Highscore Plus program.[61]

Structural Characterization from Powder Data. Powder diffraction data were analyzed with the software PANalytical X'Pert HighScore Plus. Fifteen peaks were chosen in the 2θ range 3−40°, and unit cell parameters were found using the DICVOL4 algorithm. The structure of CIP·THY$_2$ was solved by simulated annealing, performed with EXPO2014.[62] Ten runs for simulated annealing trials were set, and a cooling rate (defined as the ratio T_n/T_{n-1}) of 0.95 was used. The best solution was chosen for Rietveld refinement, which was performed with the software TOPAS 5.0.[63] The peak shape was modeled for size and strain with the Gaussian and Lorentzian functions present in TOPAS 5.0. All the hydrogen atoms were fixed in calculated positions. Refinement converged with χ^2 = 1.84 and R_{wp} = 6.51%. Rietveld refinement is shown in the Supporting Information (Figure SI-1). Structural data for all compounds investigated in this work are listed in Table SI-1.

Variable Temperature X-ray Diffraction. X-ray powder diffractograms in the 3−40° 2θ range were collected for CIP·CAR$_4$ and CIP·THY$_4$ on a PANalytical X'Pert PRO automated diffractometer, equipped with an X'Celerator detector and an Anton Paar TTK 450 system for measurements at controlled temperature. Data were collected in open air in Bragg−Brentano geometry using Cu Kα radiation without a monochromator. Thermal programs were selected on the basis of TGA results.

Single Crystal X-ray Diffraction. Single crystal X-ray diffraction data for CIP·CAR$_4$ and CIP·THY$_4$ were collected at room temperature and at 250 K, respectively, with an Oxford Diffraction X'Calibur equipped with a graphite monochromator and a CCD detector. Unit cell parameters for all compounds discussed herein are reported in Table SI-1. The structures were solved by the Intrinsic Phasing methods and refined by least-squares methods against F^2 using SHELXT-2016[64] and SHELXL-2018[65] with Olex^2 interface.[66] Non-hydrogen atoms were refined anisotropically. Hydrogen atoms were added in calculated positions. The software Mercury 4.1.2[67] was used to analyze and represent the crystal packing. Crystal data can be obtained free of charge via www.ccdc.cam.ac.uk/conts/retrieving.html (or from the Cambridge Crystallographic Data Centre, 12 Union Road, Cambridge CB21EZ, UK; fax: (+44)1223-336-033; or e-mail: deposit@ccdc.cam.ac.uk). CCDC 2010400−2010402.

Testing of Antimicrobial Activity. Antimicrobial activity was tested with broth microdilution, according to the guidelines of the two established organizations and committees on antimicrobial susceptibility testing, the CLSI and EUCAST.[68−70] For comparison, testing was conducted on suspensions of thymol, carvacrol, ciprofloxacin, and both physical mixtures and cocrystals of CIP·THY$_2$ and CIP·CAR$_4$, in 10 progressive concentrations ranging from 0.063 to 160 μg mL^{-1}. All suspensions were tested in parallel, using both a reference strain of E.

coli (ATCC 25922), which is susceptible to ciprofloxacin, and a ciprofloxacin-resistant E. coli strain (MIC > 32).[70]

■ RESULTS AND DISCUSSION

Cocrystals of Ciprofloxacin with Carvacrol. The cocrystallization of ciprofloxacin with CAR resulted in the formation of the cocrystal CIP·CAR$_4$, characterized by a 1:4 stoichiometry. Figure 1a shows how the carboxylate group on
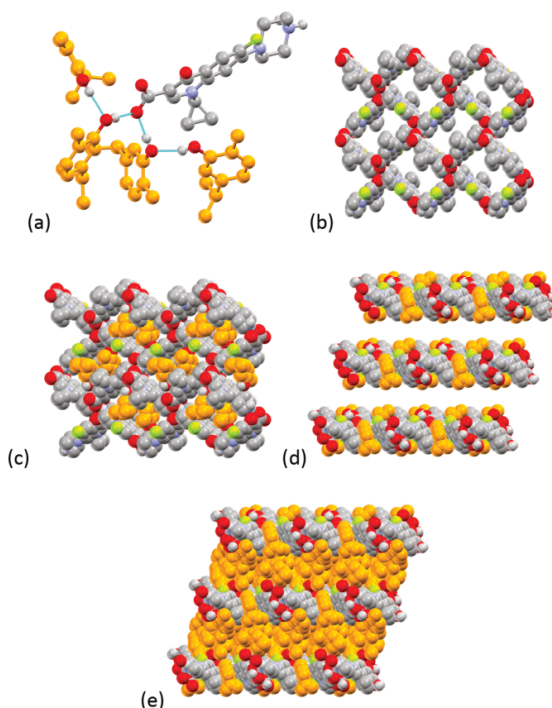

Figure 1. Hydrogen-bonding interactions between ciprofloxacin and the carvacrol molecules in crystalline CIP·CAR$_4$ (a). The ciprofloxacin molecules also interact with each other via hydrogen bonds; they are arranged in nets (b) filled with a quarter of the CAR molecules (c), thus forming parallel layers (d) alternating with thick layers of CAR molecules (e). H$_{CH}$ hydrogens were omitted for clarity. Carbon atoms of CAR are given in orange.

ciprofloxacin interacts via hydrogen bonds with the −OH group of two molecules of CAR, while the remaining two CAR molecules in the formula unit form OH···O$_{OH}$ hydrogen bonds with other CAR molecules. Each ciprofloxacin molecules interacts via NH$^+$···O$_{COO^-}$ and COO$^-$···HN$^+$ hydrogen bonds with four neighboring ciprofloxacin molecules. Figure 1c shows an interesting feature of the molecular packing in crystals of CIP·CAR$_4$, namely a layered structure: one layer is formed by ciprofloxacin and two (referred by symmetry) CAR molecules, while the second layer is exclusively formed by the remaining three CAR molecules. This feature is of help in understanding the thermal behavior of the cocrystal (see below), and it is shared with the cocrystal of ciprofloxacin with THY. Segregation of CAR and THY has also been observed in cocrystals with acridine.[71]

The study of the thermal behavior of CIP·CAR$_4$ via DSC allows one to observe, on heating, the presence of multiple endothermic events at 80, 92, and 109 °C (peak temperatures,

see Figure SI-7), followed by exothermic events. This is an indication that CAR molecules are released stepwise from the crystal, and each loss of CAR is immediately followed by recrystallization to a cocrystal with different stoichiometry. The last step corresponds to complete loss of CAR and recrystallization of ciprofloxacin. The stepwise loss of CAR from CIP·CAR$_4$ to CIP is summarized in Scheme 2.

Scheme 2. Solid-State Transformations upon Heating for the 1:4 Cocrystals of Ciprofloxacin (CIP) Zwitterion with Carvacrol (CAR) and Thymol (THY)^a
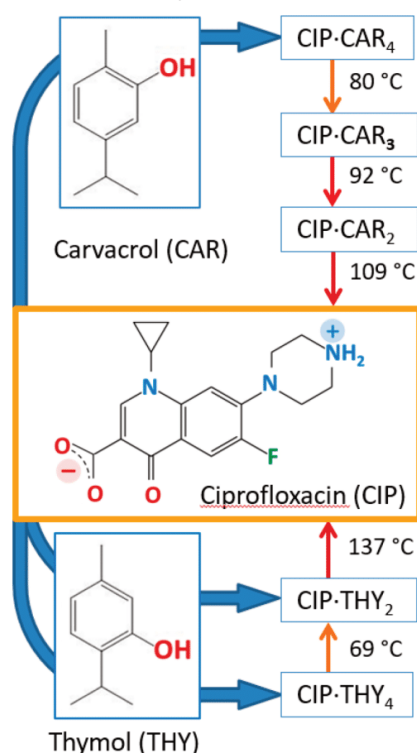
^{a}Temperatures are from DSC measurements (peak values, see Supporting Information).

The series of solid-to-solid transformations occurring upon heating crystalline CIP·CAR$_4$ was also followed by variable temperature X-ray powder diffraction (see Figure SI-3). The temperatures at which the transformations occur from CIP·CAR$_4$ to CIP·CAR$_3$, then to CIP·CAR$_2$ and finally to CIP, are in agreement (80, 100, and 110 °C, respectively) with the DSC values. Thermal gravimetric analysis, on the contrary, is not as informative (see Figure SI-13), and its trace shows a single, broad event corresponding to the loss of all CAR molecules per formula unit (weight loss ca. 63%) in the temperature range 60−150 °C. This is attributable to the low volatility of CAR, which leaves the crystal but does not evaporate from the sample in the TGA experiment. VT-XRPD experiments confirmed this observation: two samples of CIP·CAR$_4$ were first converted into CIP·CAR$_3$ and CIP·CAR$_2$, respectively, and then they were cooled to room temperature. In both cases, partial reformation of CIP·CAR$_4$ could be observed; i.e., excess

of CAR was still available in the powder samples at the end of the heating cycles.

The results of the VT-XRPD measurements were useful for the preparation of the intermediate phases CIP·CAR$_2$ and CIP·CAR$_3$ as pure materials. In both cases samples of CIP·CAR$_4$ were heated to the transition temperatures (ca. 80 and 100 °C, respectively) and kept at these temperatures for 30 min, to allow for complete transformation; the samples were then cooled to 40 °C and kept at this temperature for 3−4 h to allow for complete evaporation of the excess CAR. TGA measurements on these pure samples (see Figures SI-15 and SI-16) allowed to confirm the CIP·CAR$_3$ and CIP·CAR$_2$ stoichiometries. Once formed, all cocrystals of ciprofloxacin with CAR are stable. Even after 50 days in the open air, no change of crystalline phase was observed.

Cocrystals of Ciprofloxacin with Thymol. Thymol is a solid at ambient conditions, but it melts at 51.5 °C.[44] For this reason, the same cocrystallization approach used for ciprofloxacin with CAR was applied here, and ciprofloxacin was dissolved in excess melted THY (see Experimental Part). Upon slow cooling of the mixture two types of single crystals were recovered, and both were characterized via X-ray single crystal diffraction. The first type of crystals turned out to be pure THY, identified on the basis of CSD data (refcode IPMEPL[72]), while crystals of the second type were characterized as the new cocrystal CIP·THY$_4$. Data were collected at 250 K, to avoid loss of THY during data collection. In terms of crystal structure, CIP·THY$_4$ closely resembles CIP·CAR$_4$, as is evident from Figure 2.

Figure 2a shows how ciprofloxacin interacts via hydrogen bonds with the −OH group of three molecules of THY, while the remaining THY molecules in the formula unit form an OH···O$_{OH}$ hydrogen bond with another THY molecule. As observed in CIP·CAR$_4$, each ciprofloxacin molecules interacts via hydrogen bonds with four neighboring ciprofloxacin molecules, thus forming a 2D-net (see Figure 2b) filled with THY molecules (Figure 2c). The most relevant analogy, however, is represented by the layered organization, as thick layers of THY intercalate between the ciprofloxacin/THY layers, as shown in Figures 2, part d and e.

Ciprofloxacin and THY were also made to mechanochemically react in 1:4 stoichiometric ratio in a ball milling experiment, in the presence of two drops of ethanol. This time, however, a new solid was obtained, characterized by a powder diffraction pattern different from those of the starting materials and of CIP·THY$_4$, although peaks of unreacted THY were still present. The synthesis via ball milling was thus repeated with lower quantities of THY, and a pure phase was obtained with the 1:2 stoichiometric ratio, as confirmed by TGA (see Figure SI-14). The new cocrystal CIP·THY$_2$ was structurally characterized from powder data (see Experimental Part), since all attempts to grow single crystals were unsuccessful. Figure 3a shows the hydrogen-bonding interactions of ciprofloxacin with the two independent THY molecules. As in CIP·THY$_4$ the CIP molecules form a 2D net (Figure 3b), with ciprofloxacin molecules connected via hydrogen bonds; parallel nets (Figure 3c) are intercalated with THY molecules, which also partially enter the CIP layers with the −OH groups (Figure 3d).

Pure CIP·THY$_4$ was also obtained by slurry in EtOH with an excess of THY; the resulting solid was then left in the air for 72 h, for the excess of THY to sublimate. A DSC measurement on CIP·THY$_4$ thus obtained (Figure SI-8) shows two endother-

95
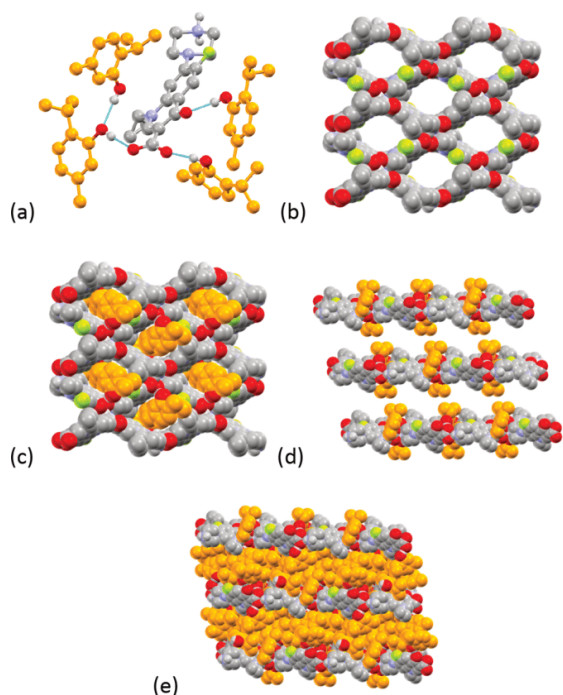
Figure 2. Hydrogen-bonding interactions between ciprofloxacin and the thymol molecules in crystalline CIP·THY$_4$ (a). The ciprofloxacin molecules also interact with each other via hydrogen bonds; they are arranged in nets (b) filled with a quarter of the THY molecules (c), thus forming parallel layers (d) alternating with thick layers of THY molecules (e). H$_{CH}$ hydrogens were omitted for clarity. Carbon atoms of THY are given in orange.

mic events, at ca. 69 °C and at 137 °C, respectively. VT-XRPD experiments (Figure SI-5) confirmed that the first event corresponds to the transformation of CIP·THY$_4$ into CIP·THY$_2$, while the second one leads to complete loss of THY. The stepwise loss of THY and the thermal transformation of CIP·THY$_4$, first into CIP·THY$_2$ and then into CIP, are summarized in Scheme 2.

Antimicrobial Activity. The antimicrobial activity of the cocrystals CIP·CAR$_4$ and CIP·THY$_2$, chosen because they could easily be obtained mechanochemically as pure phases, was compared with that of the pure components, as well as with that of physical mixtures of CIP and CAR/THY in adequate stoichiometric ratios, against a reference strain of *E. coli* (ATCC 25922), which is susceptible to the ciprofloxacin component. Pure samples of CIP·CAR$_4$ and CIP·THY$_4$ obtained as described above were used.

Concerning strain ATCC 25922, ciprofloxacin showed growth inhibition at 4 μg/mL, while THY and CAR were not effective by themselves and did not show growth inhibition. The physical mixtures of CIP and CAR and of CIP and THY in 1:4 and 1:2 ratios, respectively, resulted in growth inhibition at ca. 10 μg/mL, which, upon normalization, approximately corresponds to the inhibition effect of pure ciprofloxacin. Interestingly, both CIP·CAR$_4$ and CIP·THY$_2$ cocrystals showed growth inhibition at ca. 2 μg/mL concentration; normalizing these quantities on the base of the cocrystals formula units, it can be seen that CIP·CAR$_4$ and CIP·THY$_2$ are ca. 6 and 4 times more efficient, respectively, with respect to pure ciprofloxacin.

■ CONCLUSIONS

The study of cocrystals is at the forefront of crystal engineering because it offers a viable route to prepare, often with nonexpensive and environmentally friendly solvent free (mechanochemical) methods, novel materials for a variety of applications well beyond the pharmaceutical field. For instance,
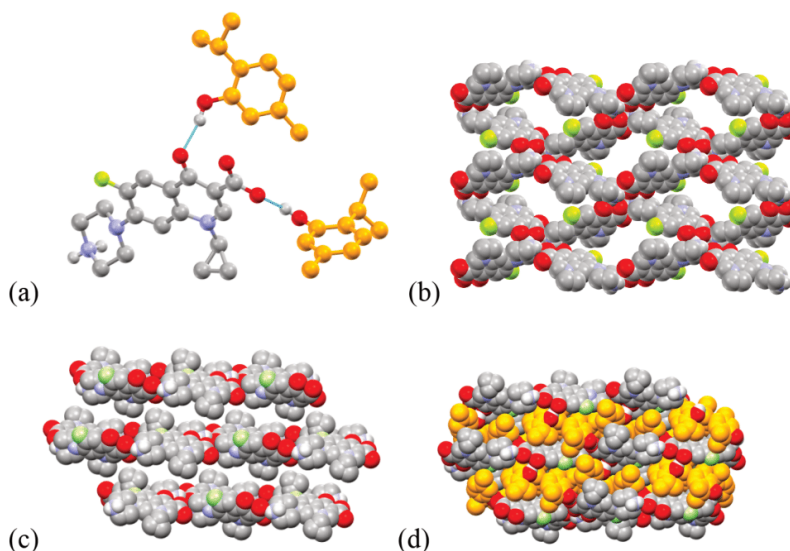
Figure 3. Hydrogen-bonding interactions between ciprofloxacin and the thymol molecules in crystalline CIP·THY$_2$ (a). As in CIP·THY4, the CIP molecules form 2D-nets (b and c), filled with the −OH extremities of the intercalated thymol layers (d). H$_{CH}$ hydrogens were omitted for clarity. Carbon atoms of THY are given in orange.

it has been amply shown that cocrystallization approaches can be used to produce materials that can be used as fertilizers, nutrients and enzyme inhibitors in the agrochemical field.[17−19] There are also indications that cocrystals could be used in an area of increasing global importance, such as that of antimicrobial resistance. In the case of proflavine, for example, it has been possible to demonstrate that cocrystallization of proflavine with CuCl and AgNO$_3$ yield materials, namely PF· CuCl and PF·AgNO$_3$ that appear to perform better in terms of antimicrobial activity than proflavine and the inorganic salts, separately.[43]

In this paper, we have reported the preparation and characterization of a series of cocrystals obtained by cocrystallizing by slurry and/or ball-milling the antibiotic ciprofloxacin (CIP) with carvacrol (CAR) and thymol (THY), which are also known to exert antibacterial activity. CIP forms compounds in 1:4 ratio with both coformers. While CIP· CAR$_4$ is stable and loses CAR in stepwise manner upon heating with formation of the phases CIP·CAR$_3$ and CIP· CAR$_2$, while CIP·THY$_4$ is unstable and loses THY spontaneously at room temperature with formation of stable CIP·THY$_2$.

The idea was that of verifying whether cocrystallization of a known antibiotic with herbal medicinal products could indeed represent a viable route to improve the properties of ciprofloxacin. Preliminary antimicrobial testing against a reference strain of *E. coli* (ATCC 25922), susceptible to ciprofloxacin, clearly indicated that cocrystals CIP·CAR$_4$ or CIP·THY$_2$ have the comparable bacteriostatic activity, and that this is significantly better than ciprofloxacin alone. If one takes into account that THY and CAR appear to be not effective on their own, or in physical mixture with ciprofloxacin, it appears that association with ciprofloxacin in the cocrystals enhances significantly its efficacy. These encouraging preliminary results require an in depth systematic study, which is under way.

ASSOCIATED CONTENT

🔘 Supporting Information

The Supporting Information is available free of charge at https://pubs.acs.org/doi/10.1021/acs.cgd.0c00900.

    XRPD patterns, DSC, and TGA (PDF)

Accession Codes

CCDC 2010400−2010402 contain the supplementary crystallographic data for this paper. These data can be obtained free of charge via www.ccdc.cam.ac.uk/data_request/cif, or by emailing data_request@ccdc.cam.ac.uk, or by contacting The Cambridge Crystallographic Data Centre, 12 Union Road, Cambridge CB2 1EZ, UK; fax: +44 1223 336033.

AUTHOR INFORMATION

Corresponding Author

   Dario Braga − *Molecular Crystal Engineering Laboratory, Dipartimento di Chimica "Giacomo Ciamician", Università di Bologna, 40126 Bologna, Italy;* ⊙ orcid.org/0000-0003-4162-4779; Email: dario.braga@unibo.it

Authors

   Oleksii Shemchuk − *Molecular Crystal Engineering Laboratory, Dipartimento di Chimica "Giacomo Ciamician", Università di Bologna, 40126 Bologna, Italy;* ⊙ orcid.org/0000-0003-3003-3922

   Simone d'Agostino − *Molecular Crystal Engineering Laboratory, Dipartimento di Chimica "Giacomo Ciamician", Università di Bologna, 40126 Bologna, Italy;* ⊙ orcid.org/0000-0003-3065-5860

   Cecilia Fiore − *Molecular Crystal Engineering Laboratory, Dipartimento di Chimica "Giacomo Ciamician", Università di Bologna, 40126 Bologna, Italy*

   Vittorio Sambri − *Dipartimento di Medicina Specialistica, Diagnostica e Sperimentale Università di Bologna, 40138 Bologna, Italy; Laboratorio Unico Centro Servizi AUSL Romagna, U.O. Microbiologia, Pievesestina (FC), Italy*

   Silvia Zannoli − *Laboratorio Unico Centro Servizi AUSL Romagna, U.O. Microbiologia, Pievesestina (FC), Italy*

   Fabrizia Grepioni − *Molecular Crystal Engineering Laboratory, Dipartimento di Chimica "Giacomo Ciamician", Università di Bologna, 40126 Bologna, Italy;* ⊙ orcid.org/0000-0003-3895-0979

Complete contact information is available at: https://pubs.acs.org/10.1021/acs.cgd.0c00900

Notes

The authors declare no competing financial interest.

REFERENCES

(1) Desiraju, G. R.; Parshall, G. W. Crystal engineering: the design of organic solids. *Materials science monographs* **1989**, 54.
(2) Almarsson, O.; Zaworotko, M. J. Crystal engineering of the composition of pharmaceutical phases. Do pharmaceutical co-crystals represent a new path to improved medicines? *Chem. Commun.* **2004**, 1889−1896.
(3) Blagden, N.; de Matas, M.; Gavan, P. T.; York, P. Crystal engineering of active pharmaceutical ingredients to improve solubility and dissolution rates. *Adv. Drug Delivery Rev.* **2007**, *59*, 617−630.
(4) Desiraju, G. R. Crystal engineering: a holistic view. *Angew. Chem., Int. Ed.* **2007**, *46*, 8342−8356.
(5) Braga, D.; Grepioni, F.; Maini, L.; d'Agostino, S. Making crystals with a purpose; a journey in crystal engineering at the University of Bologna. *IUCrJ* **2017**, *4*, 369−379.
(6) Aakeroy, C. B.; Salmon, D. J. Building co-crystals with molecular sense and supramolecular sensibility. *CrystEngComm* **2005**, *7*, 439−448.
(7) Babu, N. J.; Nangia, A. Solubility Advantage of Amorphous Drugs and Pharmaceutical Cocrystals. *Cryst. Growth Des.* **2011**, *11*, 2662−2679.
(8) Andre, V.; Shemchuk, O.; Grepioni, F.; Braga, D.; Duarte, M. T. Expanding the Pool of Multicomponent Crystal Forms of the Antibiotic 4-Aminosalicylic Acid: The Influence of Crystallization Conditions. *Cryst. Growth Des.* **2017**, *17*, 6417−6425.
(9) Good, D. J.; Rodriguez-Hornedo, N. Solubility Advantage of Pharmaceutical Cocrystals. *Cryst. Growth Des.* **2009**, *9*, 2252−2264.
(10) Yadav, A. V.; Shete, A. S.; Dabke, A. P.; Kulkarni, P. V.; Sakhare, S. S. Co-crystals: a novel approach to modify physicochemical properties of active pharmaceutical ingredients. *Indian J. Pharm. Sci.* **2009**, *71*, 359−370.
(11) Schultheiss, N.; Newman, A. Pharmaceutical Cocrystals and Their Physicochemical Properties. *Cryst. Growth Des.* **2009**, *9*, 2950−2967.
(12) Golob, S.; Perry, M.; Lusi, M.; Chierotti, M. R.; Grabnar, I.; Lassiani, L.; Voinovich, D.; Zaworotko, M. J. Improving Biopharmaceutical Properties of Vinpocetine Through Cocrystallization. *J. Pharm. Sci.* **2016**, *105*, 3626−3633.

(13) Shan, N.; Zaworotko, M. J. The role of cocrystals in pharmaceutical science. *Drug Discovery Today* **2008**, *13*, 440−446.

(14) Stanton, M. K.; Bak, A. Physicochemical properties of pharmaceutical co-crystals: A case study of ten AMG 517 co-crystals. *Cryst. Growth Des.* **2008**, *8*, 3856−3862.

(15) Steed, J. W. The role of co-crystals in pharmaceutical design. *Trends Pharmacol. Sci.* **2013**, *34*, 185−193.

(16) Wouters, J.; Quéré, L. *Pharmaceutical salts and co-crystals*; Royal Society of Chemistry: 2011.

(17) Honer, K.; Kalfaoglu, E.; Pico, C.; McCann, J.; Baltrusaitis, J. Mechanosynthesis of Magnesium and Calcium Salt−Urea Ionic Cocrystal Fertilizer Materials for Improved Nitrogen Management. *ACS Sustainable Chem. Eng.* **2017**, *5*, 8546−8550.

(18) Casali, L.; Mazzei, L.; Shemchuk, O.; Sharma, L.; Honer, K.; Grepioni, F.; Ciurli, S.; Braga, D.; Baltrusaitis, J. Novel Dual-Action Plant Fertilizer and Urease Inhibitor: Urea·Catechol Cocrystal. Characterization and Environmental Reactivity. *ACS Sustainable Chem. Eng.* **2019**, *7*, 2852−2859.

(19) Julien, P. A.; Germann, L. S.; Titi, H. M.; Etter, M.; Dinnebier, R. E.; Sharma, L.; Baltrusaitis, J.; Friscic, T. In situ monitoring of mechanochemical synthesis of calcium urea phosphate fertilizer cocrystal reveals highly effective water-based autocatalysis. *Chem. Sci.* **2020**, *11*, 2350−2355.

(20) Nauha, E.; Nissinen, M. Co-crystals of an agrochemical active − A pyridine-amine synthon for a thioamide group. *J. Mol. Struct.* **2011**, *1006*, 566−569.

(21) Zhang, J.; Shreeve, J. n. M. Time for pairing: cocrystals as advanced energetic materials. *CrystEngComm* **2016**, *18*, 6124−6133.

(22) Wei, X.; Ma, Y.; Long, X.; Zhang, C. A strategy developed from the observed energetic−energetic cocrystals of BTF: cocrystallizing and stabilizing energetic hydrogen-free molecules with hydrogenous energetic coformer molecules. *CrystEngComm* **2015**, *17*, 7150−7159.

(23) Kent, R. V.; Wiscons, R. A.; Sharon, P.; Grinstein, D.; Frimer, A. A.; Matzger, A. J. Cocrystal Engineering of a High Nitrogen Energetic Material. *Cryst. Growth Des.* **2018**, *18*, 219−224.

(24) Schultheiss, N.; Bethune, S.; Henck, J. O. Nutraceutical cocrystals: utilizing pterostilbene as a cocrystal former. *CrystEngComm* **2010**, *12*, 2436−2442.

(25) Bethune, S. J.; Schultheiss, N.; Henck, J. O. Improving the Poor Aqueous Solubility of Nutraceutical Compound Pterostilbene through Cocrystal Formation. *Cryst. Growth Des.* **2011**, *11*, 2817−2823.

(26) Bevill, M. J.; Vlahova, P. I.; Smit, J. P. Polymorphic Cocrystals of Nutraceutical Compound p-Coumaric Acid with Nicotinamide: Characterization, Relative Solid-State Stability, and Conversion to Alternate Stoichiometries. *Cryst. Growth Des.* **2014**, *14*, 1438−1448.

(27) Burdock, G. A.; Carabin, I. G. Generally recognized as safe (GRAS): history and description. *Toxicol. Lett.* **2004**, *150*, 3−18.

(28) Braga, D.; Grepioni, F.; Lampronti, G. I.; Maini, L.; Turrina, A. Ionic Co-crystals of Organic Molecules with Metal Halides: A New Prospect in the Solid Formulation of Active Pharmaceutical Ingredients. *Cryst. Growth Des.* **2011**, *11*, 5621−5627.

(29) Sekhon, B. S. Drug-drug co-crystals. *Daru, J. Pharm. Sci.* **2012**, *20*, 45.

(30) Braga, D.; Grepioni, F.; Maini, L.; Capucci, D.; Nanna, S.; Wouters, J.; Aerts, L.; Quere, L. Combining piracetam and lithium salts: ionic co-crystals and co-drugs? *Chem. Commun.* **2012**, *48*, 8219−8221.

(31) Bordignon, S.; Cerreia Vioglio, P.; Priola, E.; Voinovich, D.; Gobetto, R.; Nishiyama, Y.; Chierotti, M. R. Engineering Codrug Solid Forms: Mechanochemical Synthesis of an Indomethacin−Caffeine System. *Cryst. Growth Des.* **2017**, *17*, 5744−5752.

(32) Shemchuk, O.; Braga, D.; Grepioni, F. Ionic Cocrystals of Levodopa and Its Biological Precursors L-Tyrosine and L-Phenylalanine with LiCl. *Cryst. Growth Des.* **2019**, *19*, 6560−6565.

(33) Wang, L.-Y.; Bu, F.-Z.; Li, Y.-T.; Wu, Z.-Y.; Yan, C.-W. A Sulfathiazole−Amantadine Hydrochloride Cocrystal: The First Codrug Simultaneously Comprising Antiviral and Antibacterial Components. *Cryst. Growth Des.* **2020**, *20*, 3236−3246.

(34) Nugrahani, I.; Asyarie, S.; Soewandhi, S. N.; Ibrahim, S. The Antibiotic Potency of Amoxicillin-Clavulanate Co-Crystal. *Int. J. Pharmacol.* **2007**, *3*, 475−481.

(35) Bhatt, P. M.; Azim, Y.; Thakur, T. S.; Desiraju, G. R. Co-Crystals of the Anti-HIV Drugs Lamivudine and Zidovudine. *Cryst. Growth Des.* **2009**, *9*, 951−957.

(36) Almansa, C.; Mercè, R.; Tesson, N.; Farran, J.; Tomàs, J.; Plata-Salamán, C. R. Co-crystal of Tramadol Hydrochloride−Celecoxib (ctc): A Novel API−API Co-crystal for the Treatment of Pain. *Cryst. Growth Des.* **2017**, *17*, 1884−1892.

(37) Theuretzbacher, U. Global antibacterial resistance: The never-ending story. *J. Glob. Antimicrob. Resist.* **2013**, *1*, 63−69.

(38) Levy, S. B.; Marshall, B. Antibacterial resistance worldwide: causes, challenges and responses. *Nat. Med.* **2004**, *10*, S122−S129.

(39) Brown, E. D.; Wright, G. D. Antibacterial drug discovery in the resistance era. *Nature* **2016**, *529*, 336−343.

(40) de Kraker, M. E.; Davey, P. G.; Grundmann, H. Mortality and hospital stay associated with resistant Staphylococcus aureus and Escherichia coli bacteremia: estimating the burden of antibiotic resistance in Europe. *PLoS Med.* **2011**, *8*, e1001104.

(41) Li, X.; Bai, H.; Yang, Y.; Yoon, J.; Wang, S.; Zhang, X. Supramolecular Antibacterial Materials for Combatting Antibiotic Resistance. *Adv. Mater.* **2018**, *31*, 1805092.

(42) Payne, D. J.; Gwynn, M. N.; Holmes, D. J.; Pompliano, D. L. Drugs for bad bugs: confronting the challenges of antibacterial discovery. *Nat. Rev. Drug Discovery* **2007**, *6*, 29−40.

(43) Shemchuk, O.; Braga, D.; Grepioni, F.; Turner, R. J. Co-crystallization of antibacterials with inorganic salts: paving the way to activity enhancement. *RSC Adv.* **2020**, *10*, 2146−2149.

(44) Carpenter, M. S.; Easter, W. M. The Isopropyl Cresols. *J. Org. Chem.* **1955**, *20*, 401−411.

(45) Healy, A. M.; Worku, Z. A.; Kumar, D.; Madi, A. M. Pharmaceutical solvates, hydrates and amorphous forms: A special emphasis on cocrystals. *Adv. Drug Delivery Rev.* **2017**, *117*, 25−46.

(46) Morissette, S. L.; Almarsson, O.; Peterson, M. L.; Remenar, J. F.; Read, M. J.; Lemmo, A. V.; Ellis, S.; Cima, M. J.; Gardner, C. R. High-throughput crystallization: polymorphs, salts, co-crystals and solvates of pharmaceutical solids. *Adv. Drug Delivery Rev.* **2004**, *56*, 275−300.

(47) Grepioni, F.; Braga, D.; Chelazzi, L.; Shemchuk, O.; Maffei, P.; Sforzini, A.; Viscomi, G. C. Improving solubility and storage stability of rifaximin via solid-state solvation with Transcutol®. *CrystEngComm* **2019**, *21*, 5278−5283.

(48) Li, K. K.; Yin, S. W.; Yang, X. Q.; Tang, C. H.; Wei, Z. H. Fabrication and characterization of novel antimicrobial films derived from thymol-loaded zein-sodium caseinate (SC) nanoparticles. *J. Agric. Food Chem.* **2012**, *60*, 11592−11600.

(49) Nieto, G. Biological Activities of Three Essential Oils of the Lamiaceae Family. *Medicines (Basel)* **2017**, *4*, 63.

(50) Bassole, I. H.; Juliani, H. R. Essential oils in combination and their antimicrobial properties. *Molecules* **2012**, *17*, 3989−4006.

(51) Kim, J. M.; Marshall, M. R.; Cornell, J. A.; Preston, J. F., III; Wei, C. I. Antibacterial activity of carvacrol, citral, and geraniol against Salmonella typhimurium in culture medium and on fish cubes. *J. Food Sci.* **1995**, *60*, 1364−1368.

(52) Marchese, A.; Orhan, I. E.; Daglia, M.; Barbieri, R.; Di Lorenzo, A.; Nabavi, S. F.; Gortzi, O.; Izadi, M.; Nabavi, S. M. Antibacterial and antifungal activities of thymol: A brief review of the literature. *Food Chem.* **2016**, *210*, 402−414.

(53) Falcone, P.; Speranza, B.; Del Nobile, M. A.; Corbo, M. R.; Sinigaglia, M. A study on the antimicrobial activity of thymol intended as a natural preservative. *J. Food Prot.* **2005**, *68*, 1664−1670.

(54) Valero, D.; Valverde, J. M.; Martinez-Romero, A.; Guillen, F.; Castillo, S.; Serrano, M. The combination of modified atmosphere packaging with eugenol or thymol to maintain quality, safety and functional properties of table grapes. *Postharvest Biol. Technol.* **2006**, *41*, 317−327.

(55) Altieri, C.; Speranza, B.; Del Nobile, M. A.; Sinigaglia, M. Suitability of bifidobacteria and thymol as biopreservatives in

extending the shelf life of fresh packed plaice fillets. *J. Appl. Microbiol.* **2005**, *99*, 1294−1302.

(56) Persico, P.; Ambrogi, V.; Carfagna, C.; Cerruti, P.; Ferrocino, I.; Mauriello, G. Nanocomposite Polymer Films Containing Carvacrol for Antimicrobial Active Packaging. *Polym. Eng. Sci.* **2009**, *49*, 1447−1455.

(57) https://www.ema.europa.eu/en/human-regulatory/herbal-medicinal-products.

(58) Ash, M., *Handbook of preservatives*. ed.; Synapse Info Resources: 2004; carvacrol, p 576; thymol, p 1034.

(59) Flavor and Extract Manufacturers Association of the United States: "The safety standard applied by the FEMA Expert Panel is the same standard required by FDA, i.e. a "reasonable certainty of no harm." The FEMA Expert Panel only evaluates substances for GRAS status that are used to formulate flavors to be added to human foods. The Expert Panel does not evaluate food ingredients with functions other than flavoring nor does it evaluate flavorings for use in products other than human food." See https://www.femaflavor.org/gras.

(60) Mazzeo, P. P.; Carraro, C.; Monica, A.; Capucci, D.; Pelagatti, P.; Bianchi, F.; Agazzi, S.; Careri, M.; Raio, A.; Carta, M.; Menicucci, F.; Belli, M.; Michelozzi, M.; Bacchi, A. Designing a Palette of Cocrystals Based on Essential Oil Constituents for Agricultural Applications. *ACS Sustainable Chem. Eng.* **2019**, *7*, 17929−17940.

(61) Degen, T.; Sadki, M.; Bron, E.; Konig, U.; Nenert, G. The HighScore suite. *Powder Diffr.* **2014**, *29*, S13−S18.

(62) Altomare, A.; Cuocci, C.; Giacovazzo, C.; Moliterni, A.; Rizzi, R.; Corriero, N.; Falcicchio, A. EXPO2013: a kit of tools for phasing crystal structures from powder data. *J. Appl. Crystallogr.* **2013**, *46*, 1231−1235.

(63) Cohelo, A. *TOPAS-Academic*; Coelho Software: Brisbane, Australia, 2007.

(64) Sheldrick, G. M. SHELXT - integrated space-group and crystal-structure determination. *Acta Crystallogr., Sect. A: Found. Adv.* **2015**, *71*, 3−8.

(65) Sheldrick, G. M. Crystal structure refinement with SHELXL. *Acta Crystallogr., Sect. C: Struct. Chem.* **2015**, *71*, 3−8.

(66) Dolomanov, O. V.; Bourhis, L. J.; Gildea, R. J.; Howard, J. A. K.; Puschmann, H. OLEX2: a complete structure solution, refinement and analysis program. *J. Appl. Crystallogr.* **2009**, *42*, 339−341.

(67) Macrae, C. F.; Edgington, P. R.; McCabe, P.; Pidcock, E.; Shields, G. P.; Taylor, R.; Towler, M.; van De Streek, J. Mercury: visualization and analysis of crystal structures. *J. Appl. Crystallogr.* **2006**, *39*, 453−457.

(68) Clinical and Laboratory Standards Institute. *Performance standards for antimicrobial susceptibility testing; sixteenth informational supplement*, CLSI document M100-S16CLSI; CLSI: Wayne, PA, 2006.

(69) European Committee for Antimicrobial Susceptibility Testing (EUCAST) of the European Society of Clinical Microbiology and Infectious Diseases (ESCMID). Determination of minimum inhibitory concentrations (MICs) of antibacterial agents by broth dilution. *Clin. Microbiol. Infect.* **2003**, *9*, ix−xv.

(70) Wiegand, I.; Hilpert, K.; Hancock, R. E. Agar and broth dilution methods to determine the minimal inhibitory concentration (MIC) of antimicrobial substances. *Nat. Protoc.* **2008**, *3*, 163−175.

(71) Mazzeo, P. P.; Canossa, C.; Carraro, C.; Pelagatti, P.; Bacchi, A. Systematic coformer contribution to cocrystal stabilization: energy and packing trends. *CrystEngComm* **2020**, DOI: 10.1039/D0CE00291G.

(72) Thozet, A.; Perrin, M. Structure of 2-isopropyl-5-methylphenol (thymol). *Acta Crystallogr., Sect. B: Struct. Crystallogr. Cryst. Chem.* **1980**, *36*, 1444−1447.

99

3.1.1 Supporting information

Natural antimicrobials meet a synthetic antibiotic: carvacrol/thymol and ciprofloxacin cocrystals as a promising solid-state route to activity enhancement.

Oleksii Shemchuk, [a] Simone d'Agostino, [a] Cecilia Fiore, [a] Vittorio Sambri, [b] Silvia Zannoli, [c] Fabrizia Grepioni, [a] Dario Braga* [a]

[a] Dipartimento di Chimica "Giacomo Ciamician", Università di Bologna, Via Selmi, 2 – 40126 Bologna – Italy.
[b] Dipartimento di Medicina Specialistica, Diagnostica e Sperimentale Università di Bologna, Via Selmi, 2, 40126 Bologna, Italy.
[c] U.O.Microbiologia - Settore Biologia Molecolare Laboratorio Unico Centro Servizi AUSL Romagna

CRYSTALLOGRAPHIC DATA

Table SI-1. Crystal data and details of measurements

|	CIP·CAR$_4$	CIP·THY$_4$	CIP·THY$_2$
Formula	$C_{17}H_{18}FN_3O_3 \cdot 4(C_{10}H_{14}O)$	$C_{17}H_{18}FN_3O_3 \cdot 4(C_{10}H_{14}O)$	$C_{17}H_{18}FN_3O_3 \cdot 2(C_{10}H_{14}O)$
Fw (g mol^{-1})	932.19	932.19	631.77
T / K	293 (2)	250 (2)	293 (2)
Crystal system	Monoclinic	Monoclinic	Monoclinic
Space group	$P2_1/c$	$P2_1/n$	$P2_1/n$
Z, Z'	4, 1	4, 1	4, 1
a (Å)	17.2650 (12)	18.3044 (7) (1)	24.0906 (8)
b (Å)	18.2944 (11)	13.1847 (9) (1)	13.7891 (5)
c (Å)	18.0447 (10)	22.3769 (8) (1)	10.5350 (3)
α (°)	90.0	90.0	90.0
β (°)	107.480 (7)	99.509 (4)	91.068 (3)
γ (°)	90.0	90.0	90.0
V (Å^3)	5436.3 (6)	5326.2 (5)	3498.98 (19)
R_{wp}	-	-	0.065
R_p	-	-	0.049
R_{exp}	-	-	0.036
χ^2	-	-	1.84
d (mg cm^{-3})	1.139	1.163	-
μ (mm^{-1})	0.08	0.08	-
Measd reflns	23800	24732	-
Indep reflns	12454	12361	-
Reflns [I > 2σ(I)]	5294	4119	-
R_{int}	0.035	0.072	-
R[F^2 > 2σ(F^2)]	0.068	0.079	-
wR(F^2)	0.178	0.159	-

Rietveld refinement
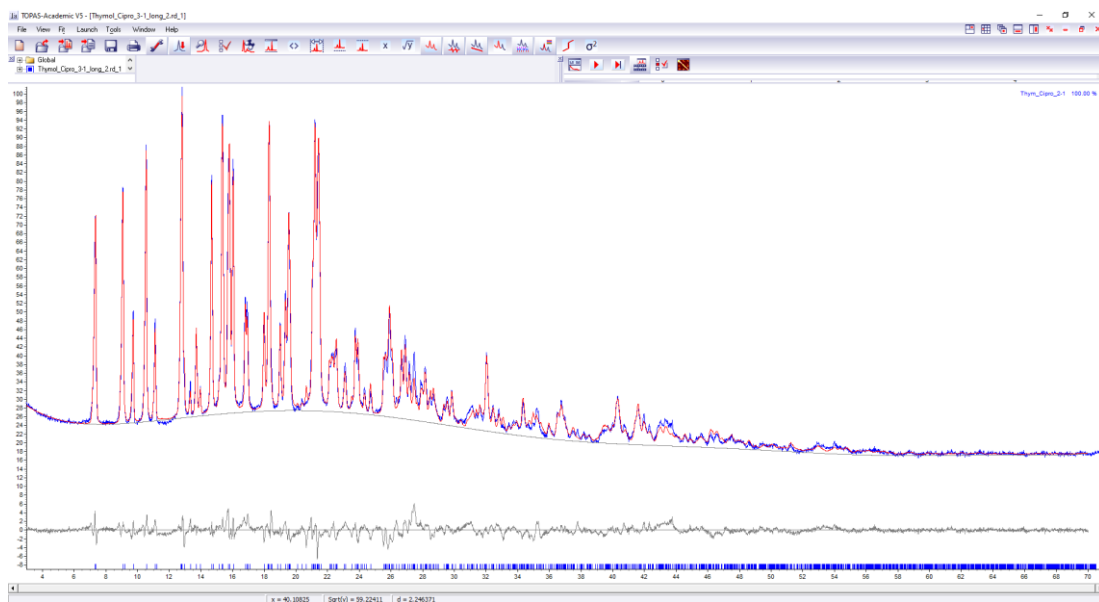
Figure SI-1. Rietveld analysis plot of CIP·THY$_2$. Red line is the calculated diffractogram, blue line is the observed diffractogram and grey line is the difference plot. Y-axis is reported as $\sqrt{y}$.
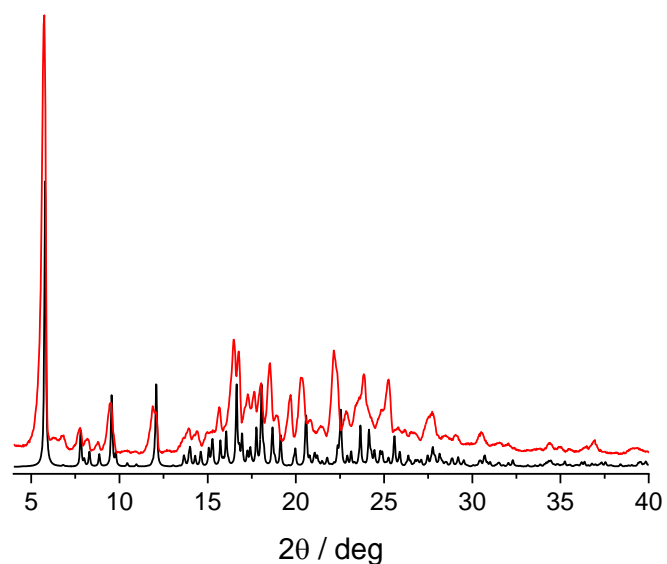
X-RAY POWDER DIFFRACTION PATTERNS
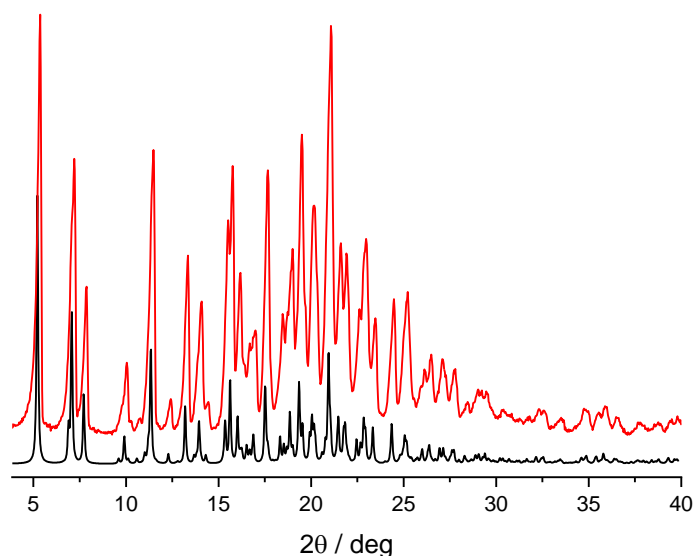
Figure SI-2. Comparison between the experimental (red) XRPD pattern of CIP·CAR$_4$, as obtained via kneading, and the pattern calculated (black) on the basis of single crystal data.
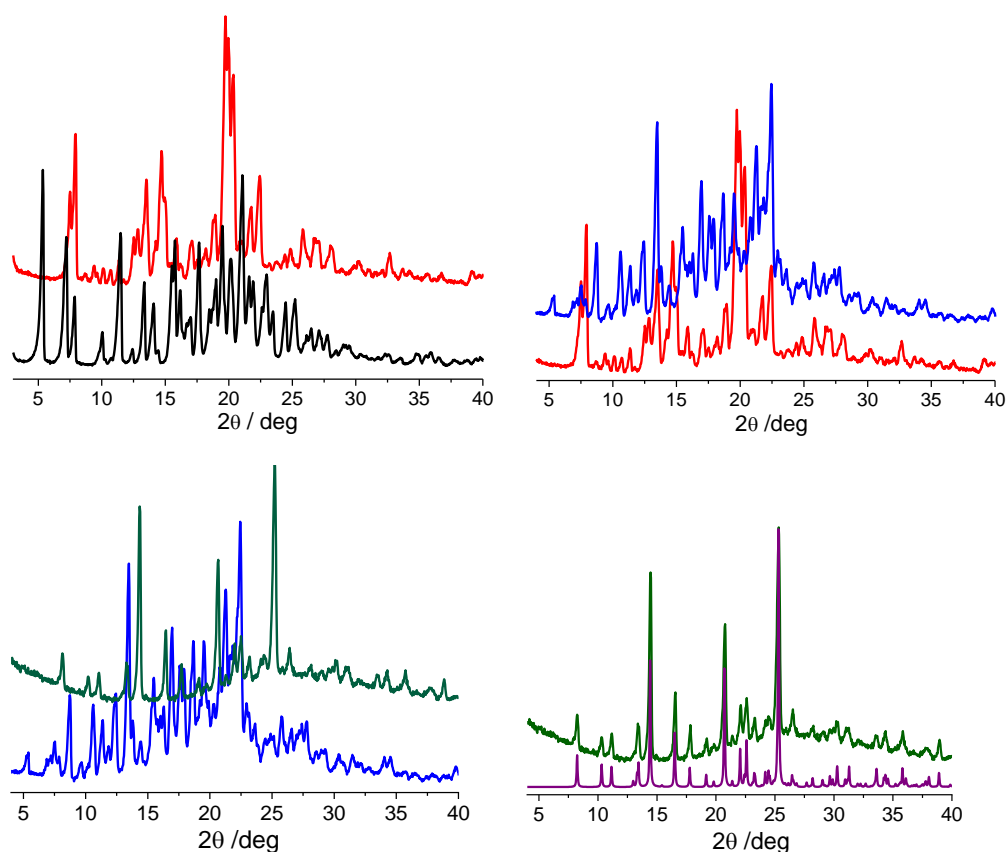
Figure SI-3. VT-XRPD for CIP·CAR$_4$. (top left) Release of one CAR molecule and transformation of CIP·CAR$_4$ (black line, RT) into CIP·CAR$_3$ (red, 80 °C); (top right) release of a second CAR molecule and transformation of CIP·CAR$_3$ (red, 80 °C) into CIP·CAR$_2$ (blue, 100 °C); (bottom left) Complete removal of CAR molecules from CIP·CAR$_2$ (blue, 100 °C) and recrystallization of pure CIP (green 110 °C); (bottom right) comparison of the experimental (green) pattern at 110 °C with the calculated (purple) one for pure CIP (from refcode UHITOV).

Figure SI-4. Comparison between the experimental (red), room temperature XRPD pattern of CIP·THY$_4$, as obtained via slurry, and the pattern calculated (black) on the basis of single crystal data collected at 250K (differences in the peaks positions are due to the difference in data collection temperatures).
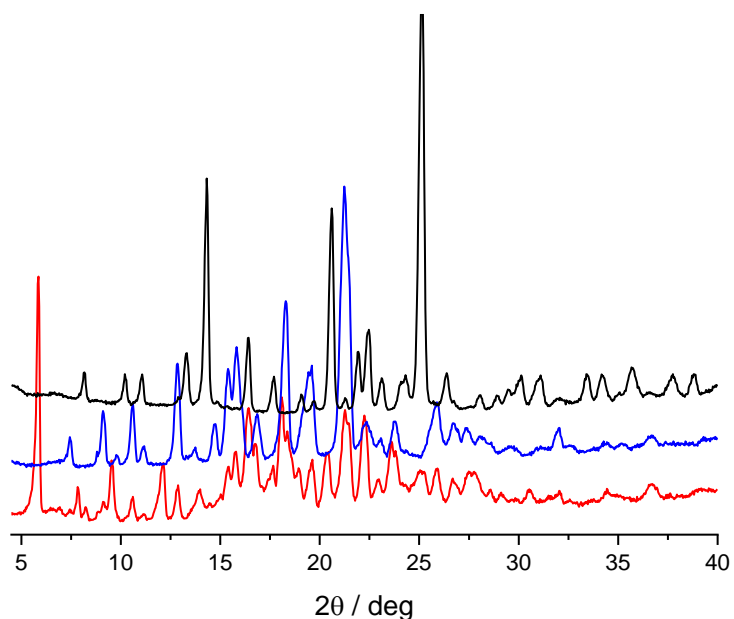
Figure SI-5. Variable temperature XRPD measurements for CIP·THY$_4$. Upon heating, thymol is released in two steps: the room temperature form (red) transforms into CIP·THY$_2$ (blue) at 70 °C, and into pure CIP (black) above 135 °C.

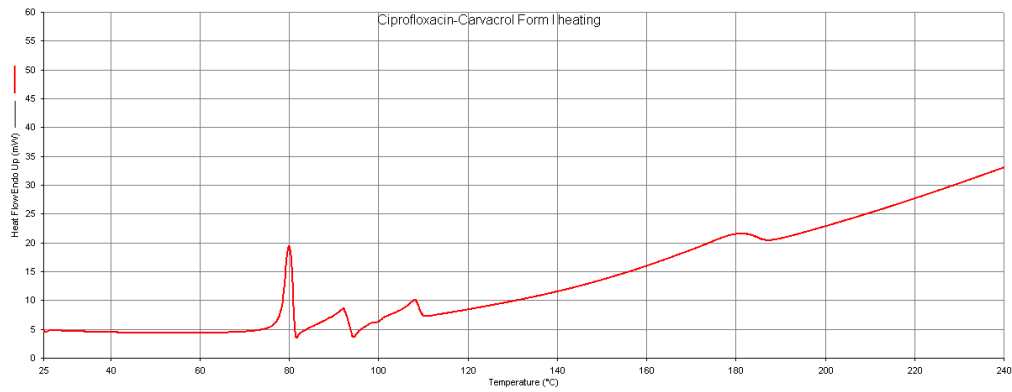## DSC AND TGA DATA
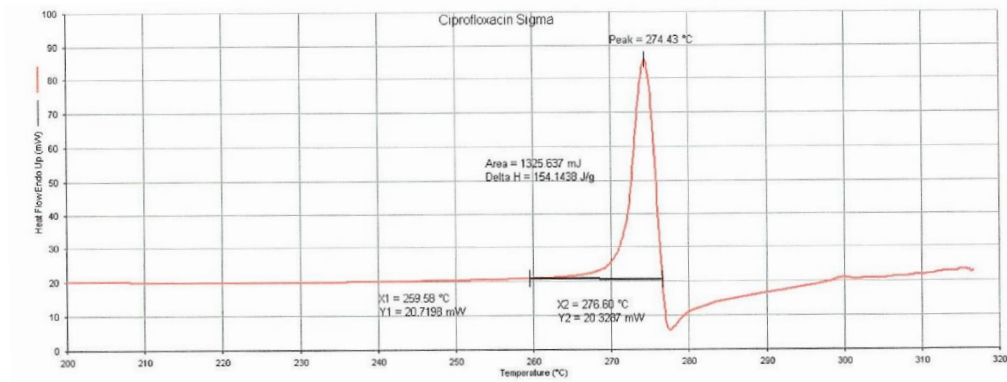
Figure SI-6. DSC trace for CIP.
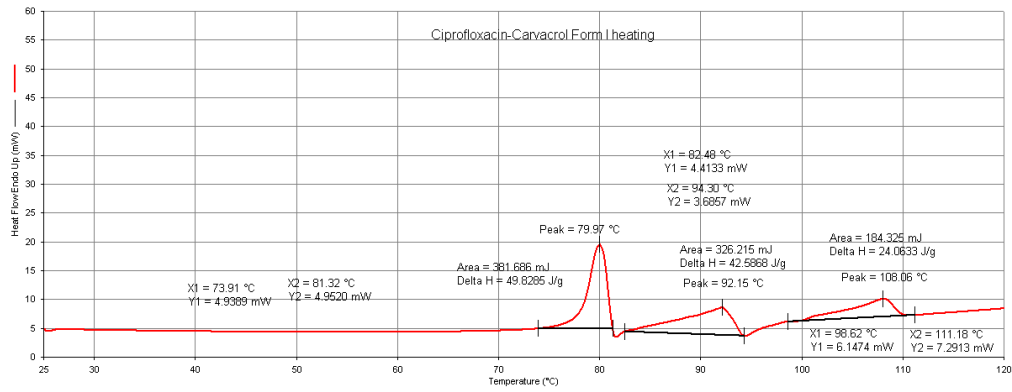
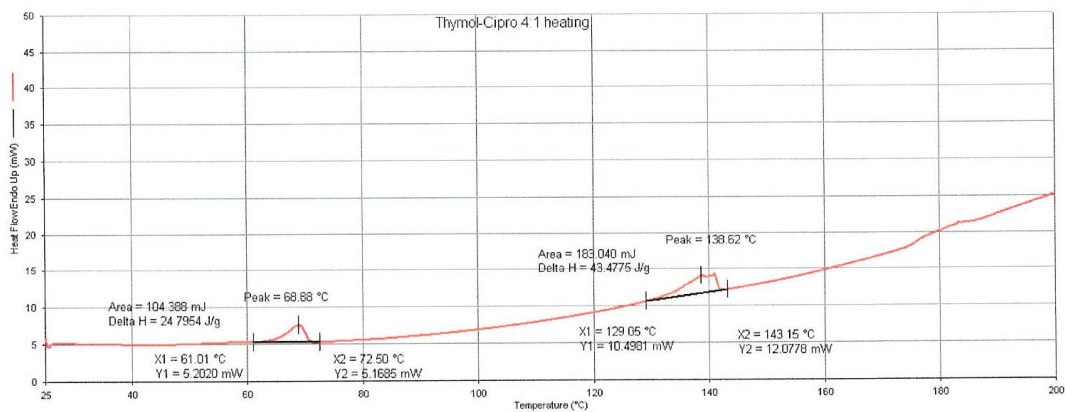**Figure SI-7.** DSC traces (the second expanded horizontally) for CIP·CAR$_4$

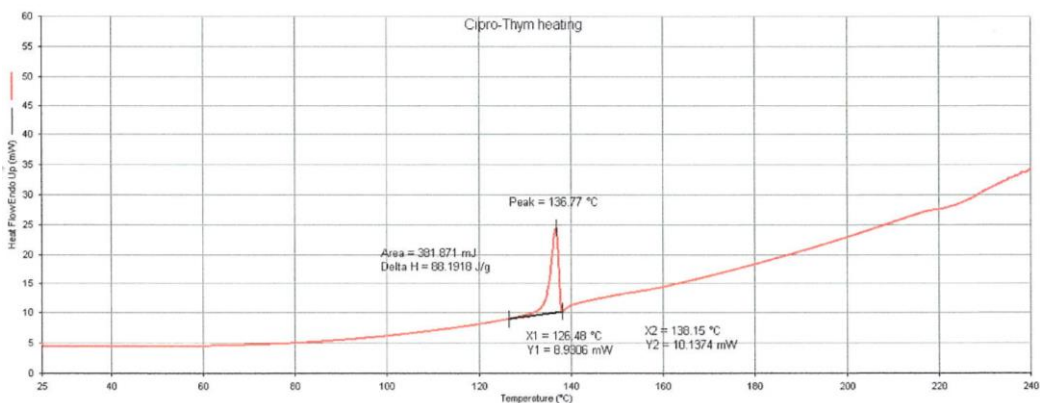**Figure SI-8**. DSC trace for CIP·THY$_4$.
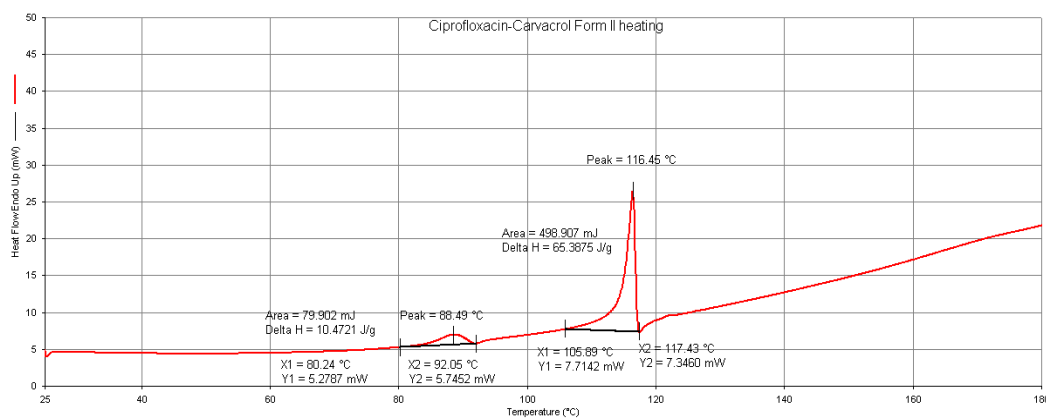

Figure SI-9. DSC trace for CIP·THY$_2$.

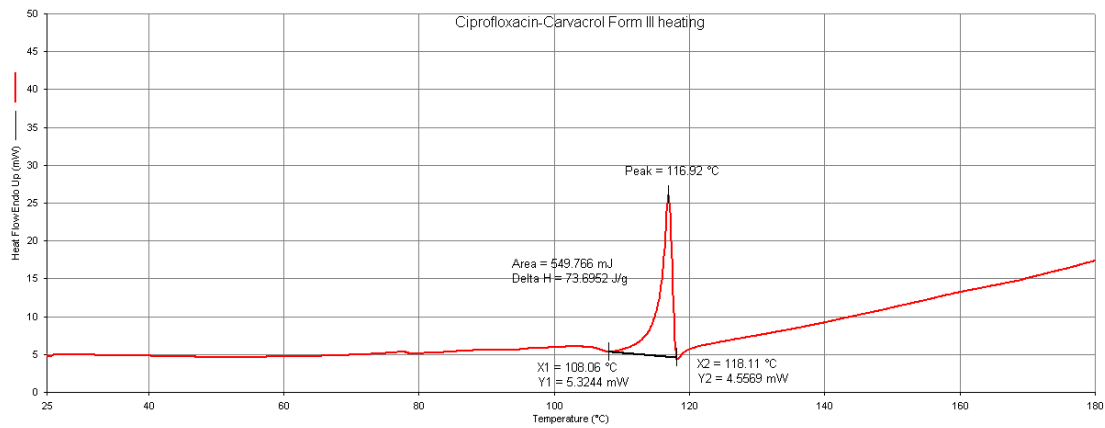**Figure SI-10**. DSC trace for CIP·CAR$_3$.

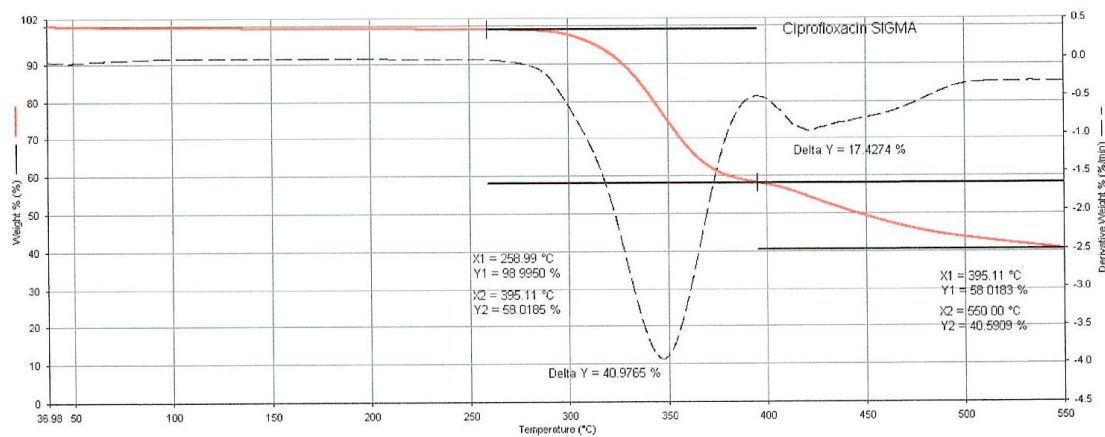**Figure SI-11**. DSC trace for CIP·CAR$_2$.
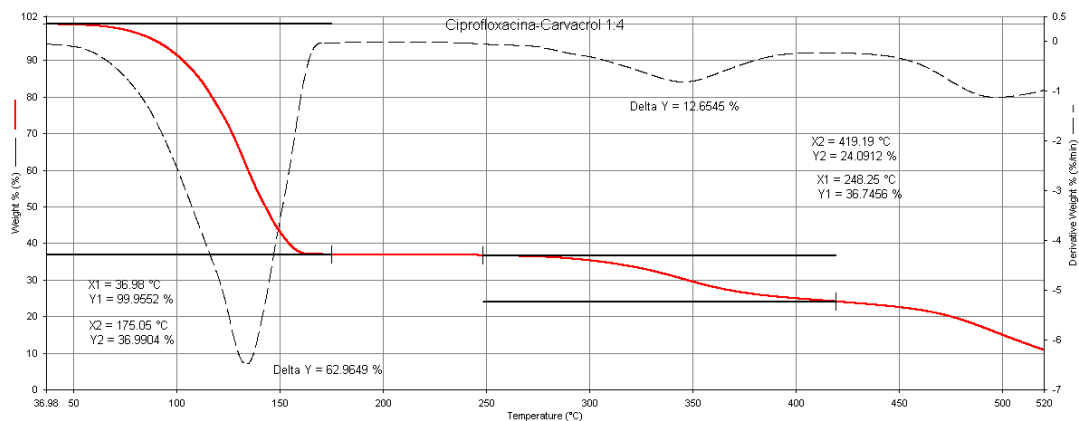

Figure SI-12. TGA trace for CIP.

Figure SI- 13. TGA traces for CIP·CAR$_4$. Note how only one large mass release (ca. 63%) corresponding to the weight of four molecules of carvacrol is observed.
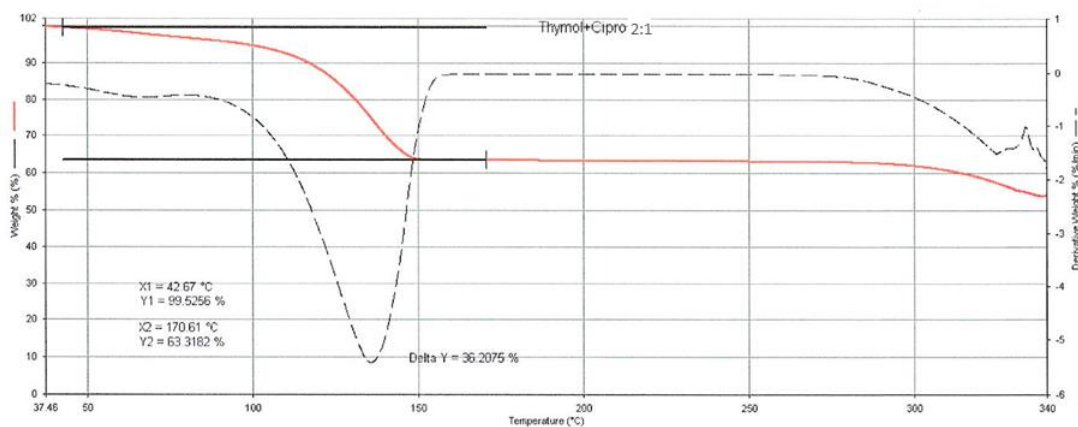
Figure SI-14. TGA trace for CIP·THY$_2$.

Figure SI-15. TGA trace for CIP·CAR$_3$.

Figure SI-16. TGA trace for CIP·CAR$_2$.

References

1)   Fabbiani, F. P. A.; Dittrich, B.; Florence, A. J.; Gelbrich, T.; Hursthouse, M. B.; Kuhs, W. F.; Shankland, N.; Sowa, H., Crystal structures with a challenge: high-pressure crystallisation of ciprofloxacin sodium salts and their recovery to ambient pressure. *CrystEngComm* **2009,** 11, (7), 1396-1406.

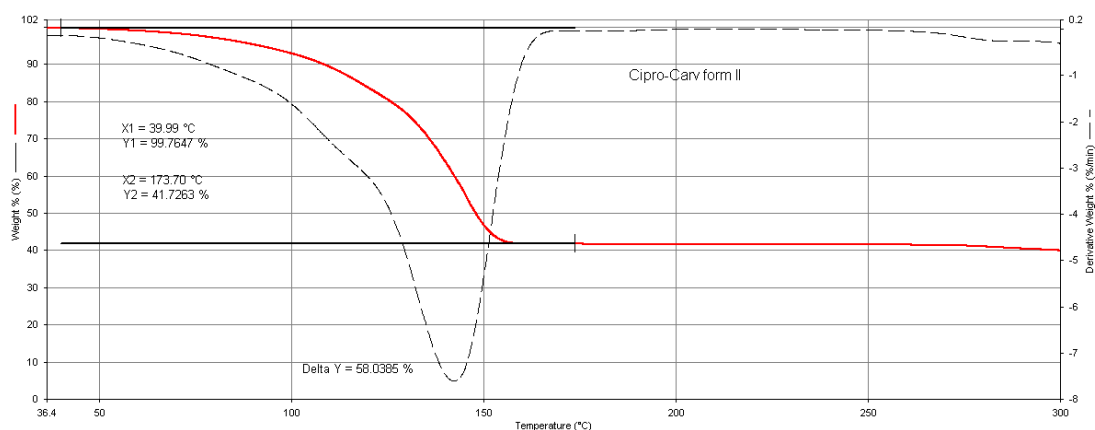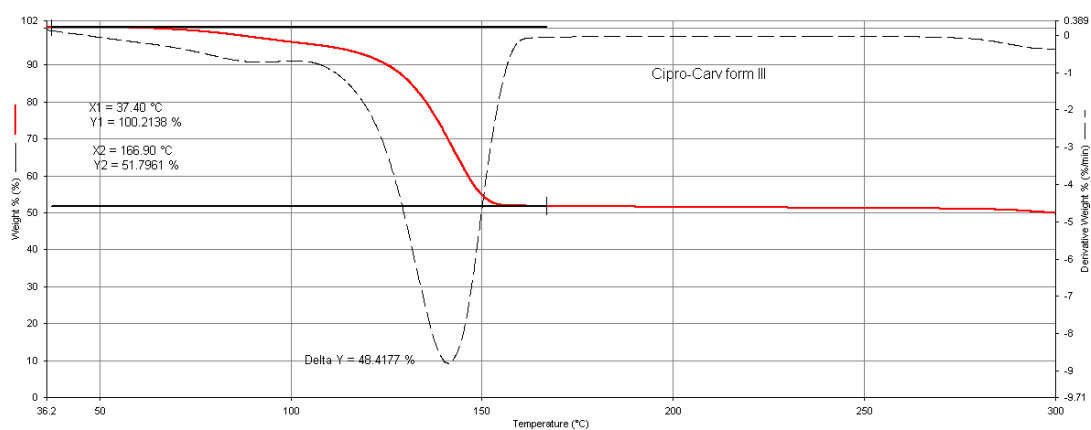## 3.2 Inhibition of the antibiotic activity of cephalosporines by co-crystallization with thymol

Abstract

Three structurally similar antibiotics of the cephalosporin (CEPH) class, namely, cephalexin (CPX), cephradine (CFD), and cefaclor (CFC), have been co-crystallized with thymol (THY) via different preparation techniques, yielding the hydrated co-crystals CPX·THY·2.5H$_2$O form I and form II, CFD· THY·2.5H$_2$O, and CFC·THY·4H$_2$O. All co-crystals were structurally characterized by single crystal and/or powder X-ray diffraction. In all co-crystals, except in the case of the elusive metastable form I of CPX·THY·2.5H$_2$O, the CEPH molecules interact with thymol only via water bridges; *i.e.*, there is no direct hydrogen bonding between CEPH molecules and THY. Preliminary antimicrobial experiments via measurements of minimal inhibitory concentration (MIC) provide clear-cut evidence that the association with thymol increases the resistance of both Gram-negative and Gram-positive bacteria to the antibiotic with respect to pure CEPH as well as to physical mixtures of CEPH with thymol.

Inhibition of the Antibiotic Activity of Cephalosporines by Co-Crystallization with Thymol

Published as part of a Crystal Growth and Design joint virtual special issue on Crystallizing the Role of Solid-State Form in Drug Delivery

Cecilia Fiore, Alessandra Baraghini, Oleksii Shemchuk, Vittorio Sambri,* Manuela Morotti, Fabrizia Grepioni, and Dario Braga*
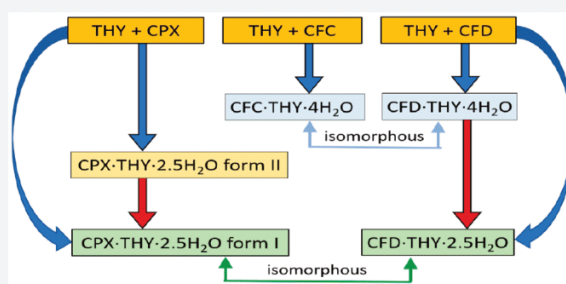
Read Online

ACCESS | Metrics & More | Article Recommendations | Supporting Information

ABSTRACT: Three structurally similar antibiotics of the cephalosporin (CEPH) class, namely, cephalexin (CPX), cephradine (CFD), and cefaclor (CFC), have been co-crystallized with thymol (THY) via different preparation techniques, yielding the hydrated co-crystals CPX·THY·2.5H$_2$O form I and form II, CFD·THY·2.5H$_2$O, and CFC·THY·4H$_2$O. All co-crystals were structurally characterized by single crystal and/or powder X-ray diffraction. In all co-crystals, except in the case of the elusive metastable form I of CPX·THY·2.5H$_2$O, the CEPH molecules interact with thymol only via water bridges; i.e., there is no direct hydrogen bonding between CEPH molecules and THY. Preliminary antimicrobial experiments via measurements of minimal inhibitory concentration (MIC) provide clear-cut evidence that the association with thymol increases the resistance of both Gram-negative and Gram-positive bacteria to the antibiotic with respect to pure CEPH as well as to physical mixtures of CEPH with thymol.

INTRODUCTION

Multicomponent molecular solids are attractive targets in the quest for novel molecular materials and are finding application in a variety of fields including pharmaceuticals,[1−6] nutraceuticals,[7−9] agrochemicals,[10−12] high-energy materials,[13−15] and pigments.[16−18] Since the solid-state packing arrangement of the building blocks (molecular and/or ionic) can dramatically affect the collective properties of the materials, it is of paramount importance to understand the relationship between the properties of the individual components and those resulting from the assembly of active ingredients and co-formers. Co-crystals have become an attractive research target, since they may provide alternative routes to new or improved properties of active molecules.[19] Pharmaceutical co-crystals composed of an active pharmaceutical ingredient (API) and a non-active ancillary co-former, selected from the Generally Recognized As Safe (GRAS) list of substances,[20] are being actively investigated by crystal engineers. It is also possible to co-crystallize an API with another API, thus forming a drug−drug (or co-drug) co-crystal.[21−27] In drug−drug co-crystals, not only the solid-state physicochemical properties of the API are altered with respect to those of the separate components, but also the pharmaceutical and biological activity may result in being significantly different because of synergistic or antagonistic effects. The first example of a co-drug was a combination of a sedative pharmaceutical pyrithyldione and a non-steroidal anti-inflammatory drug propyphenazone patented by Hoffman-La Roche in 1937.[28] In more advanced applications, APIs are chosen in a way that both have similar biological activity, and their combination as co-crystals might result in enhancement of the biological activity with respect to that of the separate components or of their physical mixture.[29−32] One of such cases has been recently reported by our research group for the co-crystals of the synthetic antibiotic ciprofloxacin with the natural antibacterial agents thymol and carvacrol (see also below).[33]

In this paper, we report our results in the co-crystallization of three representatives of the cephalosporin (CEPH) class of antibiotics, namely, cephalexin (CPX), cefradine (CFD), and cefaclor (CFC), with thymol (THY) used as a co-former (see Scheme 1).

Cephalosporins are a class of β-lactam antibiotics, extracted for the first time from the fungus *Cephalosporium acremonium*
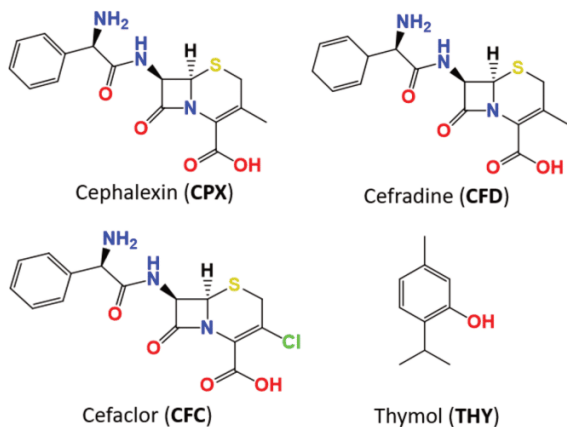
1467

Scheme 1. The First Generation Cephalosporin Antibiotics Cephalexin (CPX) and Cefradine (CFD), the Second Generation Cephalosporin Cefaclor (CFC), and the Co-Former Thymol (THY) Used in Our Study[a]

Cephalexin (**CPX**)

Cefradine (**CFD**)

Cefaclor (**CFC**)

Thymol (**THY**)

[a]CPX, CFD, and CFC were all used in their zwitterionic form.

in 1945.[34] The central nucleus of cephalosporins is formed by D-α-aminoadipic acid condensed with a β-lactam ring; this complex is called 7-aminocephalosporanic acid and represents the nucleus to which the side chains are linked for the synthesis of the various cephalosporins. The mechanism of action is carried out by synthesis inhibition of the bacterial cell wall, similarly to what was observed in the case of penicillin and derivatives.

Cephalosporins are classified into five generations according to the general characteristics of antimicrobial activity.[35] The first generation of cephalosporins, in our case cephalexin and cefradine, shows a good activity in a wide range against Gram-positive bacteria and a relatively modest activity against Gram-negative bacteria. Most of the Gram-positive cocci and oral cavity anaerobes are sensitive to the action of the first generation of cephalosporins as well as against *M. catarrhalis*, *E. coli*, *K. pneumoniae*, and *P. mirabilis*.[36] The second generation of cephalosporins is more active against Gram-negative microorganisms such as *Citrobacter* and *Enterobacter*. Cefaclor is a second-generation cephalosporin and is particularly active against *H. influenzae* and *M. catarrhalis*. In general, the second generation is more active against streptococci, *E. coli*, *P. mirabilis*, etc.[37]

Thymol [5-methyl-2-(propan-2-yl)benzenol, also known as *m*-thymol] is a natural monoterpenoid phenol derivative of *p*-cymene and is the most abundant component of the oil extracted from *Thymus vulgaris* (thyme).[38] The effective antibacterial properties of the essential oil have been investigated *in vitro* and *in vivo* against diverse Gram-negative and Gram-positive bacteria such as *S. typhimurium*, *E. coli*, and *L. monocytogenes*.[39−42] In addition to this, the herbal preparation "*Thymi aetheroleum*", listed as an "herbal medicinal product", has been assigned the GRAS (Generally Recognized As Safe) status of flavor additive[43] by FEMA (Flavor Extract Manufacturers Association).[44] The essential oils obtained from the species of the Lamiaceae family, such as the genera *Thymus*, *Ocimum*, and *Origanum* containing thymol,[45−47] have been used in the food industry since ancient times as natural preservatives in food treatment and packaging thanks to their

antimicrobial, antioxidant, and anti-inflammatory properties.[48−50] Essential oils extracted from basil (*Ocimum basilicum L.*) have been traditionally used as a medicinal plant in the treatment of headaches, coughs, diarrhea, constipation, warts, worms, and kidney malfunction.[51]

As mentioned above, co-crystallization of the antibiotic ciprofloxacin (CIP hereafter) with thymol (THY) and carvacrol (CAR) yielded two families of ciprofloxacin co-crystals, one with carvacrol, namely, CIP·CAR$_n$ (n = 2, 3, 4), and one with thymol, CIP·THY$_n$ (n = 2, 4).[33] The effect of co-crystal formation on the antibiotic activity of ciprofloxacin was evaluated by means of standard antimicrobial tests in the cases of the co-crystals CIP·CAR$_4$ and CIP·THY$_2$, and compared with the results for the pure components and their physical mixtures: in both cases, the antimicrobial tests indicated an increase of the antimicrobial activity.

Remarkably, the outcome of analogous experiments carried out with antibiotics of the CEPH family is completely different; viz., when the co-crystals with THY are administered to Gram-negative and Gram-positive bacteria, a significant *decrease* of the antimicrobial activity, and therefore an increase of the minimal inhibitory concentration (MIC) values, is observed in comparison to the pure components and to the physical mixtures. In the following, the preparation and characterization of the co-crystals of cephalexin (CPX), cefradine (CFD), and cefaclor (CFC) with thymol (THY), namely, CPX·THY·2.5H$_2$O forms I and II, CFD·THY·2.5H$_2$O, and CFC·THY·4H$_2$O, respectively, will be described and the results of the antimicrobial test discussed.

■ EXPERIMENTAL SECTION

CPX and CFD used in this work were purchased from Tokyo Chemical Industry (TCI); CFC, THY, and all solvents were purchased from Sigma-Aldrich. All reagents and solvents were used without further purification.

Solution Synthesis. *Synthesis of CFD·THY·2.5H$_2$O and CFC·THY·4H$_2$O.* In separate experiments, CFD (25 mg, 0.071 mmol) and CFC (25 mg, 0.068 mmol) were solubilized in 2 mL of water; sonication was used to accelerate the dissolution process. As thymol is insoluble in water, a solution of THY (15.9 mg, 0.106 mmol for CFD; 15.3 mg, 0.102 mmol for CFC) was prepared in 1 mL of EtOH, which was then added to both CFD and CFC aqueous solutions. The vials containing the mixture were covered with Parafilm and stored at 5 °C. A similar approach was used by Kemperman et al. in the preparation of clathrate-type complexes of cephalosporins.[59−61] Single crystals suitable for X-ray diffraction were collected after 2 days from the crystallization batches.

Synthesis of CPX·THY·2.5H$_2$O Forms I and II. CPX (25 mg, 0.072 mmol) was solubilized in 2 mL of water; sonication was used to accelerate the dissolution process. A solution obtained by dissolving THY (16.2 mg, 0.108 mmol) in 1 mL of EtOH/CH$_2$Cl$_2$ 50:50 was then added to the CPX aqueous solution. The vial containing the resulting mixture was partially covered with Parafilm and stored under a fume hood at room temperature. After 2 days, single crystals of form II were recovered, while, after 2 more days, only crystals of form I were found in the same crystallization batch.

Synthesis by Slurry. In three separate experiments, CPX (100 mg, 0.288 mmol), CFD (100 mg, 0.286 mmol), and CFC (100 mg, 0.272 mmol) were slurried with THY in a 1:1 stoichiometric ratio (43.3, 42.9, and 40.9 mg, respectively) for 48 h in 2 mL of water and 3 drops (150 μL) of EtOH. After filtration, the solid material was left to dry out under ambient conditions.

Mechanochemical Synthesis. In three separate experiments, CPX (50 mg, 0.144 mmol), CFD (50 mg, 0.143 mmol), and CFC (50 mg, 0.136 mmol) were milled with thymol in a 1:1 stoichiometric ratio (21.6, 21.5, and 20.4 mg, respectively) in a RETSCH MM200

111

(mixer mill) for 1 h (30 min + 30 min with a 5 min break) at 20 Hz milling frequency, using a 5 mL agate jar with three agate balls of 5 mm diameter; 2 drops of water (100 μL) were added to the solid mixture (liquid-assisted grinding, LAG). The product was left to dry out at room temperature and directly collected from the jar.

Crystallization. Single crystals of CFC·THY·4H$_2$O and of CPX·THY·2.5H$_2$O were crystallized from a mixture of three solvents, namely, ethanol, dichloromethane, and water. CPX·THY·2.5H$_2$O was obtained in two polymorphic forms; as form II is metastable, all solubility and antimicrobial activity measurements were carried out on form I (see below). In the case of CFD·THY·2.5H$_2$O, the structure was found to be isomorphous with that of CPX·THY·2.5H$_2$O form I. Single crystals of CPX·THY·4H$_2$O and of CFC·THY·2.5H$_2$O could not be obtained even by attempting heteroseeding crystallization with preformed crystals of isomorphous CFC·THY·4H$_2$O or CPX·THY·2.5H$_2$O form I. In the former case, the addition of the seeds of CFC·THY·4H$_2$O led to the immediate crystallization of a polycrystalline powder that was characterized as CPX·THY·2.5H$_2$O form I. Analogously, the addition of the seeds of CPX·THY·2.5H$_2$O form II to the solution of CFC and THY did not affect the crystallization, and CFC·THY·4H$_2$O was obtained.

Powder X-ray Diffraction. Room temperature powder X-ray diffraction patterns were collected on a PANalytical X'Pert Pro automated diffractometer equipped with an X'Celerator detector in Bragg−Brentano geometry, using Cu Kα radiation (λ = 1.5418 Å) without a monochromator in the 3−40° 2θ range (step size 0.033°; time/step 20 s; Soller slit 0.04 rad; anti-scatter slit $^1/_2$; divergence slit $^1/_4$; 40 mA × 40 kV).

Single Crystal X-ray Diffraction. Single crystal X-ray diffraction data were collected at RT for CFC·THY·4H$_2$O, CPX·THY·2.5H$_2$O form I, and at 100 K for CPX·THY·2.5H$_2$O form II, with an Oxford Diffraction X'Calibur instrument equipped with a graphite monochromator and a CCD detector. Unit cell parameters for all compounds discussed herein are reported in Table SI-1. The structures were solved by the intrinsic phasing methods and refined by least-squares methods against F^2 using SHELXT-2016[55] and SHELXL-2018[56] with the Olex^2 interface.[57] Non-hydrogen atoms were refined anisotropically. Hydrogen atoms were added in calculated positions. The software Mercury 4.1.2[58] was used to analyze and represent the crystal packing.

Testing of Antimicrobial Activity. Antimicrobial activity was tested by the broth microdilution method, according to the guidelines of the two established organizations and committees on antimicrobial susceptibility testing, the CLSI and EUCAST.[52,53] For comparison, tests were conducted on suspensions of thymol, CEPH, physical mixtures, and co-crystals in 10 progressive concentrations ranging from 512 to 1 μg/mL. All suspensions were tested in parallel, using as reference strains different types of bacteria pretested with different standard methods (automatic and semiautomatic) to determine their MICs.[54] Both sensitive and resistant strains, with a MIC that fell within the concentration range of 1 to 512 μg/mL, were considered.

Drug and co-crystal solutions/suspensions were prepared in the same way for all samples, namely, 30.720 mg of analyte in 15 mL of physiological solution of sodium chloride 0.45% (e.g., 30.720 mg of CEPH in 15 mL of physiological solution or 30.720 mg of co-crystal in 15 mL of physiological solution). Physical mixtures were prepared in stoichiometric ratios via simple mixing of drug dispersions and essential oil dispersions.

The antibacterial assay was carried out for all samples by using a 96-well microtiter plate; wells were filled with 50 μL of cation adjusted MH broth from well 2 to well 12; then, 100 μL of sample solution/dispersion were added and put in well 1. After that, the serial dilutions were obtained by taking 50 μL of MH broth from well 1 to well 2 and then proceeding in the same way from well 2 to well 3, etc., until well 11. This procedure resulted in 1:2 serial dilutions ranging from 512 to 1 μg/mL from well 2 to well 11. In this way, well 1 was the negative control to verify that the sample was not contaminated, while well 12 was the positive control to check for bacterial growth and was used as a comparison to evaluate the MIC well. Table SI-2 reports the results of all antimicrobial tests by comparing MIC (μg/ mL) in the cases of CEPH, of CEPH and THY as a physical mixture, and of the co-crystals for a series of both susceptible and resistant strains. The percentage molar differences in CEPH between the MIC of each CEPH and the MIC of the corresponding co-crystals are also reported (column 4).

Solubility Measurements. Solubility in water of (i) CPX (11.3 mg), CFD (10 mg), and CFC (5 mg); (ii) thymol (10 mg); and (iii) the co-crystals CFD·THY·2.5H$_2$O (10 mg), CPX·THY·2.5H$_2$O form I (9.8 mg), and CFC·THY·4H$_2$O (10 mg) was measured three times at room temperature by a stepwise procedure: each single material was suspended in 1 mL of water (quantities in mg are indicated above) in a 20 mL glass vial, and the volume of water was increased by 0.5 mL at a time; sonication (30 s^{-1} min, 95 W, 50/60 Hz) was applied after each addition. Determination of complete dissolution was based entirely on visual observation. Results are reported in Table 1.

Table 1. Solubility in Water of the Compounds Discussed Herein

| compound	solubility[a] (mg/mL)	solubility (mol/L)
THY	insoluble	insoluble
CFD	6.6(3)	1.8×10^{-2}
CPX	5.6(2)	1.5×10^{-2}
CFC	5.1(2)	1.4×10^{-2}
CFD·THY·2.5H$_2$O	1.1(3)	2.1×10^{-3}
CPX·THY·2.5H$_2$O	1.4(4)	2.6×10^{-3}
CFC·THY·4H$_2$O	1.4(3)	2.4×10^{-3}

[a]Values in parentheses are standard deviations over three measurements.

■ RESULTS AND DISCUSSION

Co-crystallization of the three cephalosporins with thymol invariably resulted in the formation of hydrated co-crystals. As discussed in the Experimental Section, the reaction between cephalosporins and thymol was conducted under three different conditions, i.e., solution, slurry, and liquid-assisted grinding (LAG). The relationship between the co-crystallization processes and the products obtained is depicted in Scheme 2.

Co-Crystallization of Cefaclor with Thymol. Co-crystallization of CFC with THY invariably resulted in the

Scheme 2. Co-Crystallization Results of Thymol (THY) with Cephalexin (CPX), Cefaclor (CFC), and Cefradine (CFD)[a]
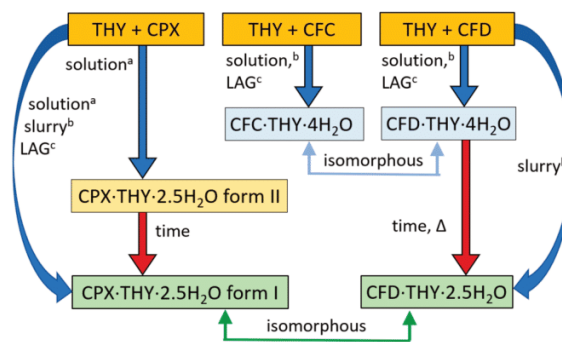
[a]Solvents used are (a) H$_2$O−EtOH−CH$_2$Cl$_2$, (b) H$_2$O−EtOH, and (c) H$_2$O.

112

formation of CFC·THY·4H$_2$O, irrespective of the process employed (see Scheme 2). Crystalline CFC·THY·4H$_2$O is composed of distinct layers of CFC and thymol molecules (Figure 1a). Water molecules are interposed in the layers of
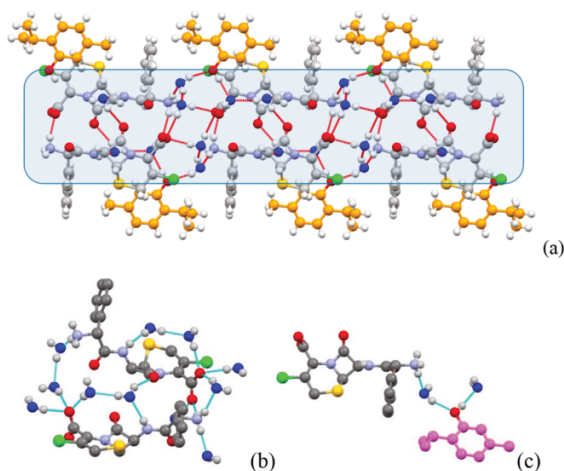
Figure 1. Crystal packing of cefaclor and thymol molecules in crystalline CFC·THY·4H$_2$O. (a) Projections in the *bc*-plane of packing portions for crystalline CFC·THY·4H$_2$O evidencing the "segregation" of the hydrophilic region (light-blue rectangle) in the structure (O$_W$ atoms in blue). (b) Hydrogen bonding interactions between CFC and water molecules and (c) between CFC, water, and THY (C$_{THY}$ in pink; H atoms omitted for clarity).

zwitterionic CFC molecules, interacting with them via hydrogen bonds. CFC molecules interact with each other via NH$_3^+$···O$_{COO}^-$ hydrogen bonds (Figure 1b), while they do not form hydrogen bonds with the hydroxyl groups of the thymol molecules (Figure 1c).

Co-Crystals of Cephalexin with Thymol. The co-crystallization of CPX with THY via ball milling with a few drops of water or via slurry in H$_2$O/EtOH solution results in the formation of CPX·THY·2.5H$_2$O. Single crystals for X-ray structural determination could only be grown with a double-layer approach at the interface of a solution of CPX in water and a solution of thymol in EtOH:CH$_2$Cl$_2$. Other choices of solvents or the use of mixtures of two solvents only yielded polycrystalline CPX·THY·2.5H$_2$O. Together with single crystals of the desired form, however, the concomitant

formation of a few crystals of a polymorphic form was detected, i.e., CPX·THY·2.5H$_2$O form II; in a matter of days, though, all crystals of form II had converted, in the presence of residual solution, into stable form I. While crystals of form I are stable under X-rays and data could be collected under ambient conditions, data for crystalline CPX·THY·2.5H$_2$O form II had to be collected at 100 K. Crystalline CPX·THY·2.5H$_2$O form II could not be detected in any other solid-state or solution experiment.
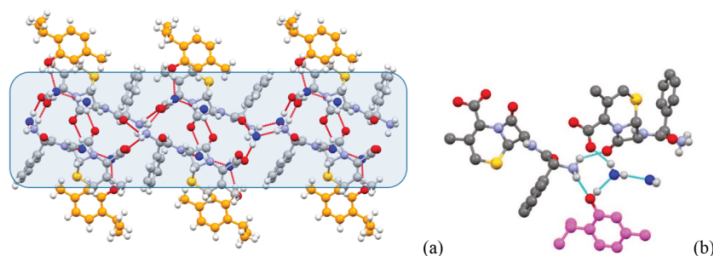
Crystalline CPX·THY·2.5H$_2$O form I is shown in Figure 2. The crystal packing resembles the one observed for CFC·THY·4H$_2$O. Once again, distinct layers of thymol and of CPX molecules are present (Figure 2a). Water molecules are interposed within the layers of CPX molecules acting as a hydrogen bonding bridge between CPX and THY molecules. O$_{H_2O}$ acts as a hydrogen bonding acceptor for H$_{OH}$ of THY molecules, and both H$_{H_2O}$, in turn, interact via OH···O$_{COO}^-$ hydrogen bonding with two different molecules of CPX (Figure 2b). CPX molecules interact via NH$_3^+$···O$_{COO}^-$ hydrogen bonds with each other (Figure 2b). The protonated amino groups of one CPX molecule interact via hydrogen bonding with the carboxylate groups of two other CPX molecules.

Segregation of the hydrophobic and hydrophilic regions is a feature also shared by crystalline CPX·THY·2.5H$_2$O form II, as is shown in Figure 3a. Figure 3b shows the absence of direct hydrogen bonding interactions between thymol and cephalexin molecules, connected one to the other via bridging water molecules.

Form I and form II of CPX·THY·2.5H$_2$O differ mainly because of the conformation due to the torsion of the carboxylate groups; see Figure 4 for a comparison.

Co-Crystals of Cefradine with Thymol. The co-crystallization of cefradine with thymol showed some similarities with both cefaclor and cephalexin (see Scheme 2). Liquid-assisted grinding resulted in the formation of the co-crystal CFD·THY·4H$_2$O, isomorphous with CFC·THY·4H$_2$O, as evidenced by a comparison of the measured XRPD pattern of CFD·THY·4H$_2$O with that calculated on the basis of single crystal data for CFC·THY·4H$_2$O (see Figure 5).

Single crystals of CFD·THY·4H$_2$O were grown in a similar way as the ones for the cefaclor co-crystal. However, these crystals were much less stable, rapidly degrading during data collection, even if the temperature was lowered to 100 K. Consequently, the crystals were left under ambient conditions for 12 h, and afterward, an XRPD pattern was collected. As it can be appreciated from Figure 6, a phase change had taken

**Figure 2.** Crystal packing of cephalexin and thymol molecules in crystalline CPX·THY·2.5H$_2$O form I. (a) Projection of a packing portion of crystalline CPX·THY·2.5H$_2$O form I, evidencing the layer of THY molecules hydrogen bonded to CPX and water molecules (O$_W$ in blue). (b) Hydrogen bonding interactions between CPX, water, and THY molecule (C$_{THY}$ in pink; H atoms omitted for clarity).

113
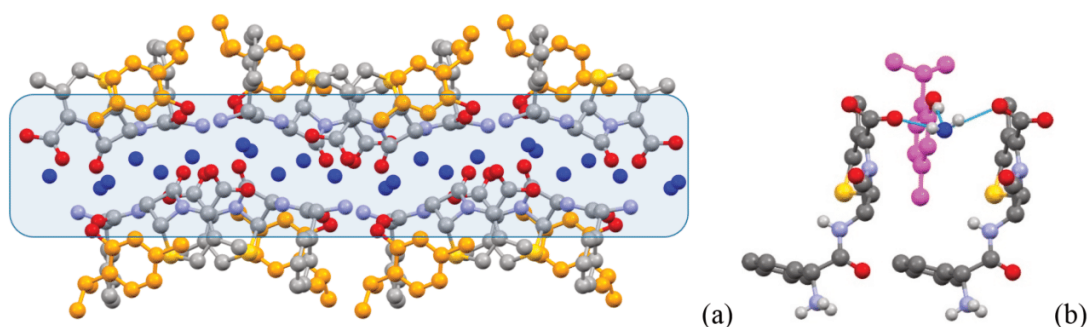
Figure 3. Segregation of the hydrophilic regions in crystalline CPX·THY·2.5H$_2$O form II (a) (H atoms and H-bonds not shown for clarity); hydrogen bonding interactions between CPX, water, and THY molecules (b); hydrogen bonding interactions mediated by a water molecule between CPX molecules (c) (carbon atoms of THY in pink, O$_W$ in blue; hydrogens omitted for clarity).
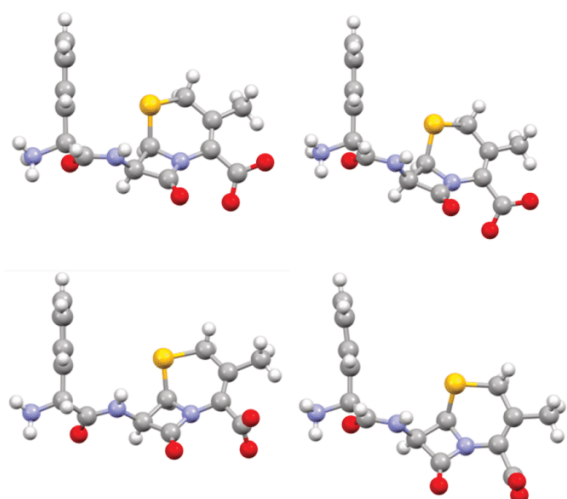
Figure 4. Conformation of the CPX molecules in form II (top) and form I (bottom): the main difference between the two forms is in the torsion of the carboxylate groups.
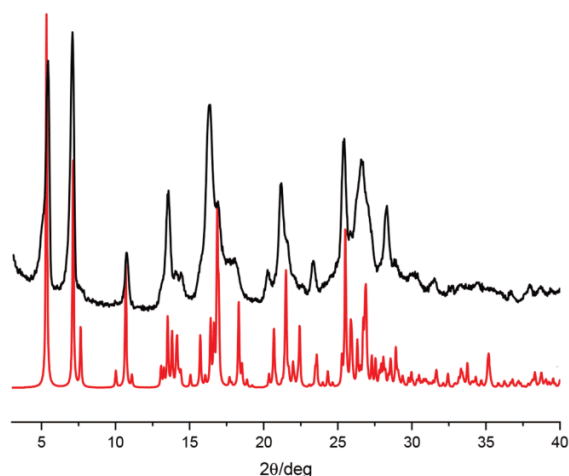
Figure 5. Comparison between the experimental powder X-ray pattern for CFD·THY·4H$_2$O (black line, top) and the one calculated on the basis of single crystal data for CFC·THY·4H$_2$O (red line, bottom).

place. This last phase was later prepared again (i) via slurry of CFD·THY·4H$_2$O and also (ii) directly from crystalline CFD·THY·4H$_2$O as obtained from the LAG process and stored under ambient conditions in a closed vial for 48 h. On the basis of the comparison of the X-ray patterns, this second form seems to be isomorphous with the stable form of CPX·THY·2.5H$_2$O, i.e., form I (see Figure 6).

Antimicrobial Activity. The results of the antimicrobial activity testing are now discussed. As described in the Experimental Section, the same strains were tested for each system. Results referring to the strains that provided growth inhibition values considered of interest for the purposes of the work are discussed. Table SI-2 lists the minimal inhibitory concentration (MIC) values for all CEPH, for CEPH and THY physical mixtures, and for the CEPH·THY·nH$_2$O co-crystals, together with the percentage concentration increase, calculated after normalization of the data, necessary for mixed systems to show the same antimicrobial effect as pure CEPH compounds. As can be seen from the examples listed in Table 2, all co-crystals were found to give growth inhibition at concentrations invariably higher than CEPH alone. In the cases where a

specific strain was found highly susceptible to the antibacterial, the corresponding co-crystals were not tested. However, when these quantities are normalized on the basis of the co-crystal formulas, differences begin to appear. Growth inhibition with CFD·THY·2.5H$_2$O requires a larger dose of cephalosporin compared to the other co-crystals described in this work. CFC·THY·4H$_2$O is considerably more efficient, as the increase of the antibiotic dose necessary to reach the MIC value is lower than that for the other systems considered. An analogous behavior could also be observed for the physical mixtures of CEPH and THY, although they present, on average, similar or slightly lower growth inhibition concentrations, based on normalized data, with respect to co-crystals. Finally, pure THY shows growth inhibition at very high values (not reported in Table 2), which are on the mg/mL scale, therefore not comparable to those for CEPH and co-crystals.

■ CONCLUSIONS

Co-crystallization of CEPH molecules with thymol was successful in yielding a class of closely related hydrated co-crystals with a 1:1 stoichiometry between the CEPH molecules

114
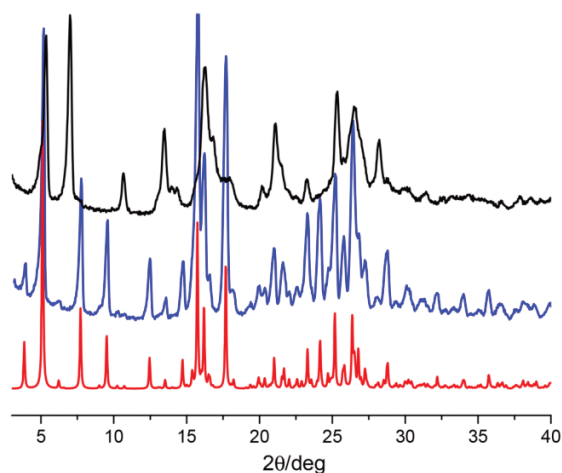
Figure 6. Comparison between the experimental XRPD patterns for CFD·THY·4H$_2$O as obtained from LAG (black line, top), the pattern obtained after 12 h under ambient conditions (blue line, middle), and the pattern calculated on the basis of single crystal data for CPX·THY·2.5H$_2$O form I (red line, bottom). As blue and red lines are superimposable, it can be inferred that a complete transformation has taken place from CFD·THY·4H$_2$O to a co-crystal isomorphous with CPX·THY·2.5H$_2$O form I, i.e., CFD·THY·2.5H$_2$O.

and THY. In all cases (with the exception of the low temperature form of CPX·THY·2.5H$_2$O), THY is not linked directly to the CEPH molecules but is linked to the antibiotic via water bridges. It is perhaps worth mentioning that all crystal structures of CPX, CFD, and CFC, currently available in the CSD database,[62] are hydrates, confirming the strong affinity of the CEPH molecules with water.

The antimicrobial activity of the co-crystals CPX·THY·2.5H$_2$O form II, CFD·THY·2.5H$_2$O, and CFC·THY·4H$_2$O was compared with that of CEPH alone, as well as with that of physical mixtures of CEPH with THY in adequate stoichiometric ratios, against a reference strain of different bacteria both susceptible and not susceptible to CEPH. THY was also tested. At variance with what was previously observed in the cases of the co-crystals of ciprofloxacin with thymol,[33] the CEPH co-crystallization products show exactly the opposite behavior in terms of antimicrobial activity. The co-crystals CPX·THY·2.5H$_2$O form II, CFD·THY·2.5H$_2$O, and CFC·THY·4H$_2$O are less effective against the bacteria than the pure active ingredient.

This apparently negative result is extremely interesting and prompts the investigation of the reasons for such a different behavior. Clearly, the two classes of antibiotics have very different biological activity (interaction with different active sites on the proteins, etc.), and the comparison cannot be between the two classes of compounds. Rather, the focus of this crystal engineering paper is on the observation that the same conceptual approach, namely, the construction of aggregates between natural antibiotics such as thymol and carvacrol and the APIs, may also cause an inhibition of the activity. This should also raise a warning, as it cannot be excluded a priori that approved substances commonly used for human consumption, as is the case of thymol, might have an impact on the pharmacological effects of antibiotics. More explorative work should be conducted with this caveat in mind.

It may also be worth noting that the solubilities in water of the co-crystals are an order of magnitude less than those of the pure CEPH (see Table 1); while the molar solubility of the CEPH molecules, when associated to THY, is significantly lower than the solubility of the free cephalosporines, THY

Table 2. Percentual Increase in Minimal Inhibition Concentration (MIC) Normalized on the Amount of CEPH (mM) for the Co-Crystals CFD·THY·2.5H$_2$O, CPX·THY·2.5H$_2$O, and CFC·THY·4H$_2$O with Respect to the Pure Cephalosporins CFD, CPX, and CFC, Respectively

	CFD·THY·2.5H$_2$O vs CFD	CPX·THY·2.5H$_2$O vs CPX	CFC·THY·4H$_2$O vs CFC
	Gram-Positive Bacteria		
Enterococcus faecalis	926	28	148
Staphylococcus aureus MRSA	926	28	148
Staphylococcus epidermidis	413	156	148
	Gram-Negative Bacteria		
Alcaligenes faecalis	413	a	398
Citrobacter freundii	a	156	a
Citrobacter koseri	a	a	24
Enterobacter cloacae	413	156	a
Enterobacter aerogenes	≥4004[c]	a	a
Escherichia coli	a	156	24
Escherichia coli ESβL+[b]	≥413[c]	924	148
Salmonella cholaeresuis	1952	156	148
Hafnia alvei	28	≥8093[c]	148
Klebsiella oxytoca	a	28	a
Morganella morganii	4004	8093	a
Proteus mirabilis ESβL+[b]	8109	1948	≥1948[c]
Proteus mirabilis	4004	3996	≥3996[c]
Providencia stuartii	1952	a	a

[a]Notes: co-crystal was not tested because the corresponding CEPH gives MIC values below the measurement limit for the specific antibacterial-susceptible strain. [b]ESβL+ stands for extended spectrum beta-lactamase. [c]The symbol ≥ is used to indicate that higher concentrations have not been investigated; therefore, the real MIC value could not be ascertained.

115

shows exactly the opposite phenomenon, becoming soluble in water.

In summary, the evaluation of the MIC values in the cases discussed herein is consistent with an inhibition effect by THY on the antibiotic activity of the three CEPH molecules upon formation of co-crystals with THY. The inhibition is less pronounced with the new generation cephalosporines. However, whether this inhibition is due to a different permeabili[63] of the CEPH co-crystals or, more simply, to the difference in solubility of the co-crystals with respect to the CEPH on their own needs to be investigated further with *ad hoc* studies *in vivo* also by considering the opposite behavior shown by the co-crystals of ciprofloxacin with thymol, which appears to be more soluble by a factor of 2 with respect to the antibiotic.[33] Work in this direction is in progress and will be the subject of future reports.

■ ASSOCIATED CONTENT

⒮ Supporting Information

The Supporting Information is available free of charge at https://pubs.acs.org/doi/10.1021/acs.cgd.1c01435.

Single crystal and powder X-ray diffraction and antimicrobial tests (PDF)

Accession Codes

CCDC 2125511−2125513 contain the supplementary crystallographic data for this paper. These data can be obtained free of charge via www.ccdc.cam.ac.uk/data_request/cif, or by emailing data_request@ccdc.cam.ac.uk, or by contacting The Cambridge Crystallographic Data Centre, 12 Union Road, Cambridge CB2 1EZ, UK; fax: +44 1223 336033.

■ AUTHOR INFORMATION

Corresponding Authors

Vittorio Sambri − *U.O. Microbiologia - Laboratorio Unico Centro Servizi AUSL Romagna, 47522 Pievesestina di Cesena, FC, Italy; Dipartimento di Medicina Specialistica, Diagnostica e Sperimentale Università di Bologna, 40138 Bologna, Italy*; Email: vittorio.sambri@unibo.it

Dario Braga − *Dipartimento di Chimica "Giacomo Ciamician", Università di Bologna, 40126 Bologna, Italy;* ⊙ orcid.org/0000-0003-4162-4779; Email: dario.braga@unibo.it

Authors

Cecilia Fiore − *Dipartimento di Chimica "Giacomo Ciamician", Università di Bologna, 40126 Bologna, Italy*

Alessandra Baraghini − *Dipartimento di Farmacia e Biotecnologie "FABIT", Università di Bologna, 40126 Bologna, Italy*

Oleksii Shemchuk − *Institute of Condensed Matter and Nanosciences, UCLouvain, B-1348 Louvain-la-Neuve, Belgium;* ⊙ orcid.org/0000-0003-3003-3922

Manuela Morotti − *U.O. Microbiologia - Laboratorio Unico Centro Servizi AUSL Romagna, 47522 Pievesestina di Cesena, FC, Italy*

Fabrizia Grepioni − *Dipartimento di Chimica "Giacomo Ciamician", Università di Bologna, 40126 Bologna, Italy;* ⊙ orcid.org/0000-0003-3895-0979

Complete contact information is available at:
https://pubs.acs.org/10.1021/acs.cgd.1c01435

■ REFERENCES

(1) Stanton, M. K.; Bak, A. Physicochemical properties of pharmaceutical co-crystals: A case study of ten AMG 517 co-crystals. *Cryst. Growth Des.* **2008**, *8* (10), 3856−3862.

(2) Wouters, J.; Quéré, L. *Pharmaceutical salts and co-crystals*; Royal Society of Chemistry: 2011.

(3) Steed, J. W. The role of co-crystals in pharmaceutical design. *Trends Pharmacol. Sci.* **2013**, *34* (3), 185−93.

(4) Golob, S.; Perry, M.; Lusi, M.; Chierotti, M. R.; Grabnar, I.; Lassiani, L.; Voinovich, D.; Zaworotko, M. J. Improving Biopharmaceutical Properties of Vinpocetine Through Cocrystallization. *J. Pharm. Sci.* **2016**, *105* (12), 3626−3633.

(5) Guo, C.; Zhang, Q.; Zhu, B.; Zhang, Z.; Bao, J.; Ding, Q.; Ren, G.; Mei, X. Pharmaceutical Cocrystals of Nicorandil with Enhanced Chemical Stability and Sustained Release. *Cryst. Growth Des.* **2020**, *20* (10), 6995−7005.

(6) Alvarez-Lorenzo, C.; Castiñeiras, A.; Frontera, A.; García-Santos, I.; González-Pérez, J. M.; Niclós-Gutiérrez, J.; Rodríguez-González, I.; Vílchez-Rodríguez, E.; Zaṙba, J. K. Recurrent motifs in pharmaceutical cocrystals involving glycolic acid: X-ray characterization, Hirshfeld surface analysis and DFT calculations. *CrystEngComm* **2020**, *22* (40), 6674−6689.

(7) Bethune, S. J.; Schultheiss, N.; Henck, J. O. Improving the Poor Aqueous Solubility of Nutraceutical Compound Pterostilbene through Cocrystal Formation. *Cryst. Growth Des.* **2011**, *11* (7), 2817−2823.

(8) Bevill, M. J.; Vlahova, P. I.; Smit, J. P. Polymorphic Cocrystals of Nutraceutical Compound p-Coumaric Acid with Nicotinamide: Characterization, Relative Solid-State Stability, and Conversion to Alternate Stoichiometries. *Cryst. Growth Des.* **2014**, *14* (3), 1438−1448.

(9) Barbas, R.; Bofill, L.; de Sande, D.; Font-Bardia, M.; Prohens, R. Crystal engineering of nutraceutical phytosterols: new cocrystal solid solutions. *CrystEngComm* **2020**, *22* (25), 4210−4214.

(10) Nauha, E.; Nissinen, M. Co-crystals of an agrochemical active - A pyridine-amine synthon for a thioamide group. *J. Mol. Struct.* **2011**, *1006* (1−3), 566−569.

(11) Powell, K. A.; Croker, D. M.; Rielly, C. D.; Nagy, Z. K. PAT-based design of agrochemical co-crystallization processes: A case-study for the selective crystallization of 1:1 and 3:2 co-crystals of p-toluenesulfonamide/triphenylphosphine oxide. *Chem. Eng. Sci.* **2016**, *152*, 95−108.

(12) Julien, P. A.; Germann, L. S.; Titi, H. M.; Etter, M.; Dinnebier, R. E.; Sharma, L.; Baltrusaitis, J.; Friscic, T. In situ monitoring of mechanochemical synthesis of calcium urea phosphate fertilizer cocrystal reveals highly effective water-based autocatalysis. *Chemical Science* **2020**, *11* (9), 2350−2355.

(13) Kent, R. V.; Wiscons, R. A.; Sharon, P.; Grinstein, D.; Frimer, A. A.; Matzger, A. J. Cocrystal Engineering of a High Nitrogen Energetic Material. *Cryst. Growth Des.* **2018**, *18* (1), 219−224.

(14) Gamekkanda, J. C.; Sinha, A. S.; Aakeroy, C. B. Cocrystals and Salts of Tetrazole-Based Energetic Materials. *Cryst. Growth Des.* **2020**, *20* (4), 2432−2439.

(15) Tan, Y.; Liu, Y.; Wang, H.; Li, H.; Nie, F.; Yang, Z. Different Stoichiometric Ratios Realized in Energetic-Energetic Cocrystals Based on CL-20 and 4,5-MDNI: A Smart Strategy to Tune Performance. *Cryst. Growth Des.* **2020**, *20* (6), 3826−3833.

116

(16) Bucar, D. K.; Filip, S.; Arhangelskis, M.; Lloyd, G. O.; Jones, W. Advantages of mechanochemical cocrystallisation in the solid-state chemistry of pigments: colour-tuned fluorescein cocrystals. *CrystEngComm* **2013**, *15* (32), 6289−6291.

(17) Li, M. Q.; Zhang, Z.; Zhang, Q.; Peng, B.; Zhu, B.; Wang, J. R.; Liu, L. Y.; Mei, X. F. Fine-Tuning the Colors of Natural Pigment Emodin with Superior Stability through Cocrystal Engineering. *Cryst. Growth Des.* **2018**, *18* (10), 6123−6132.

(18) Karangutkar, A. V.; Ananthanarayan, L. Co-crystallization of Basella rubra extract with sucrose: Characterization of co-crystals and evaluating the storage stability of betacyanin pigments. *Journal of Food Engineering* **2020**, *271*, 109776.

(19) Guo, M.; Sun, X.; Chen, J.; Cai, T. Pharmaceutical cocrystals: A review of preparations, physicochemical properties and applications. *Acta Pharmaceutica Sinica B* **2021**, *11* (8), 2537−2564.

(20) http://www.fda.gov/Food/IngredientsPackagingLabeling/GRAS/.

(21) Thipparaboina, R.; Kumar, D.; Chavan, R. B.; Shastri, N. R. Multidrug co-crystals: towards the development of effective therapeutic hybrids. *Drug Discov Today* **2016**, *21* (3), 481−90.

(22) Kavanagh, O. N.; Albadarin, A. B.; Croker, D. M.; Healy, A. M.; Walker, G. M. Maximising success in multidrug formulation development: A review. *J. Controlled Release* **2018**, *283*, 1−19.

(23) Thakuria, R.; Sarma, B. Drug-Drug and Drug-Nutraceutical Cocrystal/Salt as Alternative Medicine for Combination Therapy: A Crystal Engineering Approach. *Crystals* **2018**, *8* (2), 101.

(24) Kaur, R.; Cavanagh, K. L.; Rodriguez-Hornedo, N.; Matzger, A. J. Multidrug Cocrystal of Anticonvulsants: Influence of Strong Intermolecular Interactions on Physiochemical Properties. *Cryst. Growth Des* **2017**, *17* (10), 5012−5016.

(25) Drozd, K. V.; Manin, A. N.; Churakov, A. V.; Perlovich, G. L. Novel drug-drug cocrystals of carbamazepine with para-aminosalicylic acid: screening, crystal structures and comparative study of carbamazepine cocrystal formation thermodynamics. *CrystEngComm* **2017**, *19* (30), 4273−4286.

(26) Liu, F.; Song, Y.; Liu, Y. N.; Li, Y. T.; Wu, Z. Y.; Yan, C. W. Drug-Bridge-Drug Ternary Cocrystallization Strategy for Antituberculosis Drugs Combination. *Cryst. Growth Des.* **2018**, *18* (3), 1283−1286.

(27) Bordignon, S.; Cerreia Vioglio, P.; Priola, E.; Voinovich, D.; Gobetto, R.; Nishiyama, Y.; Chierotti, M. R. Engineering Codrug Solid Forms: Mechanochemical Synthesis of an Indomethacin-Caffeine System. *Cryst. Growth Des.* **2017**, *17* (11), 5744−5752.

(28) Roche, F. H. Artificial Pneumothorax on Statistical Trial. *Lancet* **1937**, *229*, 597.

(29) Nugrahani, I.; Asyarie, S.; Soewandhi, S. N.; Ibrahim, S. The Antibiotic Potency of Amoxicillin-Clavulanate Co-Crystal. *International Journal of Pharmacology* **2007**, *3* (6), 475−481.

(30) Bhatt, P. M.; Azim, Y.; Thakur, T. S.; Desiraju, G. R. Co-Crystals of the Anti-HIV Drugs Lamivudine and Zidovudine. *Cryst. Growth Des.* **2009**, *9* (2), 951−957.

(31) Almansa, C.; Mercè, R.; Tesson, N.; Farran, J.; Tomàs, J.; Plata-Salamán, C. R. Co-crystal of Tramadol Hydrochloride-Celecoxib (ctc): A Novel API-API Co-crystal for the Treatment of Pain. *Cryst. Growth Des.* **2017**, *17* (4), 1884−1892.

(32) Shemchuk, O.; Braga, D.; Grepioni, F.; Turner, R. J. Co-crystallization of antibacterials with inorganic salts: paving the way to activity enhancement. *Rsc Advances* **2020**, *10* (4), 2146−2149.

(33) Shemchuk, O.; d'Agostino, S.; Fiore, C.; Sambri, V.; Zannoli, S.; Grepioni, F.; Braga, D. Natural Antimicrobials Meet a Synthetic Antibiotic: Carvacrol/Thymol and Ciprofloxacin Cocrystals as a Promising Solid-State Route to Activity Enhancement. *Cryst. Growth Des.* **2020**, *20* (10), 6796−6803.

(34) Nath, A. P.; Balasubramanian, A.; Ramalingam, K. Cephalosporins: An imperative antibiotic over the generations. *Int. J. Res. Pharm. Sci.* **2020**, *11*, 623−629.

(35) Rossi, F.; Cuomo, V.; Riccardi, C. *Farmacologia, Principi di base e applicazioni terapeutiche*, 3rd ed.; Edizioni Minerva Medica: 2017; pp 698−701.

(36) Beers, M. H.; Fletcher, A. J.; Jones, T. V.; Porter, R.; Berkwitz, M.; Kaplan, J. L. *The Merck manual of medical information*, 2nd home ed.; Merck Research Laboratories: Whitehouse Station, NJ, 2003.

(37) Brunton, L.; Blumenthal, D.; Buxton, I.; Parker, K. *Goodman and Gilman's Manual of Pharmacology and Therapeutics*, 1st ed.; McGraw-Hill Professional: 2007.

(38) Marino, M.; Bersani, C.; Comi, G. Antimicrobial activity of the essential oils of Thymus vulgaris L. measured using a bioimpedometric method. *Journal of Food Protection* **1999**, *62*, 1017−1023.

(39) Altieri, C.; Speranza, B.; Del Nobile, M. A.; Sinigaglia, M. Suitability of bifidobacteria and thymol as biopreservatives in extending the shelf life of fresh packed plaice fillets. *J. Appl. Microbiol.* **2005**, *99*, 1294−1302.

(40) Valero, D.; Valverde, J. M.; Martínez-Romero, D.; Guillén, F.; Castillo, S.; Serrano, M. The combination of modified atmosphere packaging with eugenol or thymol to maintain quality, safety and functional properties of table grapes. *Postharvest Biology and Technology* **2006**, *41*, 317−327.

(41) Falcone, P.; Speranza, B.; Del Nobile, M. A.; Corbo, M. R.; Sinigaglia, M. A study on the antimicrobial activity of thymol intended as a natural preservative. *Journal of Food Protection* **2005**, *68* (8), 1664−1670.

(42) Zhou, F.; Ji, B.; Zhang, H.; Jiang, H.; Yang, Z.; Li, J.; Li, J.; Yan, W. The antibacterial effect of cinnamaldehyde, thymol, carvacrol and their combinations against the foodborne pathogen salmonella typhimurium. *Journal of Food Safety* **2007**, *27*, 124−133.

(43) Ash, M.; Ash, I. *Handbook of preservatives*; Synapse Information Resources, Inc.: 2004.

(44) https://www.femaflavor.org/flavor-library/thymol.

(45) Sarwar, A.; Latif, Z. GC-MS characterisation and antibacterial activity evaluation of Nigella sativa oil against diverse strains of Salmonella. *Natural Product Research* **2015**, *29* (5), 447−451.

(46) Licata, M.; Tuttolomondo, T.; Dugo, G.; Ruberto, G.; Leto, C.; Napoli, E. M.; Rando, R.; Rita Fede, M.; Virga, G.; Leone, R.; La Bella, S. Study of quantitative and qualitative variations in essential oils of Sicilian oregano biotypes. *Journal of Essential Oil Research* **2015**, *27* (4), 293−306.

(47) Mancini, E.; Senatore, F.; Del Monte, D.; De Martino, L.; Grulova, D.; Scognamiglio, M.; Snoussi, M.; De Feo, V. Studies on chemical composition, antimicrobial and antioxidant activities of five Thymus vulgaris L. essential oils. *Molecules* **2015**, *20* (7), 12016−12028.

(48) Lee, S. J.; Umano, K.; Shibamoto, T.; Lee, K. G. Identification of volatile components in basil (Ocimum basilicum L.) and thyme leaves (Thymus vulgaris L.) and their antioxidant properties. *Food Chem.* **2005**, *91* (1), 131−137.

(49) Karapinar, M.; Esen Aktuğ, Ş. Inhibition of foodborne pathogens by thymol, eugenol, menthol and anethole. *Int. J. Food Microbiol.* **1987**, *4* (2), 161−166.

(50) Mendes, S. S.; Bomfim, R. R.; Jesus, H. C. R.; Alves, P. B.; Blank, A. F.; Estevam, C. S.; Antoniolli, A. R.; Thomazzi, S. M. Evaluation of the analgesic and anti-inflammatory effects of the essential oil of Lippia gracilis leaves. *Journal of Ethnopharmacology* **2010**, *129* (3), 391−397.

(51) Simon, J. E. Q. J.; Murray, J. G. Basil: A Source of Essential Oils. In *Advances in New Crops*; Janick, J., Simon, J. E., Eds.; Timber Press: Portland, OR, 1990; pp 484−489.

(52) Clinical and Laboratory Standards Institute. Performance standards for antimicrobial susceptibility testing; sixteenth informational supplement. CLSI document M100-S16CLSI, Wayne, PA; 2006.

(53) European Committee for Antimicrobial Susceptibility Testing (EUCAST) of the European Society of Clinical Microbiology and Infectious Diseases (ESCMID). Determination of minimum inhibitory concentrations (MICs) of antibacterial agents by broth dilution. *Clin. Microbiol. Infect.* **2003**, *9* (8), ix−xv.

(54) Wiegand, I.; Hilpert, K.; Hancock, R. E. Agar and broth dilution methods to determine the minimal inhibitory concentration (MIC) of antimicrobial substances. *Nat. Protoc* **2008**, *3* (2), 163−175.

117

(55) Sheldrick, G. M. SHELXT - integrated space-group and crystal-structure determination. *Acta Crystallogr. A Found. Adv.* **2015**, *71* (1), 3−8.

(56) Sheldrick, G. M. Crystal structure refinement with SHELXL. *Acta Crystallogr. C Struct. Chem.* **2015**, *71* (1), 3−8.

(57) Dolomanov, O. V.; Bourhis, L. J.; Gildea, R. J.; Howard, J. A. K.; Puschmann, H. OLEX2: a complete structure solution, refinement and analysis program. *J. Appl. Crystallogr.* **2009**, *42* (2), 339−341.

(58) Macrae, C. F.; Edgington, P. R.; McCabe, P.; Pidcock, E.; Shields, G. P.; Taylor, R.; Towler, M.; van De Streek, J. Mercury: visualization and analysis of crystal structures. *J. Appl. Crystallogr.* **2006**, *39*, 453−457.

(59) Kemperman, G. J.; de Gelder, R.; Dommerholt, F. J.; Raemakers-Franken, P. C.; Klunder, A. J. H.; Zwanenburg, B. Clathrate-Type Complexation of Cephalosporins with *β*-Naphthol. *Chem. - Eur. J.* **1999**, *5* (7), 2163−2168.

(60) Kemperman, G. J.; de Gelder, R.; Dommerholt, F. J.; Raemakers-Franken, P. C.; Klunder, A. J. H.; Zwanenburg, B. Induced fit phenomena in clathrate structures of cephalosporins. *Journal of the Chemical Society-Perkin Transactions 2* **2000**, No. 7, 1425−1429.

(61) Kemperman, G. J.; de Gelder, R.; Dommerholt, F. J.; Klunder, A. J. H.; Zwanenburg, B. Molecular selectivity and cooperativity in the clathrate-type complexation of cephradine. *Eur. J. Org. Chem.* **2002**, *2002* (2), 345−350.

(62) Groom, C. R.; Bruno, I. J.; Lightfoot, M. P.; Ward, S. C. The Cambridge Structural Database. *Acta Crystallogr. B Struct Sci. Cryst. Eng. Mater.* **2016**, *B72*, 171−179.

(63) Ropponen, H. K.; Richter, R.; Hirsch, A. K. H.; Lehr, C. M. Mastering the Gram-negative bacterial barrier - Chemical approaches to increase bacterial bioavailability of antibiotics. *Adv. Drug. Delivery Rev.* **2021**, *172*, 339−360.

118

3.2.1 Supporting information

Inhibition of antibiotic activity of cephalosporines by cocrystallization with thymol

Cecilia Fiore,[a] Alessandra Baraghini,[e] Oleksii Shemchuk,[b] Vittorio Sambri,[c,d] Manuela Morotti,[c] Fabrizia Grepioni,[a] Dario Braga[a]*

[a] Dipartimento di Chimica "Giacomo Ciamician", Università di Bologna, Via Selmi, 2 – 40126 Bologna – Italy.
[b] Institute of Condensed Matter and Nanosciences, UCLouvain, 1 Place Louis Pasteur, B-1348 Louvain-la-Neuve, Belgium
[c] U.O. Microbiologia - Laboratorio Unico Centro Servizi AUSL Romagna, Pievesestina (FC), Italy
[d] Dipartimento di Medicina Specialistica, Diagnostica e Sperimentale Università di Bologna, Via Massarenti 9, 40138 Bologna, Italy.
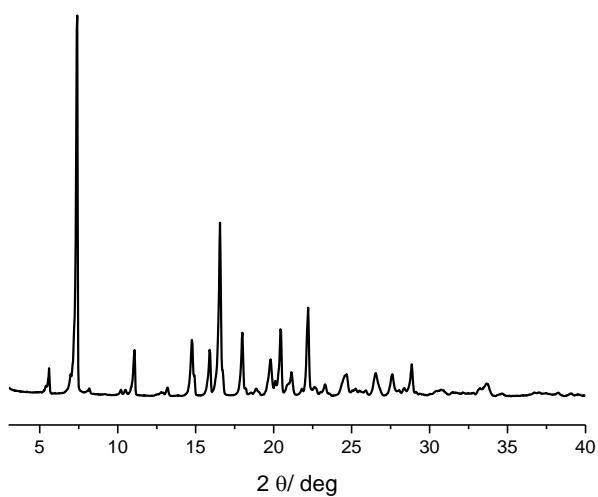[e] Dipartimento di Farmacia e Biotecnologie "FABIT", Università di Bologna, Via Belmeloro 6, 40126 Bologna, Italy.
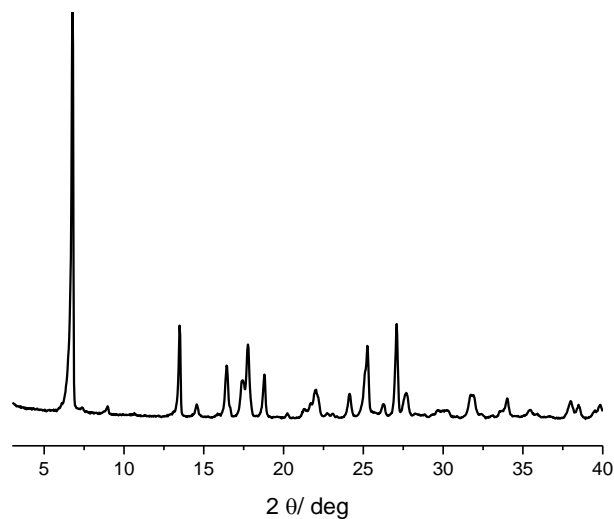
X-RAY POWDER DIFFRACTION PATTERNS
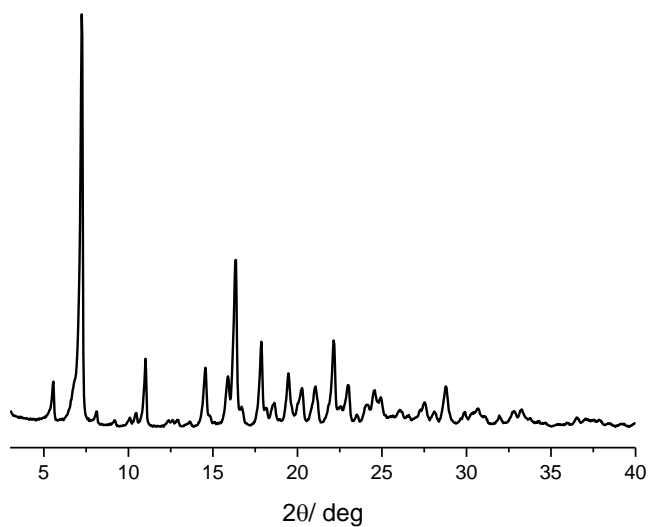
Figure SI-1. XRPD pattern of Cephalexin reagent as purchased from Tokyo Chemical Industry (TCI).

Figure SI-2. XRPD pattern of Cefradine reagentas purchased from Tokyo Chemical Industry (TCI).

Figure SI-3. XRPD pattern of Cefaclor reagent as purchased from Sigma-Aldrich.

120

CRYSTALLOGRAPHIC DATA

Table SI-1. Crystal data and details of measurements for CFC·THY·4H$_2$O, CPX·THY·2.5H$_2$O form I, and CPX·THY·2.5H$_2$O form II.

	CFC·THY·4H$_2$O	CPX·THY·2.5H$_2$O form I	CPX·THY·2.5H$_2$O form II
Chemical formula	C$_{15}$H$_{14}$ClN$_3$O$_4$S·C$_{10}$H$_{14}$O ·4H$_2$O	C$_{16}$H$_{17}$N$_3$O$_4$S·C$_{10}$H$_{14}$O ·2.5H$_2$O	C$_{16}$H$_{17}$N$_3$O$_4$S·C$_{10}$H$_{14}$O ·2.5H$_2$O
M$_r$ /g mol^{-1}	590.08	542.64	542.64
Crystal system	triclinic	monoclinic	monoclinic
Space group	$P1$	$P2_1$	$P2_1$
a / Å	7.0028(5)	17.3012(15)	12.6380(12)
b / Å	13.3272(8)	7.0697(5)	14.6478(14)
c / Å	17.2598(11)	22.9330(16)	15.5629(14)
α / °	73.450(5)	90	90
β / °	85.474(5)	93.416(7)	102.464(9)
γ / °	75.071(6)	90	90
V / Å^3	1491.94(18)	2800.0(4)	2813.1(5)
Z, Z'	2, 1	4, 2	4, 2
T / K	298	298	100
d / mg cm^{-3}	1.314	1.00	1.281
μ / mm^{-1}	0.25	0.17	0.16
Measd reflns	22403	23383	13691
Indep reflns	13809	12900	7730
Reflns with I > 2σ(I)	7873	6612	6546
R$_{int}$	0.047	0.041	0.043
$R1$ [F^2 > 2σ(F^2)]	0.083	0.066	0.057
$wR(F^2)$	0.239	0.108	0.131

https://www.ccdc.cam.ac.uk and have been allocated the accession numbers CCDC 2125511-2125513.

ANTIMICROBIAL TESTS

Table SI-2. MICs (µg/mL) for CEPH, CEPH and THY as a physical mixture and for the cocrystals.

Gram Positive Bacteria	CFD	CFD+THY physical mixture	CFD·THY·2.5H$_2$O	% increase
Staphylococcus aureus MRSA	8	32	128	926
Staphylococcus epidermidis	8	64	64	413
Enterococcus faecalis	8	128	128	926
Gram Negative Bacteria	CFD	CFD+THY physical mixture	CFD·THY·2.5H$_2$O	% increase
Enterobacter cloacae	64	256	512	413
Enterobacter aerogenes	8	$\geq 512^b$	$\geq 512^b$	≥ 4004
Escherichia coli ESβL+	64	256	$\geq 512^b$	≥ 413
Salmonella cholaeresuis	16	32	512	1952
Hafnia alvei	256	512	512	28
Morganella morganii	8	512	512	4004
Proteus mirabilis ESβL+^{a}	4	512	512	8109
Proteus mirabilis	4	256	256	4004
Providencia stuartii	16	512	512	1952
Alcaligenes faecalis	8	64	64	413
Gram Positive Bacteria	**CPX**	CPX+THY physical mixture	CPX·THY·2.5H$_2$O	% increase
Staphylococcus aureus MSSA	4	8	8	28
Staphylococcus epidermidis	32	64	128	156
Enterococcus faecalis	128	256	256	28
Gram negative Bacteria	**CPX**	CPX+THY physical mixture	CPX·THY·2.5H$_2$O	% increase
Citrobacter freundii	16	32	64	156
Enterobacter cloacae	128	256	512	156
Eschericchia coli	4	16	16	156
Eschericchia coli ESβL+^{c}	32	256	512	924
Klebsiella oxytoca	4	8	8	28
Salmonella cholaeresuis	8	16	32	156
Hafnia alvei	4	128	$\geq 512^b$	≥ 8093
Morganella morganii	4	512	512	8093
Proteus mirabilis ESβL+^{c}	16	256	512	1948
Proteus mirabilis	8	128	512	3996
Staphylococcus aureus MSSA	4	8	8	28
Staphylococcus epidermidis	32	64	128	156
Enterococcus faecalis	128	256	256	28

Gram Positive Bacteria	CFC	CFC+THY physical mixture	CFC·THY·4H$_2$O	% increase
Staphylococcus aureus MSSA	16	64	64	148
Staphylococcus aureus MRSA	16	32	64	148
Staphylococcus epidermidis	64	64	256	148
Enterococcus faecalis	16	64	64	148
Gram Negative Bacteria	CFC	CFC+THY physical mixture	CFC·THY·4H$_2$O	% increase
Citrobacter koseri	64	64	128	24
Escherichia coli ESβL+[a]	128	256	256	24
Escherichia coli	64	32	256	148
Salmonella cholaeresuis	32	64	128	148
Hafnia alvei	128	512	512	148
Haemophilus influenzae	16	32	64	148
Alcaligenes faecalis	64	256	512	398
Proteus mirabilis ESβL+[a]	16	512	≥ 512[b]	≥ 1948[b]
Proteus mirabilis	8	256	≥ 512[b]	≥ 3996[b]

Notes: (a) The percentual increase indicates the difference in the amount of CEPH required for MIC of each CEPH and the MIC of the corresponding cocrystals; (b) the symbol ≥ is used to indicate that higher concentrations have not been investigated, therefore the real MIC value cannot be known; (c) ESβL+ stands for extended spectrum β-lactamase.

3.3 Levofloxacin and Ciprofloxacin cocrystals with flavonoids: solid-state investigation for a multi-target strategy against Helicobacter pylori

Abstract

The call for new therapeutic solutions to take over the contemporary problem of antimicrobial resistance is requesting a prompt and direct answer from the scientific community. In this work, the focus turned to proposing a synergistic approach for effective therapeutic strategies against *Helicobacter pylori.*

The crystal engineering tool of co-crystallization provided us the right instrument to obtain novel materials, active against *H. pylori.* The solid-state combination of two antibiotics of the fluoroquinolone class, namely levofloxacin (LEVO) and ciprofloxacin (CIP), with three flavonoids, called quercetin (QUE), myricetin (MYR) and hesperetin (HES), resulted in the formation of four main co-crystals: LEVO-QUE, LEVO-MYR, 2LEVO-HES, and CIP-QUE. All the co crystals discussed in this work were obtained *via* different synthetic methodologies, including mechanochemical approaches.

Intriguing results were obtained from some preliminary antibacterial tests, aiming to compare the performance *versus H. pylori* of the novel co-crystals with the ones of the respective physical mixtures and isolated components.

3.3.1 Introduction

Helicobacter pylori is a Gram-negative and transmissible pathogen that colonizes the human stomach causing chronic infections that result in several gastric disorders, such as peptic ulceration, gastric adenocarcinoma, and MALT lymphoma. Most gastric cancer diagnoses are attributable to *H. pylori* infection indeed.[1,2] Like other superbugs, *H. pylori* rapidly develops resistance to the standard therapies leading to a significant decrease in their efficacy and eradication cure rates between 70 and 50%.[3] Moreover, only a few antibiotics (such as amoxicillin, clarithromycin, metronidazole, tetracycline, levofloxacin and rifabutin) can be used effectively for the eradication of *H. pylori* in clinical practice, typically when administrated to patients as combination therapies constituting two or three of these antibiotics, an acid inhibitor and/or a bismuth component that brings additional antibiotic effect and mucosal protection against aggressive factors.[4,5] Following the limited choice of effective therapeutics and the extensive use of certain antibiotics in the general population, rapid development of primary antibiotic resistance in *H. pylori* has been noted.[3]

The fluoroquinolones levofloxacin and ciprofloxacin have a broad spectrum of activity against gram-positive and gram-negative bacteria. Levofloxacin-based regimens to treat *H. pylori* infections are usually triple-therapies including a proton-pump inhibitor (PPI) and amoxicillin.[6–9] In recent studies was observed that the efficacy of levofloxacin-containing therapy is decreasing, most likely due to increased primary resistance.[3,10] In order to offer an alternative to the standard therapies for the treatment of H. pylori infection, in few studies also the efficacy of ciprofloxacin-based regimen has been explored.[11,12]

The World Health Organization (WHO)[13] and the World Gastroenterology Organization (WGO)[14] have included H. pylori in their list of "priority pathogens" for which new antibiotics are urgently needed and with this pressing need for novel therapeutic options, the scientific community's interest in traditional medicine and the use of natural products as sources of novel antibacterial drugs have been reinforced.[15]

In recent work we have demonstrated that there is a role for crystal engineers in these new frontiers of antimicrobial drugs discovery. Co-crystallization, a crystal engineering tool, provides alternative routes to the synthesis of new materials and/or to the enhancement of the properties of active molecules.[16,17] The basic idea is that the solid-state association of an active ingredient with a molecular component belonging to the GRAS family *(generally recognized as safe)* may allow to explore new ways to enhance and/or alter, in a synergistic way, the overall antimicrobial performance.[18,19]

Nowadays, bioactive compounds isolated from different plants, fruits, vegetables, beverages, etc., have gained interest in the scientific community due to their beneficial effects in human health.[20,21] Flavonoids are a large family of naturally occurring bioactive compounds present in various species and in a wide variety. Plant flavonoids play an important role in the protection against pathogenic microorganisms, such as bacteria, fungi and viruses.[15,22–24]

In this work, in order to tackle the AMR problem in *H. pylori*, we have investigated the outcome of the co-crystallization of two antibiotics of the fluoroquinolone class, namely levofloxacin and ciprofloxacin, with three natural compounds of the flavonoid family: quercetin, myricetin and hesperetin. Quercetin (QUE) is an important phytochemical, a flavonol, belonging to the flavonoid group of polyphenols. It is widely distributed in various fruits, vegetables, beverages as well as in flowers, leaves, and seeds.[25] QUE

possesses many pharmacological activities such as antioxidant,[26,27] anticancer,[28,29] anti-inflammatory,[30–32] antimicrobial,[32–34] *etc.* Myricetin (MYR) is a flavonoid of the flavone type, present as well in many vegetables, fruits, nuts, berries and herbs.[35] MYR exhibits antioxidant properties, free radical-scavenging effects and more beneficial properties.[36–42] Hesperetin (HES) is another flavonoid, of the flavanone class.[43] HES possess different activities as well, such as antioxidant, anti-inflammatory, antimicrobial and anticarcinogenic.[44–46]

The antibacterial activity and bioavailability of flavonoids are affected by various parameters, such as molecular conformation, hydrophobicity, solubility, etc.[47,48] However, the exact mechanisms of the antibacterial effects of flavonoids are not clear, but several mechanisms, such as interference with bacterial DNA synthesis, bacterial movement, cytoplasmic membrane permeability and the inhibition of bacterial metalloenzymes, have been proposed.[22,33,49]

As with other phytochemicals, the antimicrobial activity of flavonoids appears multifactorial while acting against different molecular targets in the pathogen instead of having one specific action site.[22,33]
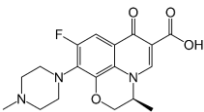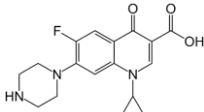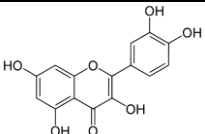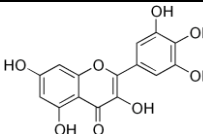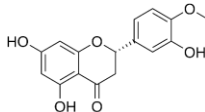
Bacterial transcriptional and post-transcriptional regulators (TR and PTR) have emerged for their significant potential as novel drug targets.[50] Targeting a bacterial TR that controls a cluster of fundamental genes is an example of a specific multitargeting approach, with high specificity for the pathogens. HsrA, also referred to as HP1043, is a conserved and essential TR that is involved in the tight regulation of a plethora of housekeeping and essential genes. This regulator is a response regulator of a two-component system, but it is an orphan of its cognate sensor histidine kinase. Due to its involvement in crucial pathways for the viability of the bacterium, HsrA is an optimal

novel target for antimicrobial drug discovery.[50–52] Recent studies have demonstrated that a group of flavonoids can inhibit HsrA regulatory function resulting in antimicrobial activity against *H. pylori*. [44,53] Therefore, the concept of creating a co-crystal of an antibiotic with a flavonoid used as co-former is the first example of a multitarget approach that involves a bacterial TR, essential for the bacterium.

In this work we report the preparation and structural characterization of three co-crystals of levofloxacin (LEVO) obtained by combining the fluoroquinolone with the flavonoids quercetin (QUE), myricetin (MYR) and hesperetin (HES), the co-crystal products obtained will be named LEVO-QUE-EtOH, LEVO-MYR-EtOH and 2LEVO-HES, respectively. A single co-crystal product was obtained in the case of the co-crystallization of ciprofloxacin with the flavonoid QUE, named CIP-QUE.

LEVO-QUE-EtOH and LEVO-MYR-EtOH received a heating treatment before to be used for the antimicrobial tests, to ensure that the product tested were completely ethanol free. In Table 1. are reported the molecular structure diagrams of the compounds used in this work.

Table 1. Molecular structure diagrams of the fluoroquinolones and flavonoids used in this work.

FLUOROQUINOLONES		FLAVONOIDS		
LEVOFLOXACIN	CIPROFLOXACIN	QUERCETIN	MYRICETIN	HESPERETIN

The stoichiometric ratio, composition, and purity of the products presented herein were confirmed by ^{1}H NMR spectroscopy and thermal analysis (TGA, DSC). (Data for ^{1}H NMR

spectroscopy, TGA and DSC analysis are reported in the Supporting information section S1 and S2 respectively). A solid-state characterization was also performed for all the co-crystals discussed herein using X-ray powder diffraction and single crystal X-ray diffraction (only in the case of LEVO-QUE).

3.3.2 Experimental section

Materials and methods All reagents and solvents used in this work were purchased from Sigma-Aldrich or TCI Europe and then used without further purification.

3.3.2.1 Solid-state synthesis

All the products were obtained using a 1:1 or 2:1 stoichiometry between the fluoroquinolone and the flavonoid.

From ball-milling equipment All the co-crystals were synthesized mechanochemically using a Retsch MM200 Mixer Mill, operated at a frequency of 25 Hz for 2 hours, with 5 mL agate jars and 2 agate balls of 5 mm diameter and ethanol liquid assisted grinding (LAG) (100 µL). A 1:1 stoichiometry of the reagents was first tried, successfully giving a novel pure phase of LEVO-QUE-EtOH, LEVO-MYR-EtOH and CIP-QUE. In the single case of the 2LEVO-HES synthesis, the 1:1 stoichiometry gave an incomplete reaction, with an excess of the HES component, this suggesting the preference of forming a 2:1 co-crystal. Then the 2:1 synthesis was performed, using 2 equivalents of the LEVO reagent. In this condition it was possible to obtain a pure phase of the 22LEVO-HES co-crystal. The products were left to dry out at room temperature, collected from the jar and analyzed with XRPD.

From slurry Co-crystals of LEVO-QUE-EtOH, LEVO-MYR-EtOH and CIP-QUE were synthesized from slurry in ethanol (1 mL) in a 1:1 stoichiometric ratio of the reactants. For each reactant, 0.5 mmol were used (mass quantities reported in Table 2) and the

reaction was let to stir at room temperature for 3 days in a 10 mL glass vial closed with a *PE pressure plug,* carefully kept in dark to prevent a possible degradation of the flavonoids. The same procedure was applied for the synthesis of the 2:1 2LEVO-HES co-crystal in which 0.25 mmol of HES were used instead. The solid products were recovered and analyzed after filtration and drying.

Table 2. Mass quantities of the materials used in this work (expressed in mg)

	Quercetin	Myricetin	Hesperetin	Levofloxacin	Ciprofloxacin
mg	151.12	159.12	75.57	180.68	165.67

Synthesis from solution Only one synthetic experiment carried out in the dark at 0°C, in a 3 mL ethanol solution, gave some crystals of LEVO-QUE that were analyzed. Each crystal shows the presence of "*pockets*" filled with a highly disordered ethanol. The quality of the data obtained from the collection of these crystals was not publishable, but it was possible to get information about the structure, the co-crystal composition and the main interactions taking place. All the other attempts to obtain single crystals suitable for analysis failed due to the incompatible and poor solubility of the reagents, the instability of the flavonoids in the solution media, fast degradation, light and temperature sensitivity.

3.3.2.2 Solid-state characterization

Single-crystal X-ray diffraction (SCXRD) Structural data for LEVO-QUE-EtOH were collected at room temperature with an Oxford Diffraction X'Calibur diffractometer equipped with a graphite monochromator and a CCD detector. The structures were solved by the Intrinsic Phasing methods and refined by least squares methods against F^2

using SHELXT-2016 and SHELXL-2018 [54] with Olex2 interface.[55] Non-hydrogen atoms were refined anisotropically. Hydrogen atoms were added in calculated positions. The software Mercury 2020.2.0 [56] was used to analyze and represent the crystal packing. Because of the presence of highly disordered solvent, it was not possible to reach the desired standard of diffraction data. Nonetheless the experiment allowed to reliably establish the gross structural features of the co-crystal. All the other attempts to repeat the co-crystallization of LEVO-QUE failed, making it impossible to recollect single-crystal data.

Powder X-ray diffraction Room-temperature powder X-ray diffraction patterns were collected on a PANalytical X'Pert Pro automated diffractometer equipped with an X'Celerator detector in Bragg-Brentano geometry, using Cu Kα radiation (λ = 1.5418 Å) without monochromator in the 3-40° 2θ range (step size: 0.033°; time/step: 20 s; Soller slit: 0.04 rad; anti-scatter slit: ½; divergence slit: ¼; 40 mA*40 kV).

Variable-temperature X-ray powder diffraction (VT-XRPD) X-ray powder diffractograms in the 3–40° 2θ range were collected, for all the co-crystals discussed in this work, with a PANalytical X'Pert PRO automated diffractometer, equipped with an X'Celerator detector and an Anton PaarTTK 450 system for measurements at controlled temperature. Data were collected in open air in Bragg–Brentano geometry using Cu Kα radiation, without a monochromator.

Differential scanning calorimetry (DSC) DSC measurements were performed for all the co-crystals with a Perkin–Elmer Diamond instrument. The samples (3–5 mg) were placed in sealed aluminium pans, and heating was carried out at 10 °C min⁻¹ in the temperature range 30-300°C.

Thermogravimetric analysis (TGA) TGA measurements for all co-crystals were performed using a Perkin-Elmer TGA7 instrument in the temperature range 30-300 °C under an N_2 gas flow, at a heating rate of 10 °C min^{-1}.

3.3.2.3 ^{1}H NMR spectroscopy

All the NMR spectra were recorded for starting materials and products discussed in this work with a Varian MR400, operating at the frequency of 400 MHz on proton, equipped with PFG (*Pulse Field Gradient*) ATB (*AutoSwitchable Broadband*) Probes.

3.3.2.4 Antimicrobial activity tests

All the tests were performed after confirming the composition of the co-crystals prepared in this work. Objects of the following test procedures were: LEVO-QUE, LEVO-MYR (both de-solvated), 2LEVO-HES and CIP-QUE.

The antimicrobial activity of the tested compounds against *Helicobacter pylori* was assessed by the broth microdilution method according to CLSI and EUCAST guidelines. All solutions/suspensions were tested in parallel, using *H. pylori* G27 strain with different standard methods to determine their minimal inhibitory concentrations (MICs) and minimal bactericidal concentrations (MBCs).

Drugs, flavonoids, and co-crystals were tested in 11 progressive concentrations ranging from 512 to 0.5 µg/mL. Compounds solutions/suspensions were all prepared following the same procedure: 20 mg of analyte in 10 mL of physiological solution (0.9% NaCl) to a final concentration of 2 mg/mL; physical mixtures were prepared simply by mixing drug dispersions/solution and flavonoid dispersions in stoichiometric ratios.

The antibacterial assay was carried out using a 96-well microtiter plate; the first column of wells was filled with 100 µL of 2X Brucella broth supplemented with 10% fetal bovine serum (FBS) and the subsequent columns were filled with 100 µL of 1X Brucella broth

supplemented with 5% FBS. Then, 100 µL of sample solution/dispersion was added in the first column, obtaining a concentration of 1 mg/mL. The two-fold serial dilutions were obtained by taking 100 µL from column 1 and mixing it with 1X broth in column 2 and then proceeding in the same way from column 2 to well 3, and so. The volume withdrawn from the last column was discarded, leaving 100 µL in all the wells. Afterwards, 100 µL of bacteria diluted in the same supplemented broth medium was added in each well to a final concentration of 1.0×10^5 CFU/mL. The whole procedure resulted in 1:2 serial dilutions ranging from 512 to 0.5 µg/mL from well 1 to well 11. Negative controls were used to verify that the compounds solutions/suspensions were not contaminated, while a positive control was added to check for bacterial growth and fitness. The positive control was used as a comparison to evaluate the MIC and the MBC. Plates were incubated in a CO_2-controlled incubator (9% CO_2) at 37 °C and examined visually after 72h. MIC values were defined as the lowest concentration of compound that inhibited the visible growth of bacteria after 72h of incubation. For MBC determinations, 10 µL aliquots of diluted bacterial cultures around the MIC were spotted on Brucella broth agar supplemented with 5% FBS and incubated for 48h in a 9% CO_2 environment at 37 °C. MBC was defined as the lowest concentration of compound that prevented the growth of ≥99.9% of *H. pylori* G27. Each experiment was performed in triplicate to confirm the results.

3.3.3   Results and Discussion
#### 3.3.3.1   *Co-crystallization with levofloxacin*
The co-crystallization of levofloxacin with quercetin led to a 1:1 stoichiometric product, from all the synthetic strategies mentioned in the experimental part: slurry, ball milling and solution and it was called LEVO-QUE-EtOH. The solution experiment was carried out

in dark at 0°C to prevent the possible degradation of the flavonoid QUE in the solution media. Tiny crystals were obtained and analyzed with a single crystal diffractometer. The data obtained from the collection was not suitable for publication but allowed us to determine the structural motifs and main intermolecular interactions taking place.

Figure 1. shows how the carboxylic group of LEVO interacts via hydrogen bond with one −OH group on the catechol ring of QUE and another -OH on the chromone core of QUE interacts with one nitrogen on the piperazine ring of LEVO. The chromone core of QUE also describes a hydrogen bonded dimer of the O−H⋯O type with a chromone core on another QUE molecule. In terms of graph set notation [57] the hydrogen bonded cycle can be described as $^{2}_{2}R(10)$, *viz*. a ten member ring with two hydrogen bond donors and two acceptor atoms.
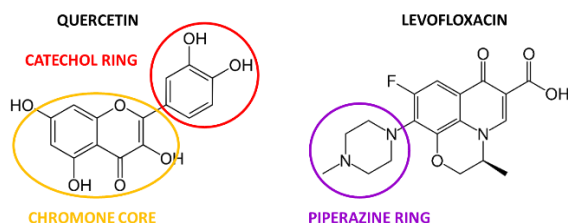

Scheme 1. Molecular structure diagrams of QUE and LEVO with the main functionalities involved in the H-bond interactions depicted in bright colors.
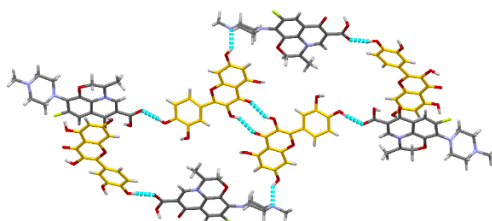

Figure 1. Hydrogen bond interactions in LEVO-QUE, disordered EtOH was omitted for clarity.

The hydrogen bond interactions form a continuous pattern, which expands in a 3D network (see Figure 2). In terms of molecular packing, the π-π stacking arrangements adopted by the aromatic units of LEVO and QUE is particularly noteworthy. The two

molecules facing each other establish a strong pattern of π-π interactions, with short interplanar distances between 3.36(1) and 3.39(1) Å (Figure 3). This feature is especially relevant in the contest of this work as it will be instrumental in understanding the structural features of the other related co-crystals.
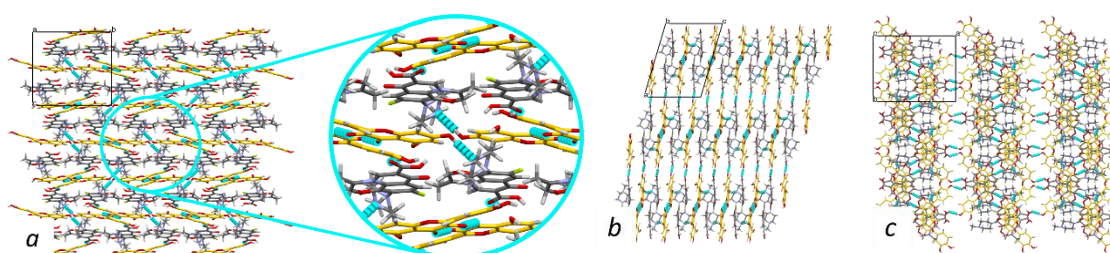

Figure 2. Packing view along *a, b, c* evidencing the H-bond 3D network (dotted lines in light blue). Disordered EtOH omitted for clarity.
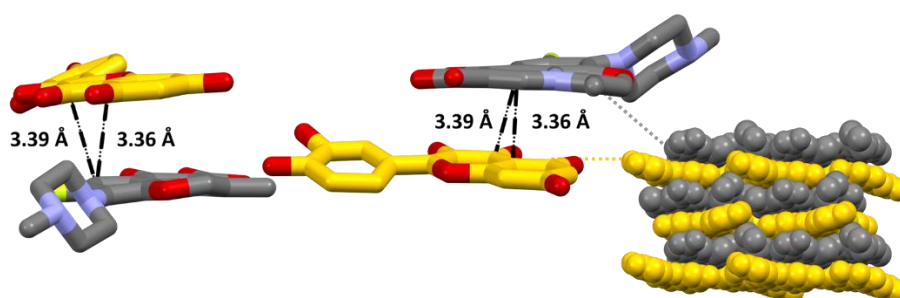
Figure 3. Focus on the interplanar π-π interactions (dashed black lines) between LEVO and QUE and a packing overview along the *a*-axis, showing the layered structure of LEVO-QUE-EtOH described by the π-π stacking arrangements of the two molecules. (LEVO in grey, QUE in yellow). Hydrogen atoms and ethanol were omitted for sake of clarity.

Thanks to the structural data, it was also possible to analyse the X-ray diffraction pattern accordingly to the interactions described above. The focus goes again to the π-staking between LEVO and QUE. In this sense, it was possible to identify in the diffraction pattern the region of reflections corresponding to the π-interactions of our interest. As a matter of fact, the diffraction pattern of LEVO and QUE as well as of LEVO-QUE all share

the same feature, namely strong diffraction peaks in the region 25-27 of 2θ, which are diagnostic of the presence of an important π-π interaction corresponding to a spacing in the range of 3.3(1)-3.5(1) Å. In Figure 4. is reported the calculated pattern from X-ray single crystal data for LEVO-QUE-EtOH, where it is noticeable the presence of diffraction peaks in the region 25-27 of 2θ.
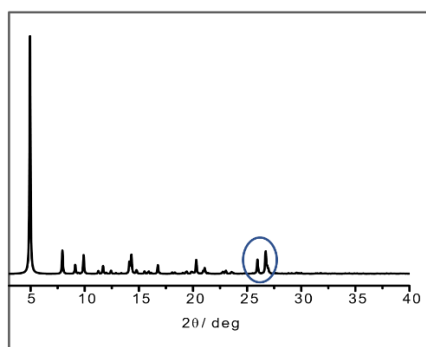
Figure 4. Calculated X-ray diffraction patter from single-crystal data of LEVO-QUE-EtOH. Highlighted with a blue circle the region of interest in the pattern.

The presence of this feature in both parent crystals of LEVO and QUE and in the LEVO-QUE co-crystal as well as in the LEVO-MYR co-crystals (see below) is indicative of the persistence of this packing motif.

Co-crystals of levofloxacin with myricetin, named LEVO-MYR, were also obtained in a 1:1 stoichiometry from both slurry and ball milling synthetic strategies.

Co-crystals of LEVO-QUE and LEVO-MYR obtained from the slurry experiment were analyzed with a variable temperature X-ray diffraction experiment (VTXRPD) to check for a possible change in the crystal phase after the heating treatment. For LEVO-QUE we observed a phase change starting around 80°C to reach the completeness at 120°C. In the case of LEVO-MYR the phase-change started already at room temperature and ended around 120°C. This change in the crystal phase was attributed to the gradual loss of ethanol and/ water from the LEVO-QUE and LEVO-MYR co-crystals. By comparing the

136

XRPD patterns we observed that both the solvate and the de-solvated phase in the case of LEVO-QUE and LEVO-MYR are isomorphous.

To support this discussion, Figure 5. reports a comparison of the XRPD patterns of the starting materials LEVO and QUE and the ones of the co-crystal LEVO-QUE-EtOH **(a)** and LEVO-MYR-EtOH **(b)** products obtained via slurry, ball milling, and after the VTXRPD experiment (named LEVO-QUE and LEVO-MYR), where a change in the crystal phase is noticeable. It is also possible to observe in LEVO-MYR-EtOH and LEVO-MYR, in the region between 25-27 = 2θ, strong diffraction peaks that we assigned to the π-stacking interactions.
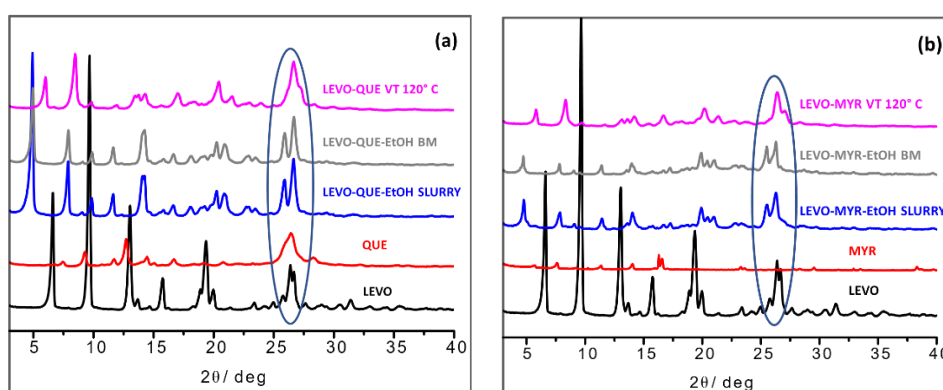
Figure 5. From bottom to top: XRPD patterns of LEVO (in black), QUE (in red), LEVO-QUE-EtOH **(a)** and LEVO-MYR-EtOH **(b)** products from slurry (in blue), LEVO-QUE-EtOH **(a)** and LEVO-MYR-EtOH **(b)** products from ball-milling synthesis (in grey), LEVO-QUE **(a)** and LEVO-MYR **(b)** after VTXRPD, measured at 120°C (in magenta). The circle in dark blue is evidencing the area in the pattern that corresponds to the π-stacking interactions described above.

Beside sharing similar features in terms of structure, LEVO-QUE-EtOH and LEVO-MYR-EtOH also show a similar thermal behaviour. In fact, the XRPD patterns of LEVO-MYR (before and after the VTXRPD experiment) are strictly comparable with the ones of LEVO-QUE-EtOH and LEVO-QUE respectively. In Figure 6. we report the comparison of the XRPD patterns for LEVO-MYR-EtOH and LEVO-QUE-EtOH before and after the VTXRPD experiment.
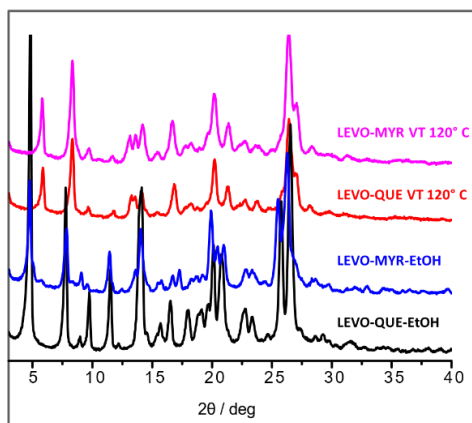
Figure 6. From bottom to top: LEVO-QUE-EtOH (in black) and LEVO- MYR-EtOH (in blue) slurry products before the VTXRPD experiment, LEVO- QUE and LEVO-MYR after the VTXRPD measured at 120°C. The circle in blue is evidencing the area in the pattern that corresponds to the π-stacking interactions described above.

At variance with the stoichiometry observed with LEVO-QUE and LEVO-MYR, the co-crystallization of levofloxacin with hesperetin led to a 2:1 stoichiometric product (2LEVO:1HES) from all synthetic strategies. After trying different stoichiometric ratios, we were able to confirm by XRPD, ^{1}H NMR spectroscopy and thermal analysis the chemical composition and purity of the 2LEVO-HES co-crystals. In the 2LEVO-HES co-crystal two molecules of levofloxacin are interacting with one molecule of hesperetin. Ideally, by looking at the diffraction pattern, we can propose also for 2LEVO-HES the presence of the π-stacking interactions between one LEVO and one HES, being present the strong diffraction peaks around 25-27 = 2θ. See Figure 7. where the XRPD patterns of 2LEVO-HES, are compared with those of the starting materials with emphasis on the peaks discussed above.
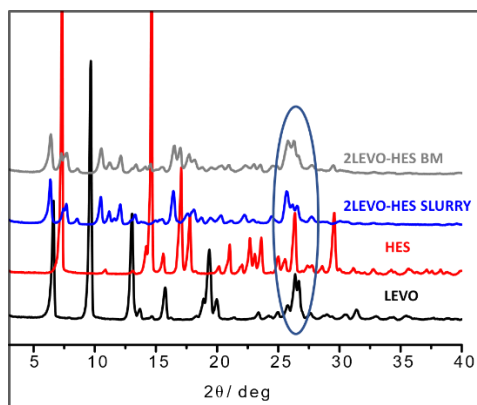
Figure 7. From bottom to top: XRPD patterns of LEVO (in black), HES (in red), 2LEVO-HES product from slurry (in blue) and 2LEVO-HES product from ball milling synthetic procedure (in grey). The dark blue circle is outlining the area of the diffraction pattern between 25-27 = 2θ of our interest, corresponding to π-π stacking arrangements of distances around 3.3(1)-3.5(1) Å.

In contrast with the previous cases of LEVO-QUE-EtOH and LEVO-MYR-EtOH, the VTXRPD experiment carried out for the 2LEVO-HES product from slurry did not show any event to be mentioned, this proving once again the stable and pure composition of the co-crystal.

3.3.3.2 Co-crystallization with ciprofloxacin

For the other fluoroquinolone used in this work, ciprofloxacin (CIP), only the co-crystallization with quercetin gave as result the formation of a novel crystalline phase of a 1:1 stoichiometry, named CIP-QUE. The other flavonoids, object of this discussion, seem to be unsuitable to make co-crystals with ciprofloxacin. Various synthetic approaches were tried, always resulting in a physical mixture of the starting materials. For CIP-QUE all the solid-state synthetic procedures let to the 1:1 product while the solution synthesis failed in all the attempt, to be ascribing to the very low solubility of CIP in a large variety of solvents. The stoichiometric composition was confirmed by ^{1}H NMR spectroscopy, dissolving a very small amount of material due to the low solubility of both CIP and CIP-QUE. In the ^{1}H NMR spectrum of CIP was also observed the presence

of some organic impurities that were carried along the synthetic procedures and found

also in the ^{1}H NMR spectrum of the co-crystal product.

Regarding the solid-state characterization of the novel phase, XRPD was used to prove

the formation of a co-crystal. Once again, by analyzing the X-ray diffraction patter, it was

possible to assume the presence of a π-stacking of the kind largely discussed earlier.

Here after, Figure 8. displays the comparison of the XRPD patterns of CIP, QUE and CIP-

QUE co-crystal products from slurry and ball-milling, pointing out the region in the

patterns mentioned above.
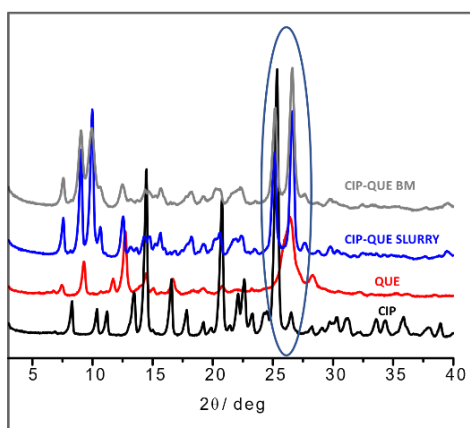
Figure 8. From bottom to top: XRPD patterns of CIP (in black), QUE (in red) CIP-QUE product from slurry (in blue) and CIP-QUE product from ball-milling synthesis. The circle in dark blue outlines the region in the pattern between 25-27 = 2θ discussed above.

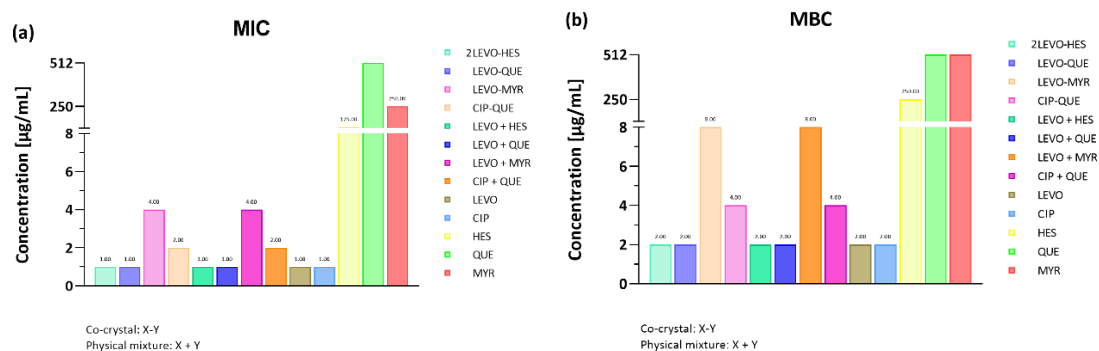### 3.3.3.3 Antimicrobial activity

The high MICs for flavonoids against *H. pylori* G27 strain is in contrast with data

presented in other studies,[44,53] where lower values showed high potential for this class

of molecules. However, the antimicrobial activity assays show a possible synergic effect

between the antibiotic and the flavonoid, especially in the case of levofloxacin and the

flavonoids hesperetin and quercetin. MICs obtained were the same for co-crystal and

antibiotic alone, but it should be taken into account the important difference arising

from the lower quantity of levofloxacin, in terms of moles, present in the co-crystal suspensions($\frac{1}{2}$ *ca.* of LEVO in LEVO-QUE and $\frac{2}{3}$ *ca.* of LEVO in 2LEVO-HES) with respect to levofloxacin alone.

Interestingly, no significant difference was observed between the co-crystal suspensions and the physical mixtures. These results may indicate that the two chemicals co-crystalize when physically mixed under the experimental conditions of the antimicrobial assays. In Table 3. are reported the MIC and MBC values for each entry considered in this work.

Entry	*H. pylori* G27	
	MIC [mg/L]	MBC [mg/mL]
2LEVO-HES	1	2
LEVO-QUE	1	2
LEVO-MYR	4	8
CIP-QUE	2	4
LEVO	1	2
CIP	1	2
HES	125	250
QUE	512	512
MYR	250	512
LEVO + HES	1	2
LEVO + QUE	1	2
LEVO + MYR	4	8
CIP + QUE	2	4

Table 3. Minimal inhibitory and bactericidal concentration values of co-crystals, physical mixtures, and single compounds. *H. pylori* G27 strain was used to perform the antimicrobial assays.

Figure 9. Histogram representation of the minimal inhibitory **(a)** and bactericidal **(b)**.

In spite of the low antimicrobial activity of the tested flavonoids, the combination with an antibiotic suitable to form a co-crystal can be a new and advanced approach to reduce the overall amount of antibiotic used for the treatment, while preserving the same antimicrobial efficacy on *H. pylori* infection.

3.3.4 Conclusions

In the need of alternatives to the common drug discovery process, to reduce costs, time and energy investments, co-crystallization and supramolecular aggregation techniques are offering us a viable and eco-friendly route to design and prepare novel pharmaceutical materials with desired modified properties. [58–61]

In this work we have reported the preparation and characterization of a series of co-crystals obtained by co-crystallizing *via* solid-state green methodologies two antibiotics of the fluoroquinolone class, namely levofloxacin and ciprofloxacin with three flavonoids: quercetin, myricetin and hesperetin. As a result, we prepared and characterized four novel co-crystals, called LEVO-QUE, LEVO-MYR, 2LEVO-HES and CIP-QUE. These co-crystals were then tested against *Helicobacter pylori*, a bacterium included in the list of "priority pathogens", according to the WHO.[13]

Our strategic multitarget approach resulted in a very interesting outcome. In fact, no significant difference in the antimicrobial activity was observed between the co-crystal suspensions and the physical mixtures used as comparison reference, while they exceptionally preserve, in both cases, the antimicrobial efficacy of the original antibiotics alone. There could be two possible outcomes to discuss regarding these peculiar results. First, we can reason about how the presence of the co-former appears to significantly affect the values of MIC and MBC), needing a lower *dose* of the antibiotic to get same effect. And second, the fact that the co-crystal and the physical mixture are equally performing may indicate that either LEVO and CIP form aggregates with the flavonoids, under the experimental conditions, resulting in comparable efficacies with the respective co-crystals, or that the presence of the co-former allows for a different mechanism of antimicrobial action.

Regarding this inspiring new trend, we call for a more specific biological investigation on the possible mechanism of action of supramolecular aggregates and co-crystals, to finally make the first steps into the great mystery that is the relationship between solid-state chemistry and the biological world.

References

(1) Dunn, B. E.; Cohen, H.; Blaser, M. J. Helicobacter Pylori. *Clin. Microbiol. Rev.* **1997**, *10* (4), 720–741. https://doi.org/10.1128/CMR.10.4.720.

(2) McColl, K. E. L. Clinical Practice. Helicobacter Pylori Infection. *N. Engl. J. Med.* **2010**, *362* (17), 1597–1604. https://doi.org/10.1056/NEJMCP1001110.

(3) Tshibangu-Kabamba, E.; Yamaoka, Y. Helicobacter Pylori Infection and Antibiotic Resistance — from Biology to Clinical Implications. *Nat. Rev. Gastroenterol. Hepatol. 2021 189* **2021**, *18* (9), 613–629. https://doi.org/10.1038/s41575-021-00449-x.

(4) Yang, H.; Guan, L.; Hu, B. Detection and Treatment of Helicobacter Pylori: Problems and Advances. *Gastroenterol. Res. Pract.* **2022**, *2022*. https://doi.org/10.1155/2022/4710964.

(5) Hooi, J. K. Y.; Lai, W. Y.; Ng, W. K.; Suen, M. M. Y.; Underwood, F. E.; Tanyingoh, D.; Malfertheiner, P.; Graham, D. Y.; Wong, V. W. S.; Wu, J. C. Y.; Chan, F. K. L.; Sung, J. J. Y.; Kaplan, G. G.; Ng, S. C. Global Prevalence of Helicobacter Pylori Infection: Systematic Review and Meta-Analysis. *Gastroenterology* **2017**, *153* (2), 420–429. https://doi.org/10.1053/J.GASTRO.2017.04.022.

(6) Nista, E. C.; Candelli, M.; Cremonini, F.; Cazzato, I. A.; Di Caro, S.; Gabrielli, M.; Santarelli, L.; Zocco, M. A.; Ojetti, V.; Carloni, E.; Cammarota, G.; Gasbarrini, G.; Gasbarrini, A. Levofloxacin-Based Triple Therapy vs. Quadruple Therapy in Second-Line Helicobacter Pylori Treatment: A Randomized Trial. *Aliment. Pharmacol. Ther.* **2003**, *18* (6), 627–633. https://doi.org/10.1046/J.1365-2036.2003.01676.X.

(7) Di Caro, S.; Franceschi, F.; Mariani, A.; Thompson, F.; Raimondo, D.; Masci, E.; Testoni, A.; La Rocca, E.; Gasbarrini, A. Second-Line Levofloxacin-Based Triple Schemes for Helicobacter Pylori Eradication. *Dig. Liver Dis.* **2009**, *41* (7), 480–485. https://doi.org/10.1016/J.DLD.2008.09.013.

(8) Gisbert, J. P.; Pérez-Aisa, Á.; Bermejo, F.; Castro-Fernández, M.; Almela, P.; Barrio, J.; Cosme, Á.; Modolell, I.; Bory, F.; Fernández-Bermejo, M.; Rodrigo, L.; Ortuño, J.; Sánchez-Pobre, P.; Khorrami, S.; Franco, A.; Tomas, A.; Guerra, I.; Lamas, E.; Ponce, J.; Calvet, X. Second-Line Therapy with Levofloxacin after Failure of Treatment to Eradicate Helicobacter Pylori Infection: Time Trends in a Spanish Multicenter Study of 1000 Patients. *J. Clin. Gastroenterol.* **2013**, *47* (2), 130–135. https://doi.org/10.1097/MCG.0B013E318254EBDD.

(9) Perna, F.; Zullo, A.; Ricci, C.; Hassan, C.; Morini, S.; Vaira, D. Levofloxacin-Based Triple Therapy for Helicobacter Pylori Re-Treatment: Role of Bacterial Resistance. *Dig. Liver Dis.* **2007**, *39* (11), 1001–1005. https://doi.org/10.1016/J.DLD.2007.06.016.

(10) Drlica, K.; Malik, M. Fluoroquinolones: Action and Resistance. *Curr. Top. Med. Chem.* **2005**, *3* (3), 249–282. https://doi.org/10.2174/1568026033452537.

(11) Forsmark, C. E.; Mel Wilco, C.; Cello, J. P.; Margaretten, W.; Lee, B.; Sachdeeva, M.; Satow, J.; Sande, M. A. Ciprofloxacin in the Treatment of Helicobacter Pylori in Patients with Gastritis and Peptic Ulcer. *J. Infect. Dis.* **1990**, *162* (4), 998–999. https://doi.org/10.1093/INFDIS/162.4.998.

(12) Dresner, D.; Coyle, W.; Nemec, R.; Peterson, R.; Duntemann, T.; Lawson, J. M. Efficacy of Ciprofloxacin in the Eradication of Helicobacter Pylori. *South. Med. J.* **1996**, *89* (8), 775–778. https://doi.org/10.1097/00007611-199608000-00004.

(13)   HELICOBACTER   PYLORI   /   *World   Health   Organisation*
        https://monographs.iarc.who.int/wp-content/uploads/2018/06/mono100B-15.pdf
        (accessed 2023-01-13).

(14)   *Helicobacter   Pylori | World   Gastroenterology   Organisation*.
        https://www.worldgastroenterology.org/guidelines/helicobacter-pylori (accessed 2023-
        01-13).

(15)   Anand, U.; Nandy, S.; Mundhra, A.; Das, N.; Pandey, D. K.; Dey, A. A Review on
        Antimicrobial Botanicals, Phytochemicals and Natural Resistance Modifying Agents from
        Apocynaceae Family: Possible Therapeutic Approaches against Multidrug Resistance in
        Pathogenic   Microorganisms.   *Drug   Resist.   Updat.*   **2020**,   *51*.
        https://doi.org/10.1016/J.DRUP.2020.100695.

(16)   Qiao, N.; Li, M.; Schlindwein, W.; Malek, N.; Davies, A.; Trappitt, G. Pharmaceutical Co-
        Crystals: An   Overview.   *Int   J   Pharm*   **2011**,   *419*   (1–2),   1–11.
        https://doi.org/10.1016/j.ijpharm.2011.07.037.

(17)   Duggirala, N. K.; Perry, M. L.; Almarsson, Ö.; Zaworotko, M. J. Pharmaceutical Co-crystals:
        Along the Path to Improved Medicines. *Chem. Commun.* **2015**, *52* (4), 640–655.
        https://doi.org/10.1039/C5CC08216A.

(18)   Fiore, C.; Baraghini, A.; Shemchuk, O.; Sambri, V.; Morotti, M.; Grepioni, F.; Braga, D.
        Inhibition of the Antibiotic Activity of Cephalosporines by Co-Crystallization with Thymol.
        Cryst. Growth Des. **2022**, *22* (2), 1467–1475. https://doi.org/10.1021/ACS.CGD.1C01435.

(19)   Shemchuk, O.; d'Agostino, S.; Fiore, C.; Sambri, V.; Zannoli, S.; Grepioni, F.; Braga, D.
        Natural Antimicrobials Meet a Synthetic Antibiotic: Carvacrol/Thymol and Ciprofloxacin
        Co-crystals as a Promising Solid-State Route to Activity Enhancement. *Cryst. Growth Des.*
        2020. https://doi.org/10.1021/acs.cgd.0c00900.

(20)   Kosalec, I.; Rai, M. Natural Antimicrobials: An Introduction. *Promis. Antimicrob. from Nat.
        Prod.* **2022**, 3–13. https://doi.org/10.1007/978-3-030-83504-0_1.

(21)   Promising Antimicrobials from Natural Products. *Promis. Antimicrob. from Nat. Prod.*
        2022. https://doi.org/10.1007/978-3-030-83504-0.

(22)   Havsteen, B. H. The Biochemistry and Medical Significance of the Flavonoids. *Pharmacol.
        Ther.* **2002**, *96* (2–3), 67–202. https://doi.org/10.1016/S0163-7258(02)00298-X.

(23)   Lalani, S.; Poh, C. L. Flavonoids as Antiviral Agents for Enterovirus A71 (EV-A71). *Viruses*
        2020, *12* (2), 184. https://doi.org/10.3390/v12020184.

(24)   Panche, A. N.; Diwan, A. D.; Chandra, S. R. Flavonoids: An Overview. *J. Nutr. Sci.* **2016**, *5*,
        e47. https://doi.org/10.1017/JNS.2016.41.

(25)   Anand David, A. V.; Arulmoli, R.; Parasuraman, S. Overviews of Biological Importance of
        Quercetin: A   Bioactive   Flavonoid.   *Pharmacogn.   Rev.*   **2016**,   *10*   (20),   84–89.
        https://doi.org/10.4103/0973-7847.194044.

(26)   Xu, D.; Hu, M. J.; Wang, Y. Q.; Cui, Y. L. Antioxidant Activities of Quercetin and Its
        Complexes   for   Medicinal   Application.   *Molecules*   **2019**,   *24*   (6),   1123.
        https://doi.org/10.3390/molecules24061123.

(27)   Zhang, M.; Swarts, S. G.; Yin, L.; Liu, C.; Tian, Y.; Cao, Y.; Swarts, M.; Yang, S.; Zhang, S. B.;
        Zhang, K.; Ju, S.; Olek, D. J.; Schwartz, L.; Keng, P. C.; Howell, R.; Zhang, L.; Okunieff, P.
        Antioxidant Properties of Quercetin. *Adv. Exp. Med. Biol.* **2011**, *701*, 283–289.
        https://doi.org/10.1007/978-1-4419-7756-4_38.

(28) Hisaka, T.; Sakai, H.; Sato, T.; Goto, Y.; Nomura, Y.; Fukutomi, S.; Fujita, F.; Mizobe, T.; Nakashima, O.; Tanigawa, M.; Naito, Y.; Akiba, J.; Ogasawara, S.; Nakashima, K.; Akagi, Y.; Okuda, K.; Yano, H. Quercetin Suppresses Proliferation of Liver Cancer Cell Lines in Vitro. *Anticancer Res* **2020**, *40* (8), 4695–4700. https://doi.org/10.21873/anticanres.14469.

(29) Zhou, J.; Fang, L.; Liao, J.; Li, L.; Yao, W.; Xiong, Z.; Zhou, X. Investigation of the Anti-Cancer Effect of Quercetin on HepG2 Cells in Vivo. *PLoS One* **2017**, *12* (3), e0172838. https://doi.org/10.1371/journal.pone.0172838.

(30) González-Segovia, R.; Quintanar, J. L.; Salinas, E.; Ceballos-Salazar, R.; Aviles-Jiménez, F.; Torres-López, J. Effect of the Fl Avonoid Quercetin on Infl Ammation and Lipid Peroxidation Induced by Helicobacter Pylori in Gastric Mucosa of Guinea Pig. *J Gastroenterol* **2008**, *43*, 441–447. https://doi.org/10.1007/s00535-008-2184-7.

(31) Guan, F.; Wang, Q.; Bao, Y.; Chao, Y. Anti-Rheumatic Effect of Quercetin and Recent Developments in Nano Formulation. *RSC Adv* **2021**, *11* (13), 7280–7293. https://doi.org/10.1039/d0ra08817j.

(32) Azeem, M.; Hanif, M.; Mahmood, K.; Ameer, N.; Chughtai, F. R. S.; Abid, U. An Insight into Anticancer, Antioxidant, Antimicrobial, Antidiabetic and Anti-Inflammatory Effects of Quercetin: A Review. *Polym. Bull.* **2022**, 1–22. https://doi.org/10.1007/S00289-022-04091-8.

(33) Cushnie, T. P. T.; Lamb, A. J. Antimicrobial Activity of Flavonoids. *Int. J. Antimicrob. Agents* **2005**, *26* (5), 343–356. https://doi.org/10.1016/J.IJANTIMICAG.2005.09.002.

(34) Lenard, N.; Henagan, T. M.; Lan, T.; Nguyen, A.; Bhattacharya, D. Antimicrobial Activity of Quercetin: An Approach to Its Mechanistic Principle. *Mol. 2022, Vol. 27, Page 2494* **2022**, *27* (8), 2494. https://doi.org/10.3390/MOLECULES27082494.

(35) Semwal, D. K.; Semwal, R. B.; Combrinck, S.; Viljoen, A. Myricetin: A Dietary Molecule with Diverse Biological Activities. *Nutr. 2016, Vol. 8, Page 90* **2016**, *8* (2), 90. https://doi.org/10.3390/NU8020090.

(36) Park, K. S.; Chong, Y.; Kim, M. K. Myricetin: Biological Activity Related to Human Health. *Appl. Biol. Chem.* **2016**, *59* (2), 259–269. https://doi.org/10.1007/S13765-016-0150-2.

(37) Tong, Y.; Zhou, X. M.; Wang, S. J.; Yang, Y.; Cao, Y. L. Analgesic Activity of Myricetin Isolated from Myrica Rubra Sieb. et Zucc. Leaves. *Arch. Pharmacal Res. 2009 324* **2009**, *32* (4), 527–533. https://doi.org/10.1007/S12272-009-1408-6.

(38) Ha, T. K.; Jung, I.; Kim, M. E.; Bae, S. K.; Lee, J. S. Anti-Cancer Activity of Myricetin against Human Papillary Thyroid Cancer Cells Involves Mitochondrial Dysfunction–Mediated Apoptosis. *Biomed. Pharmacother.* **2017**, *91*, 378–384. https://doi.org/10.1016/j.biopha.2017.04.100.

(39) Yang, Z. J.; Wang, H. R.; Wang, Y. I.; Zhai, Z. H.; Wang, L. W.; Li, L.; Zhang, C.; Tang, L. Myricetin Attenuated Diabetes-Associated Kidney Injuries and Dysfunction via Regulating Nuclear Factor (Erythroid Derived 2)-like 2 and Nuclear Factor-ĸB Signaling. *Front. Pharmacol.* **2019**, *10* (JUN), 647. https://doi.org/10.3389/FPHAR.2019.00647.

(40) Jiang, M.; Zhu, M.; Wang, L.; Yu, S. Anti-Tumor Effects and Associated Molecular Mechanisms of Myricetin. *Biomed. Pharmacother.* **2019**, *120*. https://doi.org/10.1016/j.biopha.2019.109506.

(41) Gordon, M. H.; Roedig-Penman, A. Antioxidant Activity of Quercetin and Myricetin in Liposomes. *Chem. Phys. Lipids.* **1998**, *97* (1), 79–85. https://doi.org/10.1016/s0009-3084(98)00098-x.

(42) Taheri, Y.; Suleria, H. A. R.; Martins, N.; Sytar, O.; Beyatli, A.; Yeskaliyeva, B.; Seitimova, G.; Salehi, B.; Semwal, P.; Painuli, S.; Kumar, A.; Azzini, E.; Martorell, M.; Setzer, W. N.; Maroyi, A.; Sharifi-Rad, J. Myricetin Bioactive Effects: Moving from Preclinical Evidence to Potential Clinical Applications. *BMC Complement. Med. Ther. 2020 201* **2020**, *20* (1), 1–14. https://doi.org/10.1186/S12906-020-03033-Z.

(43) Srimathi Priyanga, K.; Vijayalakshmi, K. Investigation of Antioxidant Potential of Quercetin and Hesperidin: An in Vitro Approach. *Asian J Pharm Clin Res* **2017**, *10* (11), 83–86. https://doi.org/10.22159/ajpcr.2017.v10i11.20260.

(44) González, A.; Casado, J.; Lanas, Á. Fighting the Antibiotic Crisis: Flavonoids as Promising Antibacterial Drugs Against Helicobacter Pylori Infection. *Front. Cell. Infect. Microbiol.* **2021**, *11*, 671. https://doi.org/10.3389/FCIMB.2021.709749.

(45) González, A.; Salillas, S.; Velázquez-Campoy, A.; Espinosa Angarica, V.; Fillat, M. F.; Sancho, J.; Lanas, Á. Identifying Potential Novel Drugs against Helicobacter Pylori by Targeting the Essential Response Regulator HsrA. *Sci. Rep.* **2019**, *9* (1), 1–13. https://doi.org/10.1038/s41598-019-47746-9.

(46) Chadha, K.; Karan, M.; Bhalla, Y.; Chadha, R.; Khullar, S.; Mandal, S.; Vasisht, K. Co-crystals of Hesperetin: Structural, Pharmacokinetic, and Pharmacodynamic Evaluation. *Cryst. Growth Des.* **2017**, *17* (5), 2386–2405. https://doi.org/10.1021/ACS.CGD.6B01769.

(47) Manach, C.; Scalbert, A.; Morand, C.; Rémésy, C.; Jiménez, L. Polyphenols: Food Sources and Bioavailability. *Am. J. Clin. Nutr.* **2004**, *79* (5), 727–747. https://doi.org/10.1093/AJCN/79.5.727.

(48) Manach, C.; Williamson, G.; Morand, C.; Scalbert, A.; Rémésy, C. Bioavailability and Bioefficacy of Polyphenols in Humans. I. Review of 97 Bioavailability Studies. *Am. J. Clin. Nutr.* **2005**, *81* (1), 230S-242S. https://doi.org/10.1093/AJCN/81.1.230S.

(49) Mirzoeva, O. K.; Grishanin, R. N.; Calder, P. C. Antimicrobial Action of Propolis and Some of Its Components: The Effects on Growth, Membrane Potential and Motility of Bacteria. *Microbiol. Res.* **1997**, *152* (3), 239–246. https://doi.org/10.1016/S0944-5013(97)80034-1.

(50) Roncarati, D.; Scarlato, V.; Vannini, A. Targeting of Regulators as a Promising Approach in the Search for Novel Antimicrobial Agents. *Microorg. 2022, Vol. 10, Page 185* **2022**, *10* (1), 185. https://doi.org/10.3390/MICROORGANISMS10010185.

(51) Zannoni, A.; Pelliciari, S.; Musiani, F.; Chiappori, F.; Roncarati, D.; Scarlato, V. Definition of the Binding Architecture to a Target Promoter of HP1043, the Essential Master Regulator of Helicobacter Pylori. *Int. J. Mol. Sci.* **2021**, *22* (15), 7848. https://doi.org/10.3390/IJMS22157848/S1.

(52) Vannini, A.; Roncarati, D.; Agostino, F. D'; Antoniciello, F.; Scarlato, V. Insights into the Orchestration of Gene Transcription Regulators in Helicobacter Pylori. *Int. J. Mol. Sci. 2022, Vol. 23, Page 13688* **2022**, *23* (22), 13688. https://doi.org/10.3390/IJMS232213688.

(53) González, A.; Salillas, S.; Velázquez-Campoy, A.; Espinosa Angarica, V.; Fillat, M. F.; Sancho, J.; Lanas, Á. Identifying Potential Novel Drugs against Helicobacter Pylori by Targeting the Essential Response Regulator HsrA. *Sci. Reports 2019 91* **2019**, *9* (1), 1–13. https://doi.org/10.1038/s41598-019-47746-9.

(54) Sheldrick, G. SHELXT: Integrating Space Group Determination and Structure Solution. *Acta Crystallogr. Sect. A Found. Adv.* **2014**, *70* (a1), C1437–C1437.

https://doi.org/10.1107/S2053273314085623.

(55) Altomare, A.; Cuocci, C.; Giacovazzo, C.; Moliterni, A.; Rizzi, R.; Corriero, N.; Falcicchio, A. EXPO2013: A Kit of Tools for Phasing Crystal Structures from Powder Data. *urn:issn:0021-8898* **2013**, *46* (4), 1231–1235. https://doi.org/10.1107/S0021889813013113.

(56) MacRae, C. F.; Sovago, I.; Cottrell, S. J.; Galek, P. T. A.; McCabe, P.; Pidcock, E.; Platings, M.; Shields, G. P.; Stevens, J. S.; Towler, M.; Wood, P. A. Mercury 4.0: From Visualization to Analysis, Design and Prediction. *J. Appl. Crystallogr.* **2020**, *53* (1), 226–235. https://doi.org/10.1107/S1600576719014092.

(57) Bernstein, J.; Davis, R. E.; Shimoni, L.; Chang, N. -L. Patterns in Hydrogen Bonding: Functionality and Graph Set Analysis in Crystals. *Angew. Chemie Int. Ed. English* **1995**, *34* (15), 1555–1573. https://doi.org/10.1002/ANIE.199515551.

(58) Sekhon, B. S. Drug-Drug Co-Crystals. *DARU, J. Pharm. Sci.* **2012**, *20* (1), 1–2. https://doi.org/10.1186/2008-2231-20-45.

(59) Shemchuk, O.; D'Agostino, S.; Fiore, C.; Sambri, V.; Zannoli, S.; Grepioni, F.; Braga, D. Natural Antimicrobials Meet a Synthetic Antibiotic: Carvacrol/Thymol and Ciprofloxacin Co-crystals as a Promising Solid-State Route to Activity Enhancement. *Cryst. Growth Des.* **2020**, *20* (10), 6796–6803. https://doi.org/10.1021/acs.cgd.0c00900.

(60) Bordignon, S.; Vioglio, P. C.; Priola, E.; Voinovich, D.; Gobetto, R.; Nishiyama, Y.; Chierotti, M. R. Engineering Codrug Solid Forms: Mechanochemical Synthesis of an Indomethacin–Caffeine System. *Cryst. Growth Des.* **2017**, *17* (11), 5744–5752. https://doi.org/10.1021/ACS.CGD.7B00748.

(61) Byrn, S. R.; Pfeiffer, R. R.; Stephenson, G.; Grant, D. J. W.; Gleason, W. B. Solid-State Pharmaceutical Chemistry. *Chem. Mater.* **1994**, *6* (8), 1148–1158. https://doi.org/10.1021/CM00044A013.

(62) Farhadi, F.; Khameneh, B.; Iranshahi, M.; Iranshahy, M. Antibacterial Activity of Flavonoids and Their Structure–Activity Relationship: An Update Review. *Phytother Res* **2019**, *33* (1), 13–40. https://doi.org/10.1002/ptr.6208.

3.3.5 Supporting information

Levofloxacin and Ciprofloxacin cocrystals with *flavonoids:*
**solid-state investigation for a multi-target strategy against *Helicobacter pylori.***

Cecilia Fiore [a], Federico Antoniciello [b], Davide Roncarati [b], Vincenzo Scarlato [b] and Dario Braga [a].

[a] Dipartimento di Chimica "Giacomo Ciamician", University of Bologna, Via Selmi, 2 – 40126   Bologna – Italy.
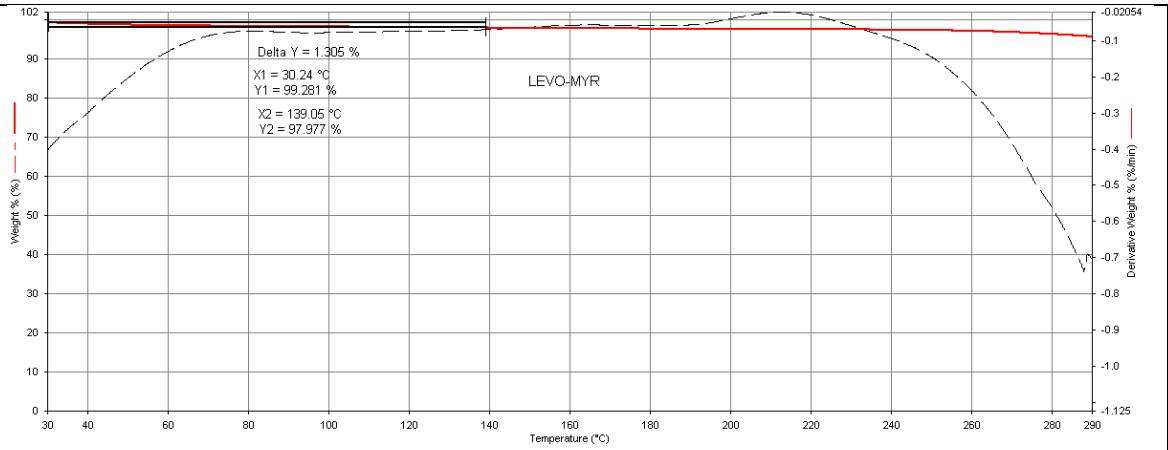[b] Dipartimento di Farmacia e Biotecnologie, University of Bologna, Via Belmeloro 6, – 40126, Bologna – Italy.

TGA AND DSC DATA

LEVO-QUE-EtOH	
DSC	
TGA	
LEVO-MYR-EtOH	
DSC	
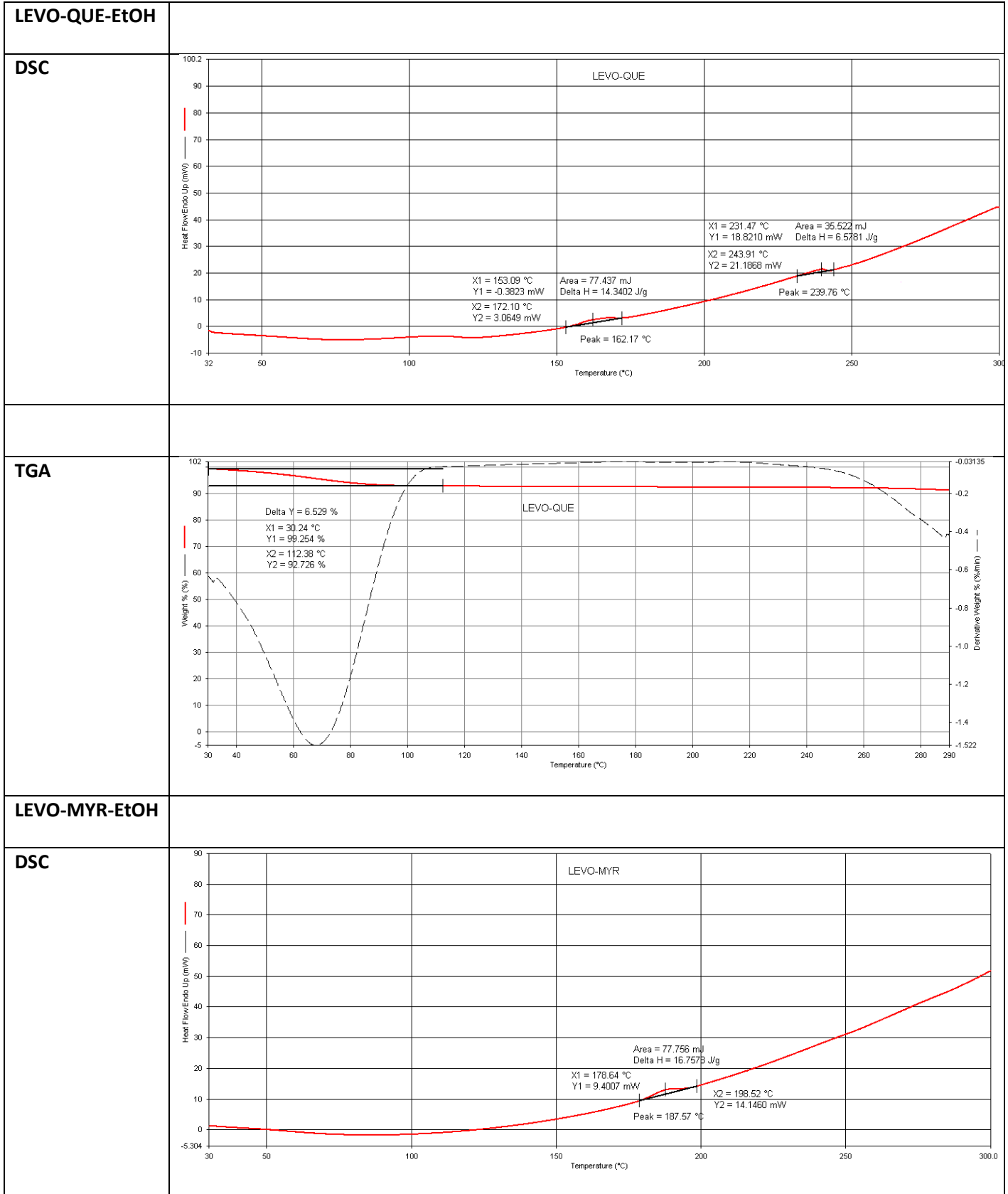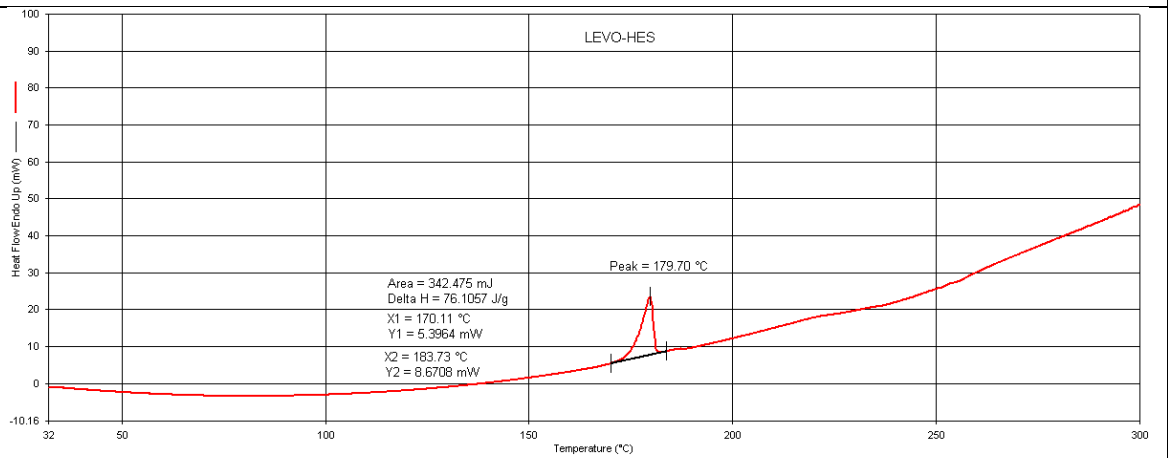
TGA	
2LEVO-HES	
DSC	
TGA	
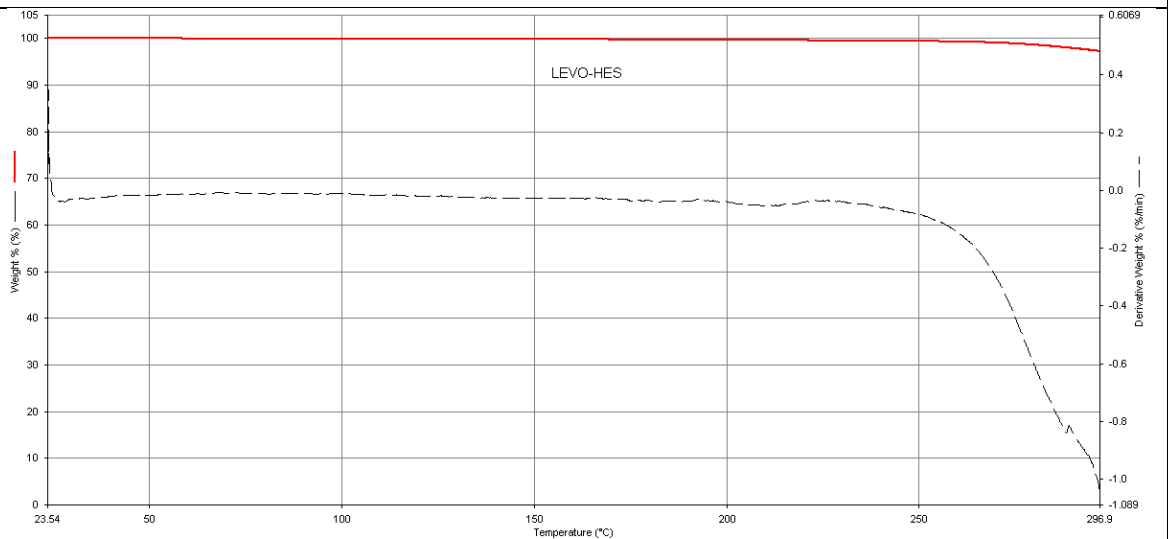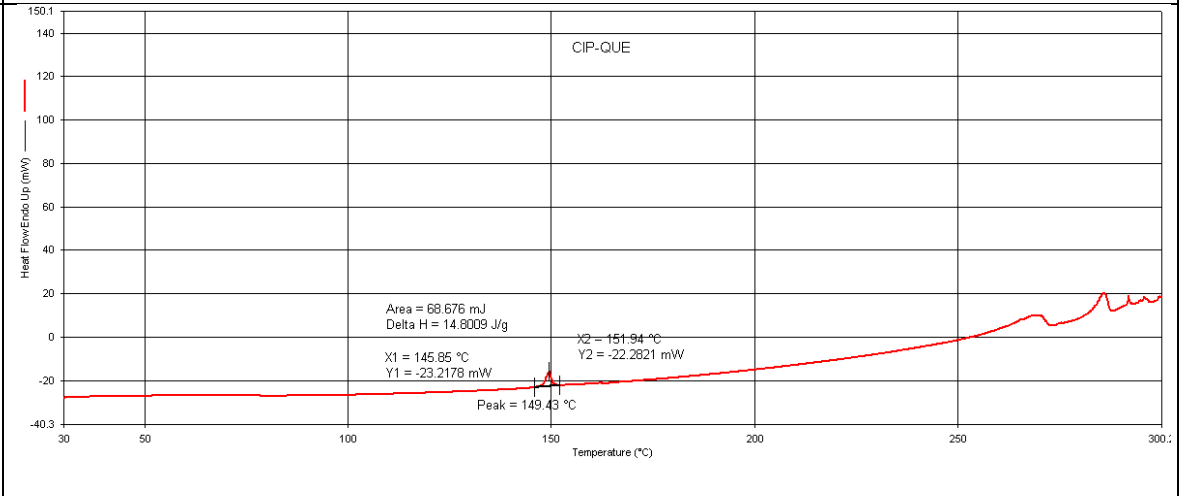
| CIP-QUE	
DSC	
TGA	
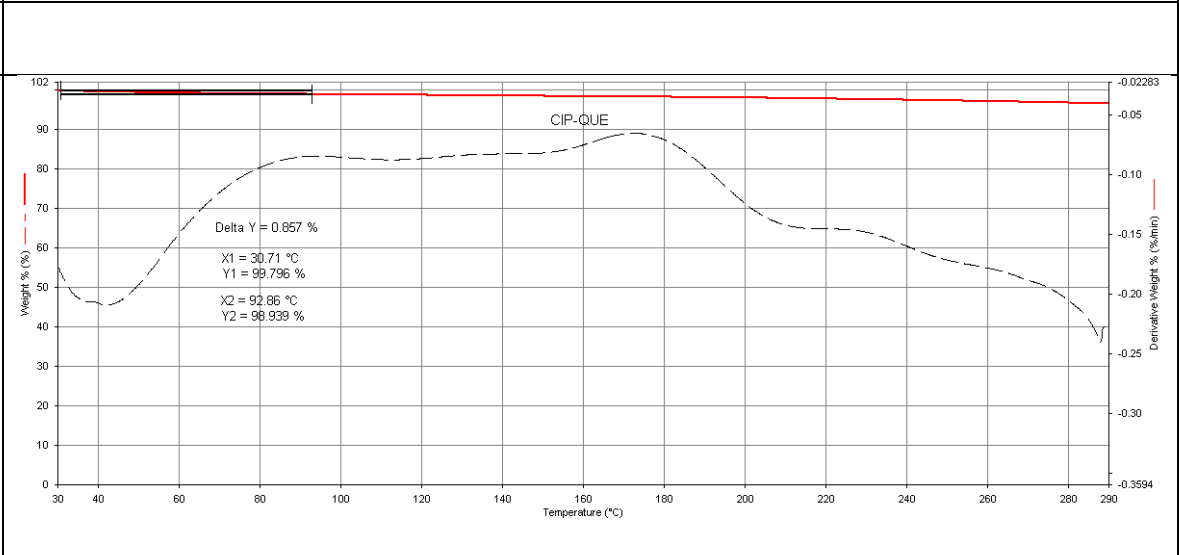
¹H NMR spectroscopy
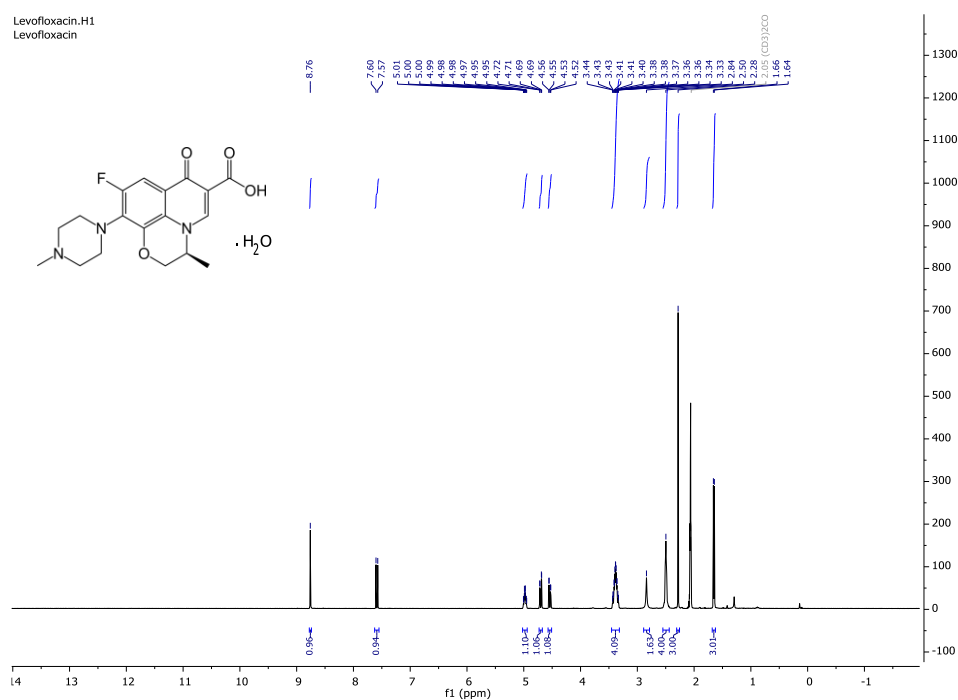
LEVOFLOXACIN: ¹H NMR (401 MHz, Acetone-*d₆*) δ 8.76 (s, 1H), 7.59 (d, *J* = 12.4 Hz, 1H), 5.02 – 4.94 (m, 1H), 4.70 (dd, *J* = 11.5, 1.8 Hz, 1H), 4.54 (dd, *J* = 11.5, 2.3 Hz, 1H), 3.39 (m , 4H), 2.50 (s, 4H), 2.28 (s, 3H), 1.65 (d, *J* = 6.8 Hz, 3H). **H₂O:** 2.84 (s, 2H).
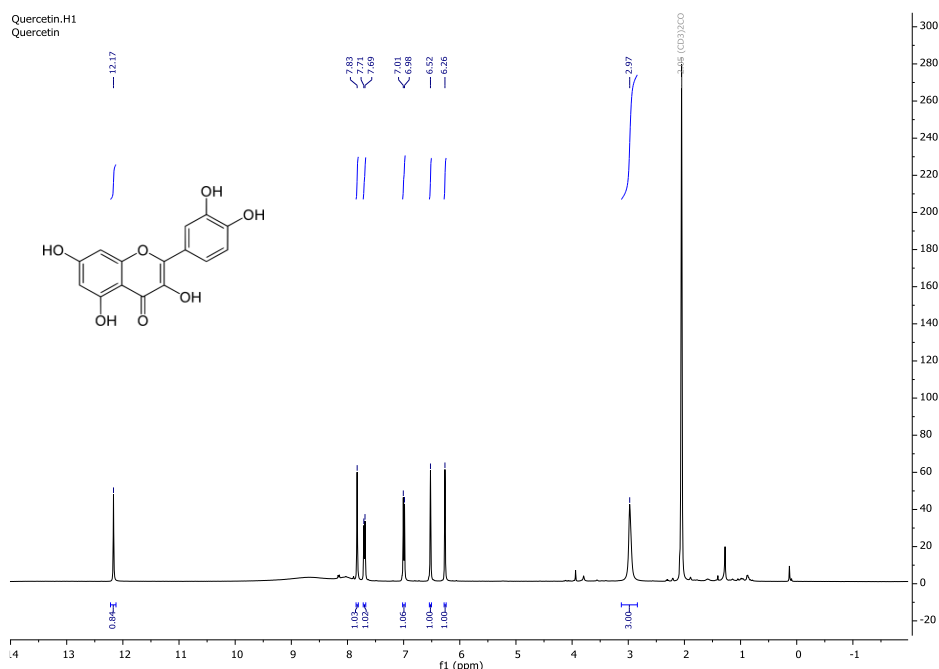
QUERCETIN: ¹H NMR (401 MHz, Acetone-*d₆*) δ 12.17 (s, 1H), 7.83 (s, 1H), 7.70 (d, *J* = 8.4 Hz, 1H), 7.00 (d, *J* = 8.5 Hz, 1H), 6.52 (s, 1H), 6.26 (s, 1H), 2.97 (s, 3H).
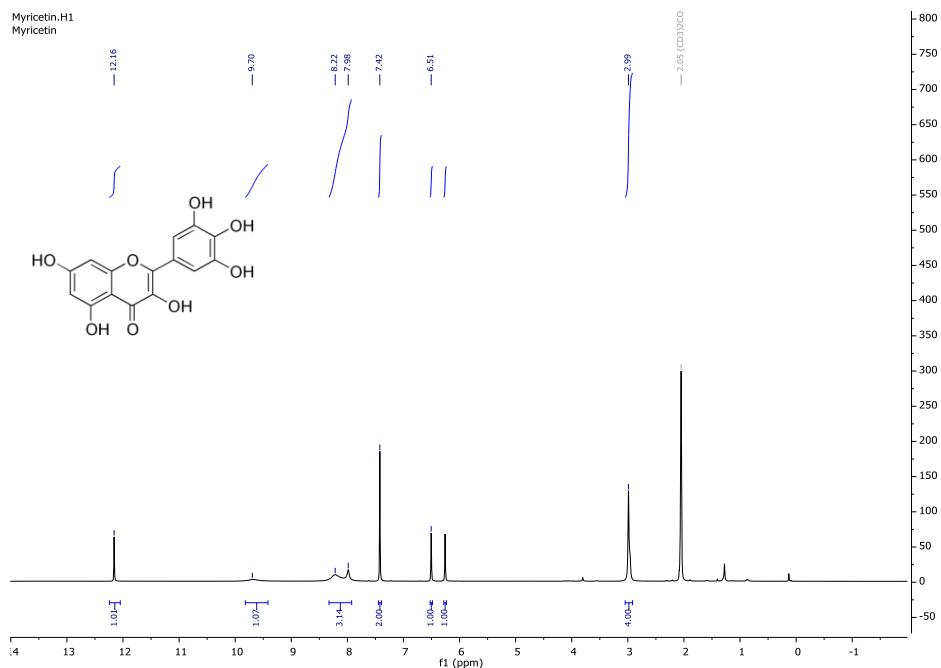
MYRICETIN: ^{1}H NMR (401 MHz, Acetone-d_6) δ 12.16 (s, 1H), 9.70 (s, 1H), 8.10 (d, J = 93.4 Hz, 3H), 7.42 (s, 2H), 6.51 (s, 1H), 6.26 (d, J = 2.1 Hz, 1H), 2.99 (s, 4H – MYRICETIN + H_2O/SOLVENT).
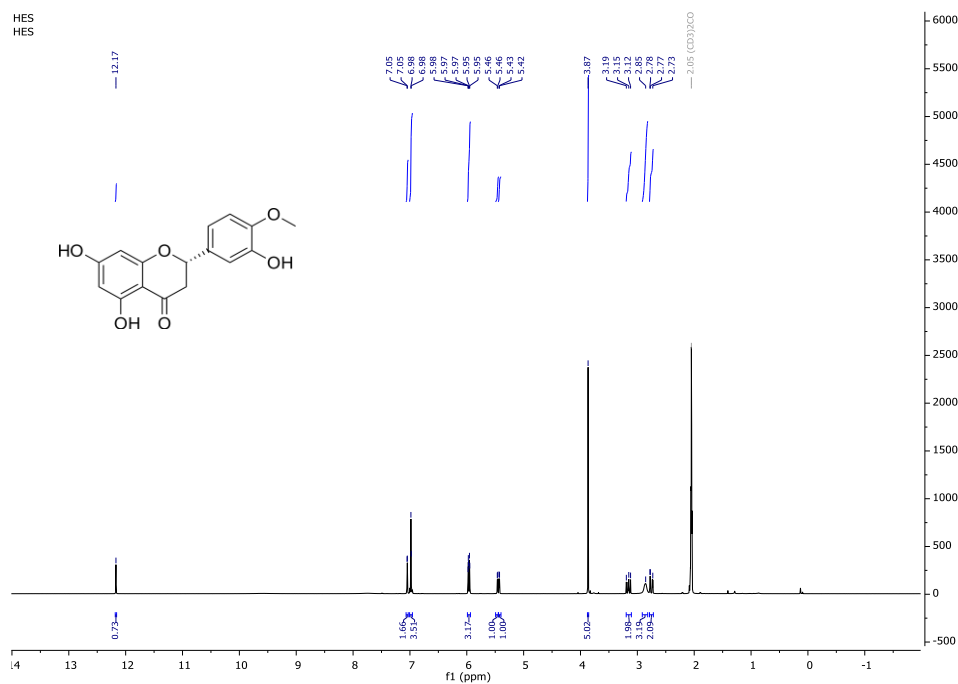
HESPERETIN: ^{1}H NMR (401 MHz, Acetone-d_6) δ 12.17 (s, 1H), 7.05 (d, J = 1.4 Hz, 2H), 6.98 (d, J = 2.0 Hz, 4H), 5.99 – 5.94 (m, 3H), 5.46 (d, J = 3.1 Hz, 1H), 5.43 (d, J = 3.1 Hz, 1H). -O-CH_3 + solvent impurity :3.87 (s, 5H), SOLVENTS RESIDUES 3.20 – 3.11 (m, 2H), 2.85 (s, 3H), 2.79 – 2.72 (m, 2H).
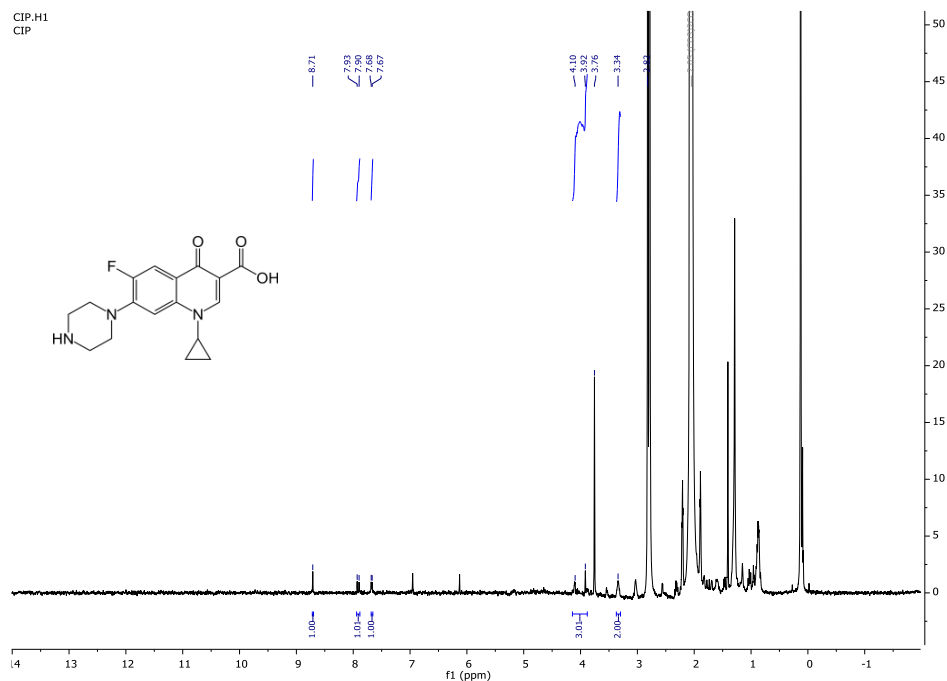
CIPROFLOXACIN: analysis of the spectrum incomplete due to the low quality of signals belonging to CIP and too the presence of impurities covering the signals of interest. ^{1}H NMR (401 MHz, Acetone-d_6) δ 8.71 (s, 1H), 7.91 (d, J = 13.6 Hz, 1H), 7.68 (d, J = 7.0 Hz, 1H), 4.01 (d, J = 72.0 Hz, 3H), 3.34 (s, 2H).
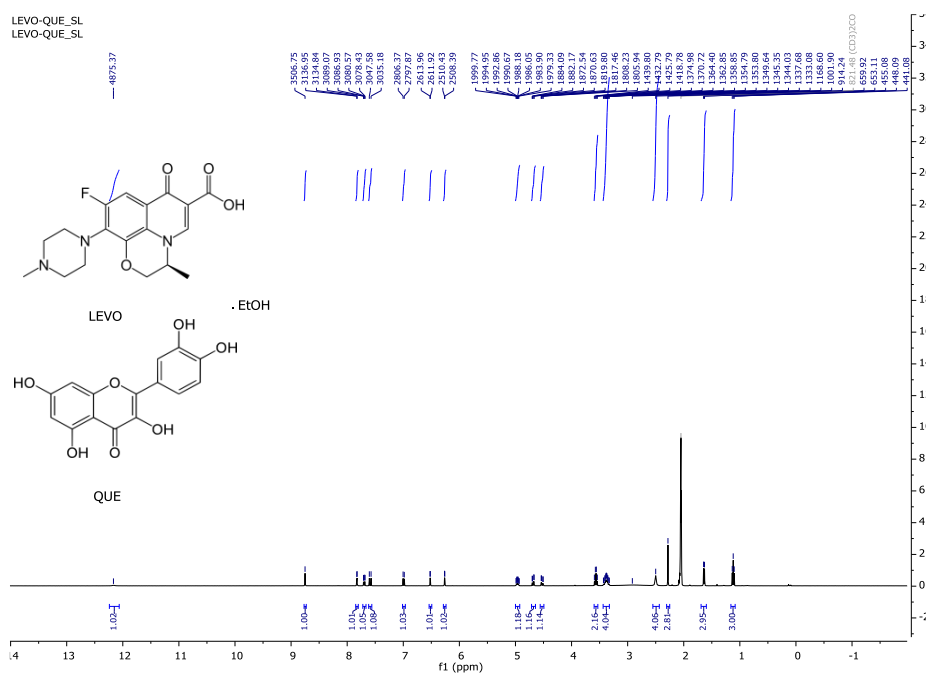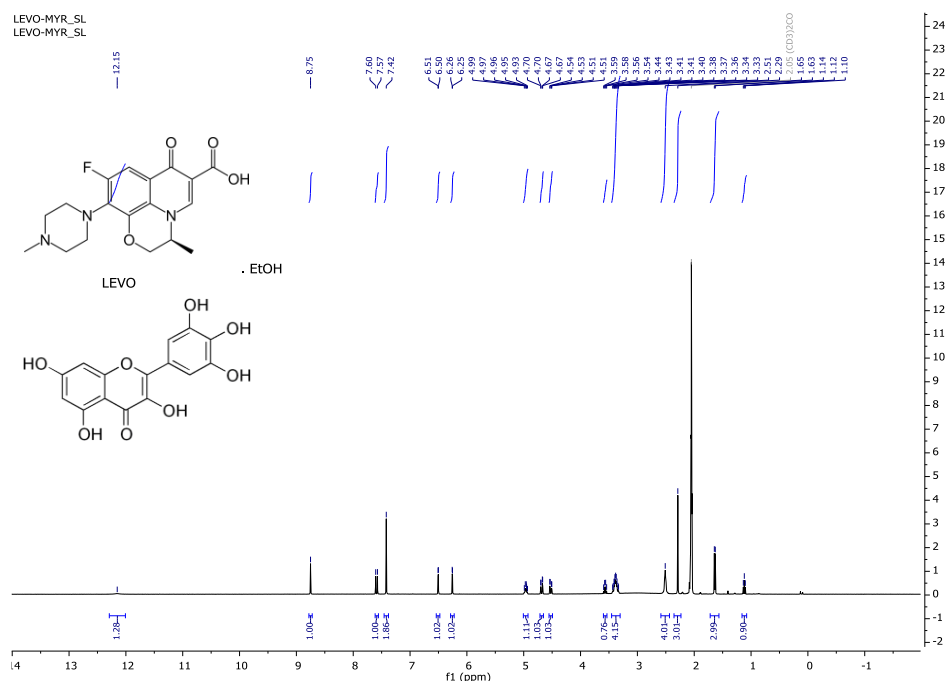

LEVO-QUE-EtOH: ^{1}H NMR (401 MHz, Acetone-d_6) δ 12.17 (s, 1H), 8.75 (s, 1H), 7.83 (d, J = 2.1 Hz, 1H), 7.70 (dd, J = 8.5, 2.1 Hz, 1H), 7.59 (d, J = 12.4 Hz, 1H), 6.99 (d, J = 8.5 Hz, 1H), 6.52 (d, J = 2.0 Hz, 1H), 6.26 (d, J = 2.0 Hz, 1H), 4.96 (m, 1H), 4.68 (dd, J = 11.5, 1.9 Hz, 1H), 4.52 (dd, J = 11.5, 2.3 Hz, 1H), 3.57 (q, J = 7.0 Hz, 2H), 3.44 – 3.33 (m, 4H), 2.50 (s, 4H), 2.28 (s, 3H), 1.64 (d, J = 6.8 Hz, 3H), **EtOH -CH$_2$** :3.57 (q, J = 7.0 Hz, 2H), **-CH$_3$**: 1.12 (t, J = 7.0 Hz, 3H).

155
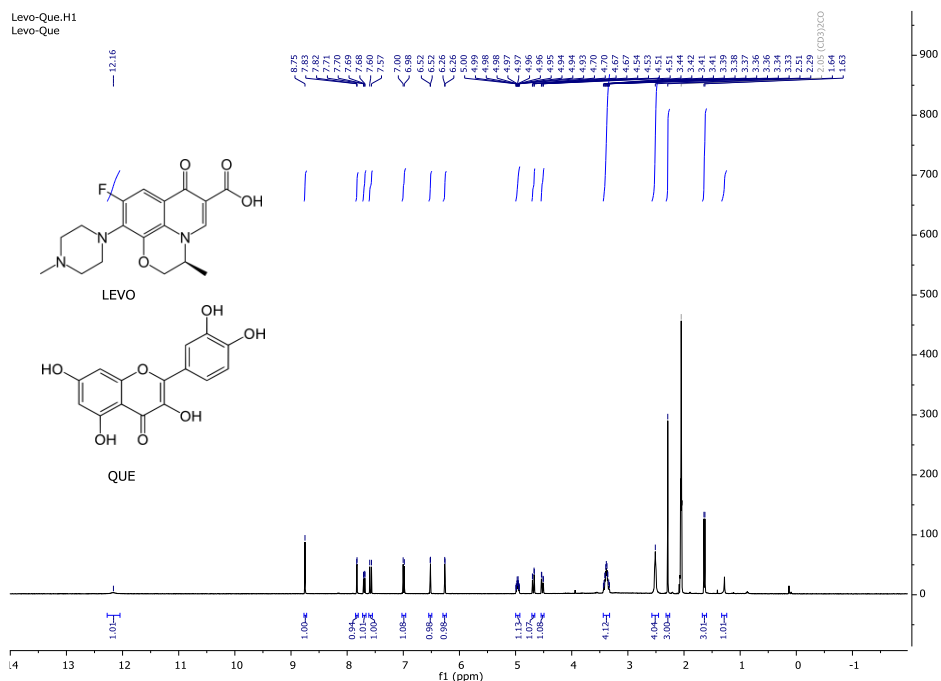
LEVO-QUE after VTXRPD : ^{1}H NMR (401 MHz, Acetone-d_6) δ 12.16 (s, 1H), 8.75 (s, 1H), 7.83 (d, *J* = 2.1 Hz, 1H), 7.70 (dd, *J* = 8.5, 2.1 Hz, 1H), 7.58 (d, *J* = 12.4 Hz, 1H), 6.99 (d, *J* = 8.5 Hz, 1H), 6.52 (d, *J* = 1.9 Hz, 1H), 6.26 (d, *J* = 2.0 Hz, 1H), 4.96 (m, 1H), 4.68 (dd, *J* = 11.5, 1.8 Hz, 1H), 4.52 (dd, *J* = 11.5, 2.3 Hz, 1H), 3.44 – 3.33 (m, 4H), 2.51 (s, 4H), 2.29 (s, 3H), 1.64 (d, *J* = 6.8 Hz, 3H), 1.28 (s, 1H).


LEVO-MYR-EtOH: ^{1}H NMR (401 MHz, Acetone-d_6) δ 12.15 (s, 1H), 8.75 (s, 1H), 7.59 (d, *J* = 12.4 Hz, 1H), 7.42 (s, 2H), 6.50 (d, *J* = 2.0 Hz, 1H), 6.26 (d, *J* = 2.0 Hz, 1H), 5.01 – 4.92 (m, 1H), 4.68 (dd, *J* = 11.5, 1.9 Hz, 1H), 4.52 (dd, *J* = 11.5, 2.3 Hz, 1H), 3.38 (m, 4H), 2.51 (s, 4H), 2.29 (s, 3H), 1.64 (d, *J* = 6.8 Hz, 3H). **EtOH -CH₂:**3.57 (q, *J* = 7.0 Hz, 0.76H), **-CH₃:**1.12 (t, *J* = 7.0 Hz, 0.90H).
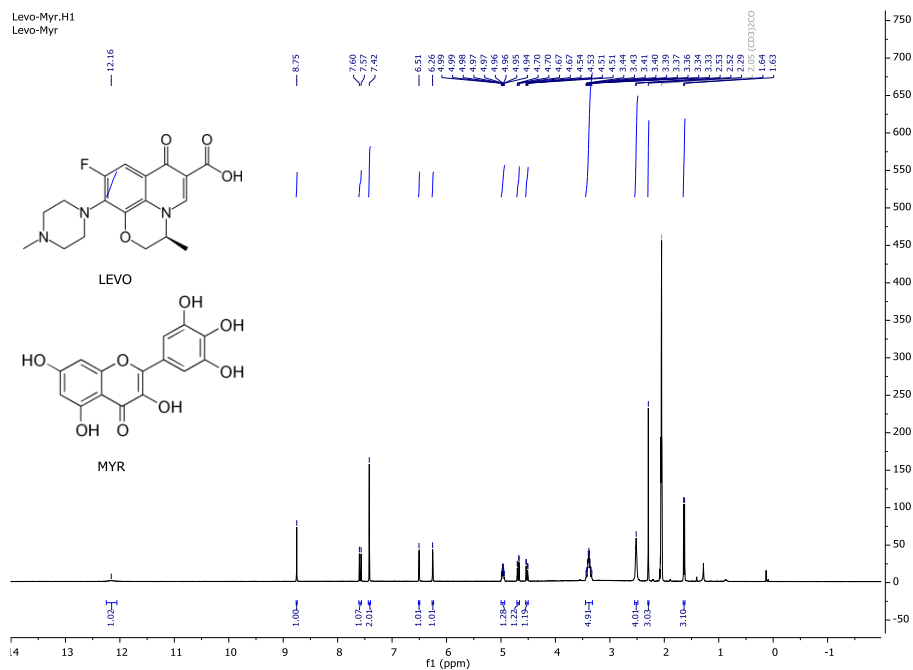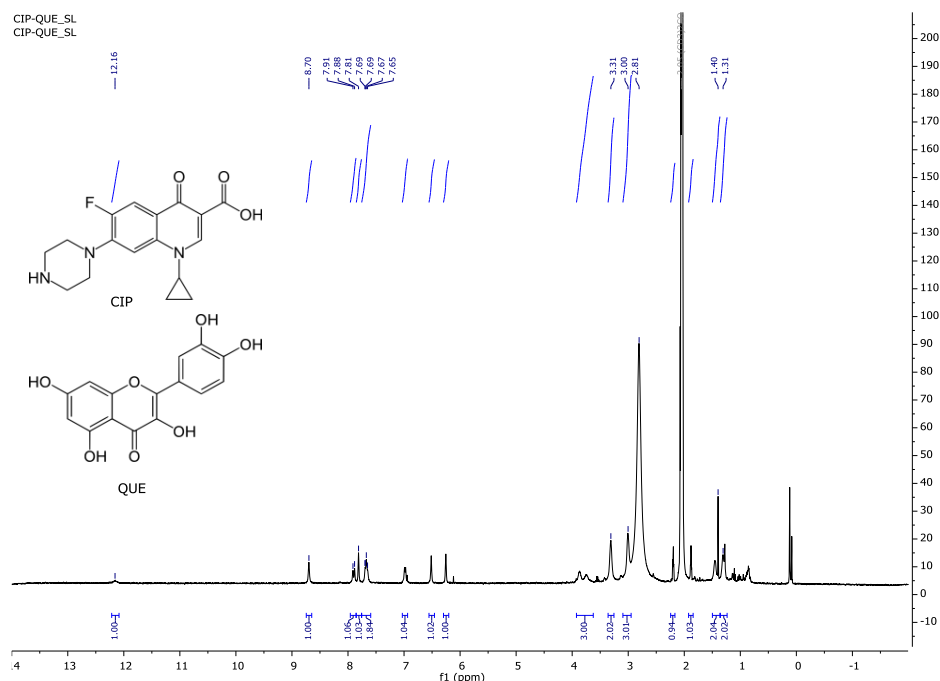
LEVO-MYR after VTXRPD ^{1}H NMR (401 MHz, Acetone-d_6) δ 12.16 (s, 1H), 8.75 (s, 1H), 7.58 (d, *J* = 12.4 Hz, 1H), 7.42 (s, 2H), 6.51 (s, 1H), 6.26 (s, 1H), 5.00 – 4.93 (m, 1H), 4.68 (dd, *J* = 11.5, 1.8 Hz, 1H), 4.52 (dd, *J* = 11.6, 2.3 Hz, 1H), 3.45 – 3.32 (m, 5H), 2.55 – 2.49 (m, 4H), 2.29 (s, 3H), 1.64 (d, *J* = 6.8 Hz, 3H).
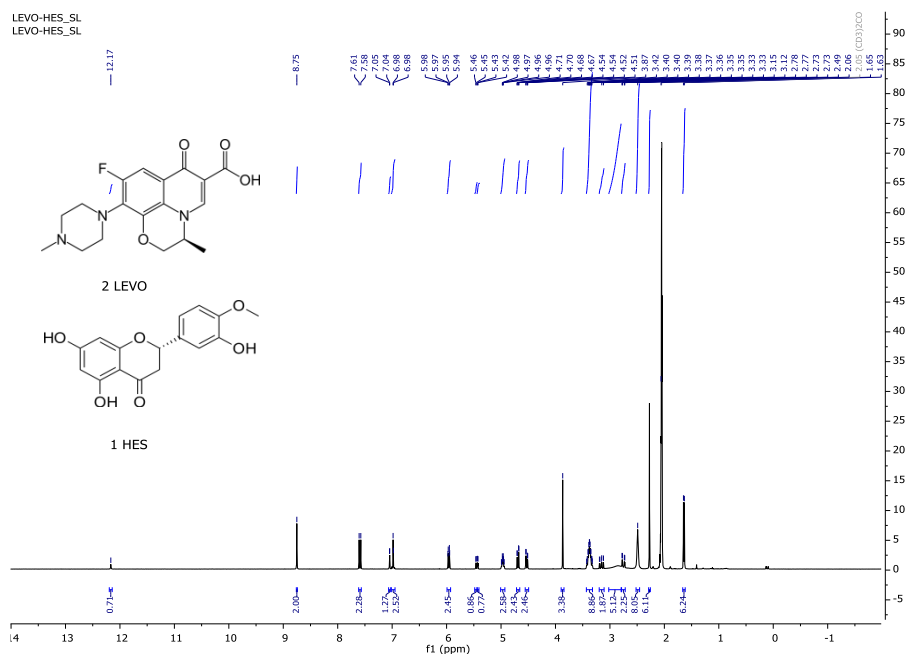
2LEVO-HES before VTXRPD: ^{1}H NMR (401 MHz, Acetone-d_6) δ 12.17 (s, 1H), 8.75 (s, 2H), 7.59 (d, *J* = 12.4 Hz, 2H), 7.05 (d, *J* = 1.3 Hz, 1.5H), 6.98 (d, *J* = 2.1 Hz, 3H), 5.96 (dd, *J* = 10.5, 2.1 Hz, 2H), 5.46 (d, *J* = 3.0 Hz, 1H), 5.43 (d, *J* = 3.0 Hz, 1H), 4.97 (m, 3H), 4.69 (dd, *J* = 11.5, 1.9 Hz, 2H), 4.53 (dd, *J* = 11.5, 2.3 Hz, 2H), 3.87 (s, 3H), 3.38 (th, *J* = 12.1, 4.3 Hz, 8H), 3.16 (dd, *J* = 17.1, 12.6 Hz, 2H), 2.85 (s, 5H), 2.75 (dd, *J* = 17.1, 3.1 Hz, 2H), 2.49 (s, 8H), 2.27 (s, 6H), 1.64 (d, *J* = 6.8 Hz, 6H).
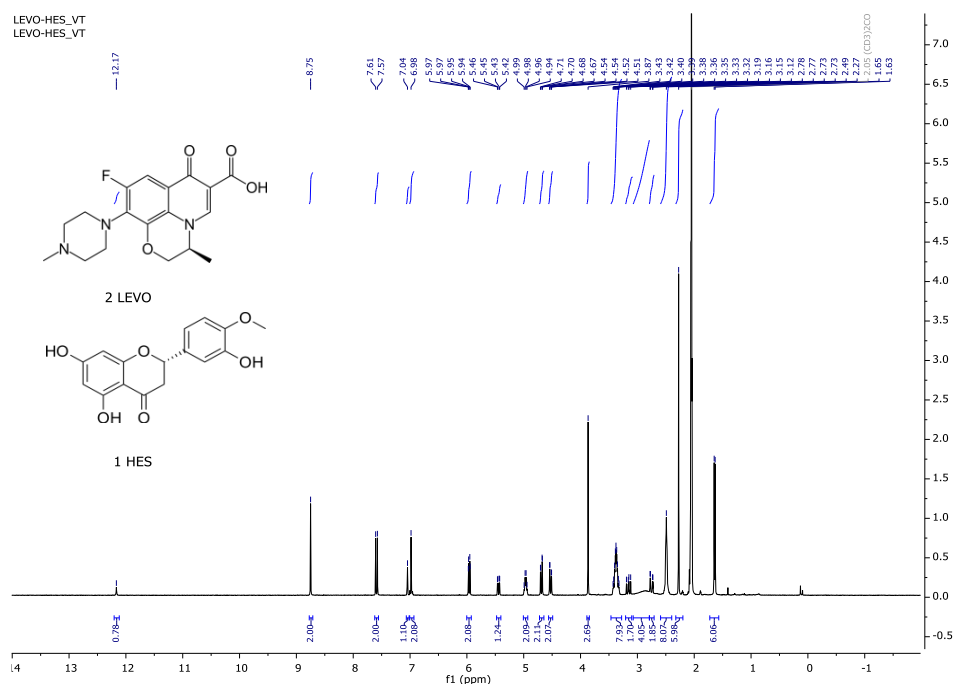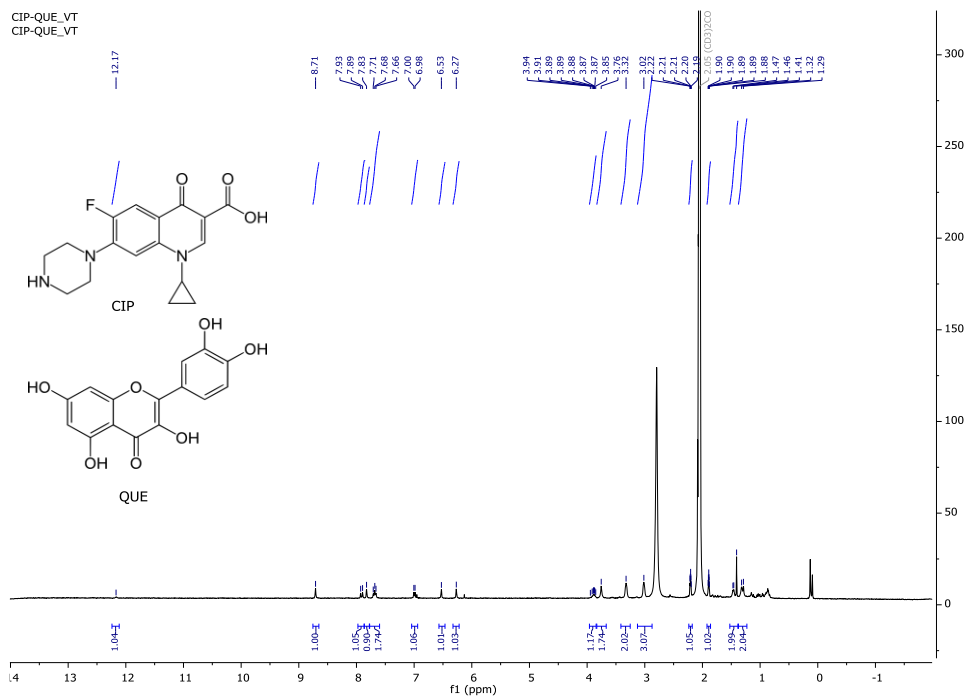
2LEVO-HES after VTXRPD: ^{1}H NMR (401 MHz, Acetone-d_6) δ 12.17 (s, 1H), 8.75 (s, 2H), 7.59 (d, J = 12.4 Hz, 2H), 7.04 (s, 1H), 6.98 (s, 2H), 5.96 (dd, J = 10.5, 2.1 Hz, 2H), 5.44 (dd, J = 12.6, 3.0 Hz, 1H), 4.97 (q, J = 6.8 Hz, 2H), 4.69 (dd, J = 11.5, 1.9 Hz, 2H), 4.53 (dd, J = 11.6, 2.3 Hz, 2H), 3.87 (s, 3H), 3.38 (qt, J = 10.6, 4.3 Hz, 8H), 3.16 (dd, J = 17.1, 12.6 Hz, 2H), 3.07 − 2.79 (m, 4H), 2.75 (dd, J = 17.1, 3.1 Hz, 2H), 2.49 (s, 8H), 2.27 (s, 6H), 1.64 (d, J = 6.8 Hz, 6H).

CIP-QUE before VTXRPD: ^{1}H NMR (401 MHz, Acetone-d_6) δ 12.16 (s, 1H), 8.70 (s, 1H), 7.90 (d, J = 11.6 Hz, 1H), 7.81 (s, 1H), 7.76 − 7.59 (m, 2H), 7.03 − 6.94 (m, 1H), 6.52 (s, 1H), 6.25 (s, 1H), 3.81 (d, J = 49.0 Hz, 3H), 3.31 (s, 2H), 3.00 (s, 3H), 2.20 (dd, J = 4.5, 2.3 Hz, 1H), 1.88 (p, J = 2.2 Hz, 1H), 1.40 (s, 2H), 1.31 (s, 2H).

CIP-QUE after VTXRPD: ^{1}H NMR (401 MHz, Acetone-d_6) δ 12.17 (s, 1H), 8.71 (s, 1H), 7.91 (d, J = 13.2 Hz, 1H), 7.83 (s, 1H), 7.77 − 7.60 (m, 2H), 6.99 (d, J = 8.2 Hz, 1H), 6.53 (s, 1H), 6.27 (s, 1H), 3.96 − 3.84 (m, 1H), 3.76 (s, 2H), 3.32 (s, 2H), 3.02 (s, 3H), 2.21 (dt, J = 4.2, 2.2 Hz, 1H), 1.92 − 1.86 (m, 1H), 1.53 − 1.39 (m, 2H), 1.31 (d, J = 13.0 Hz, 2H).

Conclusions

The frame of this doctoral project was the synthesis through solid-state methods, and the characterization and overall performance evaluation, of novel crystalline materials obtained by combining, with a crystal engineering approach, molecules and/or metal complexes of known antimicrobial activity.

The increasing concern in the development of antimicrobial resistance is motivating the quest for new materials to be used in the battle against pathogens. Co-crystallization, whether from solution or from mechanochemical solvent-free methods, has been used to synthesize new materials and/or to enhance the properties of active molecules.

With this idea in mind, the research activity was focused on two main lines summarized as follows:

1. Design, preparation and characterization of novel metal-based antimicrobials, whereby organic molecules with known antimicrobial properties are combined with metal atoms also known to exert antimicrobial action.

2. Design, preparation and characterization of co-crystals obtained by combining antibacterial APIs (*active pharmaceutical ingredients*) with natural antimicrobials.

1. Regarding the first line of my research activity, we have shown that co-crystallization of antibacterial compounds or GRAS molecules with metal salts is indeed a viable, eco-friendly, and inexpensive way to obtain new materials with enhanced antibacterial properties. Indeed, molecular inorganic-organic hybrid compounds obtained by coordinating organic molecules with metals have been shown to possess enhanced

antimicrobial properties with respect to those of the separate components on their own or in physical mixture.

The first systems successfully synthesized by both solution and solid-state methods (mechanochemically), and structurally characterized, are two novel compounds of the antibacterial proflavine with $ZnCl_2$, namely $ZnCl_3(HPF)$ and $[HPF]_2[ZnCl_4]\cdot H_2O$. Crystallization from solution yielded higher purity target products, which were subsequently utilized for the investigation of the antimicrobial activity. In terms of antimicrobial activity, the two compounds appear to be 1.5 to 2 times more efficient towards the pathogen indicator strains with respect to the reagents and towards AgNO3 used as a standard of metal antimicrobial activity.

A second project developed, belonging to the same research line, regards the preparation, characterization and antimicrobial activity evaluation of novel coordination polymers obtained by co-crystallizing the amino acids arginine and histidine, as both enantiopure L and racemic DL forms, with the salts $Cu(NO_3)_2$ and $AgNO_3$.

In this study, the antimicrobial activity has been investigated to explore the effect of chirality in the cases of enantiopure and racemic forms. The compounds were prepared by mechanochemical, slurry and solution methods and characterized by X-ray single-crystal, powder diffraction and, in the cases of the silver compounds, by solid-state NMR spectroscopy.

The antimicrobial activity of the materials mentioned above was tested by the group of the Professor Raymond J. Turner, at the University of Calgary, Alberta – Canada.

2. The second line of my research has been focused on the design and characterization of co-crystals obtained by combining antibacterial APIs (*active pharmaceutical*

ingredients) with natural antimicrobials. In this research project we have shown that co-crystallization provides alternative routes to the synthesis of new materials and/or to the enhancement of the properties of active molecules. Herein co-crystallization strategies are applied to approach the problem of the antimicrobial resistance.

For this purpose, the first goal was fulfilled by co-crystallizing the antibiotic ciprofloxacin (CIP) via slurry and/or ball-milling with carvacrol (CAR) and thymol (THY), natural products belonging to the GRAS family, also known to exert antimicrobial activity. As a result, two families of ciprofloxacin cocrystals with carvacrol, CIP·CARn (n = 2, 3, 4) and with thymol, CIP·THYn (n = 2, 4), were obtained and their solid- state characterization and thermal behaviour was carried out.

The effect of co-crystals formation on the antibiotic activity of ciprofloxacin has also been evaluated by means of standard antimicrobial tests in the case of CIP·CAR4 and CIP·THY2 and compared with the results for the pure components and their physical mixtures. Preliminary antimicrobial testing clearly indicated that cocrystals CIP·CAR4 and CIP·THY2 have a comparable bacteriostatic activity, and that this is significantly better than the one of ciprofloxacin alone. These results were very encouraging and for this reason more work was done in this sense, following the same approach.

As a follow up of the previous inspiring results, the second project of this research line focuses on the co-crystallization of three representatives of the cephalosporin (CEPH) class of antibiotics, namely, cephalexin (CPX), cefradine (CFD), and cefaclor (CFC) with thymol (THY) used as a co-former. The co-crystals of CPX, CFD, and CFC with THY, namely, CPX·THY·2.5H2O forms I and II, CFD·THY·2.5H2O, and CFC·THY·4H2O, respectively, were prepared via solid-state synthesis (ball milling/slurry) and/or solution methods, characterized, and their antimicrobial performance was evaluated.

Remarkably, the outcome of the experiments carried out with antibiotics of the CEPH family was at variance with that of ciprofloxacin (CIP) discussed above. The evaluation of the MIC values for the co-crystals of CEPH with THY showed a systematic inhibition effect with respect to the activity of CEPH alone and in physical mixture with THY. This difference has been explained on the basis of a drastic reduction in solubility of the co-crystals with respect to the pure component, which may affect the permeability of the bacterial cell membrane.

The multitarget approach used in the previous cases has been finally applied to the case of the co-crystallization of the antibiotic levofloxacin (LEVO) and ciprofloxacin (CIP) with the flavonoids quercetin (QUE), myricetin (MYR) and hesperetin (HES) resulted in a very interesting outcome. In fact, no significant difference in the antimicrobial activity was observed between the co-crystals and the physical mixtures used as comparison reference, while they preserve, both co-crystals and physical mixtures, the antimicrobial efficacy of the original antibiotics alone.

All the antimicrobial tests reported for this section were performed by the research group of the Professor Vittorio Sambri and collaborators (ciprofloxacin and cephalosporines with carvacrol and thymol), and the group of the Professor Vincenzo Scarlato and collaborators (work in progress on levofloxacin and ciprofloxacin with flavonoids) at the University of Bologna- Italy.

Forward look

This thesis is a "proof of concept": crystal engineering-based strategies can indeed be applied to bring solid state chemistry beyond the boundaries of chemistry into the realm of biology, pharmacology, and medicine. The work of my thesis demonstrated that potentially useful new materials and drugs can be prepared by simple mixing of know

compounds and that the combination activates synergistic interactions that can, in some cases, improve the antimicrobial target properties, as designed.

The diversity of results obtained within the two lines of investigation, whether based on metal complexes and coordination polymers or on molecular cocrystals formed by organic molecules and active pharmaceutical ingredients, calls for a deeper and case-oriented biological investigation on the mechanism of action of co-crystals and supramolecular aggregates with the microorganisms. In order to be addressed, these very relevant aspects require expertise in the pharmaceutical and biotechnological domains, for a better understanding of the factors controlling the different behaviours evidenced in the studies reported herewith when the co-crystals and coordination complexes/polymers are brought in contact/proximity of the microorganisms.

ACKNOWLEDGEMENTS

I would like to thank Dr. Oleksii Shemchuk for his awesome contribution in the first year of my PhD and for his great patience in teaching me the *"know how"* of crystal engineering.

I must thank Prof. Dr. Tomislav Friščić for hosting me in his group for 4 months at the McGill University – Montreal, Canada and for supporting my research activity.

He's been a great supervisor and an amazing friend.

Dr. Katia Rubini is acknowledged for her time and experience performing DSC and TGA analysis.

Dr. Stefano Grilli is acknowledged for his wise suggestions and ideas, for providing me access to the NMR facility and carrying out NMR experiments.

Dr. Simone d'Agostino is acknowledged for his kind support to the group and the Molecular Crystal Engineering lab.

Personal thanks

There are no words to describe how thankful I am to my Mum and Dad for bringing me to this world and supporting me in my studies and in every decision and step I made.

Many, many thanks to my boyfriend and life-mate Samet Ocak, who always tried to sustain me in all the *mental breakdowns*, fixing what was needed to be fixed, and who enthusiastically shared with me the most intense period of our lives.

Not to mention my group of friends, *"Gli amici dell' aperitivo",* who were born ready and committed to grab a drink or two and chat of our daily events, in dark and bright moments.

I must also thank my professors Dario and Fabrizia and all my colleagues, for being patient and tolerative with my moods, the extravagancy, and my -sometimes- indelicate way to express opinions and feelings - *about science and not*.

I'm surely not going to change the world with this science, but I'm willing to leave a small trace in it.

Sincerely, thank you all.